UNIVERSIDADE DE LISBOA
FACULDADE DE CIÊNCIAS

A mathematical model of the phosphoinositide pathway in human pulmonary epithelial cells

"*Documento Definitivo"*

Doutoramento em Biologia
Especialidade de Biologia de Sistemas

Daniel Vigário Olivença

Tese orientada por:
Prof. Dr. Francisco R Pinto
Prof. Dr. Eberhard O Voit

Documento especialmente elaborado para a obtenção do grau de doutor

2018

UNIVERSIDADE DE LISBOA

FACULDADE DE CIÊNCIAS

A mathematical model of the phosphoinositide pathway in human pulmonary epithelial cells

Doutoramento em Biologia

Especialidade de Biologia de Sistemas

Daniel Vigário Olivença

Tese orientada por:

Prof. Dr. Francisco R Pinto

Prof. Dr. Eberhard O Voit

Júri:

Presidente:

- Doutor Rui Manuel dos Santos Malhó, Professor Catedrático da Faculdade de Ciências da Universidade de Lisboa

Vogais:

- Doutor Rui Davide Martins Travasso, Investigador Principal da Faculdade de Ciências e Tecnologia da Universidade de Coimbra
- Doutora Isabel Cristina Almeida Pereira Rocha, Professora Auxiliar da Escola de Engenharia da Universidade do Minho
- Doutora Susana de Almeida Mendes Vinga Martins, Professora Associada do Instituto Superior Técnico da Universidade de Lisboa
- Doutora Margarida Sofia Pereira Duarte Amaral, Professora Catedrática da Faculdade de Ciências da Universidade de Lisboa
- Doutor Francisco Rodrigues Pinto, Professor Associado com Agregação da Faculdade de Ciências da Universidade de Lisboa (orientador)

Documento especialmente elaborado para a obtenção do grau de doutor

Daniel Vigário Olivença foi bolseiro de doutoramento no âmbito to Programa doutoral BioSys em Sistemas Biológicos, Genómica Funcional & Integrativa (FCT/PD/00065/2012) da Faculdade de Ciências da Universidade de Lisboa, financiado pela Fundação para a Ciência e Tecnologia do Ministério da Educação e Ciência, Bolsa FCT / SFRH / BD / 52486 / 2014.

2018

Daniel Vigário Olivença foi bolseiro de doutoramento no âmbito to Programa doutoral BioSys em Sistemas Biológicos, Genómica Funcional & Integrativa (FCT/PD/00065/2012) da Faculdade de Ciências da Universidade de Lisboa, financiado pela Fundação para a Ciência e Tecnologia do Ministério da Educação e Ciência, Bolsa FCT / SFRH / BD / 52486 / 2014.

Acknowledgments

A special acknowledgement goes to my supervisors, Prof. Dr. Francisco R Pinto and Prof. Dr. Eberhard O Voit, who hosted me in their labs and started my journey into the modelling field. The list of acknowledgments due to them is longer than the reader can bear but I must highlight the patience towards my many shortcomings, the profound knowledge of the field and the natural kindness that characterized both of them. I was truly blessed with the opportunity to work with them.

I would like to thank my Bioinformatics lab companions: Gonçalo Nogueira, Inês Fernandes Ramos, Marina Luque and Nuno Domingues. I would like to mention also the former lab members Daniel Vilar and Flávia Penim.

I would like to thank all the GER group – Gene Expression and Regulation group, Afonso Mota, André Matos, Camilo Simanca, Hugo Santos, Inês Martins, Iga Rawica, Lúcia Heitor, Marcelo Pereira, Marta Correia, Miguel Pereira, Tânia Marques and especially to Prof. Dr. Margarida Gama Carvalho.

Special thanks also deserve my colleagues from all classes of the BioSys PhD. Thanks for the patience and help given in the breaks and lunch hours, when you probably would like to talk about lighter subjects and I would ask something related to work. Your sacrifice was not gone unnoticed. Thank you for facilitating the understanding of an area that was foreign to me.

I would like to thank to the personnel in Prof. Dr. Voit's LBSA – Laboratory for Biological Systems Analysis. Thank you for the help, conversations, suggestions and ideas. A special thanks goes to Dr. Luis L Fonseca for valuable insights about my work, translating and helping me navigate the American culture and bureaucracy. It always was a pleasure to work with him.

Thanks to Prof. Dr. Paulo Matos and Prof. Dr. Peter Jordan for giving me the opportunity the experience the exhilarating roller coaster that is wet lab work. Thanks to their lab staff, especially to Dr. Patricia Barros, who carried or dragged me throughout this experience.

I would like to thanks to the members of Amaral for receiving me in their weekly lab meetings, for their patience and knowledge. A special thanks for prof. Margarida Ramos for her insights in physiology and to prof. Carlos Farinha for his insights on whatever was in my mind at the moment.

To the person responsible for this PhD and the BIOISI program to exist, prof. Margarida Amaral. I find Portuguese people to be risk adverse to the point of inaction for fear of failing and very conscious not to disturb others even when the discomfort they cause would serve as a motivation for people to grow and improve. Prof. Margarida has none of these defects. Thank you for your courage. She also had the idea that became my PhD project, her lab supplied the data that for model validation and has an immense knowledge on Cystic Fibrosis.

I would also like to thank to all my friends outside the "lab life," who helped me throughout this PhD.

To my family, especially to my mum and dad: Thanks! Thank you also to all members of my family that believed in me. Finally, my heartfelt gratitude goes to Rita, for her patience and understanding.

Summary

Cystic fibrosis is a condition caused by mutations in the cystic fibrosis transmembrane conductance regulator (CFTR), a chloride and bicarbonate channel. The epithelial sodium channel (ENaC) may also be affected. The defective function of these ion channels is thought to reduce the airway surface liquid (ASL) and lead to the accumulation of mucus in the airways that characterizes the disease and causes the recurrent pulmonary infections and inflammation that will ultimately destroy the lungs of the affected subjects.

Phosphoinositides are rare signaling lipids that constitute a complex network regulating many cellular processes. One of phosphoinositides' many functions is as cell membrane protein regulators, and several studies implicate phosphatidylinositol 4,5-biphosphate ($PI(4,5)P_2$) in ENaC regulation.

Diacylglycerol kinase (DGK), an enzyme of the phosphoinositide pathway that catalyses the phosphorylation of diacylglycerol (DAG) into phosphatidic acid (PA). When DGK is inhibited, it will cause the moderation of ENaC function, and this could be exploited as a therapeutic in cystic fibrosis. But the mechanism of ENaC regulation by DGK is not completely understood. The usually accepted hypothesis is that DGK influences $PI(4,5)P_2$ production by halting the phosphoinositide recycling.

In Chapter 2 we present a model of the phosphoinositide pathway that simulates one square micrometer of the inner layer of the membrane. The objective of this project was to create a model that could simulate the phosphoinositide pathway and be used to study how perturbations to the pathway impact the levels of pertinent lipids, especially the ones known to affect ENaC.

The model replicates the steady-state of the phosphoinositide pathway as recorded in the literature and replicates most known dynamic phenomena. Furthermore, sensitivity analysis demonstrates that the model is robust to moderate perturbations to the parameters. The model suggests that the main source of material to the $PI(4,5)P_2$ pool is a flux representing the direct transformation of phosphatidylinositol (PI) into $PI(4,5)P_2$ that defies the traditional view that the main source is the sequential phosphorylation of phosphoinositol into phosphatidylinositol 4-phosphate (PI(4)P) by the enzyme phosphoinositol 4-kinase (PI4K) followed by the transformation to

$PI(4,5)P_2$ by phosphoinositide 4-phosphate 5-kinase I (PIP5KI). The model also suggests that phosphatidylinositol 5-phosphate (PI(5)P) could be a significant source for $PI(4,5)P_2$ production. We compared the model results to data from a siRNA screens, where the expression of several enzymes in the pathway were knocked down and the activity of ENaC was monitored. Our model suggests control strategies where the activity of the enzyme PIP5KI or the PI4K+PIP5KI+DVL protein complex are decreased and cause an efficacious reduction in $PI(4,5)P_2$ levels while avoiding undesirable alterations in other phosphoinositide pools.

In Chapter 3 we present a model that enables the study of the interplay between ENaC, CFTR, airway surface liquid (ASL), $PI(4,5)P_2$ and the protein SPLUNC1 (short palate, lung, and nasal epithelial clone). It presents a good fit to experimental observations, and the available data can constrain the model's parameters without ambiguities. The model analysis shows that ASL at the steady state is sensitive to small changes in $PI(4,5)P_2$ abundance, particularly in cystic fibrosis conditions, which suggests that manipulation of phosphoinositide metabolism may promote therapeutic benefits for cystic fibrosis patients.

Finally, in Chapter 4, we bring the phophoinositide pathway and ENaC/ASL model together. These models enabled us to study DGK and ENaC and strongly suggest that, contrary to the usually accepted hypothesis, this regulation is effected by the control of $PI(4,5)P_2$ production by the PIP5KI that in turn is controlled by PA, the product of DGK.

In this work we also use a model of the phosphoinositide cycle to test the hypothesis that DGK influence $PI(4,5)P_2$ production by halting the phosphoinositide recycling. This model is unable to replicate the available data if the activation of PIP5KI by PA is not implemented, which strengthens our belief that ENaC regulation by phosphoinositides is accomplished through PA and PIP5KI.

Key Words: Cystic fibrosis, ENaC, phosphoinositides.

Resumo

A fibrose quística é uma condição causada por mutações no regulador da condutância transmembranar da fibrose quística (CFTR), um canal de cloreto e bicarbonato. É um distúrbio autossómico recessivo monogénico: monogénico porque é um distúrbio causado por um único gene defeituoso; autossómico porque o gene está num autossoma, um cromossoma que não é um cromossoma sexual; recessivo porque a condição só se expressa se um indivíduo tiver duas cópias do gene defeituoso. Esta doença foi descrita pela primeira vez em 1938, mas somente em 1989 o gene causador foi identificado. Apesar da causa ser conhecida há 29 anos, uma cura definitiva para esta doença ainda não foi encontrada.

A fibrose quística surge por mau funcionamento das glândulas exócrinas do organismo (as de secreção externa). Existe uma grande variabilidade nos fenótipos dos pacientes com fibrose quística. Após o nascimento, os sintomas mais comuns são a concentração elevada de cloreto no suor e, em mais 85% dos pacientes, a insuficiência pancreática. Inicialmente, a insuficiência pancreática era considerada a principal complicação da fibrose quística, sendo os problemas pulmonares uma consequência da desnutrição. Hoje em dia, corrigidos os problemas pancreáticos e de desnutrição, as complicações a nível pulmonar mantêm-se.

Embora os pulmões não estejam afetados no nascimento, inflamações e infeções por bactérias aparecerão pouco depois. Isso é causado, acredita-se, pela acumulação de muco. Esta é uma consequência de um transporte deficiente de iões, ou seja, redução da secreção de cloreto e aumento da absorção de sódio. Inflamação continuada e infeções por bactérias como Pseudomonas aeruginosa irão desencadear uma resposta inflamatória persistente. A infeção e a inflamação contínuas acabarão por destruir os pulmões e esta é a principal causa de morbilidade e mortalidade dos indivíduos com fibrose quística.

É uma das doenças genéticas mais comuns, sendo os indivíduos caucasianos os mais atingidos. Segundo a Associação Nacional de Fibrose Quística, na Europa, em média, 1 em cada 2000 – 6000 recém-nascidos tem a doença. Em Portugal, estima-se que nasçam por ano cerca de 20–40 crianças com fibrose quística. A nível mundial, estima-

se que 75000 pessoas sofram da doença e que 7 milhões sejam portadores do gene defeituoso.

O canal epitelial de sódio (ENaC) também pode ser afetado, aumentando a absorção de sódio e água. A função defeituosa desses canais iónicos promove a acumulação de muco espesso nos brônquios, o que caracteriza a doença e causa as infeções pulmonares recorrentes e a inflamação que acabará por destruir os pulmões dos indivíduos afetados. Vários estudos apontam para uma regulação do ENaC por fosfatidilinositóis, especialmente o fosfatidilinositol 4,5-bifosfato ($PI(4,5)P_2$) e o fosfatidilinositol 3,4,5-trifosfato ($PI(3,4,5)P_3$).

Os fosfatidilinositóis são lipídios raros com várias funções que constituem uma rede complexa que regula muitos processos celulares. Uma das muitas funções dos fosfatidilinositóis é como reguladores de proteínas da membrana celular, e vários estudos implicam que o $PI(4,5)P_2$ na regulação ENaC.

A diacilglicerol quinase (DGK) é um enzima da via dos fosfatidilinositóis que catalisa a fosforilação do diacilglicerol (DAG) em ácido fosfatídico (PA). Inibição do DGK causa a moderação a função do ENaC e isso pode ser explorado como uma estratégia terapêutica na fibrose quística. Mas o mecanismo de regulação do ENaC pelo DGK não é completamente entendido. A hipótese geralmente aceite é que o DGK influencia a produção de $PI(4,5)P_2$ interrompendo a reciclagem dos fosfatidilinositóis.

Esta hipótese tem alguns problemas. DGK e ENaC estão localizados na membrana plasmática, enquanto a síntese de fosfatidilinositóis se dá no retículo endoplasmático. Não é claro como o ácido fosfatídico produzido na membrana plasmática influencia um processo que ocorre no retículo endoplasmático. Também não é claro como os fosfatidilinositóis, produzidos no retículo endoplasmático, vão afetar o ENaC que está na membrana plasmática.

Neste trabalho testamos uma hipótese alternativa. O PA gerado pelo DGK ativa o PIP5KI, o enzima que catalisa a transformação de PI(4)P em $PI(4,5)P_2$. Sugerimos que, quando o DGK é inibido, a diminuição de PA vai reduzir a produção de $PI(4,5)P_2$, que por sua vez irá moderar a atividade do ENaC. Esta hipótese tem a vantagem de ter um menor número de intervenientes e de todos estarem localizados na membrana plasmática.

No Capítulo 2 apresentamos um modelo da via dos fosfatidilinositóis que simula a camada interna de um micrometro quadrado de membrana. O objetivo foi criar um modelo que pudesse simular a via dos fosfatidilinositóis e ser usado para estudar como as perturbações na via afetam os níveis dos lipídios, especialmente aqueles que regulam o ENaC.

O modelo replica as quantidades dos fosfatidilinositóis que constituem a via, conforme registrado na literatura, e replica os fenómenos dinâmicos mais conhecidos. Além disso, a análise de sensibilidade demonstra que o modelo é robusto relativamente a perturbações moderadas dos parâmetros. O modelo sugere que a principal fonte de material para o pool $PI(4,5)P_2$ é um fluxo que representa a transformação direta de fosfatidilinositol (PI) em $PI(4,5)P_2$, que desafia a visão tradicional de que a fonte principal é a transformação de fosfatidilinositol em fosfatidilinositol 4-fosfato (PI(4)P) pelo enzima fosfatidilinositol 4-quinase (PI4K) e, seguidamente, a transformação deste lípido em $PI(4,5)P_2$ pelo enzima fosfatidilinositol 4-fosfato 5-quinase I (PIP5KI). O modelo também sugere que fosfatidilinositol 5-fosfato (PI(5)P) poderia ser uma fonte significativa para a produção de $PI(4,5)P_2$. Comparámos os resultados do modelo com os dados da atividade do ENaC perturbada com inibições da expressão de vários enzimas da via recorrendo a siRNA. O nosso modelo sugere estratégias de controle onde a atividade do enzima PIP5KI ou do complexo de proteínas PI4K + PIP5KI + DVL estão diminuídas e causam uma redução eficaz nos níveis de $PI(4,5)P_2$, evitando alterações indesejáveis em outros pools de fosfatidilinositóis.

No Capítulo 3 apresentamos um modelo que permite o estudo da interação entre ENaC, CFTR, líquido que cobre a superfície das vias aéreas (ASL), $PI(4,5)P_2$ e o clone curto epitelial de palato, pulmão e nariz (SPLUNC1). Este modelo apresenta um bom ajuste às observações experimentais e os dados disponíveis restringem os parâmetros do modelo sem ambiguidades. A análise do modelo mostra que a ASL é sensível a pequenas mudanças na abundância de $PI(4,5)P_2$, particularmente nas condições de fibrose quística, o que sugere que a manipulação do metabolismo do fosfatidilinositóis pode promover benefícios terapêuticos para pacientes com fibrose quística.

Finalmente, no Capítulo 4, juntámos o modelo da via dos fosfatidilinositóis e o modelo ENaC / ASL. Estes modelos permitem estudar a regulação do ENaC pelo DGK e sugerem que, ao contrário da hipótese geralmente aceite, esta regulação seja efetuada

pelo controle da produção de $PI(4,5)P_2$ pelo PIP5KI que por sua vez é controlado por PA, o produto de DGK.

Ainda neste trabalho, usámos um modelo do ciclo dos fosfatidilinositóis para testar a hipótese de que o DGK influencia a produção de $PI(4,5)P_2$ interrompendo a reciclagem dos fosfatidilinositóis. Este modelo não reproduz os dados experimentais se não for implementado a ativação do PIP5KI pelo PA, o que reforça a nossa conclusão de que a regulação do ENaC pelos fosfatidilinositóis se processa através do PA e do PIP5KI.

Apesar destes resultados, que sugerem que a manipulação dos níveis de fosfatidilinositóis seja uma estratégia promissora para proceder à moderação da atividade do ENaC, é prudente salientar que os fosfatidilinositóis influenciam muitos processos celulares e várias proteínas de membrana. Baixar os níveis de $PI(4,5)P_2$ e de PA tem grande probabilidade de originar efeitos imprevisíveis ou indesejados.

Palavras-Chave : Fibrose quística, ENaC, fosfatidilinositóis.

De acordo com o disposto no artigo 24º do Regulamento de Estudos de Pós-Graduação da Universidade de Lisboa, Despacho nº 7024/2017, publicado no Diário da República – 2ª Série – nº 155 – 11 de Agosto de 2017, foram utilizados nesta dissertação resultados incluídos nos seguintes artigos:

1. Olivença, D. V., Uliyakina, I., Fonseca, L. L., Amaral, M., Voit, E., & Pinto, F. R. (2018). A Mathematical Model of the Phosphoinositide Pathway. *Scientific Reports*, *8*, 1–12. https://doi.org/10.1038/s41598-018-22226-8

E por fim dois manuscritos já submetidos:

1. Olivença, D. V., Fonseca, L. L., Voit, E. O., & Pinto, F. R. (2018). Thickness of the airway surface liquid layer in the lung is affected in cystic fibrosis by compromised synergistic regulation of the ENaC ion channel. [submitido e apresentado no Capítulo 3]
2. Olivença, D. V., Voit, E. O., & Pinto, F. R. (2018). ENaC regulation by phospholipids and SPLUNC1 protein explained through mathematical modelling [submitido e apresentado no Capítulo 4]

No cumprimento do disposto da referida deliberação, o autor esclarece serem da sua responsabilidade, exceto quando referido o contrário, a execução das experiências que permitiram a elaboração dos resultados apresentados, assim como da interpretação e discussão dos mesmos. Os resultados obtidos por outros autores foram incluídos com a autorização dos mesmos para facilitar a compreensão dos trabalhos e estão assinalados nas respetivas figuras e metodologias.

Table of Contents

List of Figures

List of Tables

Abbreviations

AKT - Protein Kinase B, a serine/threonine-specific protein kinase

ASL - Airway surface liquid

ATP - Adenosine triphosphate

BST - Biochemical systems theory

cAMP - Cyclic adenosine monophosphate

CF - Cystic fibrosis

CFTR - Cystic fibrosis transmembrane conductance regulator

DAG - Diacylglycerol

DGK - Diacylglycerol kinase

DVL - Segment Polarity Protein Dishevelled Homolog DVL

ENaC - Epithelium sodium channel

ER - Endoplasmic reticulum

GMA - Generalized mass action

GPCRs - G protein coupled receptors

INPP5 - Inositol polyphosphate 5-phosphatases

IP_3 - Inositol triphosphate

LPP - Phosphatidate phosphatase

LPTs - Lipid transport proteins

MCSs - Membrane contact sites

MDCK cells - Madin-Darby Canine Kidney Epithelial Cells

MM - Michaelis-Menten

MTM - Myotubularin

N - Number of active ENaC channels in the membrane

NEDD4-2 - Neural precursor cell expressed developmentally down-regulated protein 4 - 2

OCRL - Lowe Oculocerebrorenal Syndrome Protein; OCRL is an INPP5

ODE - Ordinary Differential Equation

PA - Phosphatidic acid

PC - Phosphatidylcholine

PDK1 - Phosphoinositide-dependent kinase 1

PE - Phosphatidylethanolamine

PI - Phosphatidylinositol

PI(3)P - Phosphatidylinositol 3-phosphate

$PI(3,4)P_2$ - Phosphatidylinositol 3,4-bisphosphate

$PI(3,4,5)P_3$ - Phosphatidylinositol 3,4,5-triphosphate

$PI(3,5)P_2$ - Phosphatidylinositol 3,5-bisphosphate

PI(4)P - Phosphatidylinositol 4-phosphate

$PI(4,5)P_2$ - Phosphatidylinositol 4,5-bisphosphate

PI(5)P - Phosphatidylinositol 5-phosphate

PI3K - Phosphatidylinositol 3 kinase

PI4K - Phosphoinositide 4-kinase

PIKfyve - FYVE finger-containing phosphoinositide kinase.

PIP5KI - Phosphatidylinositol-4-phosphate 5- kinase I

PKA - Protein kinase A

PKC - Protein kinase C

PLC - Phospholipase C

PLD - Phospholipase D

PLIP - PTEN-like lipid phosphatase

P_o - Open probability of ENaC

PS - Phosphatidylserine

PTEN - Phosphatase and tensin homolog

SAC - Suppressor of actin

SHIP1 - SH2 domain-containing phosphatidylinositol 5′-phosphatase

SKIP - Skeletal muscle and kidney enriched inositol polyphosphate phosphatase

SPLUNC1 - Short palate lung and nasal epithelial clone 1

SYNJ - Synaptojanins

TPIP - PTEN-Like Inositol Lipid Phosphatase

Wnt3a - Wingless-Type MMTV Integration Site Family, Member 3A

WT - Wild type

Chapter 1. **Introduction**

1.1. Modelling

A model is a partial representation or abstraction of a system of interest.

As Griffiths [1] puts it, "…the world is very complex and hard to understand, no matter how brainy you are. To make things easier to grasp, reality is generally broken down into bite-size chunks. These chunks are abstracted from the real world and simplified into things called models."

We use models for several reasons: to help us understand and explain a system, test our assumptions or hypotheses and make predictions. Models are especially well suited for testing the interactions between elements of a system. An important feature of model construction is to distinguish the components that are relevant to answer the questions at hand from the ones that are not. By only using the relevant features, researchers can simplify a study and potentially notice details that could be masked or shadowed by non-essential complexity.

Models are always approximations of the system under study and, because of this, no model is entirely correct. As a consequence, one should always judge models by their usefulness than for their alleged correctness.

Also, a model that is closer to the structure of the system of interest is not necessarily a better model. Take for example the London underground maps in Figure 1.1, an example taken from Walter Kolch's talks. In the beginning of the XXth Century, the maps where geographically accurate, but this made them disorganised and confusing. Today, the maps are much more abstract, and simplicity is as important as the accuracy of representation. This compromise makes them more efficient in their function of conveying information (Kolch, conference communication, 2017).

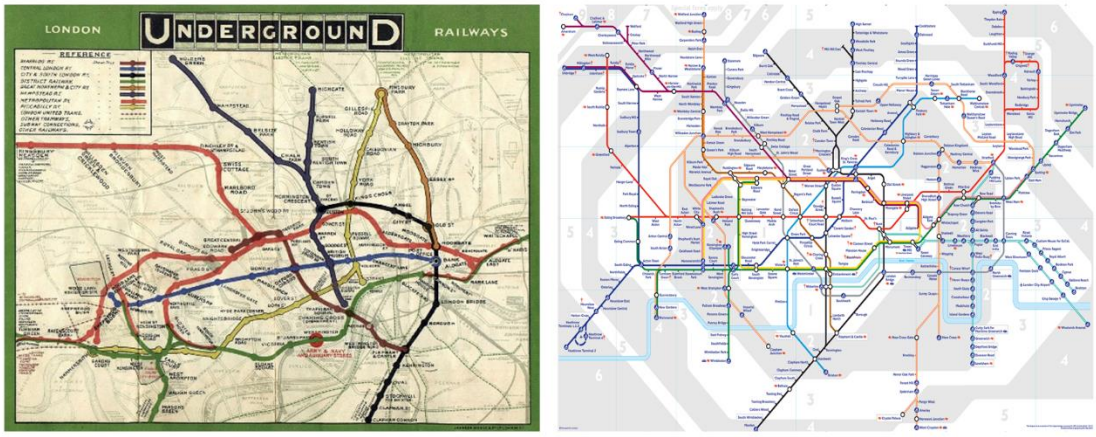

Figure 1.1. Maps of London underground.

(Left) Old London underground map that is geographically accurate. (Right) Modern London underground map: A simpler and a better conveyer of information [2], [3].

There are many different types of models and many ways to classify them. Let's refer to some examples that are close to biochemistry. Conceptual models are representations of a system that have been used constantly and from the dawn of humanity, like maps or workflow charts. *In vivo* models are organisms that hopefully function more or less in the same way as the organism that is actually of interest; an example is the use of a lab rat as a substitute for the human organism. Due to the complexity of these organisms, which sometimes overshadows the system under study, the rise of ethical concerns with animal experimentation and their great maintenance cost, many researchers use *in vitro* models. These are simplifications of the conditions of the *in vivo* models, like a Petri dish with culture medium. Continuing this line of abstraction, we arrive at computer-based models (also known as *in silico* models, if the use of cod Latin is not a problem), which are the subject of this work. These are computational representations and mathematical descriptions of a system and they are the most versatile type of models. These different types of models shouldn't be used individually but be used together, to exploit their advantages and mitigate their limitations.

1.2. Biochemical Systems Theory

Biochemical systems theory (BST) is a mathematical modelling framework for biochemical systems, based on ordinary differential equations (ODE), in which processes are represented using power-laws. It was developed by Savageau [4]–[6],

Voit [7]–[9], and many others. The objective of this field of study is to find general laws, or at least appropriate representations, that govern the biochemical processes and use then to build models that mimic biochemical systems.

BST is useful because biochemical systems are difficult to study. Also, researchers have a very limited toolbox to work with. A biochemist studying an organism or a biological system is like a person from the XVIIIth Century trying to understand, with notions of the scientific method, how a computer works [10], [11]. He will unplug it from the socket and find out if it will not work. He will open the computer and remove a piece and see if it still works or if its function is affected in some manner. Or he will add several similar components in the same machine and see what happens. To complicate things even further, these biological "computers" appear in all sorts of shapes and sizes, their components were designed to have many redundancies and display a fair amount of variability. Like a computer with multiple heterogeneous hard drives with different operating systems.

As mentioned before, biochemists have been using *in vivo* and *in vitro* models for some while, but these are usually costly and time consuming. Also, some promising perturbations are simply not feasible with current technology, are very difficult to perform in a lab, or simply unethical. With mathematical and computational models, we can execute many simulations in the same time it takes to make a single wet lab experiment and at a fraction of the cost. Also, the control we have over a model is much greater than what we have over a biological system. There is a trade-off, however, as computer-based models are artificial approximations and their results must be validated in the original biological system in order to be certain that simulation results are not unintended artefacts.

BST is a canonical modelling framework which offers valuable guidelines for the design, analysis and simulation of biological systems. Once the biochemical map is drafted, the rules of BST make the construction of the mathematical model a straightforward process.

In BST, all fluxes are represented as products of power-laws. Equation 1.1 shows the general representation of a flux in this framework.

$$v_{a\to b} = \gamma_{a\to b} \times \prod_{j=1}^{n+m} X_j^{f_{a\to b,j}} \tag{1.1}$$

$v_{a\to b}$ represents flux from a to b, X_j represent the different dependent or independent variables that affect the flux and n and m are the number of dependent and independent variables respectively. $\gamma_{a\to b}$ is the rate constant of the flux and $f_{a\to b,j}$ is the kinetic order of the X_j variable in the $\boldsymbol{v}_{a\to b}$ flux. The rate constant and kinetic orders are parameters that can be calculated using information from data, from the literature, or present in databases with enzyme functional data like BRENDA [12].

But why this formalism? Biochemical reactions are well represented by the Michaelis-Menten (MM) equation if the conditions underlying this formalism apply, but these conditions are seldom truly satisfied in living cells. Furthermore, MM is a rational function, which has the drawback that sums of rational functions are difficult to deal analytically. Power-laws are alternatives that become linear in log space, even in high dimensions. They can be designed directly based on data and knowledge of a pathway, and they are also good approximations for MM equations, especially near the operating point, which is typically the steady state of the system. They can efficiently simulate nonlinear behaviors in the S-system form (1.13 [6], [8] and provide an analytical solution for the steady-states.

MM equations have the form

$$v = \frac{\mathrm{Vmax} \cdot [S]}{Km + [S]} \tag{1.2}$$

v is the rate of reaction represented by in this specific flux, Vmax is the maximum velocity achieved by the reaction, Km is the Michaelis constant that represents the concentration of substrate needed for the reaction to progress at a rate half of the Vmax and [S] represents the concentration of subtract.

Bode [13] found that a rational function in log-space is linearized in a part of its domain (Figure 1.2). To understand the log-space, consider a function of areal variable x, f(x); in Log space the abscissa are $\log(x_i)$ and the ordinate is $\log(f(x_i))$.

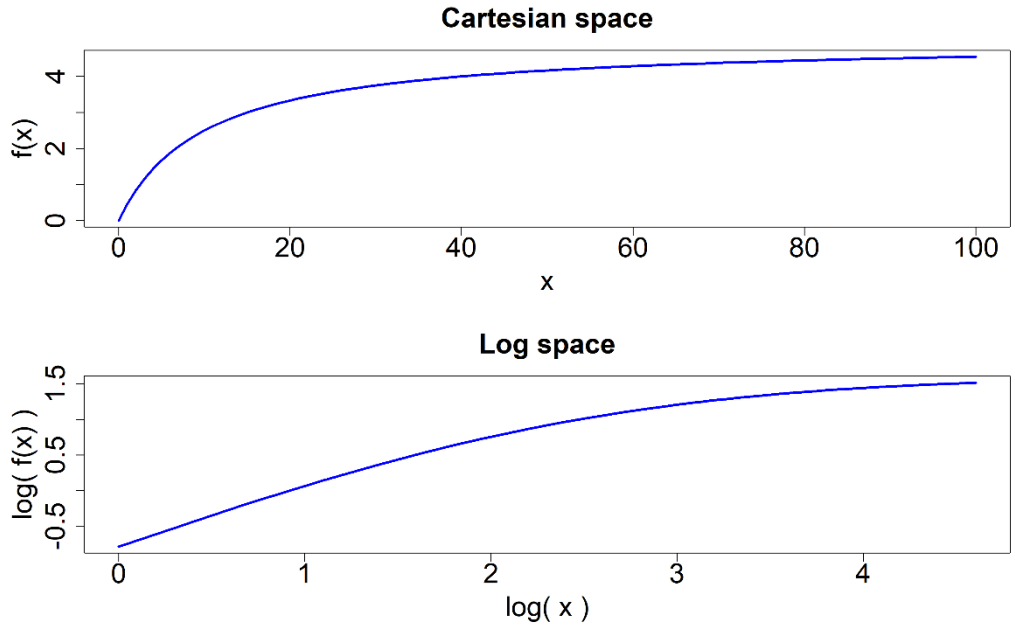

Figure 1.2. Representation of the rational function f(x) = 5x / (10 + x) in Cartesian space (top) and in log-space (bottom).

In the latter, the function plot is more similar to a linear function, at least in the initial part.

Any function that is differentiable at the operating point can be approximated with a power law, and saturating functions typically become more linear, which increases the range of valid approximation.

Taylor, with his well-known formula, proposed the approximation of any function with a polynomial. If we use a first-order polynomial, this will not produce a good approximation of the whole function, only at the operating point will we get a satisfactory approximation. This operating point is a value from a region of interest of the function's domain. For example, it is a point in a region that we believe will supply the function with most of its inputs.

$$f(x) \simeq f(p) + \frac{f'(p)}{1!}(x - p) \qquad (1.3)$$

Let's use Taylor's formula to approximate a function in log space to a first-degree polynomial (Figure 1.3). Here, log represents the natural logarithm.

$$\log\left[f(x)\right] \simeq \log\left(f(p)\right) + \frac{d\log\left(f(p)\right) \Big/ d\log(p)}{1!}\left(\log(x) - \log(p)\right) \qquad (1.4)$$

Let's turn our attention to the derivative and try to simplify it.

$$\frac{d\log\left(f(p)\right)}{d\log(p)} = \frac{\dfrac{d\log\left(f(p)\right)}{dp}}{\dfrac{d\log(p)}{dp}} = \frac{\dfrac{d\left(f(p)\right)}{dp}}{\dfrac{f(p)}{p}} = \frac{d\left(f(p)\right)}{dp} \times \frac{p}{f(p)} \qquad (1.5)$$

So we can write (1.4) as

$$\log\left[f(x)\right] \simeq \log\left(f(p)\right) + \frac{d\left(f(p)\right)}{dp} \times \frac{p}{f(p)} \times \left(\log(x) - \log(p)\right) \qquad (1.6)$$

This is a linear function in log-space. We can write it in reduced form *m[log(x)]+b* where

$$\begin{aligned} m &= \frac{d\left(f(p)\right)}{dp} \times \frac{p}{f(p)} \\ b &= \log\left(f(p)\right) - \frac{d\left(f(p)\right)}{dp} \times \frac{p}{f(p)} \times \log(p) \end{aligned} \qquad (1.7)$$

Now we have an approximation, in log-space, of a linear function to the rational function. Let's write the approximation in Cartesian space.

$$\begin{aligned} &\log\left(f(x)\right) \simeq m \times \log(x) + b \Leftrightarrow f(x) \simeq e^{m \times \log(x) + b} \Leftrightarrow \\ &\Leftrightarrow f(x) \simeq e^{\log\left(x^m\right)} \times e^b \Leftrightarrow f(x) \simeq x^m \times e^b \end{aligned} \qquad (1.8)$$

The function, written in this form, is a power law. The power of the dependent variable is called a *kinetic order* and is usually represented with a *g* and the multiplicative constant is called the *rate constant* and usually represented with a γ.

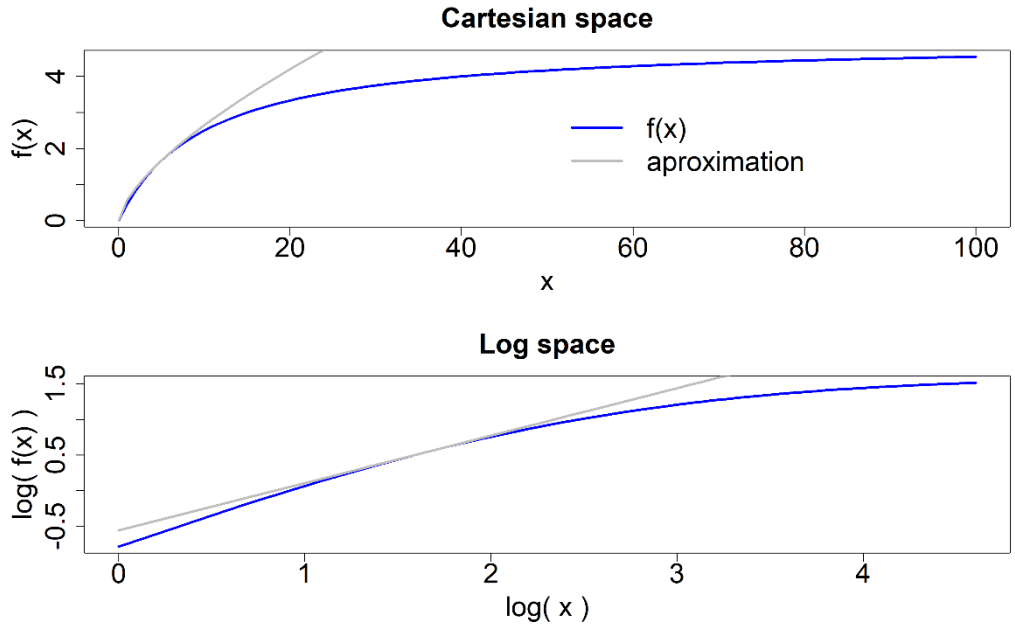

Figure 1.3. Representation of the rational function f(x) = 5x / (10 + x) in Cartesian space (top) and in log-space (bottom) in blue.

In grey, the power law approximation at operating point x=5.

In practice, the kinetic order will be calculated in following manner:

$$g = \text{kinetic order} = \frac{d\left(f\left(x\right)\right)}{dx} \times \frac{x}{f\left(x\right)}\bigg|_{x=\text{operating point}} \qquad (1.9)$$

$$\gamma = \text{rate constant} = f\left(x\right) \times x^{-g}\Big|_{x=\text{operating point}}$$

For multiple variable functions the calculations are similar and for that and more information please see Voit [7], [8].

Because the MM equations are so important, let's turn our attention to the power-law approximation for these equations. We need to calculate the rate constants and kinetic orders, and these can be calculated from *Km* values, specific activities and quantities of the enzymes obtained from BRENDA [12] and Genecards databases.

The kinetic order, for a given concentration of substrate (*S*), is

$$
\begin{aligned}
&kinetic\,order = \frac{d(v)}{d[S]} \times \frac{[S]}{v}\bigg|_{x=\text{operating point}} = \\
&= \frac{d}{d[S]} \frac{\text{Vmax} \cdot [S]}{Km + [S]} \times \frac{[S]}{\frac{\text{Vmax} \cdot [S]}{Km + [S]}}\bigg|_{[S]=\text{operating point}} = \\
&= \frac{\text{Vmax} \cdot (Km + [S]) - \text{Vmax} \cdot [S]}{(Km + [S])^2} \times \frac{[S](Km + [S])}{\text{Vmax} \cdot [S]}\bigg|_{[S]=\text{operating point}} = \\
&= \frac{Km}{Km + [S]}\bigg|_{[S]=\text{operating point}}
\end{aligned}
\tag{1.10}
$$

The rate constants are computed for a given substrate concentration *S* with specific activities and quantities of the enzymes. Note that Vmax = specific activity * enzyme quantity.

$$
\begin{aligned}
&\text{rate constant} = \frac{\text{Vmax.}[S]}{Km + [S]} \times [S]^{-\text{kinetic order}} = \\
&= \frac{\text{specific activity} \times \text{enzyme amount} \times [S]}{Km + [S]} \times [S]^{-\text{kinetic order}}
\end{aligned}
\tag{1.11}
$$

In the construction of the differential equations there are three options: Generalized Mass Action (GMA), S-systems and Half-systems.

The GMA format of ordinary differential equations consists of a sum of all fluxes that are directly related to a dependent variable. Examples of a generic GMA system are given in Eq. 1.12.

$$
\begin{aligned}
&\frac{dX_i}{dt} = \sum_{s=1}^{a} \left(n_{s \to i} \times v_{s \to i} \right) - \sum_{p=1}^{b} \left(m_{i \to p} \times v_{i \to p} \right) \\
&v_{i \to j} = \gamma_{i \to j} \cdot E_{i \to j} \cdot X_i^{f_{i \to j}}
\end{aligned}
\tag{1.12}
$$

X_i represent the dependent variables, which are quantities that change due to the action of the model. $v_{s \to i}$ and $v_{i \to p}$ represent influxes and effluxes of the dependent variable, $\gamma_{i \to i}$ represent the rate constant of the flux and $E_{i \to i}$ the amount of enzyme that catalyze

the reaction represented by the flux. $n_{s\to i}$ and $m_{i\to p}$ are the stoichiometric coefficients for the influxes and effluxes. *a* denote the number of influxes and b the number of outfluxes of material for the X_i dependent variable. With GMA one sees directly what the contribution of each flux is, but in general, no analytical solution for the differential equations is available. We can go around this difficulty with numerical integrators and the enormous computational power available to us nowadays by calculating approximated solutions.

In S-systems, the input and output fluxes are condensed into a single input and a single output term. The result is

$$\frac{dX_i}{dt} = \alpha_i \prod_{j=1}^{n+m} X_j^{g_{ij}} - \beta_i \prod_{j=1}^{n+m} X_j^{h_{ij}} \tag{1.13}$$

α_i and β_i are constants, X_j are dependent and independent variables that influence variable X_i and g_{ij} and h_{ij} are kinetic orders. *n* and *m* are the number of dependent and independent variables respectively.

With this approach we no longer see the contribution of individual fluxes directly, although these fluxes can be reconstructed. In return, we can calculate an exact analytical solution for the system's steady state [9] as can be seen in Box 1.

Finally, in half-systems, all fluxes are assembled into one term.

$$\frac{dX_i}{dt} = \pm\delta_i \prod_{j=1}^{n+m} X_j^{k_{ij}} \tag{1.14}$$

δ_i is a constant, one for each dependent variable. X_j are dependent and independent variables that influence the equation variable and k_{ij} is a kinetic order. *n* and *m* are the number of dependent and independent variables respectively. This format is the simplest, but it is inconvenient for metabolic modelling as it does not permit non-trivial steady states where no variable is 0.

Box 1 – Calculation of the S-systems steady states.

We start with an S-system

$$\frac{dX_i}{dt}=\alpha_i \prod_j X_j^{g_{ij}} - \beta_i \prod_j X_j^{h_{ij}}$$

To calculate the steady states, we substitute the left side of the equations by zero.

$$0=\alpha_i \prod_j X_j^{g_{ij}} - \beta_i \prod_j X_j^{h_{ij}} \Leftrightarrow \alpha_i \prod_j X_j^{g_{ij}} = \beta_i \prod_j X_j^{h_{ij}}$$

Let's put logarithms on both sides of the equations to transform the multiplications into sums of logarithms.

$$\log\left(\alpha_i \prod_j X_j^{g_{ij}}\right) = \log\left(\beta_i \prod_j X_j^{h_{ij}}\right) \Leftrightarrow \log\left(\alpha_i\right) + \sum_{j=1} g_{ij} \times \log\left(X_j\right) = \log\left(\beta_i\right) + \sum_j h_{ij} \times \log\left(X_j\right)$$

Now let's isolate $log(X_j)$ to obtain an expression from the solution.

$$\sum_{j=1} g_{ij} \times \log\left(X_j\right) - \sum_j h_{ij} \times \log\left(X_j\right) = \log\left(\beta_i\right) - \log\left(\alpha_i\right) \Leftrightarrow \sum_{j=1} \left[\left(g_{ij} - h_{ij}\right) \times \log\left(X_j\right)\right] = \log\left(\frac{\beta_i}{\alpha_i}\right)$$

The sum on the *j* index has n dependent and m independent variables. So we can divide the sum in the following way.

$$\sum_{j=1}^{n} \left[\left(g_{ij} - h_{ij}\right) \times \log\left(X_j\right)\right] + \sum_{j=n+1}^{n+m} \left[\left(g_{ij} - h_{ij}\right) \times \log\left(X_j\right)\right] = \log\left(\frac{\beta_i}{\alpha_i}\right)$$

Usually, independent variables are known, so the second sum is known.

$$\sum_{j=1}^{n} \left[\left(g_{ij} - h_{ij}\right) \times \log\left(X_j\right)\right] = \log\left(\frac{\beta_i}{\alpha_i}\right) - \sum_{j=n+1}^{n+m} \left[\left(g_{ij} - h_{ij}\right) \times \log\left(X_j\right)\right]$$

Now, for convenience, let's write the equations in matrix form.

$\sum_{j=1}^{n} \left[\left(g_{ij} - h_{ij}\right) \times \log\left(X_j\right)\right]$ will be written as $A_D . \vec{y}_D$

$\sum_{j=n+1}^{n+m} \left[\left(g_{ij} - h_{ij}\right) \times \log\left(X_j\right)\right]$ will be written as $A_I . \vec{y}_I$

$\log\left(\frac{\beta_i}{\alpha_i}\right)$ will be written as $\vec{b}$

$$A_D . \vec{y}_D = \vec{b} + A_I . \vec{y}_I \Leftrightarrow \vec{y}_D = A_D^{-1} . \vec{b} + A_D^{-1} . A_I . \vec{y}_I$$

1.2.1. Parameter estimation

After the construction of the system equations, the next task is to populate the model's parameters with values. This is considered the bottleneck of model construction, as it is typically difficult and very time consuming. In biology and biochemistry, assigning values is not an easy task due to the great variability present in biological systems, for

example metabolites [14]. Even more unfortunate for modelers is that this difficulty drive biologists and biochemists to avoid reporting concrete values altogether [15].

There are multiple methods to perform parameter estimation. Unfortunately, there is no known methodology that produces consistently the best results for every case. The standard methods are divided into top-down and bottom-up approaches. Bottom-up methods consist of studying parts of the system using, for example, kinetic information from the literature or from wet lab experiments and assemble these parts into flux representations. Top-down approaches consist of algorithms like, for example, least square regression that will search the parameter space for values that best fit the model to available data. Both approaches have positive and negative features. Bottom-up approaches usually need extensive parameter tuning to fit properly the experimental data and top-down approaches are slow and sometimes produce parameter values with doubtful biological relevance. An intermediate approach is to start with a bottom-up approach and use a top-down strategy to fill the holes in the information or to fine-tune the model to an acceptable fit.

After the model is complete, the next task is to study the steady state values. Because there is no change in the values of the dependent variables when the system is at steady state, one can substitute the left side of the differential equations with zero and try to find solutions. Unfortunately, this is not always possible explicitly, but one can turn to numerical integrators, that will provide an approximate solution.

1.2.2. Steady state stability

System steady states are stable if after slightly perturbed the system returns to the previous steady state; or unstable if after a small perturbation the system goes to a different steady state or enters in a different dynamic regime like, for example, oscillations.

A convenient way to study steady state stability is to calculate the eigenvalues of the Jacobian matrix of the system. These eigenvalues are often complex numbers. If the real parts of all eigenvalues are negative, the system has a stable steady state. If the imaginary part is different from zero, the system can exhibit oscillations.

To understand the intuition behind this, let’s start with a very simple equation.

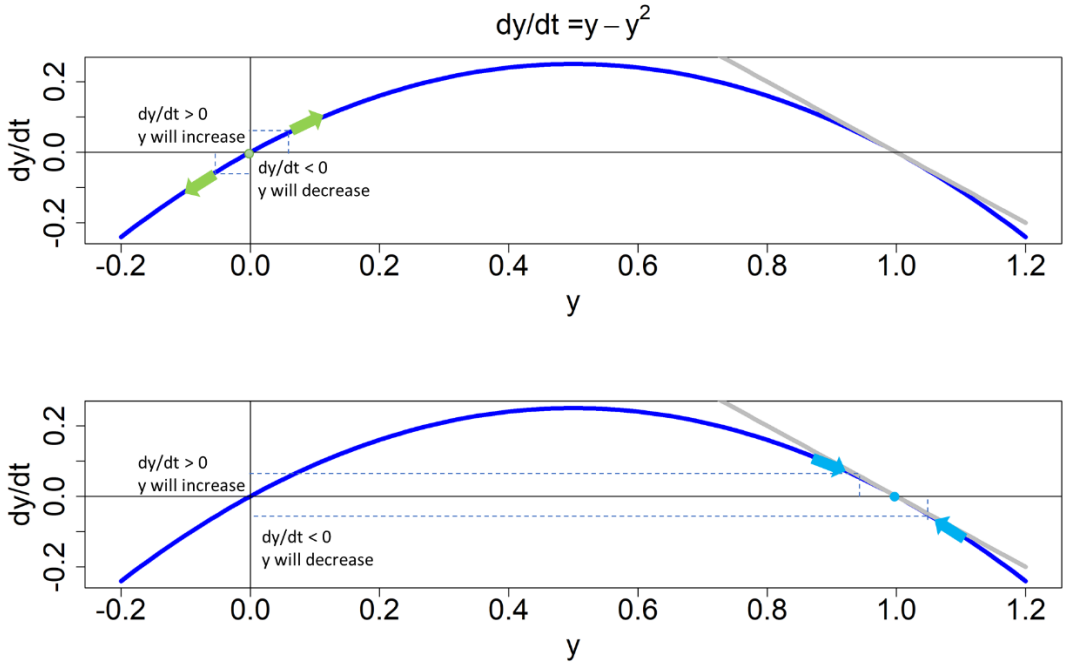

Figure 1.4. Analysis of the stability of the two steady states in dy/dt = y – y^2.

(top) 0 is an unstable steady state and the function will slip away from it if perturbed. (bottom) 1 is a stable steady state and will return to it if slightly perturbed.

As can be seen in Figure 1.4, this equation has two steady states: 0 and 1. The equivalent of a Jacobian for this function is its derivative with respect to y: 1 – 2y. For the steady state at 0, we obtain df/dy(0) = 1, so 0 is a unstable steady state. For y = 1, df/dy(1) = -1, so 1 is a stable steady state. The fundamental concept here is that the function dy/dt = f(y) gives the rate of change of y. So, if dy/dt is positive, y will increase and a negative dy/dt will signal a decrease in y. Note that in one dimension the use of the derivative was unnecessary because the sign of the function would suffice.

In multidimensional systems, the intuition is analogous, with eigenvalues of the Jacobian matrix taking the place of the derivative. Positive eigenvalues indicate that there are directions that the function uses to distance itself from a steady state. All negative eigenvalues signal that, near a stable steady state, in every direction, the function will converge back to the former stable steady state.

1.2.3. Sensitivity analysis

In a model that is representing a system we can distinguish three types of quantities: dependent variables, independent variables and parameters. Dependent variables have their value determined by the model. This does not happen to independent variables and parameters. The distinction between these last two is subtle. Independent variables describe elements of the environment or within the system that influence the system but are not altered by the system. Parameters describe characteristics intrinsic to the system that do not change during a computational experiment or that are in a time scale so different from the object of study that their change will be too slow to be relevant [7]. To provide an example, consider a phosphorylation reaction catalyzed by an enzyme. The quantity of product and substrate are dependent variables, the quantity of enzyme is an independent variable and the rate constant and kinetic order of the reaction are parameters.

In a sensitive analysis one will perturb the independent variables or parameters to measure their influence on the dependent variables, typically at the steady state. Each independent variable and parameter value will be increased by a small amount (usually 1%) and the new steady states of the dependent variables will be recorded [8]. Next, these values are compared to the old steady states to access the magnitude and sign of the change. Of special interest are alterations in the dependent variables that are higher than 1% of the unperturbed steady state. We call these sensitivities high sensitivities, while the ones with absolute value lower than 1% are low sensitivities. In mathematical terms, sensitivities are the partial derivatives of the dependent variable at steady state with respect to one of the parameters. Note that an ODE system is composed of the derivatives of the dependent variable functions with respect to time, so these cannot be directly used to study sensitivities. However, sensitivities are easily computed at the steady state. Good models have mainly low sensitivities because this will make the model resistant to normal perturbations. But there are exceptions, like signaling systems where high sensitivities relate to signal amplification [8].

Other techniques for assessing sensitivity exist if the use of a steady state is not convenient. In this approach we can use a time course of the model and alter the parameters one by one, recording the originated time courses. The sensitivity is

accessed by calculating the sum of the absolute differences of the original time course to the ones originated by the perturbations in the parameters.

Sensitivity analysis has two types of results: sensitivities and logarithmic gains. They are essentially the same, calculated in the same fashion and interpreted in the same way. The difference between the two is that logarithmic gains are attained from independent variables and sensitivities from parameters [16].

The results of the sensitivity analysis are conditional on the parameter set that provides realistic steady-state values and replicates observed phenomena. However, multiple small or intermediate errors in parameter values could collectively have a larger impact on performance of the system. To address this question, combined sensitivities can be studied using a Monte-Carlo approach. We can assign uncertainty to every parameter and create new parameter sets and use these to study local sensitivity. This allows us to investigate whether the distributions of sensitivities might suggest a different behavior associated with a parameter change than the one suggested by the local sensitivities. Generally, if the sensitivity of a parameter exhibits great variability, it might suggest a lack of system robustness [17].

1.2.4. Identifiability analysis

If a model is only slightly perturbed even in response to large changes in a parameter value, how can we know what is the parameter value that best replicates observed data? This question becomes more complicated if the sensitivities of two or more parameters are correlated and the increase in one can be compensated with an alteration in one or multiple parameters. The issue is related to the existence of infinite parameter combinations that produce essentially the same model output. This redundancy is especially important if we want to suggest an experimental design to populate the model with parameters values. These issues are related to the problem of parameter identifiability, which is defined as the ability to identify the true value of a model parameter [18].

There are two types of identifiability. Global or structural identifiability asks if parameters are identifiable at all. For example, if two parameters are correlated for any data, changing one will compensate the other alteration. In this way, we will never know the two parameters' true values using the model's behavior. Local or practical

identifiability concerns conditions that can make parameters identifiable. Parameters are locally non-identifiable if this can be reverted by, for example, adding more data or adding data of a different nature.

The method described by Srinath and Gunawan [18] and Yao *et al.* [19] can be used to find the best identifiable parameters, which is based on the local sensitivity matrix. For each column of the matrix, the Euclidian norm is calculated and the column with the highest magnitude is selected. If the magnitude exceeds a certain threshold, the parameter corresponding to this column is identifiable. This column is removed from the local sensitivity matrix. The projection of the removed column on the remaining columns is computed and subtracted from them. This procedure creates a new local sensitivity matrix. The process is repeated until the highest magnitude is below the threshold. All remaining parameters are considered non-identifiable.

1.3. Cystic Fibrosis

Cystic Fibrosis (CF) is a monogenic autosomal recessive disorder. It is called monogenic because it is a disorder caused by a single defective gene. It is autosomal because the gene is in an autosome, a chromosome that is not a sex chromosome. It is recessive because the condition only expresses itself if an individual has two copies of the abnormal gene [20].

This diseased was first described in 1938, but only in 1989 the gene causing CF was identified [21]–[23]. CF patients present mutations in two alleles of the Cystic Fibrosis Transmembrane Conductance Regulator (*CFTR*) gene, that encode a chloride (Cl^-) channel. The gene that encodes CFTR resides on the long arm of chromosome 7 at q31.2, consists of 27 exons and 26 introns, is approximately 190 kb in size and encodes a protein of 1,480 amino acids. As of March of 2018, 2026 mutations were identified in the *CFTR* gene [24] and 312 CFTR mutations have been confirmed as CF-causing in the CFTR2 database [25] and they are usually classified as shown in Figure 1.5. Of the different mutations, F508Del, the deletion of a phenylalanine in the position 508, accounts for 70% of CF chromosomes and 50% of CF patients in the United States are homozygous for this mutation [26].

CFTR is expressed in many epithelial cells, including sweat duct, airway, pancreatic duct, intestine, biliary tree, and vas deferens [26]. It only transports the chloride ion

down the electrochemical gradient: in the sweat gland CFTR absorbs chloride into the epithelial cell, in the gut CFTR secretes chloride from the epithelial cell and in the lung CFTR can do both, secretion or absorption, depending on the direction of the gradient [27].

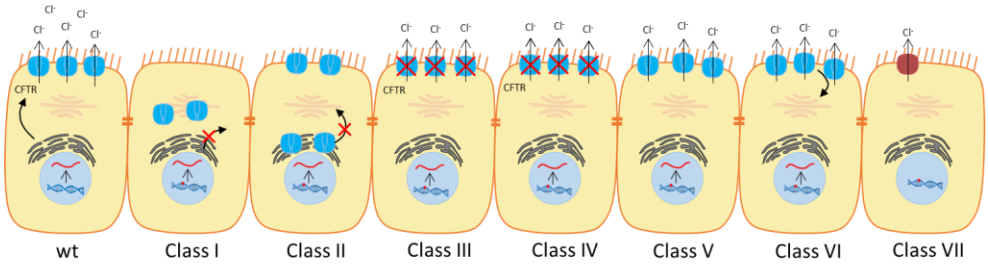

CFTR defect	–	No protein	No traffic	Impaired gating	Decreased conductance	Less protein	Less stable	No mRNA
Mutations examples	–	GLy542X, Trp1282X	F508del N1303K	G551D G551S	R117H R334W	A455E, 3849+10 kbC→T	N287Y 4326delTC	dele2,3(21 kb), 1717-1G→A
Frequency (% of patients)	–	10%	>70%	4%	3%	3%		
CFTR protein								
Membrane location	Good	No	Very low	Present	Present	Reduced	Reduced	No
Function	Good	No	Poor	Poor	Partly	Good	Good	No
Corrective therapy	–	Rescue synthesis	Rescue traffic	Restore channel activity	Restore channel activity	Correct splicing	Promote stability	Unrescuable
Drug	–	Read-through compounds	Correctors VX-809 VX-661	Potentiators VX-770 Genistein	Potentiators VX-770 Genistein	RNA based strategies AONs	Stabilizers Cavosonstat	Bypass therapies

Figure 1.5. Classes for CF mutations.

(Used with permission from the author, Sofia Ramalho, and complemented with information from Fajac and Wainwright [28])

There is a great variability in the phenotypes of CF patients [26], [27]. Still, at birth, the most common symptoms are elevated sweat chloride concentration and more than 85% CF patients have pancreatic insufficiency that will cause impaired development due to malnutrition [26]. Initially, pancreatic insufficiency was thought to be the major complication of CF, causing lung problems through severe malnutrition, but that point of view changed.

While the lungs are unaffected at birth, inflammation and infections by bacteria will appear shortly after. This is caused, it is thought, by an accumulation of thick, dehydrated mucus. This is a consequence of ion transport deregulation, namely, reduced chloride secretion and increased sodium absorption. Continued inflammation

and infections by bacteria like *Pseudomonas aeruginosa* will elicit a persistent neutrophilic inflammatory response. The continuous infection and inflammation will ultimately destroy the lungs and this is the major cause of morbidity and mortality for individuals with CF [26].

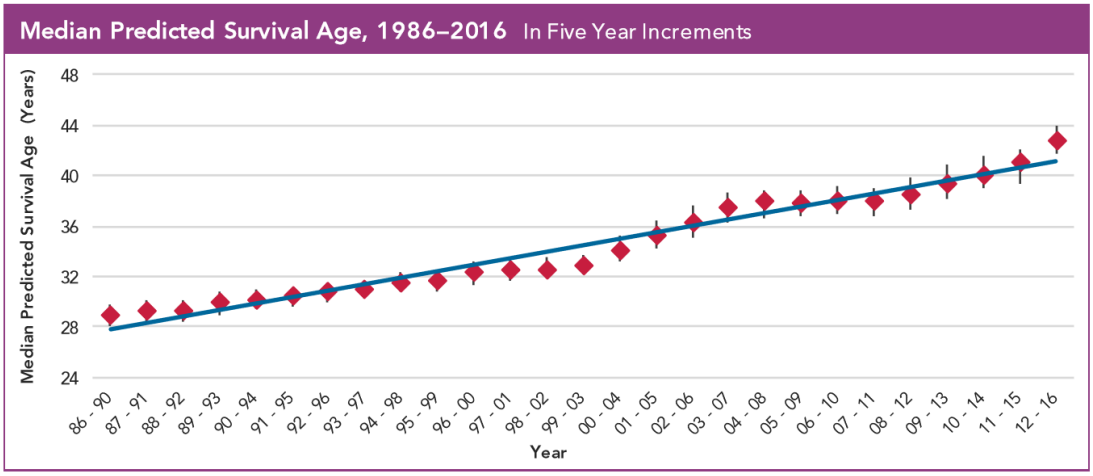

**Using the currently recommended method for calculating median predicted survival.*

Figure 1.6. Life expectancy evolution of CF patients.

(Reproduced and adapted with permission of the Cystic Fibrosis foundation [29])

Initially, health care providers focused on treating CF symptoms but recently the focus shifted to correcting the mutated CFTR. This led to the development of compounds like the corrector lumacaftor (VX-809) that corrects the protein folding, increasing the number of CFTR protein molecules that are trafficked to the cell surface. Also, the potentiator ivacaftor (VX-770) improves the open probability of the channel. At the beginning, these compounds were only effective for a small percentage of cases and types of mutations, but new advances were made and they are now approved for use in the most common mutations [30] and commercialized with the name Orkambi. Still, there are mutations which cannot be treated with these compounds.

A better understanding of the disease and improvements in the therapeutics have led to a dramatic improvement of the life expectancy of CF patients [29], [31], as can be seen in Figure 1.6. As a consequence, soon, the majority of the CF patients will be adult [32] and this is already a fact in the US [29].

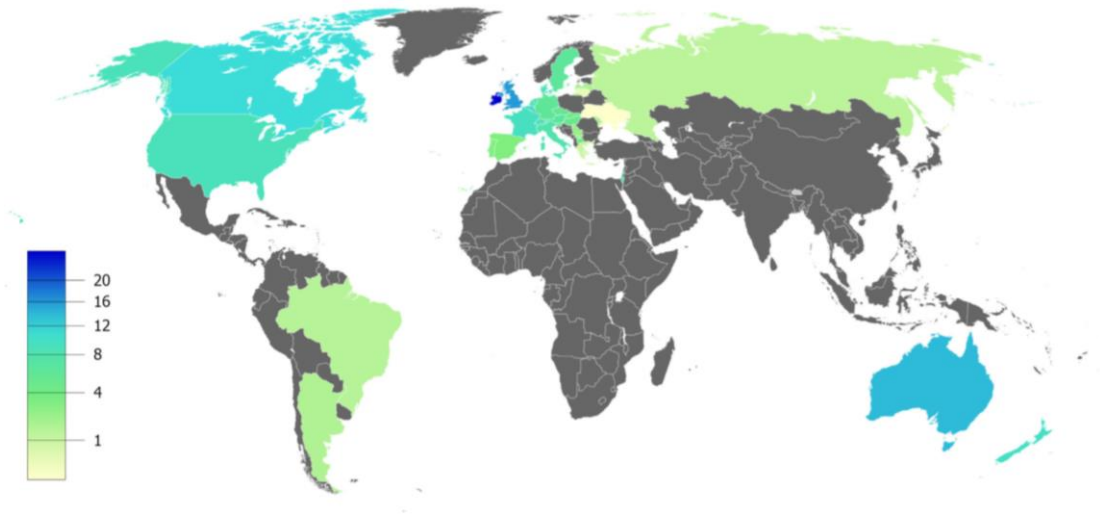

Figure 1.7. Estimated prevalence of cystic fibrosis per 100,000 habitants.

Data compiled from the latest registry reports of Europe (European Cystic Fibrosis Society [ECFS], 2016), United States (Cystic Fibrosis Foundation [CFF], 2015), Canada (Cystic Fibrosis Canada [CFC], 2016), Australia (Cystic Fibrosis Federation Australia [CFFA], 2016) and Brazil (Brazilian Cystic Fibrosis Study Group [GBEFC], 2016). Grey represents no available data. [33]

In a 2004 study on the prevalence of cystic fibrosis in the European Union by Philip M. Farrell [34], 27 European Union countries had 35806 CF patients for a total population of 486,114,000, resulting in a mean prevalence of 7.37 per 100,000, similar to the United States. In the same study, Portugal had a total population of 10,524,000 and 285 CF patients which corresponds to a prevalence of 2.71 per 100000. It is interesting to note that in the European Lung White Book Respiratory Health and Disease in Europe, 2nd Ed [31] a decrease of CF incidence was reported for countries where new-born screening for CF has been introduced and they attribute this to the couples alternative reproductive choices after the birth of a first CF child. A map in Figure 1.7 shows an estimate of CF prevalence in several countries.

It is not clear why CF became the most common autosomal disease in Caucasians. A popular belief among researchers is that mutations in CFTR may confer a degree of protection against some diseases like cholera and other secretory diarrhoeas and typhoid fever. Poolman *et al.* [35] advanced the hypothesis that tuberculosis is the main force behind the selection of CF genes in Caucasian populations. They provide

molecular, clinical and temporal-geographical distribution evidence supporting this hypothesis. The main argument is that only tuberculosis had enough selective pressure over the human population to generate the observed frequencies of CF. The casualties and time of effect of other candidates like cholera or typhoid fever were not enough to cause a selection on a protected population.

1.4. ENaC regulation

The epithelial sodium channel is a membrane bound heterotrimeric protein, i.e., it is formed by three out of four possible heterologous subunits: α, δ, β, or γ. Usually, one ENaC channel is composed with a α, β and γ. EnaC is ubiquitinated by NEDD4-2, an E3 ubiquitin ligase [36].

In the lungs, there is paracellular permeability for water and ions. ENaC Na transport generates a transepithelial potential difference that is the driving force of ion transport [37]. In this tissue, CFTR secretes chloride and bicarbonate. In CF, CFTR function is deficient and the transport of sodium through ENaC is thought to be up-regulated. This will cause a decrease of ions and water in the extracellular space by the lack of chloride secretion and hyperabsorption of sodium. This is one of the causes of the accumulation of mucus in the lungs that characterizes CF [38] and it is believed to make the lungs of CF patients very susceptible to infections of which *Pseudomonas aeruginosa* remains the most strongly associated with clinical disease severity, frequency of hospitalization and decreased survival [32]. But this is not generally accepted. Other researchers, presenting trans-epithelial conductance data in pigs, argue that ENaC function is normal in CF [39]. In mice, CFTR mutations do not cause CF like symptoms in lungs, but inhibition of NEDD4-2 [40] or overexpression of β-ENaC subunit [41] will cause lung-CF like symptoms.

Chemical inhibitors of ENaC, such as amiloride, denzanil or PS552, which are typically used with other therapeutic substances, yield disappointing results because their effect is sustained for a short period of time or dysregulate ENaC in other organs, as for example in the kidneys [38].

In the sweat grands, on the other hand, the tighter epithelia with less water permeability compels both CFTR and ENaC to absorb ions in a coordinated fashion [37]. This means that ENaC activity is directly proportional to CFTR activity. Consequently, ENaC

function is downregulated in CF sweat glands, because there is no CFTR activity [42]. This will lead to the salt rich sweet that characterizes CF.

The mechanism of ENaC and CFTR interactions is still unknown [43] [38] [44].

Initially, it has believed that CFTR regulated ENaC through PKA and cAMP [45] but this was disproved [42].

Berdiev *et al.* [44] present strong arguments in favor of a protein interaction between ENaC and CFTR. A protein that could be important for the interaction between ENaC and CFTR is COMMD1. This protein binds to CFTR and protects it from ubiquitination [46], while it has the opposite effect on ENaC [47]. A lack of CFTR could remove COMMD1 from the plasma membrane and produce the observed ENaC activity increase.

Farinha and Matos [48] have shown evidence that RAB GTPases control the transport of both CFTR and ENaC and also play a role in the recycling/degradation of these channels.

Tarran and colleagues [49], [50] explain the relation between CFTR and ENaC in the following way. These authors believe that the protein SPLUNC1 (short palate, lung, and nasal epithelial clone) regulates the number of ENaCs and consequently the air surface liquid (ASL) height. When ASL is high, SPLUNC1 will be diluted and not interact with ENaC. This will increase ENaC numbers in the cell membrane, which in turn will increase the absorption of sodium and water and decrease the ASL height. When the ASL is low, SPLUNC1 will associate with the sodium channel and promote its disassembly, ubiquitination and internalization of the α and γ subunits [50]. This will reduce the numbers of ENaC, reduce the absorption of sodium and water and increase the ASL height.

This conceptual model can also explain the interaction between CFTR and ENaC. SPLUNC1 is inactivated by low pH levels. This chloride channel also secretes bicarbonate, increasing the extracellular pH. In CF, without CFTR, the more acidic extracellular environment will inactivate SPLUNC1 and cause the observed ENaC up-regulation through the increase of channel numbers in the plasma membrane. Tarran and colleagues developed and are currently testing a compound that has the ENaC

activity of SPLUNC1 and is insensitive to pH. The results are very promising so far [51].

It is known that ENaC is influenced by phosphoinositides [52]–[54]. Negatively charged phosphoinositides like $PI(4,5)P_2$ and $PI(3,4,5)P_3$ interact with positively charged lysine residues (K+) at the N terminus of β- and γ-ENaC [54] which are important for channel activation. This interaction will cause a change in the conformation of ENaC, releasing the extracellular loops and enabling them to be cleaved by proteases [55]. This cleavage will increase the open probability of ENaC.

The search for compounds that normalize ENaC activity led Almaça *et al.* [38] to perform a silencing RNA screen with a live cell automatic microscopy assay, which enabled the functional assessment of ENaC activity in human respiratory epithelial cells. They found that the phosphoinositide pathway was the most enriched among the silenced mRNAs that significantly changed ENaC activity and identified diacylglycerol kinase (DGK) has a promising therapeutic target.

DGK catalyzes the transformation of diacylglycerol (DAG) into phosphatidic acid (PA). PA is the precursor for the formation of all phosphoinositides lipids, including $PI(4,5)P_2$. Almaça *et al.* propose that DGK inhibition stops the transformation of DAG into PA, and consequently stops the production of $PI(4,5)P_2$. This leads to the depletion of the $PI(4,5)P_2$ pool and to the decrease of ENaC open probability [38]. The problem with this hypothesis is that the transformation from PA into inositol lipids occurs in the ER, not in the plasma membrane. It seems improbable that a change in PA in the plasma membrane will affect a process in the ER that subsequently will almost immediately influence the levels of $PI(4,5)P_2$ or $PI(3,4,5)P_3$ in the plasma membrane. Also, the PA pool is much smaller than the PI pool. The study of mechanisms of how DGK affects the phosphoinositide pathway is the main focus of this PhD project.

PA can also activate PIP5KI, the enzyme that transforms PI(4)P into $PI(4,5)P_2$ [56]–[59]. This alternative mechanism is more plausible than Almaça's *et al.* hypothesis for two reasons: PA activation of PIP5KI is a process that occurs only in the plasma membrane and this hypothesis is much simpler, *i.e.*, involves fewer components, transports and cell compartments than the alternative.

1.5. Phosphoinositide pathway

Phosphoinositides are rare lipids present in the cell membranes representing about 1% of total cellular phospholipids, and with phosphatidylinositol, the unphosphorylated species, representing about 10% [60]. The percentages of major lipid groups in a mammalian cell can be seen in Table 1.1.

All phospholipids are directly or indirectly derived from PA [61], [62]. The *de novo* synthesis of this lipid occurs in the ER. PA can be transformed by phosphatidic acid phosphatase-1 (PAP-1) into DAG, that will supply the Kennedy pathway to become PC, PE and PS. Alternatively, PA can be transformed into CDP-DAG that will be the base for phosphatidylinositol (PI) and the phosphoinositides, the inositol lipids [62].

Table 1.1. Percentages of major lipid groups in a mammalian cell.
Adapted from [62].

	Percentage of total lipids
Phosphatidylcholine (PC)	45–55
Phosphatidylethanolamine (PE)	15–25
Phosphatidylinositol (PI)	10–15
Phosphatidylserine (PS)	5–10
Phosphatidic acid (PA)	1–2
Sphingomyelin (SM)	5–10
Cardiolipin (CL)	2–5
Phosphatidylglycerol (DAG)	<1
Glycosphingolipids	2–5
Cholesterol	10–20

The phospholipids can be transported to the different cell compartments by lipid transport proteins (LPT's), membrane contact sites and vesicles [62], [63] and there is evidence that vesicle transport of lipids is not as relevant as the others [62].

Phosphoinositides are phospholipids that are formed by a glycerol backbone that has three carbons, which are usually called positions SN1, SN2 and SN3, as can be seen in Table 1.2. Two fatty acids are attached to positions SN1 and SN2; stearic acid (18:0) being the most common in the SN1 position and arachidonic acid (20:4) at SN2 [64]. At position SN3, an inositol group is attached by a phosphodiester bond, forming the polar head that gives these lipids a negative charge.

The inositol ring of phosphatidylinositol can be phosphorylated in the third, fourth and sixth carbons, and these phosphorylations give rise to the different subspecies of phosphoinositides: PI(3)P, PI(4)P, PI(5)P, PI(3,4)P_2, PI(3,5)P_2, PI(4,5)P_2 and finally PI(3,4,5)P_3. The information on inositol lipids is presented in Tables 1.4 to 1.11 located at the end of the present subsection.

Inositol lipids represent 10% to 15% of all cellular phospholipids, but they are not as structurally important as, for example, PC, which represents around 50% of all phospholipids in eukaryotic cell membranes [62]. Phosphoinositides have many functions and influence almost every cell process. They function as identifiers to the different cell membranes, as second messengers, precursors to other signaling molecules, as membrane protein docking sites and regulators, shape the cell membrane, control vesicular trafficking, and organelle physiology, as well as a variety of other tasks [63].

We now have an idea of the total amount of inositol lipids in mammalian cells, but there is some variation in the number presented by the different authors, as can be seen in Table 2.1. Alexis Traynor-Kaplan and colleagues [65] found differences in the amount of inositol lipids in different types of cells.

Unfortunately, the exact amount of inositol lipids in each cellular organelle is still unknown. In this work, when necessary, we follow the principle observed in phospholipids by Vance [62], that "…,in general, the differences in lipid composition are quantitative rather than qualitative."

Table 1.2. Structure, percentage and cellular localization of phosphoinositides.

Adapted from [66]. Structural representations created with the online drawing tool of the Lipid maps site.

Name	PI3P	PI4P	PI5P	PI34P2	PI35P2	PI45P2	PI345P3
Structure	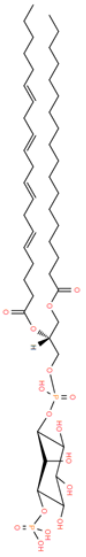	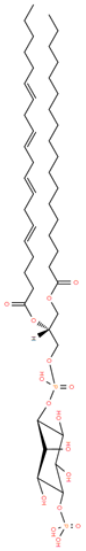	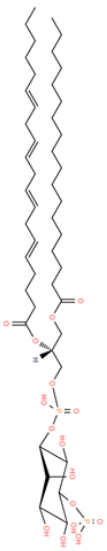	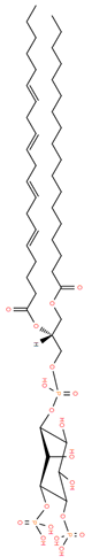	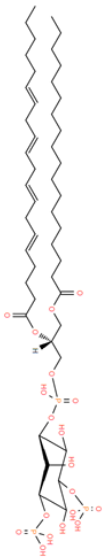	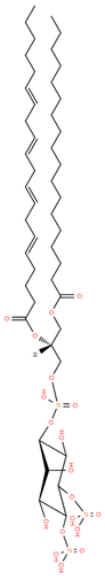	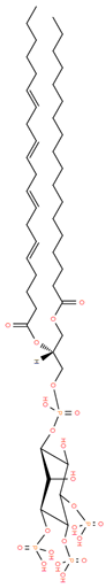
% of Pis (Viaud et al. 2017)	.05% - 1.5%	10%	.1% - .5%	.1% - 1%	.1% - 1%	10%	.1% - 1%
Cellular localization (Viaud et al. 2017)	Endosomes	Golgi apparatus Plasma membrane*	Plasma membrane Golgi apparatus Nucleus	Endosomes Plasma membrane	Endosomes Lysosomes	Plasma membrane	Plasma membrane

(http://www.lipidmaps.org/tools/structuredrawing/StrDraw.pl?Mode=SetupGPStrDraw).

*Not present in the original Table by Viaud, but the presence of PI(4)P in the plasma membrane is supported by Balla [63], De Creane *et al.* [67] and, strangely enough, by Viaud et al. [66], in the same paper where the Table originated.

Also, one can still subdivide the subspecies of phosphoinositides relative to their acyl chain composition. Despite much more work being needed for identifying the different

acyl chains in the different subspecies of phosphoinositides, some progress was made by Alexis Traynor-Kaplan and colleagues [65].

In higher plants, the PI : PIP : $PI(4,5)P_2$-ratio is 100:1.7:1.3 according to radio labeling. $PI(4,5)P_2$ levels are about 10 times lower than in animals or lower plants, PI(4)P makes up 80% of monophosphorylated phosphoinositides and PI(5)P amounts to 3% to 18%, which is far more than the 2% in animals. No $PI(3,4,5)P_3$ exists but PTEN, the $PI(3,4,5)P_3$ phosphatase, does. In *Arabidopsis*, $PI(3,4)P_2$ was never recorded [77]

Concerning the cellular location of phosphoinositides, some information is available concerning the major inositol lipids present in the different organelles. Unfortunately, there are still many unanswered questions that are fundamental to a complete understanding of the phosphoinositide distribution in the cell. For example, we know that the total cellular amounts of PI(4)P and $PI(4,5)P_2$ are similar but we are not certain that this also happens in the plasma membrane. We know that PI is much more abundant than PI(4)P or $PI(4,5)P_2$, that it is very common in the ER and that this organelle has a membrane much larger that the plasma membrane. Considering these facts, I wonder if the ratios between PI, PI(4)P and $PI(4,5)P_2$ in the plasma membrane are similar to the ratio for the total cell.

The different subspecies of phosphoinositides interconvert into each other. These interconversions are represented in Figures 2.1; the enzymes that are responsible for these interconversions were extensively reviewed in a paper by Sazaki and colleagues [78]. The modelling of this reaction network is the subject of Chapter 2 of this thesis.

$PI(4,5)P_2$ is a substrate for PLC (Phospholipase C) that cleaves the phosphoinositide into IP_3 and DAG. DAG is then converted into PA that can be transported to the ER. PA is also created *de novo* in the ER. In the ER, PA can supply the Kennedy pathway or be transformed into PI that can subsequently be transported to the plasma membrane and be phosphorylated into $PI(4,5)P_2$. This is commonly known as the phosphoinositide cycle that suggests a close system view of the phosphoinositides in a cell. An attempt to model this view of the phosphoinositides was proposed by Suratekar *et al*. [79]. A representation of the phosphoinositide cycle is presented in Figure 1.8.

This view is very dependent on lipid transport proteins (LPTs). Our knowledge about these proteins has seen great developments in the last years. Still, we are far from completely identifying and understanding LPTs.

PTEN has been known to be a tumor suppressor for almost twenty years [63]. This phosphatase hydrolyses the third position of the inositol ring in $PI(3,4,5)P_3$ and to a lesser degree $PI(3,4)P_2$ [63], [78], [80]. As a phosphatase, it blocks the AKT/$PI(3,4,5)P_3$ pathway. As a nuclear protein, it activates proteins responsible for DNA repair and chromosome stability [72], [81].

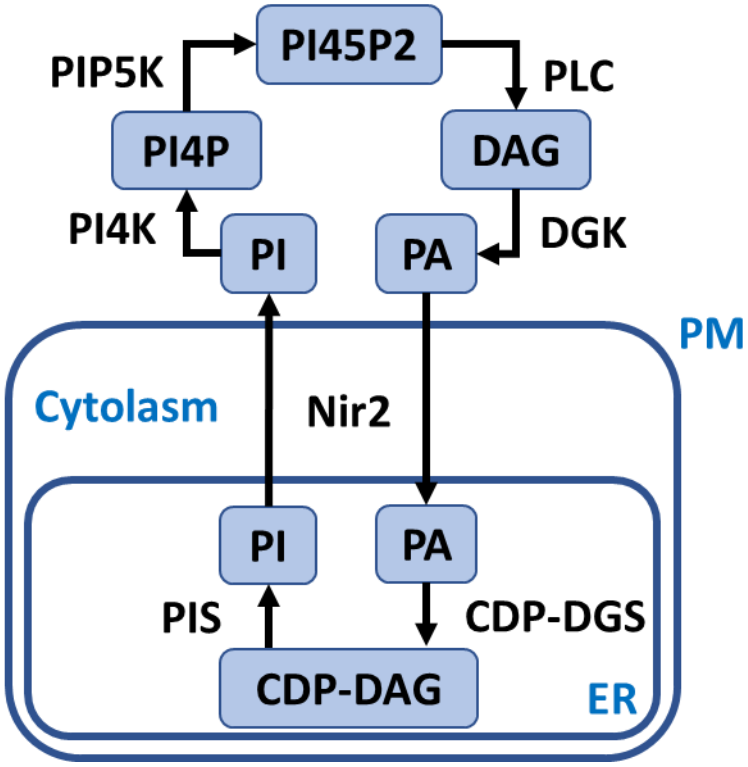

Figure 1.8. Representation of the phosphoinositide cycle.

In this simplified representation of the cycle, is shown the transformations that occur in the ER and in the plasma membrane. Nir2 is an LTP that transports PI and PA between the ER and the plasma membrane.

PI3KI phosphorylates the third position of the inositol ring in $PI(4,5)P_2$ into $PI(3,4,5)P_3$, the inverse reaction of PTEN. The product of PI3KI will activate AKT, also known as protein kinase B that controls cell energetic and metabolism functions, start a series of

processes preceding cell division and proliferation and plays a key role in cancer development [63], [81].

Bryant, and others [80], [82], reported that $PI(4,5)P_2$ marks the apical membrane and $PI(3,4,5)P_3$ the basolateral side of epithelial cells. From the literature it is clear that the distribution of $PI(3,4,5)P_3$ exists in the basolateral side, while it is very rare, if not absent in the apical part. Things are less clear concerning the distribution of $PI(4,5)P_2$. In many images we see the apical site marked with $PI(4,5)P_2$ [80] and read sentences like " PIP_2 is apically localized …" [83] or "*PIP2* localizes to *apical* membranes" [84]. These statements cause the spread of the idea that, in a polarized cell, $PI(4,5)P_2$ is increased in the apical part of the plasma membrane and $PI(3,4,5)P_3$ is the dominant phosphoinositide in the basolateral part.

The pool of $PI(3,4,5)P_3$ is sixteen times smaller than the $PI(4,5)P_2$ pool, simply too small for its consumption to cause a noticeable increase in $PI(4,5)P_2$. Also, our model presented in Chapter 2 predicts, at best, an increase in $PI(4,5)P_2$ of only 5% when we pass from a basal to apical configuration of the membrane. This increase is too small to be detected with the usual florescence microscopy technics.

To increase the confusion, there are data that support both hypotheses, the more recent and more plausible of which points to the uniform distribution of $PI(4,5)P_2$ along the plasma membrane [75].

My belief is that $PI(4,5)P_2$ levels are similar in both parts of the membrane. What makes the apical and basolateral sides of the membrane different concerning the lipid content is $PI(3,4,5)P_3$, which is present in the basolateral part and absent in the apical part. PTEN and PI3KI are responsible for this difference. PTEN, by being present in the apical part and at the tight junctions, PI3KI is located in the basolateral part of the membrane.

There is a fair amount of regulation involving PTEN, PI3KI, $PI(4,5)P_2$ and $PI(3,4,5)P_3$ [72], [82], [85]. Both these enzymes are activated by their products causing two parallel and opposite positive feedback loops. Also, $PI(3,4,5)P_3$ accumulation promotes the release of PTEN from the plasma membrane [85].

Table 1.3. Features of PI

PI (phosphoinositol)
Cellular location Ubiquitous phospholipid in eukaryotic cells. Greater concentrations in the plasma membrane and in the ER. [67]
Quantities 80% - 90% of inositol lipids in human cells. [63][63] [68] [69] [66] 10% of phospholipids in human cells. [60]
Generation PA is transformed into CDP-DAG that together with inositol forms PI. PI synthesis occurs in the cytoplasmic face of the ER membrane, the Golgi, mitochondria and microsomes. [86] The enzyme catalyzing this reaction is PtdIns synthase. PI is also created by hydrolysis of PI(3)P, PI(4)P and PI(5)P. The enzymes that catalyze these reactions are myotubularins (MTM1), myotubularins related phosphatases (MTM1-4, MTM6, MTM7) and suppressor of actin 1 (SAC1). [78]
Degradation / Consumption PI is transformed into PI(3)P by PI3KIII, PI(4)P by PI4K and PI(5)P by PIKfyve. [78]
Functions Marker of the ER membrane. Precursor to the phosphoinositide's.
Open questions What is percentage of PI in the ER and in the plasma membrane. What is the rate of *de novo* synthesis of PI in the ER?

Table 1.4. Features of PI(3)P

PI(3)P (Phosphatidylinositol 3-Phosphate)

Cellular location
Enriched in membranes of early endosomes [87] and multivehicular bodies.

Quantities
0.05 to 1.5% of phosphoinositide's in human cells. [66]
Less than 15% of monophosphorylated phosphoinositides. [60]

Generation
PI3P is created from PI mainly by PI3KIII. It is also created by hydrolysis of $PI(3,5)P_2$ by FIG4 and $PI(3,4)P_2$ by INPP4. [78]

Degradation / Consumption
PI(3)P is hydrolyzed to PI by SAC1, MTM1-4,6-8 and SYNJs.
PI(3)P is phosphorylated in the 5^{th} position into $PI(3,5)P_2$ by PIKfyve. [78]

Functions
Involved in the endosomal sorting of proteins, sorting of endosomes to the membrane, the lysosome and returning to the Golgi and the formation of the MVB. [88]

Open questions
What is the amount of PI(3)P in the plasma membrane?

Table 1.5. Features of PI(4)P

PI(4)P (Phosphatidylinositol 4-Phosphate)

Cellular location
Golgi membrane and plasma membrane. [89] [90]
Secretory vesicles [91]. Late endosomes and lysosome [87].

Quantities
10% of phosphoinositides. [66]
45% of monophosphorylated phosphoinositides in human cells. [60]

Generation
PI(4)P is created from PI by PI4K's.
PI(4)P is created by hydrolysis of $PI(4,5)P_2$ by INPP5, ORCL and also SAC2, SYNJ1/2 and SKIP. Is also created from $PI(3,4)P_2$ by PTEN. [78]

Degradation / Consumption
PI(4)P is phosphorylated in the 5^{th} position by PIP5KI's. It is also phosphorylated in the 3^{rd} position by PI3KII.
PI(4)P is hydrolyzed to PI by SYNJ1/2 and SAC1. [78]

Functions
Marks the Golgi membrane.
Is a precursor for $PI(4,5)P_2$.
OSBP locates to the Golgi though interaction with PI(4)P and ARF. It exchanges PI(4)P in the Golgi for sterols in the ER. This ER PI(4)P is rapidly transformed to PI by SACs phosphatases. [92]
ORP5 and ORP8 localize to ER contact sites with the plasma membrane or the mitochondria. They exchange PS from the ER by PI(4)P from the plasma membrane and mitochondria. [93]

Open questions
What is the ratio between the amount of PI(4)P in the Golgi and the plasma membrane?
What is the amount of PI(4)P that is transported by LTP's and vesicles from the Golgi to the ER and from the Golgi to the plasma membrane?
Is the PI(4)P consumed or degraded during the vesicle migration?
How much SAC phosphatases are in the ER? What makes them so effective in degrading PI(4)P?

Table 1.6. Features of PI(5)P

PI(5)P (Phosphatidylinositol 5-Phosphate)

Cellular location
PI(5)P is present in the plasma membrane, endosome and nucleus in small amounts. [67]

Quantities
Similar to PI(3)P. [63]
0.1 - 0.5% of phosphoinositides. [66]
Less than 10% of monophosphorylated phosphoinositides. [60]

Generation
PI(5)P can be generated from PI by PIKfyve.
PIKfyve will also produce $PI(3,5)P_2$ out of PI(3)P. $PI(3,5)P_2$ will then be hydrolyzed at the 3rd position by myotubularins. This will generate the bulk of PI(5)P.
PI(5)P is also produced by the hydrolysis of $PI(4,5)P_2$ in the 4th position into by SYNJ1/2 and TMEM55. [78]

Degradation / Consumption
PI(5)P can be phosphorylated in the 4th position by PIP5KII (also known as PIP4KII).
PI(5)P can be hydrolyzed to PI by SYNJ1/2 and SAC1. [78]

Functions
Some scholars believe that PI(5)P is just a byproduct of errors that occur in the process of phosphorylating and hydrolysis of phosphoinositides. [94][74]
Modulating the transcriptional activity of chromatin regulator ING2 in the nucleus.
In the plasma membrane, PI(5)P is involved in actin remodeling by the activation of RAC1, thus influencing cell migration [95].
Endosomal protein sorting through interaction with TOM1. [96]

Open questions
The role of PI(5)P in human cells is still poorly understood.

Table 1.7. Features of $PI(3,4)P_2$

$PI(3,4)P_2$ (Phosphatidylinositol 3,4-bisphosphate)

Cellular location
Mainly in the plasma membrane. [60]

Quantities
0.1 – 1% of phosphoinositides. [66]
Less than 10% of phosphoinositides. [60]

Generation
$PI(3,4)P_2$ is mainly produced by phosphorylation of the 3rd position of PI(4)P by PI3KII.
It is also produced by hydrolysis of the 5th position of $PI(3,4,5)P_3$ by INPP5, ORCL and also SAC2, SYNJ1/2, SKIP and SHIP2. [78]

Degradation / Consumption
$PI(3,4)P_2$ can be hydrolyzed in the 4th position by INPP4 to produce PI(3)P.
It also can be hydrolyze in the 3rd position by PTEN to produce PI(4)P. [78]

Functions
Recruits AKT, phosphoinositide-dependent kinase 1 (PDK1) or Pleckstrin to the plasma membrane. [97]
Rule in endocytosis, signaling in early endosomes and clathrin-coated pits maturation. [98]

Open questions
It is still unclear whether $PI(3,4)P_2$ and its effector protein Lpd regulate focal adhesion dynamics and migration in breast cancer cells. [99]

Table 1.8. Features of $PI(3,5)P_2$

$PI(3,5)P_2$ (Phosphatidylinositol 3,5-bisphosphate)
Cellular location Mostly on early endosomes and lysosome. [100] [101]
Quantities Less than 5% of phosphoinositides. [67] 7 to 50 fold less than PI(5)P. [76] 0.1 – 1% of phosphoinositides. [66]
Generation $PI(3,5)P_2$ is generated by phosphorylation PI(3)P 5^{th} position by PIKfyve. [78]
Degradation / Consumption $PI(3,5)P_2$ is hydrolyzed in the 3^{rd} position by myotubularin's (MTMR) to produce the bulk of the PI(5)P pool. SAC1, SAC3 and SYNJ1/2 also hydrolyze $PI(3,5)P_2$ in the 5^{th} position to generate PI(3)P. [78]
Functions $PI(3,5)P_2$ plays an essential role in protein sorting at the late endosomes and in the multivehicular body. Also involved in autophagy. [102]
Open questions The upstream pathways and many of the downstream pathways specific for $PI(3,5)P_2$ are poorly understood.

Table 1.9. Features of $PI(4,5)P_2$

$PI(4,5)P_2$ (Phosphatidylinositol 4,5-bisphosphate)
Cellular location Mainly located in the plasma membrane. [63], [100]
Quantities 45% of phosphoinositide's in human cells and 90% of biphosphorylated phosphoinositides. [100] Around 2% of cellular inositol lipids. [63] 10% of phosphoinositides. [66]
Generation $PI(4,5)P_2$ is created from PI(4)P by PIP5KI. $PI(4,5)P_2$ is created from PI(5)P by PIP5KII. (apparently in the Golgi???) $PI(4,5)P_2$ is created from $PI(3,4,5)P_3$ by PTEN and TPIP. There is evidence of scaffolding of PI4K and PIP5KI kinases to essentially rapidly produce $PI(4,5)P_2$ from the much abundant PI. [78]
Degradation / Consumption $PI(4,5)P_2$ is phosphorylated in the 3rd position into $PI(3,4,5)P_2$ by PI3KI. $PI(4,5)P_2$ is hydrolyzed in the 5th position into PI(4)P by INPP5, ORCL and also SAC2, SYNJ1/2 and SKIP. PI(4,5)P2 is hydrolyzed in the 4th position into PI(5)P by SYNJ1/2 and TMEM55. SYNJ1/2 has the ability to hydrolyze the 4th and 5th position of phosphoinositides, being able to transform $PI(4,5)P_2$ rapidly into PI. [78]
Functions Identifier of the plasma membrane. [63] Precursor for $PI(3,4,5)P_3$. Precursor for IP_3 and DAG, important in calcium ER release. [63] Actin cytoskeleton and endocytic regulator. [100] At the nucleus, $PI(4,5)P_2$ regulates pre-mRNA splicing and gene expression though poly(A) polymerase, termed Star-PAP. [103], [104]
Open questions What is the $PI(4,5)P_2$, PI ratio in the plasma membrane? Can the manipulation of the levels of $PI(4,5)P_2$ be an effective means to influence the activity of proteins in the plasma membrane?

Table 1.10. Features of $PI(3,4,5)P_3$

$PI(3,4,5)P_3$ (Phosphatidylinositol 3,4,5-trisphosphate)

Cellular location
Mainly in the plasma membrane. [67]

Quantities
Less than 5% of total phosphoinositides. [60]
0.1 - 1% of total phosphoinositides. [66]
Almost non-detectable in quiescent cells.
Intracellular level rapidly and transiently increases up to 100-fold in response to an agonist. [105]

Generation
Created by PI3KI from $PI(4,5)P_2$. [78]
There is evidence that scaffolding kinases can transform PI to $PI(3,4,5)P_3$. [106]

Degradation / Consumption
$PI(3,4,5)P_3$ is transformed back into $PI(4,5)P_2$ by PTEN or TPIP.
$PI(3,4,5)P_3$ is also hydrolyzed in the 5^{th} position. [78]

Functions
Control of cell proliferation and cell survival, cytoskeleton dynamics, cell motility, membrane trafficking and apoptosis by interacting with the Arf GTPases family, PDK1 and AKT kinases and phospholipase C. [107], [108]

Open questions
In the apical part of a polarized epithelial cell, the absence of $PI(3,4,5)P_3$ is accompanied by an increase of $PI(4,5)P_2$? There is experimental evidence that supports both sides, but the evidence with better quality points to no alteration of $PI(4,5)P_2$ levels. [75]

1.6. Thesis outline

The biological motivation and theoretical background for this work are introduced in Chapter 1.

There were four objectives to this PhD project that were accomplished and reported in the central chapters of this thesis. The first objective was to build a dynamic model of the phosphoinositide pathway, which is reported in Chapter 2.

The creation of an ENaC/ASL model (described in Chapter 3) enabled us to achieve the second objective, namely, to expand the model to include ion channels. This task was completed in the paper presented in Chapter 4 with the joining of the phosphoinositide and the ENaC/ASL models.

Throughout the three aforementioned Chapters, the third objective, the search for therapeutic approaches in the context of cystic fibrosis was implemented.

Finally, in Chapter 5, two suggested experiments are proposed, completing the fourth objective of planning laboratory experiments. Also, in this Chapter, the results of Chapters 2, 3 and 4 are revisited, discussed and directions for future research are proposed.

1.6. References

[1] E. Griffiths, “What is a Model ?,” 2010. [Online]. Available: https://63587809-a-bf11e6be-s-sites.googlegroups.com/a/ncsu.edu/emily-griffiths/whatisamodel.pdf.

[2] D. Graham-Smith, “The History Of The Tube Map,” 2018. [Online]. Available: https://londonist.com/2016/05/the-history-of-the-tube-map. [Accessed: 03-Jul-2018].

[3] Mayor of London, “Transport for London - Tube,” 2018. [Online]. Available: https://tfl.gov.uk/maps/track/tube. [Accessed: 03-Jul-2018].

[4] M. A. Savageau, “Biochemical systems analysis. I. Some mathematical properties of the rate law for the component enzymatic reactions.,” *J. Theor. Biol.*, vol. 25, no. 3, pp. 365–9, Dec. 1969.

[5] M. Savageau, *Biochemical Systems Analysis*. 1976.

[6] M. A. Savageau, “Introduction to S-systems and the underlying power-law formalism,” *Math. Comput. Model.*, vol. 11, no. C, pp. 546–551, 1988.

[7] E. O. Voit, *Computational analysis of biochemical systems: a practical guide for biochemists and molecular biologists*. Cambridge, U.K.: Cambridge University Press, 2000.

[8] E. O. Voit, *A first course in systems biology*. Garland Science,Taylor & Francis Group, 2013.

[9] E. O. Voit, “Biochemical systems theory: a review,” *ISRN Biomath.*, vol. 2013, pp. 1–53, 2013.

[10] Y. Lazebnik, “Can a biologist fix a radio? - Or, what I learned while studying apoptosis,” *Biochem.*, vol. 69, no. 12, pp. 1403–1406, 2004.

[11] M. A. Savageau, “Reconstructionist molecular biology.,” *New Biol.*, vol. 3, no. 2, pp. 190–197, 1991.

[12] I. Schomburg *et al.*, “BRENDA: integrated reactions, kinetic data, enzyme function data, improved disease classification.,” 2015. .

[13] H. W. Bode, *Network Analysis and Feedback Amplifier Design*. New York: D. Van Nostrand Co., 1945.

[14] M. A. Savageau, “Enzyme kinetics in vitro and in vivo: Michaelis-Menten revisited,” in *Principles of Medical Biology, volume 4, part 1*, E. Bittar, Ed.

Elsevier, 1995, pp. 93–146.

[15] R. Milo and R. Phillips, *Cell Biology By the Numbers.*, no. June. Garland Science,Taylor & Francis Group, 2015.

[16] K. Soetaert and T. Petzoldt, "Inverse Modelling, Sensitivity and Monte Carlo Analysis in R Using Package FME," *J. Stat. Softw.*, vol. 33, no. 3, pp. 1–28, 2010.

[17] E. Kent, S. Neumann, U. Kummer, and P. Mendes, "What can we learn from global sensitivity analysis of biochemical systems?," *PLoS One*, vol. 8, no. 11, 2013.

[18] S. Srinath and R. Gunawan, "Parameter identifiability of power-law biochemical system models," *J. Biotechnol.*, vol. 149, no. 3, pp. 132–140, 2010.

[19] K. Z. Yao, B. M. Shaw, B. Kou, K. B. McAuley, and D. W. Bacon, "Modeling Ethylene/Butene Copolymerization with Multi-site Catalysts: Parameter Estimability and Experimental Design," *Polym. React. Eng.*, vol. 11, no. 3, pp. 563–588, 2003.

[20] World Health Organisation, "The molecular genetic epidemiology of cystic fibrosis," p. 26, 2004.

[21] J. R. Riordan *et al.*, "Identification the Cystic Fibrosis Gene : Cloning and Characterization of Complementary DNA," *Science*, vol. 245, pp. 1066–1073, 1989.

[22] B. Kerem *et al.*, "Identification of the cystic fibrosis gene: genetic analysis.," *Science*, vol. 245, no. 4922, pp. 1073–80, 1989.

[23] J. Rommens *et al.*, "Identification of the cystic fibrosis gene: chromosome walking and jumping," *Science*, vol. 245, no. 4922, pp. 1059–1065, 1989.

[24] R. Dorfman *et al.*, "Cystic Fibrosis Mutation Database (CFTR1)," 2011. [Online]. Available: http://www.genet.sickkids.on.ca/cftr/StatisticsPage.html. [Accessed: 15-Mar-2018].

[25] U. C. Foundation, J. H. University, and T. H. for S. Children, "The Clinical and Functional TRanslation of CFTR (CFTR2)," 2011. [Online]. Available: http://www.cftr2.org. [Accessed: 15-Mar-2018].

[26] P. B. Davis, "Cystic fibrosis since 1938," *Am. J. Respir. Crit. Care Med.*, vol. 173, no. 5, pp. 475–482, 2006.

[27] M. L. Drumm, A. G. Ziady, and P. B. Davis, “Genetic Variation and Clinical Heterogeneity in Cystic Fibrosis,” *Annu. Rev. Pathol.*, vol. 7, pp. 267–282, 2012.

[28] I. Fajac and C. E. Wainwright, “New treatments targeting the basic defects in cystic fibrosis,” *Press. Medicale*, vol. 46, no. 6P2, pp. e165–e175, 2017.

[29] C. F. Foundation, “Cystic Fibrosis Foundation Patient Registry 2016 Annual Data Report,” 2017.

[30] J. L. Taylor-Cousar *et al.*, “Lumacaftor/ivacaftor in patients with cystic fibrosis and advanced lung disease homozygous for F508del-CFTR.,” *J. Cyst. Fibros.*, vol. 17, no. 2, pp. 228–235, 2017.

[31] European Respiratory Society, *The European Lung White Book Respiratory Health and Disease in Europe*, 2nd ed. Sheffield, UK., 2013.

[32] T. Ong and B. W. Ramsey, “Update in cystic fibrosis 2014,” *Am. J. Respir. Crit. Care Med.*, vol. 192, no. 6, pp. 669–675, 2015.

[33] M. Lopes-Pacheco, “CFTR modulators: Shedding light on precision medicine for cystic fibrosis,” *Front. Pharmacol.*, vol. 7, no. 275, pp. 1–20, 2016.

[34] P. M. Farrell, “The prevalence of cystic fibrosis in the European Union,” *J. Cyst. Fibros.*, vol. 7, no. 5, pp. 450–453, 2008.

[35] E. M. Poolman and A. P. Galvani, “Evaluating candidate agents of selective pressure for cystic fibrosis.,” *J. R. Soc. Interface*, vol. 4, no. 12, pp. 91–98, 2007.

[36] J. Almaça *et al.*, “AMPK controls epithelial Na+ channels through Nedd4-2 and causes an epithelial phenotype when mutated,” *Pflugers Arch. Eur. J. Physiol.*, vol. 458, no. 4, pp. 713–721, 2009.

[37] M. A. Mall and L. J. V. Galietta, “Targeting ion channels in cystic fibrosis,” *J. Cyst. Fibros.*, vol. 14, no. 5, pp. 561–570, 2015.

[38] J. Almaça *et al.*, “High-content siRNA screen reveals global ENaC regulators and potential cystic fibrosis therapy targets,” *Cell*, vol. 154, no. 6, 2013.

[39] O. A. Itani *et al.*, “Human cystic fibrosis airway epithelia have reduced Cl- conductance but not increased Na+ conductance,” *Proc. Natl. Acad. Sci.*, vol. 108, no. 25, pp. 10260–10265, 2011.

[40] T. Kimura *et al.*, “Deletion of the ubiquitin ligase Nedd4L in lung epithelia causes cystic fibrosis-like disease.,” *Proc. Natl. Acad. Sci. U. S. A.*, vol. 108, no. 8, pp. 3216–21, 2011.

[41] Z. Zhou *et al.*, "The ENaC-overexpressing mouse as a model of cystic fibrosis lung disease," *J. Cyst. Fibros.*, vol. 10, no. SUPPL. 2, pp. S172–S182, 2011.

[42] M. M. Reddy, M. J. Light, and P. M. Quinton, "Activation of the epithelial Na+ channel (ENaC) requires CFTR Cl- channel function.," *Nature*, vol. 402, no. 6759, pp. 301–4, 1999.

[43] A. G. Palma, B. A. Kotsias, and G. I. Marino, "Artículo especial funciones de los canales iónicos CFTR y ENaC.," *Med. (Buenos Aires)*, vol. 74, pp. 133–139, 2014.

[44] B. K. Berdiev, Y. J. Qadri, and D. J. Benos, "Assessment of the CFTR and ENaC association," *Mol Biosyst.*, vol. 5, no. 2, pp. 123–127, 2009.

[45] M. J. Stutts, B. C. Rossier, and R. C. Boucher, "Cystic Fibrosis Transmembrane Conductance Regulator Inverts Protein Kinase A-mediated Regulation of Epithelial Sodium Channel Single Channel Kinetics," *J. Biol. Chem.*, vol. 272, no. 22, pp. 14037–14040, 1997.

[46] L. Drévillon *et al.*, "Commd1-mediated ubiquitination regulates CFTR trafficking," *PLoS One*, vol. 6, no. 3, 2011.

[47] Y. Ke, A. G. Butt, M. Swart, Y. F. Liu, and F. J. McDonald, "COMMD1 downregulates the epithelial sodium channel through Nedd4-2," *Am J Physiol Ren. Physiol*, vol. 298, no. 6, pp. F1445-1456, 2010.

[48] C. M. Farinha and P. Matos, "Rab GTPases regulate the trafficking of channels and transporters – a focus on cystic fibrosis," *Small GTPases*, vol. 1248, no. May, pp. 00–00, 2017.

[49] R. Tarran and M. R. Redinbo, "Mammalian short palate lung and nasal epithelial clone 1 (SPLUNC1) in pH-dependent airway hydration," *Int J Biochem Cell Biol.*, pp. 130–135, 2014.

[50] C. S. Kim, S. Ahmad, T. Wu, W. G. Walton, M. R. Redinbo, and R. Tarran, "SPLUNC1 is an allosteric modulator of the epithelial sodium channel," *FASEB J.*, Jan. 2018.

[51] D. W. Scott *et al.*, "SPX-101 is a novel ENaC-targeted therapeutic for cystic fibrosis that restores mucus transport," *AJRCCM*, pp. 1–47, 2017.

[52] O. Pochynyuk, V. Bugaj, and J. D. Stockand, "Physiologic regulation of the epithelial sodium channel by phosphatidylinositides," *Curr. Opin. Nephrol.*

Hypertens., vol. 17, no. 5, pp. 533–540, 2008.

[53] H.-P. Ma and D. C. Eaton, "Acute regulation of epithelial sodium channel by anionic phospholipids.," *J. Am. Soc. Nephrol.*, vol. 16, no. 11, pp. 3182–3187, 2005.

[54] K. Kunzelmann, T. Bachhuber, R. Regeer, D. Markovich, J. Sun, and R. Schreiber, "Purinergic inhibition of the epithelial Na+ transport via hydrolysis of PIP2.," *FASEB J.*, vol. 19, pp. 142–143, 2005.

[55] P. Kota *et al.*, "The N-terminal domain allosterically regulates cleavage and activation of the epthelial sodium channel," *J. Biol. Chem.*, vol. 289, no. 33, pp. 23029–23042, 2014.

[56] A. Moritz, P. N. De Graan, W. H. Gispen, and K. W. Wirtz, "Phosphatidic acid is a specific activator of phosphatidylinositol-4-phosphate kinase.," *J. Biol. Chem.*, vol. 267, no. 11, pp. 7207–7210, 1992.

[57] G. H. Jenkins, P. L. Fisette, and R. A. Anderson, "Type I phosphatidylinositol 4-phosphate 5-kinase isoforms are specifically stimulated by phosphatidic acid.," *J. Biol. Chem.*, vol. 269, no. 15, pp. 11547–54, Apr. 1994.

[58] D. R. Jones, M. A. Sanjuan, and I. Mérida, "Type I alpha phosphatidylinositol 4-phosphate 5-kinase is a putative target for increased intracellular phosphatidic acid," *FEBS Lett.*, vol. 476, no. 3, pp. 160–165, 2000.

[59] M. Jarquin-Pardo, A. Fitzpatrick, F. J. Galiano, E. A. First, and J. N. Davis, "Phosphatidic acid regulates the affinity of the murine phosphatidylinositol 4-phosphate 5-kinase-1β for phosphatidylinositol-4-phosphate," *J. Cell. Biochem.*, vol. 100, no. 1, pp. 112–128, 2007.

[60] B. Payrastre, K. Missy, S. Giuriato, S. Bodin, M. Plantavid, and M. P. Gratacap, "Phosphoinositides: Key players in cell signalling, in time and space," *Cellular Signalling*, vol. 13, no. 6. Pergamon, pp. 377–387, 01-Jun-2001.

[61] K. Athenstaedt and G. Daum, "Phosphatidic acid, a key intermediate in lipid metabolism," *European Journal of Biochemistry*. 1999.

[62] J. E. Vance, "Phospholipid Synthesis and Transport in Mammalian Cells," *Traffic*, vol. 16, no. 1, pp. 1–18, 2015.

[63] T. Balla, "Phosphoinositides: tiny lipids with giant impact on cell regulation," *Physiol. Rev.*, vol. 93, no. 3, pp. 1019–1137, 2013.

[64] S. L. Marcus AJ, Ullman HL, “Lipid composition of subcellular particles of human blood platelets,” *J. Lipid Res.*, vol. 10, pp. 108–114, 1969.

[65] A. Traynor-Kaplan *et al.*, “Fatty-acyl chain profiles of cellular phosphoinositides,” *Biochim. Biophys. Acta - Mol. Cell Biol. Lipids*, vol. 1862, no. 5, pp. 513–522, 2017.

[66] J. Viaud *et al.*, “Phosphoinositides: Important lipids in the coordination of cell dynamics,” *Biochimie*, vol. 125, pp. 250–258, 2016.

[67] J. O. De Craene, D. L. Bertazzi, S. Bär, and S. Friant, “Phosphoinositides, major actors in membrane trafficking and lipid signaling pathways,” *Int. J. Mol. Sci.*, vol. 18, no. 3, 2017.

[68] G. van Meer, D. R. Voelker, and G. W. Feigenson, “Membrane lipids: where they are and how they behave.,” *Nat. Rev. Mol. Cell Biol.*, vol. 9, no. 2, pp. 112–124, 2008.

[69] C. Xu, J. Watras, and L. M. Loew, “Kinetic analysis of receptor-activated phosphoinositide turnover,” *J. Cell Biol.*, vol. 161, pp. 779–791, 2003.

[70] O. C. Ikonomov *et al.*, “The Phosphoinositide Kinase PIKfyve Is Vital in Early Embryonic Development: PREIMPLANTATION LETHALITY OF PIKfyve-/- EMBRYOS BUT NORMALITY OF PIKfyve+/- MICE,” *J. Biol. Chem.*, vol. 286, no. 15, pp. 13404–13413, 2011.

[71] Y. Zhang *et al.*, “Loss of Vac14, a regulator of the signaling lipid phosphatidylinositol 3,5-bisphosphate, results in neurodegeneration in mice.,” *Proc. Natl. Acad. Sci. U. S. A.*, vol. 104, no. 44, pp. 17518–17523, 2007.

[72] N. R. Leslie, I. H. Batty, H. Maccario, L. Davidson, and C. P. Downes, “Understanding PTEN regulation: PIP2, polarity and protein stability,” *Oncogene*, vol. 27, no. 41, pp. 5464–5476, 2008.

[73] B. H. Falkenburger, J. B. Jensen, E. J. Dickson, B.-C. Suh, and B. Hille, “Phosphoinositides: lipid regulators of membrane proteins.,” *J. Physiol.*, 2010.

[74] S. J. Bulley, J. H. Clarke, A. Droubi, M.-L. Giudici, and R. F. Irvine, “Exploring phosphatidylinositol 5-phosphate 4-kinase function.,” *Adv. Biol. Regul.*, vol. 57, pp. 193–202, Jan. 2015.

[75] S. Kolay, U. Basu, and P. Raghu, “Control of diverse subcellular processes by a single multi-functional lipid phosphatidylinositol 4,5-bisphosphate

[PI(4,5)P2].," *Biochem. J.*, vol. 473, no. 12, pp. 1681–92, 2016.

[76] A. Shisheva, "PtdIns5P: News and views of its appearance, disappearance and deeds," *Arch. Biochem. Biophys.*, vol. 538, no. 2, pp. 171–180, 2013.

[77] H. J. G. Meijer and T. Munnik, "Phospholipid-based signaling in plants.," *Annu. Rev. Plant Biol.*, 2003.

[78] T. Sasaki *et al.*, "Mammalian phosphoinositide kinases and phosphatases," *Prog. Lipid Res.*, vol. 48, no. 6, pp. 307–343, 2009.

[79] R. Suratekar, A. Panda, P. Raghu, and S. Krishna, "Evidence of sinks and sources in the phospholipase C-activated PIP $_2$ cycle," *FEBS Lett.*, pp. 1–11, 2018.

[80] D. M. Bryant and K. E. Mostov, "From cells to organs: building polarized tissue.," *Nat. Rev. Mol. Cell Biol.*, vol. 9, no. 11, pp. 887–901, 2008.

[81] S. J. Baker, "PTEN Enters the Nuclear Age," *Cell*, vol. 128, no. 1, pp. 25–28, 2007.

[82] A. Gassama-Diagne *et al.*, "Phosphatidylinositol-3,4,5-trisphosphate regulates the formation of the basolateral plasma membrane in epithelial cells.," *Nat. Cell Biol.*, vol. 8, no. 9, pp. 963–970, 2006.

[83] Wikipedia, "Epithelial polarity," 2017. [Online]. Available: https://en.wikipedia.org/wiki/Epithelial_polarity. [Accessed: 03-Jul-2018].

[84] M. Mahon, "Apical membrane segregation of phosphatidylinositol-4,5-bisphosphate influences parathyroid hormone 1 receptor compartmental signaling and localization via direct regulation of ezrin in LLC-PK1 cells," *Cell Signal*, vol. 23, no. 10, pp. 1659–1668, 2011.

[85] Y. Arai, T. Shibata, S. Matsuoka, M. J. Sato, T. Yanagida, and M. Ueda, "Self-organization of the phosphatidylinositol lipids signaling system for random cell migration," *Proc Natl Acad Sci U S A*, vol. 107, no. 27, pp. 12399–12404, 2010.

[86] B. E. Antonsson, "Purification and characterization of phosphatidylinositol synthase from human placenta.," *Biochem. J.*, vol. 297 (Pt 3, pp. 517–522, 1994.

[87] G. R. V Hammond, M. P. Machner, and T. Balla, "A novel probe for phosphatidylinositol 4-phosphate reveals multiple pools beyond the Golgi," *J. Cell Biol.*, vol. 205, no. 1, pp. 113–126, 2014.

[88] D. J. Gillooly *et al.*, "Localization of phosphatidylinositol 3-phosphate in yeast

and mammalian cells.," *EMBO J.*, vol. 19, no. 17, pp. 4577–88, Sep. 2000.

[89] A. Audhya, M. Foti, and S. D. Emr, "Distinct roles for the yeast phosphatidylinositol 4-kinases, Stt4p and Pik1p, in secretion, cell growth, and organelle membrane dynamics.," *Mol. Biol. Cell*, vol. 11, no. 8, pp. 2673–89, Aug. 2000.

[90] K. Ketel *et al.*, "A phosphoinositide conversion mechanism for exit from endosomes," *Nature*, vol. 529, no. 7586, pp. 408–412, 2016.

[91] J. Guo, M. R. Wenk, L. Pellegrini, F. Onofri, F. Benfenati, and P. De Camilli, "Phosphatidylinositol 4-kinase type IIalpha is responsible for the phosphatidylinositol 4-kinase activity associated with synaptic vesicles.," *Proc. Natl. Acad. Sci. U. S. A.*, vol. 100, no. 7, pp. 3995–4000, Apr. 2003.

[92] T. P. Levine and S. Munro, "Targeting of Golgi-Specific Pleckstrin Homology Domains Involves Both PtdIns 4-Kinase-Dependent and -Independent Components," *Curr. Biol.*, vol. 12, no. 9, pp. 695–704, Apr. 2002.

[93] R. Galmes, A. Houcine, A. R. van Vliet, P. Agostinis, C. L. Jackson, and F. Giordano, "ORP5/ORP8 localize to endoplasmic reticulum–mitochondria contacts and are involved in mitochondrial function," *EMBO Rep.*, vol. 17, no. 6, pp. 800–810, Jun. 2016.

[94] A. Gericke, N. R. Leslie, M. Lösche, and A. H. Ross, "PtdIns(4,5)P2-mediated cell signaling: Emerging principles and PTEN as a paradigm for regulatory mechanism," *Adv. Exp. Med. Biol.*, vol. 991, pp. 85–104, 2013.

[95] A. Oppelt *et al.*, "PIKfyve, MTMR3 and their product PtdIns5 *P* regulate cancer cell migration and invasion through activation of Rac1," *Biochem. J.*, vol. 461, no. 3, pp. 383–390, 2014.

[96] F. Boal *et al.*, "TOM1 is a PI5P effector involved in the regulation of endosomal maturation," *J. Cell Sci.*, vol. 128, no. 4, pp. 815–827, Feb. 2015.

[97] C. Edlich, G. Stier, B. Simon, M. Sattler, and C. Muhle-Goll, "Structure and Phosphatidylinositol-(3,4)- Bisphosphate Binding of the C-Terminal PH Domain of Human Pleckstrin," *Structure*, vol. 13, no. 2, pp. 277–286, Feb. 2005.

[98] P. T. Hawkins and L. R. Stephens, "Emerging evidence of signalling roles for PI(3,4)P2 in Class I and II PI3K-regulated pathways," *Biochem. Soc. Trans.*, vol. 44, no. 1, pp. 307–314, 2016.

[99] M. Fukumoto, T. Ijuin, and T. Takenawa, “PI(3,4)P2plays critical roles in the regulation of focal adhesion dynamics of MDA-MB-231 breast cancer cells.,” *Cancer Sci.*, vol. 108, no. 5, pp. 941–951, May 2017.

[100] G. Di Paolo and P. De Camilli, “Phosphoinositides in cell regulation and membrane dynamics.,” *Nature*, vol. 443, no. 7112, pp. 651–657, 2006.

[101] X. Li *et al.*, “Genetically encoded fluorescent probe to visualize intracellular phosphatidylinositol 3,5-bisphosphate localization and dynamics.,” *Proc. Natl. Acad. Sci. U. S. A.*, vol. 110, no. 52, pp. 21165–70, 2013.

[102] G. Odorizzi, M. Babst, and S. D. Emr, “Fab1p PtdIns(3)P 5-Kinase Function Essential for Protein Sorting in the Multivesicular Body,” *Cell*, vol. 95, no. 6, pp. 847–858, Dec. 1998.

[103] S. L. Osborne, C. L. Thomas, S. Gschmeissner, and G. Schiavo, “Nuclear PtdIns(4,5)P2 assembles in a mitotically regulated particle involved in pre-mRNA splicing.,” *J. Cell Sci.*, vol. 114, no. Pt 13, pp. 2501–11, Jul. 2001.

[104] W. Li, R. S. Laishram, and R. A. Anderson, “The novel poly(A) polymerase Star-PAP is a signal-regulated switch at the 3′-end of mRNAs,” *Adv. Biol. Regul.*, vol. 53, no. 1, pp. 64–76, Jan. 2013.

[105] S. B. Milne, P. T. Ivanova, D. DeCamp, R. C. Hsueh, and H. A. Brown, “A targeted mass spectrometric analysis of phosphatidylinositol phosphate species.,” *J. Lipid Res.*, vol. 46, no. 8, pp. 1796–802, Aug. 2005.

[106] S. Choi, A. C. Hedman, S. Sayedyahossein, N. Thapa, D. B. Sacks, and R. A. Anderson, “Agonist-stimulated phosphatidylinositol-3,4,5-trisphosphate generation by scaffolded phosphoinositide kinases,” *Nat. Cell Biol.*, vol. 18, no. 12, pp. 1324–1335, 2016.

[107] M. A. Lemmon, “Phosphoinositide Recognition Domains,” *Traffic*, vol. 4, no. 4, pp. 201–213, Apr. 2003.

[108] P. Hilpelä, M. K. Vartiainen, and P. Lappalainen, “Regulation of the actin cytoskeleton by PI(4,5)P2 and PI(3,4,5)P3.,” *Curr. Top. Microbiol. Immunol.*, vol. 282, pp. 117–63, 2004.

Chapter 2. **A Mathematical Model of the Phosphoinositide Pathway**

This Chapter is an integral reproduction of the paper:

Olivença, D. V., Uliyakina, I., Fonseca, L. L., Amaral, M., Voit, E. O., & Pinto, F. R. (2018). A Mathematical Model of the Phosphoinositide Pathway. *Scientific Reports*, *8*, 1–12. https://doi.org/10.1038/s41598-018-22226-8

2.1. Abstract

Phosphoinositides are signalling lipids that constitute a complex network regulating many cellular processes. We propose a computational model that accounts for all species of phosphoinositides in the plasma membrane of mammalian cells. The model replicates the steady-state of the pathway and most known dynamic phenomena. Sensitivity analysis demonstrates model robustness to alterations in the parameters. Model analysis suggest that the greatest contributor to phosphatidylinositol 4,5-biphosphate ($PI(4,5)P_2$) production is a flux representing the direct transformation of PI into $PI(4,5)P_2$, also responsible for the maintenance of this pool when phosphatidylinositol 4-phosphate (PI(4)P) is decreased. PI(5)P is also shown to be a significant source for $PI(4,5)P_2$ production. The model was validated with siRNA screens that knocked down the expression of enzymes in the pathway. The screen monitored the activity of the epithelium sodium channel (ENaC), which is activated by $PI(4,5)P_2$. While the model may deepen our understanding of other physiological processes involving phosphoinositides, we highlight therapeutic effects of ENaC modulation in Cystic Fibrosis (CF). The model suggests control strategies where the activities of the enzyme phosphoinositide 4-phosphate 5-kinase I (PIP5KI) or the PI4K+PIP5KI+DVL protein complex are decreased and cause an efficacious reduction in $PI(4,5)P_2$ levels while avoiding undesirable alterations in other phosphoinositide pools.

2.2. Introduction

Biological systems have evolved by improving the efficiency with which complex regulatory networks control multiple mechanisms in the cell through the fine-tuned balancing of enzymatic reactions. Phosphoinositides are important lipids that are interconverted into each other by multiple enzymatic reactions, which together constitute an example of such a complex network regulating critical cellular functions. Phosphoinositides are key signalling messengers, and several play important parts in regulating physiological processes including vesicular trafficking, transmembrane signalling, ion channel regulation, lipid homeostasis, cytokinesis and organelle identity as characteristic identifiers for different membranes in the cell[1]–[5]. It is thus not surprising that phosphoinositides play critical roles in a number of pathological conditions including immunological defence, mediating replication of a number of pathogenic RNA viruses, in the development of the parasite responsible for malaria, in tumorigenesis, Alzheimer's disease, diabetes, and numerous others[6]–[9].

The inositol head of phosphoinositides can be phosphorylated at its third, fourth and fifth carbon, thus creating different subspecies. The responsible pathway connects eight metabolites through a dense network of 21 chemical reactions, which are catalysed by 19 kinases and 28 phosphatases[10] (Figure 2.1). The resulting degree of complexity prevents simple interpretations and renders intuitive predictions of pathway behaviour and regulation unreliable. It is especially difficult to pinpoint the roles of less abundant phosphoinositides, such as phosphatidylinositol 5-phosphate (PI(5)P) and phosphatidylinositol 3,4-biphosphate ($PI(3,4)P_2$). $PI(4,5)P_2$ is present throughout the plasma membrane and considered a general marker for the cell membrane. By contrast, phosphatidylinositol 3,4,5-triphosphate ($PI(3,4,5)P_3$), marks the basolateral part of a polarized cell’s membrane but is absent from the apical part[1], [11].

Other phosphoinositides characterize intracellular membranes (Figure 2.2). Phosphatidylinositol 3,5-biphosphate ($PI(3,5)P_2$) is typical for multivesicular bodies and lysosomes, whereas PI(4)P is found in the Golgi, and phosphatidylinositol (PI) is located in the endoplasmic reticulum (ER)[12]. To achieve this distinctive variability in phosphoinositide composition among different membrane compartments, the cell must be able to modulate phosphoinositide metabolism in a targeted, localized manner.

Phosphoinositides also serve as precursors for various signalling molecules, as in the case of $PI(4,5)P_2$, which can be transformed into diacylglycerol (DAG) and inositol triphosphate (IP_3) through the action of phospholipase C (PLC). They are furthermore docking sites in the plasma membrane, for instance, for AKT (also known as Protein Kinase B) in the case of $PI(3,4,5)P_3$.

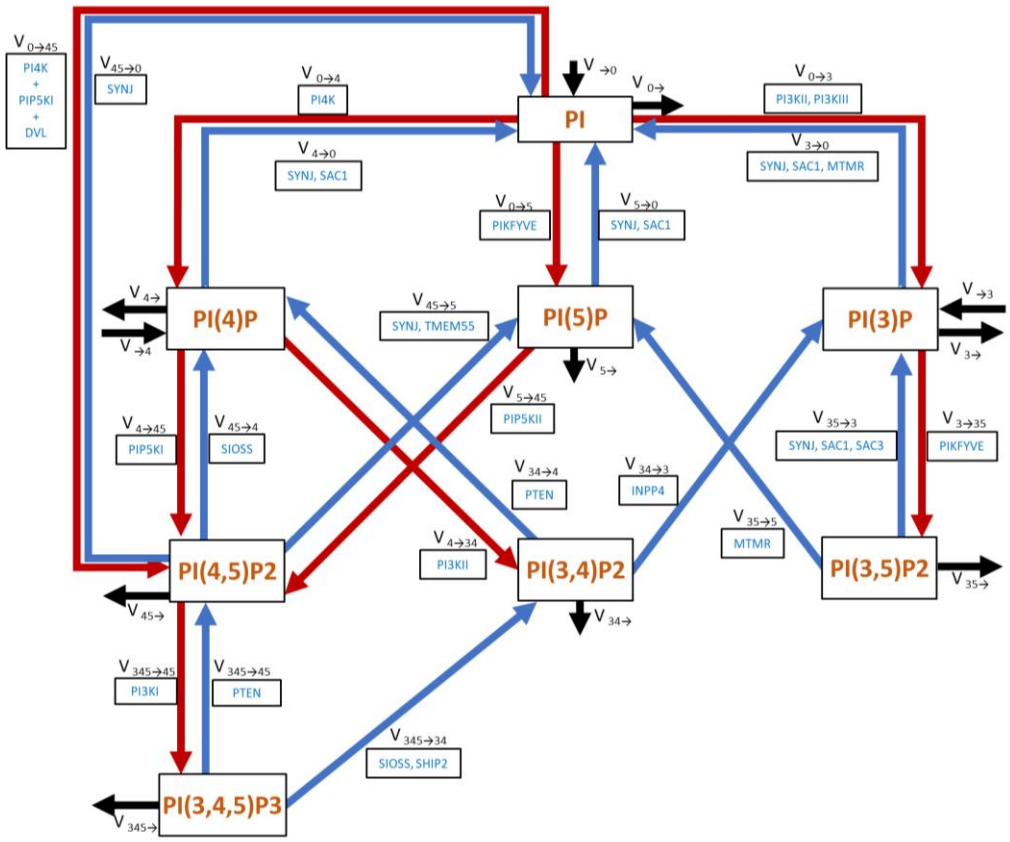

Figure 2.1. Map of the phosphoinositide pathway.

Red arrows represent fluxes of phosphorylation and blue arrows fluxes of hydrolysis. For each flux, the name ($v_{i\to j}$) and the group of enzymes that catalysed the reaction are shown. Black arrows represent influxes and effluxes of material entering and leaving the system. SIOSS is a group of phosphatases, consisting of SYNJ 1/2, INPP5 B/J/E, OCRL1, SAC2 and SKIP. PI4K + PIP5KI + DVL denotes a complex formed by the three proteins. Proteins separated by commas catalyzed the same reaction. SYNJ: Synaptojanins; INPP5: Inositol polyphosphate 5-phosphatases; OCRL1: Lowe Oculocerebrorenal Syndrome Protein; SAC2: Suppressor of actin; SKIP: Skeletal muscle and kidney enriched inositol polyphosphate phosphatase.

Interestingly, phosphoinositides are also key regulators of ion channel activity[11]. The epithelial sodium channel (ENaC) is of interest, as it plays a critical role in Cystic

Fibrosis (CF), a genetic condition caused by mutations in the gene encoding CFTR, a chloride channel that also regulates other ion conductance, namely through ENaC, across epithelia. In order to keep ENaC open, lysine residues present at the N terminus of the β and δ subunits need to be bound to $PI(4,5)P_2$[13]. This channel function is upregulated in the lungs of individuals with CF, and the increased absorption of sodium and water is considered to be the major cause of lung disease due to critical dehydration of airway surface liquid (ASL)[14]. The dehydrated ASL and consequent impairment of mucociliary clearance, in turn, is a major cause of respiratory problems in CF[13]. Thus, a better understanding of the phosphoinositide pathway is of paramount importance, as it may contribute to ameliorating the CF phenotype by manipulating the levels of $PI(4,5)P_2$, which moderate the action of ENaC.

To address the challenge of complexity, it is advantageous to resort to mathematical models, which indeed have already been proposed for particular components of the phosphoinositide pathway. Narang[12], Xu[15], Nishioka[16] and Purvis[17] proposed models mainly focused on understanding the dynamics of $PI(4,5)P_2$, PLC, IP_3 and DAG, since these molecules are directly associated with calcium release and protein kinase C (PKC) activation, which are important signalling events. Other models, such as those developed by Araia[18] and MacNamara[19], focus on $PI(4,5)P_2$, $PI(3,4,5)P_3$, phosphoinositide 3-kinase (PI3K), phosphatase and tensin homolog (PTEN) and their roles in cancer. None of these models account for all phosphoinositide species. However, the inclusion of less abundant species is important for understanding the distinctions between membrane compartments and for rationalizing the observed impact of several enzyme knock-downs on $PI(4,5)P_2$-mediated ENaC modulation[13].

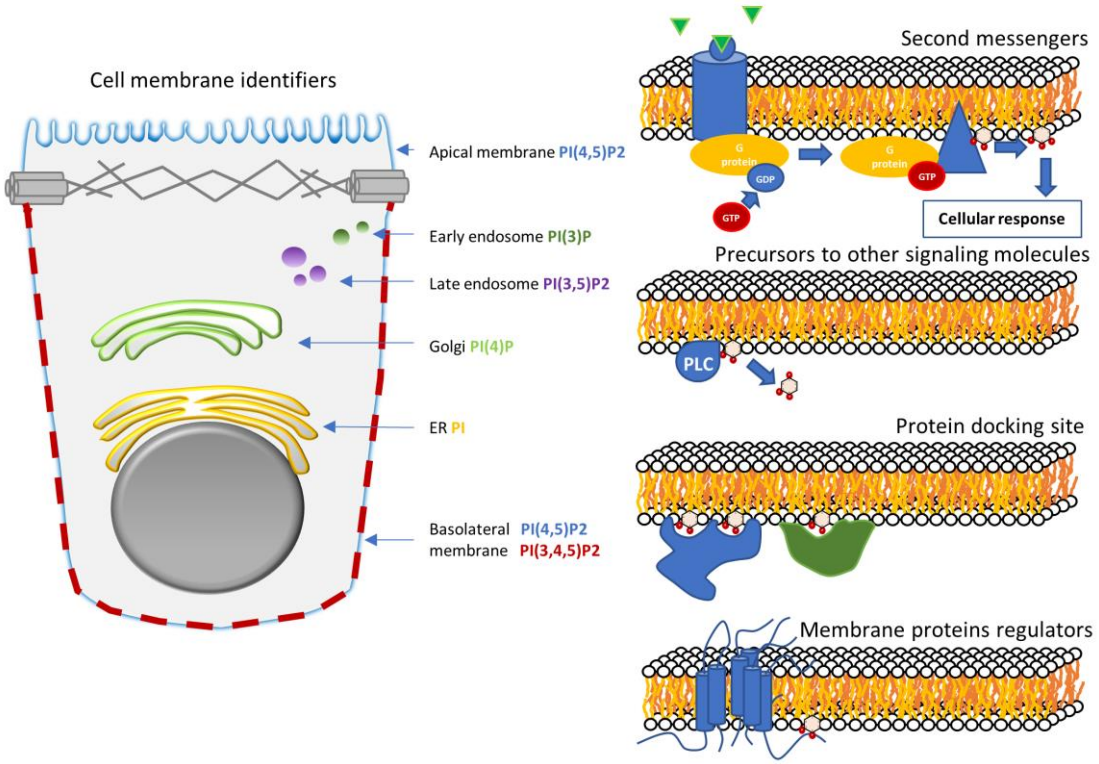

Figure 2.2. Functions of phosphoinositides in the cell.

Phosphoinositides are signalling lipids that are cell membrane identifiers. PI(4,5)P_2 marks the plasma membrane, PI(3)P the early endosomes, PI(4)P the Golgi, PI(3,5)P_2 the late endosomes, PI the ER; finally, PI(3,4,5)P_3 is present in the basolateral part of the plasma membrane and absent from the apical part. Phosphoinositides are also second messengers, precursors to other signalling molecules and membrane protein docking sites and regulators.

Here, we propose a mathematical model of the complete phosphoinositide pathway. Our primary goal is to shed light on the dynamics of this pathway. Moreover, the model will facilitate a deeper understanding of the unique composition of membranes in different compartments and thereby provide an effective tool for exploring various physiological conditions and their potential treatments, including possible therapeutic targets for CF, cancer and other diseases in which the phosphoinositide pathway plays a critical role.

2.3. Results

The prime result of this study is a mathematical model of the phosphoinositide pathway that contains all allegedly relevant molecular components and captures pertinent features of the pathway documented in the literature. The model is certainly not all-

encompassing but detailed enough to serve as a launch pad for future extensions. For instance, it is known that the actual pathway is distributed and compartmentalized. Here, we simulate it restricted to a 1 μm^2 patch of plasma membrane, which we consider spatially homogeneous. Nonetheless, the model is designed in a manner that is flexible enough to simulate membrane patches in different compartments, and once the necessary data become available to allow such an extension, it will be easy to block a given reaction *a priori* if it is known to be absent in that compartment. Alternately, one may perform the same type of parameter optimization as we have done here, but fit experimental observations in different compartments, and this strategy would lead to very low enzyme activities for the corresponding reactions.

The pathway map underlying the model is exhibited in Figure 2.1. To facilitate the presentation and discussion of results, each flux is represented by $v_{i\rightarrow j}$, and the group of enzymes catalysing it by $E_{i\rightarrow j}$, where the subscripts i and j identify the phosphorylated positions of the substrate and product phosphoinositide species, respectively. The modelled reaction network is based on a review by Balla[11], but expanded with information from other sources[2], [3], [10]. In particular, we added four fluxes: $v_{0\rightarrow 45}$, $v_{45\rightarrow 0}$, $v_{4\rightarrow 34}$ and $v_{34\rightarrow 4}$. The first, $v_{0\rightarrow 45}$, transforms PI into PI(4,5)P2 through a ternary complex of proteins PI4K, PIP5KI and DVL[20]. This complex is included as one possible molecular complex facilitating the direct channelling of PI into PI(4,5)P2, and it is possible that other protein assemblies could perform this function as well[21]. $v_{45\rightarrow 0}$ represents the opposite reaction, which is catalysed by synaptojanins, which are phosphatases that have both a 5-phosphatase domain and a suppressor of actin 1 (SAC1) domain. Balla[11] and Hsu[22] speculate that the 5-phosphatase domain can transform $PI(4,5)P_2$ into PI(4)P by feeding the SAC1 domain, which dephosphorylates PI(4)P, into PI. Although $v_{0\rightarrow 45}$ and $v_{45\rightarrow 0}$ are based on molecular mechanisms that are not generally accepted, their inclusion in the model turned out to be necessary for the maintenance of the $PI(4,5)P_2$ pool when the level of PI(4)P is low. The inclusion of $v_{4\rightarrow 34}$ has been suggested by Sasaki[10], Shewan and Mostov[3]. Di Paolo and De Camilli [2] reported the existence of both $v_{4\rightarrow 34}$ and $v_{34\rightarrow 4}$.

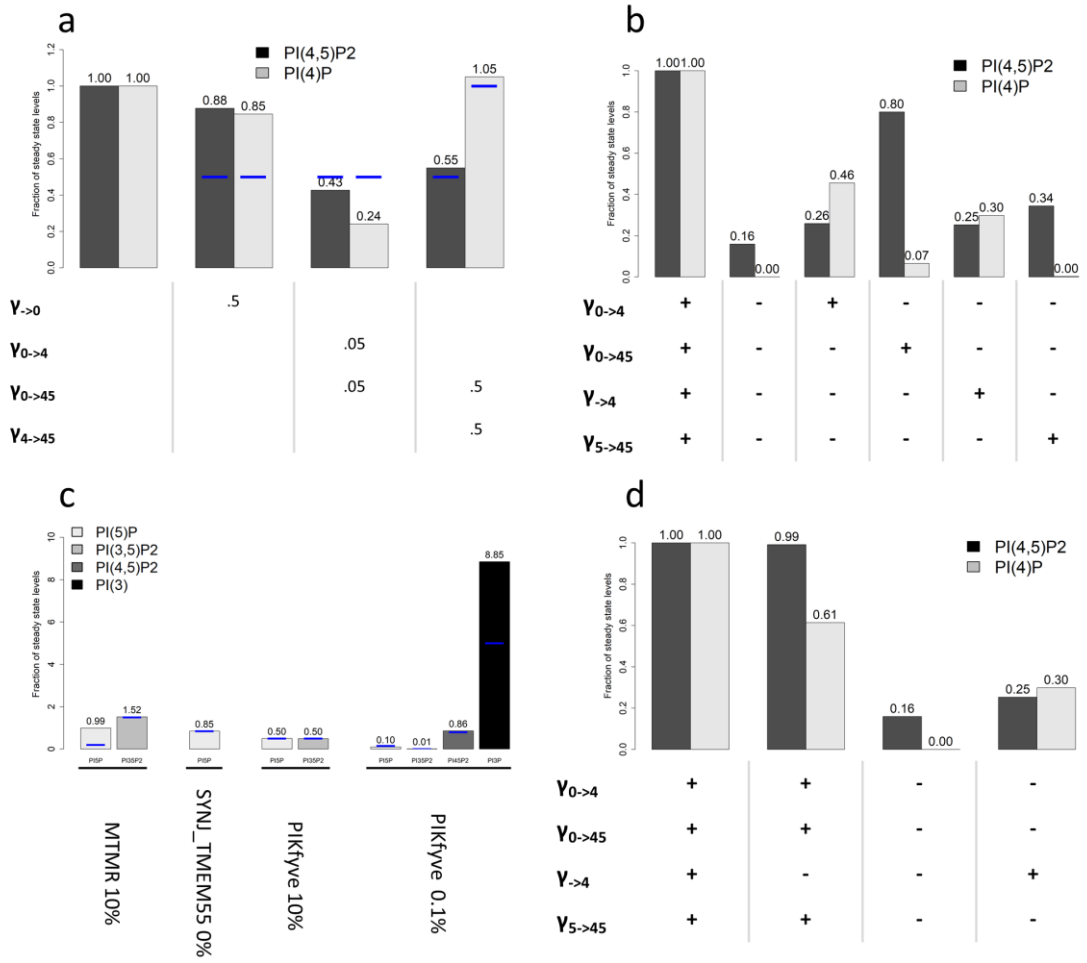

Figure 2.3. Perturbations to the phosphoinositide pathway.

Blue lines represent experimental observations and bars represent model predictions. **a)** Perturbation of PI levels, PI4K and PI5KI activities and resulting effects in PI(4,5)P_2 and PI(4)P. $\gamma_{\rightarrow 0}$ is decreased to 50% to trigger a decrease of 50% in PI. **b)** Perturbation of input fluxes to the levels of PI(4)P and PI(4,5)P_2. After stopping all inputs into PI(4)P and PI(4,5)P_2, the inputs are re-activated, one at a time, to test if they are sufficient to restore PI(4,5)P_2 levels. Enzyme knockouts were simulated by setting the rate constant of the corresponding flux to zero, except for $\gamma_{0\rightarrow 4}$, which was decreased to 20% of its original value, in order to avoid numerical errors in the simulation due to very small levels of PI(4)P. **c)** Perturbations to MTMR, SYNJ_TMEM55 and PIKfyve that were used to fit the model to the behaviour of phosphoinositides with small pools: PI5P, PI(3,5)P_2 and PI(3)P. **d)** Consequences of Golgi PI(4)P input ($\gamma_{\rightarrow 4}$) for the levels of PI(4)P and PI(4,5)P_2 pools. Golgi PI(4)P has a significant impact on the PI(4)P pool but barely affects the PI(4,5)P_2 pool. The graphs were created in R[26] and the x axis labels were added with PowerPoint.

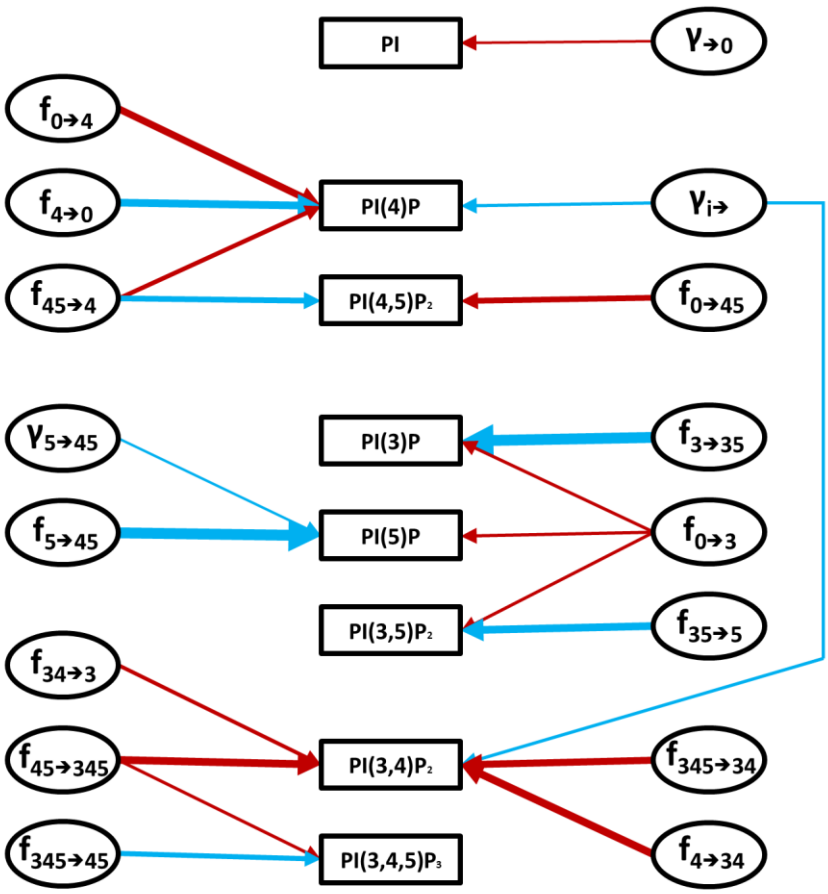

Figure 2.4. High-sensitivity network.

Arrows represent amplifying sensitivities with absolute magnitude greater than 1. Red and blue arrows represent positive and negative sensitivities, respectively. The thickness of each arrow is proportional to the magnitude of the corresponding sensitivity.

2.3.1. Consistency of the Model with Data

As described in the *Methods* section, model equations were formulated according to Biochemical Systems Theory (BST)[23], [24]. Initial parameter estimates were derived from the literature and from the BRENDA database[25]. The parameter values were subsequently optimized with a genetic algorithm such that the model matched reported phosphoinositide steady-state levels (Supplementary Table 2.1) and dynamic phenomena reported in the literature (Figure 2.3 a,c and Supplementary Table 2.2). This model successfully mimics steady-state levels and 11 out of 13 observed phenomena. The observations that were not replicated are: 1) when the PI levels are reduced, the

drop in $PI(4,5)P_2$ levels is not as evident as reported in the literature (Figure 2.3a); and 2) the knockout of myotubularin MTMR2 effects are only partially replicated (Figure 2.3c).

2.3.2. Model sensitivities

The profile of model sensitivities is a double-edged sword. On the one hand, high sensitivities make the model susceptible to unreasonable responses from small perturbations or noise. On the other hand, if the system has a signalling function, small signals must be amplified to have appropriate effects. The model presented here has a stable steady state that is mostly insensitive to parameter changes (Supplementary Table 2.8). In fact, the system is robust even to large changes in parameter values (Supplementary Figure 2.8). At the same time, the model does exhibit clusters of high sensitivities that are associated with signalling compounds, which one should expect (Figure 2.4).

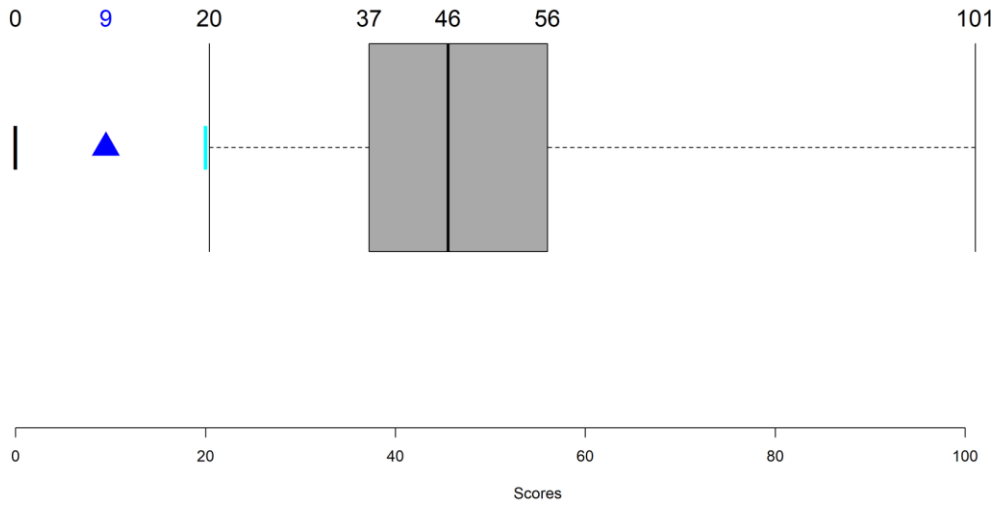

Figure 2.5. Sum of squared errors for parameter sets detected through Monte-Carlo exploration of the parameter space.
All parameter sets shown comply with the following conditions: 1. phosphoinositide steady-state levels are within the intervals retrieved from the literature; 2. the relative amounts between the phosphoinositide pools match the data; 3. influxes are less than 25% of the corresponding phosphoinositide pools; 4. effluxes are less than 7% of the corresponding phosphoinositide pools. The black bar at zero represents the score of a perfect model, the best set found by the genetic algorithm is shown as a blue triangle and the manually found set is the cyan bar. The boxplot concerns the 116 admissible alternative parameter sets. Figure created in R [26].

2.3.2.1. Analysis of low sensitivities and parameter identifiability

Even though most sensitivities are low, one must question how many of the parameters are actually identifiable. To address this question, we performed a Monte Carlo search of the parameter space, which revealed that only 166 out of 79,993 parameter sets tested yield correct steady-state levels (less than 0.15%), given an acceptable material influx into the pathway. All of these 166 solutions have a worst adjustment score than the manually fitted set and the set found with a genetic algorithm (Figure 2.5). These results suggest that the model parameterization is sufficiently specific, given the available experimental information.

2.3.2.2. High-sensitivity sub-networks

The pairs of model variables and parameters with high sensitivities (Figure 2.4) form a network that clusters into four groups around: 1) PI, which is the source of the phosphoinositides; 2) PI(4)P and $PI(4,5)P_2$, which are responsible for plasma membrane identification and $PI(4,5)P_2$ maintenance; 3) the small lipids pools (PI(3)P, PI(5)P and $PI(3,5)P_2$); and 4) $PI(3,4,5)P_3$ and its derivate $PI(3,4)P_2$.

This high-sensitivity network is reflected in a map of parameters that are best poised to serve as "master regulators" for controlling the variables in the different groups. For example, an increase in the levels of $PI(3,4,5)P_3$ and $PI(3,4)P_2$ is most easily accomplished by altering the kinetic order in the flux $V_{45\rightarrow345}$. An increase in $V_{345\rightarrow45}$ elicits a reduction of $PI(3,4,5)P_3$, which highlights the importance of PI3KI and PTEN for this part of the pathway. If simultaneous increases in the levels of the three phospholipids PI(3)P, PI(5)P and $PI(3,5)P_2$ are required, a researcher should boost $V_{0\rightarrow3}$. As an alternative, he could decrease each phospholipid independently manipulating the respective consumption fluxes.

2.3.3. New Insights into the Phosphoinositide System

The model can be used to shed light on the control of the phosphoinositide pathway. Particularly pertinent insights are described in the following subsections.

2.3.3.1. $PI(4,5)P_2$ is sensitive to PI, PI4K and PIP5KI

Model simulations replicating reported experimental results demonstrate that $PI(4,5)P_2$ is sensitive to the level of PI and to the activities of phosphoinositide 4-kinase (PI4K) and phosphoinositide 4-phosphate 5-kinase (PIP5KI) (Figure 2.3a).

2.3.3.1.1. PI4K controls $PI(4,5)P_2$ levels.

According to the literature, a knockout of phosphoinositide 4-kinase (PI4K) leads to a decrease in PI(4)P and $PI(4,5)P_2$ to 50% of their basal level[27]. Decreasing PI4K will cause not only the decrease of $v_{0\rightarrow4}$ but also $V_{0\rightarrow45}$ because this kinase is part of the protein complex that catalyses $V_{0\rightarrow45}$. The model mimics this phenomenon for $PI(4,5)P_2$ although it predicts a more severe drop in the levels of PI(4)P.

2.3.3.1.2. PIP5KI controls $PI(4,5)P_2$ levels.

One strategy for reducing $PI(4,5)P_2$ levels is to decrease the amount of PIP5KI. This mechanism is probably viable *in vivo* because a single allele of the *PIP5KI*γ gene is sufficient to sustain life in mice embryos, whereas knock-out PIP5KIγ mice die shortly after birth[28]. The same study also showed that α and β genes are not necessary to maintain viability, and their roles are still unclear. Volpicelli-Daley *et al.*[28] furthermore reported that $PI(4,5)P_2$ levels drop around 50% in PIP5KIγ KO mice. Decreasing the activities of PIP5KI ($E_{4\rightarrow45}$) and PI4K/PIP5KI ($E_{0\rightarrow45}$) to 50% in the model, reduces $PI(4,5)P_2$ to roughly 50% of its basal level.

2.3.3.1.3. PI controls $PI(4,5)P_2$ levels.

Kim[29] reported that a 50% drop in the PI pool causes a similar decrease in $PI(4,5)P_2$ levels. $PI(4,5)P_2$ in the model is sensitive to a reduction in PI but does not drop as much as reported in the literature. Specifically, a 50% drop in PI will only lead to a reduction of 11% in $PI(4,5)P_2$. A 50% drop of PI in the whole cell would also affect other membrane compartments responsible for the production of PI(3)P and PI(4)P. To include this effect, we closed $v_{\rightarrow4}$ and $v_{\rightarrow3}$. However, this intervention decreases $PI(4,5)P_2$ only to 88% of its basal level. Interestingly, PI(4)P drops to 47%. To achieve a 50% drop in the $PI(4,5)P_2$ pool we would have to shut down $v_{\rightarrow4}$ and $v_{\rightarrow3}$ completely and reduce the influx of PI,$v_{\rightarrow0}$, to 2% of its original value.

2.3.3.2. $PI(3,4,5)P_3$ levels are sensitive to the concentrations of PTEN and PI3KI

PTEN has been known to be a tumour suppressor for almost twenty years[11]. This phosphatase hydrolyzes the third position of the phosphoinositide inositol ring in $PI(3,4,5)P_3$ into $PI(4,5)P_2$ and, to a lesser degree, in $PI(3,4)P_2$ into PI(4)P [1], [10], [11]. PI3KI phosphorylates the third position of the inositol ring of $PI(4,5)P_2$ into $PI(3,4,5)P_3$, thereby catalysing the inverse reaction of PTEN. This kinase is known to control the cell energetic state and metabolism and thus playing a key role in tumorigenesis[11]. Bryant and Mostov[1] reported that $PI(3,4,5)P_3$ is present at the basolateral membrane, but absent in the apical part, of polarized epithelial cells. PTEN and PI3K are believed to be responsible for this difference. PTEN is present in the apical part and at the tight junctions, where it transforms $PI(3,4,5)P_3$ into $PI(4,5)P_2$. By contrast, PI3K is located in the basolateral part of the membrane and catalyses the opposite reaction from $PI(4,5)P_2$ to $PI(3,4,5)P_3$.

2.3.3.2.1. Regulation of PTEN and PI3KI.

Cell polarization is highly regulated through mechanisms involving PTEN, PI3K, $PI(4,5)P_2$ and $PI(3,4,5)P_3$[18], [30], [31]. We investigated to what degree high activity of PTEN (2.3e-15 mg/μm^2) and low activity of PI3KI (6.1e-16 mg/μm^2) are sufficient to deplete $PI(3,4,5)P_3$ to about 2 molecules/μm^2 and thereby mimic the apical membrane configuration. Conversely, we asked if low PTEN (3.9e-17 mg/μm^2) and high PI3KI (1.5e-14 mg/μm^2) could replicate the basolateral membrane configuration, which is rich in $PI(3,4,5)P_3$ (760 molecules/μm^2). Interestingly, model simulations readily mimicked both membrane configurations, which suggests that the model is a satisfactory approximation of the observed phenomena characterizing epithelial and basolateral membrane states (Figure 2.6).

2.3.3.2.2. Flux $v_{345\rightarrow34}$ modulates the effects of PTEN.

If the flux $v_{345\rightarrow34}$ is accelerated to values close to those ones described in the literature for SH2 domain-containing phosphatidylinositol 5-phosphatase (SHIP1), the model predicts a decrease in $PI(3,4,5)P_3$. The surprising consequence of this prediction is that this decrease will lock the membrane in a basal-like configuration and that a knockdown of PTEN will no longer increase $PI(3,4,5)P_3$ (Figure 2.6).

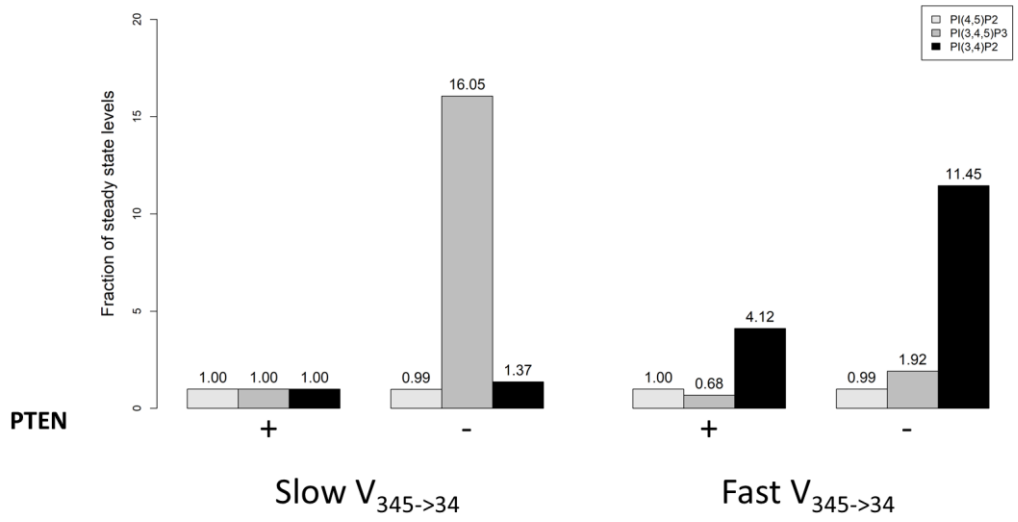

Figure 2.6. PI(3,4,5)P3 is sensitive to PTEN when $v_{345\rightarrow34}$ is slow.

A decrease in PTEN is sufficient to increase the levels of $PI(3,4,5)P_3$ and change the membrane configuration form apical (low $PI(3,4,5)P_3$) to basolateral (high $PI(3,4,5)P_3$). A fast $v_{345\rightarrow34}$ will decrease $PI(3,4,5)P_3$ and make the membrane much less sensitive to a PTEN change. A PTEN knockdown of 98.33% does not alter the amount of $PI(4,5)P_2$ in either fast or slow $v_{345\rightarrow34}$ conditions. Fast $v_{345\rightarrow34}$ increases the levels of $PI(3,4)P_2$ and makes the levels of this lipid dependent on the $PI(3,4,5)P_3$ pool. Slow $v_{345\rightarrow34}$ is modelled as $\gamma_{345\rightarrow34} = 1e11$ and $f_{345\rightarrow34} = 0.9982$. Fast $v_{345\rightarrow34}$ is modelled as $\gamma_{345\rightarrow34} = 6e13$ and $f_{345\rightarrow34} = 0.9998$. Rate constants are in molecules^{1-g} μm^{2g}/min or μm^2/min/mg where ^{g} is the kinetic order of the corresponding variable, kinetic orders are dimensionless. The graph was created in R42 and the x axis labels were added with PowerPoint.

2.3.3.3. Control of $PI(4,5)P_2$ levels

The proposed model is a powerful tool for exploring how the cell controls the phosphoinositide levels in its cell membrane. Due to the multiple functions of $PI(4,5)P_2$, including ion channel activity regulation, cell polarization, and signalling, the control of this phosphoinositide is of particular relevance.

$PI(4,5)P_2$ can be synthesized from three phosphoinositide species in addition to PI (through $v_{0\rightarrow45}$), namely PI(4)P, PI(5)P and $PI(3,4,5)P_3$ (Figure 2.1). $PI(3,4,5)P_3$ is present in low concentrations and transformed into $PI(4,5)P_2$ mainly by the phosphatase PTEN. The cellular location of this enzyme is tightly regulated, as it is located in non-

polarized cells in the cytosol and nucleus most of the time[32]. PI(5)P also exists as a small pool and its role is not clearly understood. That leaves PI(4)P as the only reasonable candidate for maintaining $PI(4,5)P_2$ levels, besides PI. PI(4)P is a substrate for the kinase PIP5KIγ and has a physiological concentration roughly similar to $PI(4,5)P_2$ pool, *i.e.*, around 10,000 molecules/μm^2. However, it has been observed that $PI(4,5)P_2$ levels can be maintained even with low PI(4)P levels[11], [27]. Figure 2.3b shows the changes in PI(4)P and $PI(4,5)P_2$ levels predicted by the model when different sources are perturbed.

2.3.3.3.1. Contribution of $v_{0\rightarrow45}$ to $PI(4,5)P_2$ levels.

The flux $v_{0\rightarrow45}$ represents the direct transformation of PI into $PI(4,5)P_2$ by means of a ternary complex of proteins containing PI4K and PIP5KI[20]. The model suggests that $v_{0\rightarrow45}$ alone can maintain 80% of the basal level of $PI(4,5)P_2$, thereby making it the main source of $PI(4,5)P_2$ (Figure 2.3b). This direct transformation of PI into $PI(4,5)P_2$ should exist to ensure the stability of the $PI(4,5)P_2$ pool, and reports in the literature[20], [33] seem to support this finding.

2.3.3.3.2. Contribution of PI(4)P influx to $PI(4,5)P_2$ levels.

The flux $v_{\rightarrow4}$ represents the amount of PI(4)P coming from the Golgi through vesicle trafficking or non-vesicle transfer (Figure 2.2), which has been reported to constitute a sizeable contribution to the maintenance of plasma membrane PI(4)P, but contributes only moderately to the maintenance of $PI(4,5)P_2$[33], [34]. Indeed, the model simulations show that $v_{\rightarrow4}$ by itself can maintain PI(4)P at 30% of its basal level and only generates a 9% increase in the $PI(4,5)P_2$ pool (Figure 2.3d).

2.3.3.3.3. Contribution of PI(5)P to $PI(4,5)P_2$ levels.

The flux $v_{5\rightarrow45}$ can maintain the $PI(4,5)P_2$ pool at 34% of its basal level (Figure 2.3b). However, the influence of this flux is highly dependent on $v_{\rightarrow3}$. If $v_{\rightarrow3}$ increases 25 times, which makes this input flux similar to the one for PI(4)P, $v_{5\rightarrow45}$ can sustain $PI(4,5)P_2$ levels at 71%. If $v_{\rightarrow3}$ increases 50 times, $v_{5\rightarrow45}$ can sustain 100% of $PI(4,5)P_2$. This result suggests that PI(5)P may have an influential role in the maintenance of $PI(4,5)P_2$ levels and function as a means of channelling material from PI(3)P toward the linear pathway of PI(4)P, $PI(4,5)P_2$ and $PI(3,4,5)P_3$.

Taken together, these results suggest that the cell employs at least four mechanisms to maintain adequate $PI(4,5)P_2$ levels. This level of redundancy highlights the importance of $PI(4,5)P_2$. Indeed, $PI(4,5)P_2$ is known as a characteristic component of the cell membrane[11], [27], and it is to be expected that down-regulation of $PI(4,5)P_2$ levels would interfere with the proper functioning of the proteins in the membrane. Compromising these proteins, in turn, would have a negative impact on fundamental processes, such as cellular nutrient intake, information sensing, chemical messaging and the secretion of waste.

2.3.4. Therapeutic Targets for the Modulation of ENaC Activity in CF

The components of the phosphoinositide pathway, and $PI(4,5)P_2$ in particular, are involved in numerous physiological processes, and our model has the potential to deepen our understanding in many of these areas. One specific motivation for us to develop this model was to explore the role of the phosphoinositide pathway in the modulation of the epithelial Na+ channel (ENaC) activity in the lung tissue of patients with CF. ENaC is a sodium and water channel whose activity is upregulated in CF. It is well established that $PI(4,5)P_2$ promotes ENaC activity[11], [35]. We have also previously identified the phosphoinositide pathway to be a key regulator of ENaC[13] . Indeed, performing an siRNA screen in the CF context using a microscopy-based live-cell assay, we identified 30 enzymes in the phosphoinositide pathway as significant modulators of ENaC activity. We performed independent siRNA knockdowns of phosphoinositide enzymes and re-evaluated ENaC activity with the same live-cell assay. Assuming that if a siRNA increases $PI(4,5)P_2$ it will enhance ENaC activity, we compared ENaC activity results (Supplementary Table 2.10) with model predictions of an siRNA effect on $PI(4,5)P_2$.

Our model predictions are consistent with four out of five siRNA assays targeting phosphoinositide kinases. As these assays were not used to calibrate model parameters, this agreement of model predictions with experimental observations supports the validity of our model. Furthermore, model simulations allow us to check if the tested siRNA perturbations may have undesirable side effects on the steady-state profile of the pathway, which were not observable in the original experiments. The results for specific pathway perturbations are discussed in the next sections.

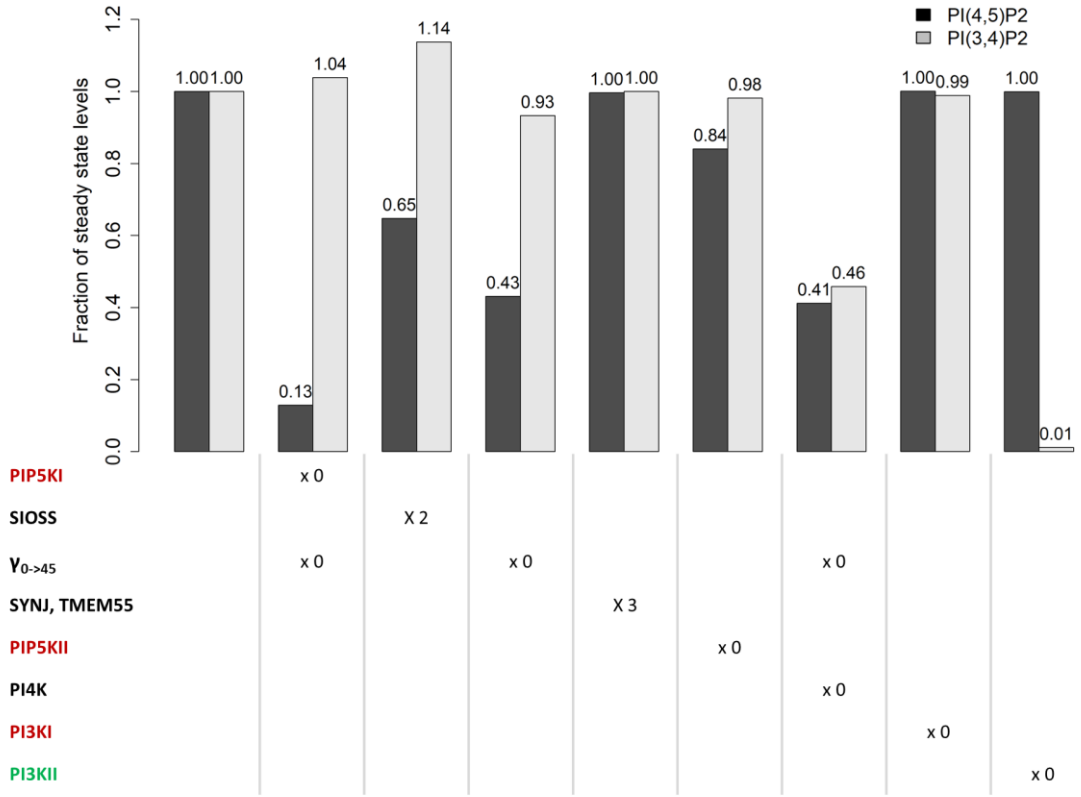

Figure 2.7. Predicted changes in PI(4,5)P2 and PI(3,4)P2 levels as a consequence of siRNA knockdown assays.

Each kinase is inactivated, one at the time, and phosphatases are upregulated. The protein complex catalysing $v_{0\rightarrow45}$ is composed of PIP5KI and PI4K; therefore, when one of these enzymes is knocked out, the complex should be also knocked out. There is also the possibility of knocking out only the complex. Enzymes are coloured according to the classification in the siRNA screens: enzymes activating ENaC are marked red, those inhibiting ENaC are marked green and those exhibiting both effects are marked black. The graph was created in R[26] and the x axis labels were added with PowerPoint.

2.3.4.1. PIP5KI

The most direct and effective way to decrease $PI(4,5)P_2$ levels is by decreasing PIP5KI ($E_{4\rightarrow45}$ and $E_{0\rightarrow45}$) or enhancing the 5-phosphatases of the SIOSS enzyme group that hydrolyse the fifth position of $PI(4,5)P_2$ ($E_{45\rightarrow4}$). It is documented in the literature that decreasing PIP5KI will significantly affect $PI(4,5)P_2$ levels[28]. The model predicts that a knock-out of PIP5KI will trigger a decrease in $PI(4,5)P_2$ to 13% of its basal steady state (Figure 2.7). The performed siRNAs validation tests corroborate the model prediction (Supplementary Table 2.10).

An alternative to trigger the decrease in $PI(4,5)P_2$ levels is to increase the activity of 5-phosphatases in the SIOSS enzyme group. Doubling the activity of this phosphatase group in the model results in a 35% decrease in $PI(4,5)P_2$ (Figure 2.7). Both our previous dataset[13] and results from the new siRNAs validation tests included in the present study (Supplementary Table 2.10) are not as conclusive about the SIOSS phosphatases, as for most of the phosphatases tested, which could be a consequence of the unspecific activity that characterizes phosphatases. For example, synaptojanins catalyse several reactions in the pathway and perturbing them would probably cause unexpected side effects.

2.3.4.2. PI4K

A PI4K knockout affects the fluxes $v_{0\rightarrow4}$ and $v_{0\rightarrow45}$. It decreases $PI(4,5)P_2$ in 59% (Figure 2.7). Accordingly, the model suggests that PI4K should be classified as an ENaC activating gene, which is in line with our previous observations[13]. An undesirable side effect within these model predictions is the change of the $PI(3,4)P_2$ concentration, a lipid involved in clathrin-coated vesicle formation and activation of AKT. According to the model, this perturbation would cause a 54% decrease in the level of $PI(3,4)P_2$.

2.3.4.3. PI4K, PIP5KI and DVL protein complex

A knockout of the protein complex formed by PI4K, PIP5KI and segment polarity protein dishevelled homolog (DVL) (PI4K+PIP5KI+DVL, $E_{0\rightarrow45}$), which transforms PI directly into $PI(4,5)P_2$, causes a 57% decrease in this lipid (Figure 2.7). This perturbation also causes a 7% decrease in the levels of $PI(3,4)P_2$. The PI4K+PIP5KI+DVL protein complex is formed upon wingless-Type MMTV Integration Site Family, Member 3A (Wnt3a) stimulation. The possibility of targeting the segment polarity protein Dishevelled homolog DVL (DVL) to suppress the formation of the protein complex is interesting because it would avoid interfering with other reactions in the pathway.

2.3.4.4. PIP5KII and SYNJ/TMEM55

An increase of SYNJ/TMEM55 ($E_{45\rightarrow5}$) phosphatases and a decrease of the kinase PIP5KII ($E_{5\rightarrow45}$) could decrease $PI(4,5)P_2$ (Figure 2.7). The model predicts that

SYNJ/TMEM55 has a negligible effect, which is consistent with the literature[11] and our previous data[13] concerning synaptojanins. However, no phosphatases belonging to the TMEM55 group were screened in the Almaça *et al.* study. Knocking out PIP5KII reduces the pool of $PI(4,5)P_2$ by 16%. PIP5KII was classified as an ENaC enhancer in both our previous screens[13] and in the present siRNA validation tests (Supplementary Table 2.10), in agreement with the model prediction. Altering PIP5KII function only causes a 2% decrease in PI(3,4)P2, however perturbing PIP5KII activities could have unforeseen consequences since the role of PI(5)P is not clearly understood and the flux catalyzed by PIP5KII, $v_{5\rightarrow45}$, is the main efflux for the PI(5)P pool.

2.3.4.5. PI3KI and PI3KII

The model predicts that $PI(4,5)P_2$ levels are insensitive to knockouts of PI3KI and PI3KII. We previously classified PI3KI as an ENaC activating gene[13], and this is corroborated here by the siRNA validation tests. The PI3KI knockdown increases the level of $PI(4,5)P_2$ if the model parameters are configured to reproduce a basolateral-like membrane composition (enriched in $PI(3,4,5)P_3$). At the same time, this simulated PI3KI knockdown decreases $PI(3,4,5)P_3$ levels, which is also known to control ENaC[11]. One should note that in polarized cells ENaC localizes to the apical part of the membrane which contains neither $PI(3,4,5)P_3$ nor PI3KI. Therefore, the effect of PI3KI on ENaC may only be observable in non-polarized cells.

The model predicts a negligible influence of PI3KII on $PI(4,5)P_2$ and $PI(3,4,5)P_3$ but causes an almost complete depletion of $PI(3,4)P_2$. We previously[13] classified PI3KII as an ENaC inhibiting gene. If this is so, the model suggests that this inhibition could be caused by the depletion of $PI(3,4)P_2$ or components not belonging to the phosphoinositide pathway.

2.4. Discussion

In this work, we developed a new mathematical model that captures the complex metabolic network of phosphoinositides. The proposed model successfully replicates the phosphoinositide metabolite levels in mammalian cells and reflects numerous observed phenomena. The model is also able to reproduce the differentiation of the cell membrane into apical and basolateral types.

Using model simulations we were able to dissect the control of the levels of $PI(4,5)P_2$, for which the low abundant phosphoinositide PI(5)P seems to have a significant role as an alternative source. This finding was not detectable in previous models of the pathway, due to their simplifying assumptions.

The results obtained here are of potential interest for a variety of physiological conditions, because the different phosphoinositides play uncounted roles in lipid signalling and membrane dynamics. Of particular interest to us was the fact that the model was helpful in explaining observed effects in a siRNA screen of ENaC modulators in CF. Namely, the model suggested targeting the enzyme that catalyses $v_{4\rightarrow45}$, PIP5KI, as the most effective way to decrease the levels of $PI(4,5)P_2$. Targeting PI4K would also reduce $PI(4,5)P_2$ levels significantly, but model simulations point to a possible undesired side effect, namely, the simultaneous reduction of $PI(3,4)P_2$ levels. Targeting the PI4K+PIP5KI+DVL protein complex does not significantly alter other lipids (Supplementary Figure 2.9) while yielding a large $PI(4,5)P_2$ reduction. Because this reduction is not as extensive as the one induced by PIP5KI targeting, it may moderate ENaC activity without drastic negative effects in the activity of other proteins regulated by $PI(4,5)P_2$.

The model also suggests that, in order to replicate phenomena retrieved from the literature, $v_{0\rightarrow45}$ should be the main flux producing $PI(4,5)P_2$. In particular, this flux may explain the maintenance of $PI(4,5)P_2$ levels when the levels of PI(4)P are low. This result suggests the importance of a close functional relationship between PI4K and PIP5KI. This relationship does not imply that the two kinases must be in physical proximity through this particular protein complex[20]. They may also work in close proximity within lipid raft-like structures, for example.

The coupling of PI4K and PIP5KI activities may define two configurations of the system. One, where the two kinases are working together closely, in which case they are more sensitive to alterations in PI and in the levels of PI4K. The other configuration is more robust in terms of $PI(4,5)P_2$ levels, where the bulk of this phosphoinositide is created through PI(4)P.

Of course, the model could be improved in the future when new experimental data regarding phosphatases and higher parameter precision are available, but this

information is much scarcer than that of kinases. For instance, it is unclear how exactly phosphatases act on the system. Their versatility may suggest the existence of competitive inhibition among their substrates, but this competition could cause substrate coupling, when all substrates of a phosphatase are influenced by the alteration of a single substrate, especially if the phosphatase is saturated[36].

Along the same lines, some kinases catalyse multiple reactions. It would thus make sense to consider substrate competition at a more general level. In preliminary studies, we already considered substrate competition, but did not detect significant differences in model behaviours.

Although the model is quite robust, it has few shortcomings. For instance, we estimated values for the parameters $\gamma_{5\rightarrow45}$, $f_{5\rightarrow45}$, $\gamma_{3\rightarrow35}$ and $\gamma_{35\rightarrow5}$, which differed somewhat from literature reports, in order to replicate the levels of PI(5)P and PI(3,5)P_2. Also, not all phenomena were fully replicated by the model: PI(4,5)P_2 did not decrease proportionally to PI, and when MTMR was reduced to 65% (simulating the knockout of MTMR2), PI(5)P did not drop to 20%, only to 98.97%. These discrepancies could be due to gaps in the information about the system. In particular, most of the quantitative data address the total cell and are not membrane specific. Also, *in vitro* experimental results used to parameterize the model may not truly replicate the system behaviour *in vivo*.

The current model does not incorporate some regulatory mechanisms which nevertheless may be implemented in future versions. For instance, Bulley *et al.*[37] report the activation of PTEN and PI3KI by their own products, as well as activation of myotubularins and PTEN, and inhibition of SHIP by PI(5)P.

Finally, because the phosphoinositide pathway acts differently in different organelle membranes[2], it could be interesting to model not only a cell membrane patch but also the membranes of the Golgi, nucleus and the endoplasmic reticulum with a multiple compartment model featuring lipid transport between them (Figure 2.2).

In spite of these simplifications, the proposed model is the first to successfully replicate phosphoinositide metabolism in the mammalian cell membranes. In contrast to earlier models, the model accounts for all known phosphoinositide species and permits unprecedented explorations of the roles of those phosphoinositide's that are

physiologically present in small amounts. The current model, as it is designed, focuses on a single, very small membrane patch of one particular compartment, the plasma membrane, and is not really geared to describe analyses of multiple compartments. One reason is that we simply do not have sufficient metabolic information about fluxes between compartments. If this information were available, we could "multiply" our model several times, eliminate those reactions that are not present in any specific sub-model and use the inter-compartmental fluxes to connect these models.

The model was used to identify the best approaches to control $PI(4,5)P_2$ levels with the goal of establishing new therapeutic targets in the context of CF. The model suggests that the most effective way to accomplish this goal is to decrease the activity of the enzyme PIP5KI ($v_{4\rightarrow45}$). Additionally, $v_{0\rightarrow45}$ was also found to be very important in the maintenance of $PI(4,5)P_2$ levels. Targeting proteins that are part of the protein complex of PI4K, PIP5KI and DVL or contribute to its control should offer an effective way to control $PI(4,5)P_2$ levels.

In this work, we tried to arrange the current knowledge on the phosphoinositide pathway into a coherent structure. This is an important tool into the understanding of a complex layer of cell regulation that is usually overlooked and can impact fields of study with great potential to improve the human well-being like CF and cancer.

2.5. Methods

2.5.1. Model Equations

A dynamical model of phosphoinositide metabolism was designed within the framework of Biochemical Systems Theory (BST)[24], [38]–[42], using ordinary differential equations (ODEs) in the format of a generalized mass action (GMA) system. In this approach, each ODE describes the dynamics of a dependent variable X_i, which is formulated as a sum of all fluxes that are directly related to this variable; furthermore, each flux $v_{i\rightarrow j}$ is formulated as a power law function, as indicated in equation (2.1).

$$\frac{dX_i}{dt} = \sum_{s=1}^{n+m} v_{s\rightarrow i} - \sum_{p=1}^{n+m} v_{i\rightarrow p} \qquad (2.1)$$
$$v_{i\rightarrow j} = \gamma_{i\rightarrow j} \cdot E_{i\rightarrow j} \cdot X_i^{f_{i\rightarrow j}}$$

n and m represent the number of dependent and indepented variables. The dependent variables (X_i) represent the actual numbers of phosphoinositide molecules (X_3: PI(3)P; X_4: PI(4)P; X_5: PI(5)P; X_{34}: PI(3,4)P_2; X_{35}: PI(3,5)P_2; X_{45}: PI(4,5)P_2; and X_{345}: PI(3,4,5)P_3), and of PI (X_0: PI) in a membrane patch of size 1μm^2. If more than one substrate contributes to the reaction, or if the reaction is modulated by other variables, the flux term in (2.1) contains these contributors as additional X's with their own powers. Because all modelled reactions transform one molecule of some phosphoinositide species into one molecule of another phosphoinositide species, all stoichiometric coefficients are 1 and Eq. (2.1), therefore, does not explicitly show these coefficients. Kinase catalysed reactions consume ATP and produce ADP, while phosphatase catalysed reactions consume H_20 and produce one phosphate ion. These four metabolites were considered to be available in sufficient quantities and not to affect reaction rates.

The model accounts for fluxes transporting PI ($v_{\rightarrow 0}$), PI(4)P ($v_{\rightarrow 4}$) and PI(3)P ($v_{\rightarrow 3}$) into the membrane from the ER, Golgi and endosome, respectively. Additionally, all included species were allowed to be transported out of the membrane via fluxes $v_{i\rightarrow}$. We assume that these effluxes follow first-order kinetics ($f_{i\rightarrow} = 1$) and share one common rate constant. The input flux values were restricted in order to allow 4.5% of the membrane phosphoinositides to recycle per minute (see *Supplementary Information*). Both influxes and effluxes represent transport of lipids that enters or exits the plasma membrane by vesicle- or non-vesicle-mediated transport. The latter can be mediated by specialized proteins like LTP's or occur spontaneously at membrane contact sites.

2.5.2. Parameter Estimation

Rate constants ($\gamma_{i\rightarrow j}$) and kinetic orders ($f_{i\rightarrow j}$) were derived from enzyme kinetic parameters obtained in BRENDA or in the literature, as detailed in the *Supplementary Information*. Enzyme activities ($E_{i\rightarrow j}$) and transport fluxes where manually set to approximate reported phosphoinositide steady-state values. This manually adjusted parameter set was used as an initial input for a genetic algorithm (detailed in *Supplemental Information*). This algorithm found a parameter set that minimized the deviations between model predictions and experimental observations and computing an adjustment score. The parameterized model was characterized through sensitivity

and identifiability analysis, and the parameter space was explored with a Monte-Carlo approach (see *Supplemental Information*).

2.5.3. Model Implementation

The model was implemented in the programming language R v3.1.0 [26] together with the package deSolve [43]. We used the ODE integration function with the LSODA method. Figures 2.1, 2.2 and 2.4 were created in MS PowerPoint, Figure 2.5 and 2.8 were created in R[26] and finally 2.3, 2.6, 2.7 and 2.9 were created in R[26] and modified in WS PowerPoint.

2.5.4. Code Availability

The R code is available in GITHUB at the following URL:

https://github.com/dolivenca/MK15_phosphoinositide_pathway_model

2.5.5. siRNA knockdown validity test

To confirm model predictions, selected phosphoinositide pathway hits identified in a large scale siRNA screen[13] were validated with an independent round of siRNA knockdown assays. Human alveolar type II epithelial A549 cells (ATCC, Cat no. CCL-185) were transfected with 2 or 3 different siRNAs targeting phosphoinositide pathway enzymes. After transfection the FMP/Amiloride live-cell assay[13] was applied to measure ENaC activity. Detailed methods and analysis are described in the *Supplementary Information*.

2.5.6. Data Availability

All data generated or analysed during this study are included in this published article. Please see Supplementary Table 2.10 in the *Supplementary Information* file.

2.6. References

[1] D. M. Bryant and K. E. Mostov, “From cells to organs: building polarized tissue.,” *Nat. Rev. Mol. Cell Biol.*, vol. 9, no. 11, pp. 887–901, 2008.

[2] G. Di Paolo and P. De Camilli, “Phosphoinositides in cell regulation and membrane dynamics.,” *Nature*, vol. 443, no. 7112, pp. 651–657, 2006.

[3] A. Shewan, D. J. Eastburn, and K. Mostov, “Phosphoinositides in cell architecture,” *Cold Spring Harb. Perspect. Biol.*, vol. 3, no. 8, pp. 1–17, 2011.

[4] A. Gericke, N. R. Leslie, M. Lösche, and A. H. Ross, “PtdIns(4,5)P2-mediated cell signaling: Emerging principles and PTEN as a paradigm for regulatory mechanism,” *Adv. Exp. Med. Biol.*, vol. 991, pp. 85–104, 2013.

[5] T. Balla, “Regulation of Ca2+ entry by inositol lipids in mammalian cells by multiple mechanisms,” *Cell Calcium*, vol. 45, no. 6, pp. 527–534, 2009.

[6] G. L. Dornan, J. A. McPhail, and J. E. Burke, “Type III phosphatidylinositol 4 kinases: structure, function, regulation, signalling and involvement in disease,” *Biochem. Soc. Trans.*, vol. 44, no. 1, pp. 260–266, 2016.

[7] H. Currinn and T. Wassmer, “The amyloid precursor protein (APP) binds the PIKfyve complex and modulates its function.,” *Biochem. Soc. Trans.*, vol. 44, no. 1, pp. 185–90, 2016.

[8] L. E. Rameh and J. T. Deeney, “Phosphoinositide signalling in type 2 diabetes: a -cell perspective,” *Biochem. Soc. Trans.*, vol. 44, no. 1, pp. 293–298, Feb. 2016.

[9] M. Vicinanza, G. D ’angelo, A. Di Campli, and M. A. De Matteis, “Function and dysfunction of the PI system in membrane trafficking,” *EMBO J.*, vol. 27, no. 19, pp. 2457–2470, 2008.

[10] T. Sasaki *et al.*, “Mammalian phosphoinositide kinases and phosphatases,” *Prog. Lipid Res.*, vol. 48, no. 6, pp. 307–343, 2009.

[11] T. Balla, “Phosphoinositides: tiny lipids with giant impact on cell regulation,” *Physiol. Rev.*, vol. 93, no. 3, pp. 1019–1137, 2013.

[12] A. Narang, K. K. Subramanian, and L. D. A., “A mathematical model for chemoattractant gradient sensing based on receptor-regulated membrane phospholipid signaling dynamics.,” *Ann. Biomed. Eng.*, vol. 29, no. 8, pp. 677–691, 2001.

[13] J. Almaça *et al.*, “High-content siRNA screen reveals global ENaC regulators

and potential cystic fibrosis therapy targets," *Cell*, vol. 154, no. 6, 2013.

[14] R. C. Boucher, "Cystic fibrosis: a disease of vulnerability to airway surface dehydration," *Trends Mol. Med.*, vol. 13, no. 6, pp. 231–240, 2007.

[15] C. Xu, J. Watras, and L. M. Loew, "Kinetic analysis of receptor-activated phosphoinositide turnover," *J. Cell Biol.*, vol. 161, pp. 779–791, 2003.

[16] T. Nishioka, K. Aoki, K. Hikake, H. Yoshizaki, E. Kiyokawa, and M. Matsuda, "Rapid Turnover Rate of Phosphoinositides at the Front of Migrating MDCK Cells.," *Mol. Biol. Cell*, vol. 19, pp. 4213–4223, 2008.

[17] J. E. Purvis, M. S. Chatterjee, L. F. Brass, and S. L. Diamond, "A molecular signaling model of platelet phosphoinositide and calcium regulation during homeostasis and P2Y1 activation.," *Blood*, vol. 112, pp. 4069–4079, 2008.

[18] Y. Arai, T. Shibata, S. Matsuoka, M. J. Sato, T. Yanagida, and M. Ueda, "Self-organization of the phosphatidylinositol lipids signaling system for random cell migration," *Proc Natl Acad Sci U S A*, vol. 107, no. 27, pp. 12399–12404, 2010.

[19] A. MacNamara, F. Stein, S. Feng, C. Schultz, and J. Saez-Rodriguez, "A single-cell model of PIP3 dynamics using chemical dimerization," *Bioorg. Med. Chem.*, vol. 23, no. 12, pp. 2868–2876, 2015.

[20] Y. Qin, L. Li, W. Pan, and D. Wu, "Regulation of phosphatidylinositol kinases and metabolism by Wnt3a and Dvl," *J. Biol. Chem.*, vol. 284, no. 34, pp. 22544–22548, 2009.

[21] S. Choi and R. A. Anderson, "IQGAP1 is a Phosphoinositide Effector and Kinase Scaffold," *Adv. Biol. Regul.*, vol. 60, no. 5, pp. 29–35, 2016.

[22] F. Hsu and Y. Mao, "The Sac domain-containing phosphoinositide phosphatases: structure, function, and disease.," *Front. Biol. (Beijing).*, vol. 8, no. 4, pp. 395 – 407, 2013.

[23] E. O. Voit, *A first course in systems biology*. Garland Science,Taylor & Francis Group, 2013.

[24] E. O. Voit, “Biochemical systems theory: a review,” *ISRN Biomath.*, vol. 2013, pp. 1–53, 2013.

[25] I. Schomburg *et al.*, “BRENDA: integrated reactions, kinetic data, enzyme function data, improved disease classification.,” 2015. .

[26] R Core Team, *R: a language and environment for statistical computing*. Vienna, Austria, 2017.

[27] G. R. V. Hammond *et al.*, “PI4P and PI(4,5)P2 are essential but independent lipid determinants of membrane identity.,” *Science (80-.).*, vol. 337, no. 6095, pp. 727–730, 2012.

[28] L. A. Volpicelli-Daley *et al.*, “Phosphatidylinositol-4-phosphate 5-kinases and phosphatidylinositol 4,5-bisphosphate synthesis in the brain,” *J. Biol. Chem.*, vol. 285, no. 37, pp. 28708–28714, 2010.

[29] Y. J. Kim, M. L. Guzman-Hernandez, and T. Balla, “A highly dynamic ER-derived phosphatidylinositol-synthesizing organelle supplies phosphoinositides to cellular membranes,” *Dev. Cell*, vol. 21, pp. 813–824, 2011.

[30] M. Zhang *et al.*, “Long lasting synchronization of calcium oscillations by cholinergic stimulation in isolated pancreatic islets.,” *Biophys. J.*, vol. 95, no. 10, pp. 4676–88, 2008.

[31] A. Gassama-Diagne *et al.*, “Phosphatidylinositol-3,4,5-trisphosphate regulates the formation of the basolateral plasma membrane in epithelial cells.,” *Nat. Cell Biol.*, vol. 8, no. 9, pp. 963–970, 2006.

[32] A. Bononi and P. Pinton, “Study of PTEN subcellular localization,” *Methods*, vol. 77, pp. 92–103, 2015.

[33] E. Delage, J. Puyaubert, A. Zachowski, and E. Ruelland, “Signal transduction pathways involving phosphatidylinositol 4-phosphate and phosphatidylinositol 4,5-bisphosphate: Convergences and divergences among eukaryotic kingdoms,” *Prog. Lipid Res.*, vol. 52, no. 1, pp. 1–14, 2013.

[34] Z. Szentpetery, P. Várnai, and T. Balla, “Acute manipulation of Golgi

phosphoinositides to assess their importance in cellular trafficking and signaling.," *Proc. Natl. Acad. Sci. U. S. A.*, vol. 107, no. 18, pp. 8225–30, 2010.

[35] O. Pochynyuk, V. Bugaj, and J. D. Stockand, "Physiologic regulation of the epithelial sodium channel by phosphatidylinositides," *Curr. Opin. Nephrol. Hypertens.*, vol. 17, no. 5, pp. 533–540, 2008.

[36] M. A. Rowland, B. Harrison, and E. J. Deeds, "Phosphatase Specificity and Pathway Insulation in Signaling Networks.," *Biophys. J.*, vol. 198, pp. 986–996, 2015.

[37] S. J. Bulley, J. H. Clarke, A. Droubi, M.-L. Giudici, and R. F. Irvine, "Exploring phosphatidylinositol 5-phosphate 4-kinase function.," *Adv. Biol. Regul.*, vol. 57, pp. 193–202, Jan. 2015.

[38] E. O. Voit and A. Sorribas, "Computer modeling of dynamically changing distributions of random variables," *Math. Comput. Model.*, vol. 31, no. 4–5, pp. 217–225, 2000.

[39] E. O. Voit, "A systems-theoretical framework for health and disease: Inflammation and preconditioning from an abstract modeling point of view," *Math. Biosci.*, vol. 217, no. 1, pp. 11–18, Jan. 2009.

[40] M. A. Savageau, "Biochemical systems analysis. I. Some mathematical properties of the rate law for the component enzymatic reactions.," *J. Theor. Biol.*, vol. 25, no. 3, pp. 365–9, Dec. 1969.

[41] E. O. Voit, *Computational analysis of biochemical systems: a practical guide for biochemists and molecular biologists*. Cambridge, U.K.: Cambridge University Press, 2000.

[42] M. A. Savageau, *Biochemical systems analysis : a study of function and design in molecular biology.* Addison-Wesley, 1976.

[43] K. Soetaert, T. Petzoldt, and R. W. Setzer, *Solving Differential Equations in R: Package deSolve.*, vol. 2. 2010.

2.7. Acknowledgements

Work supported by UID/MULTI/04046/2013 centre grant (to BioISI) and DIFFTARGET PTDC/BIM-MEC/2131/2014 grant (to MDA), both from FCT, Portugal. DO is a recipient of a PhD fellowship from BioSys PhD programme (Ref: SFRH/BD/52486/2014) and IU of SFRH/BD/69180/2010, both from FCT, Portugal. This work was supported in part by the grants MCB-1517588 (PI: EOV) of the U.S. National Science Foundation. The funding agencies are not responsible for the content of this article. The authors are also grateful to Luís Marques (BioISI) and to staff from EMBL, Heidelberg (Germany), from ALMF-Advanced Light Microscopy (Beate Neumann, Christian Tischer) core facility for technical assistance.

2.8. Supplements:

2.8.1. Supplementary methods and results

2.8.1.1. Background

We assume that phospholipids may move freely across the cell membrane and that phosphoinositides are in the inner leaflet of the plasma membrane, as reported by van Meer [1] and Fadeel [2]. Model reactions take place at the inner leaflet of a 1 μm^2 patch of plasma membrane and in an adjacent region of the cytoplasm, with a height of 0.01 μm. We assume that influxes and effluxes of lipids by diffusion from or to adjacent patches are balanced. Within this 3D environment, we suppose that the enzyme kinetics in the model follow generalized mass action processes. We do not account for the binding of cytoplasmic enzymes to the membrane prior the initialization of their catalytic activity.

2.8.1.2. Model Design

2.8.1.2.1. Transport fluxes

Transport fluxes reflect vesicle and non-vesicle-mediated transport [3]–[5]. It is unclear what percentage of the total transport is vesicle-independent. The transport can be accomplished by specialized proteins, called lipid transport proteins (LTPs), or can happen spontaneously at membrane contact sites (MCSs). We assume that these effluxes have first-order kinetics ($f_{i\rightarrow} = 1$) and have one common rate constant. This

last assumption is not trivial. For example, some species of phosphoinositides are necessary for the initiation of vesicle formation so they might have a slightly higher exit rate. At the same time, non-vesicle mediated transport is facilitated by LTPs, and LTPs with varying affinities for different phosphoinositides are presently not known. Overall, we do not possess enough information to include different efflux rate constants for each model variable.

Alberts *et al.* [6] reported that a macrophage ingests 3% of its plasma membrane per minute, while a fibroblast only ingests 1%. As a compromise, we set the amount of internalized plasma membrane due to endocytosis as 2% per minute. We added 2.5% for non-vesicle transport, resulting in a total of 4.5% per minute. The input flux values were restricted in order to allow 4.5% of the membrane phosphoinositides to recycle per minute. This setting made the levels of PI robust to alterations in other phosphoinositide pools. We also tested a level of 1% per minute. The model exhibited a similar behaviour, but the PI pool fluctuated considerably in response to alterations in other phosphoinositide pools. For example, manipulations in the PI(4)P and PI(4,5)P_2 levels caused an undue increase of more than 15% in the PI pool. Of course, it is imaginable that such fluctuations could exist and have a physiological meaning, for instance, to signal to the kinases responsible for PI(4)P and PI(4,5)P_2 production that these lipids are being depleted. However, we found no reports in the literature of this phenomenon, and therefore chose the model setting corresponding to a more stable PI pool.

2.8.1.3. Parameter Estimation

The phosphoinositide literature is vast. However, many experimental results are presented in ways that are difficult, if not impossible, to translate into numerical values of model variables or relative changes. Other publications present results that involve manipulations or perturbations of genes or proteins that are not included in our model. In the end, the experimental data used in the following to parameterize the model consist of all data from the literature that permitted reliable translation into model variables or changes in model parameters.

Each flux $v_{i\rightarrow j}$ contains three parameters, namely a rate constant $\gamma_{i\rightarrow j}$, one or more kinetic orders $f_{i\rightarrow j}$, and the available quantity of enzyme that catalyses the reaction in this flux

($E_{i \rightarrow j}$). These three types of parameters need to be estimated to populate the model equations.

If parameter values are found in the literature, they are typically given as K_m and specific activity values. Many of such values have been collected in the database BRENDA [7]. While BST does not use these parameters, they are easily converted into values for rate constants and kinetic orders of GMA model [8]. Enzyme kinetic parameters retrieved from literature and BRENDA are shown in Table 2.4.

K_m and specific activity values collected in BRENDA are in mM and µmol/min/mg respectively. Before using these parameters in the estimation of rate constants and kinetic orders, K_m's were converted to molecules/µm^2 and the specific activities to molecules/min/mg. While converting volume units to area units, we considered that the number of molecules present in a 1 µm^2 membrane patch is the same number present in a 1 µm^3 volume including the membrane patch and a thin layer of surrounding cytosol.

Table 2.4 also presents the known cellular localization of each enzyme as retrieved from UNIPROT annotations and described by Sasaki *et al.* [9]. Since the model aims to simulate a patch of the plasma membrane, enzymes should be considered if they are present in the cytosol or in the plasma membrane. This is true for all enzymes except the three SAC phosphatases. However, there is evidence that these phosphatases can control directly the levels of PI(4)P at the plasma membrane by acting at membrane contact sites between the ER and the plasma membrane [10].

For enzymes that are present in multiple cellular compartments it is difficult to assess their relative contributions to the catalysis of a given reaction in each of the compartments. This lack of information is not critical in our approach since the parameters defining the amount of enzyme catalysing each flux in the plasma membrane patch ($E_{i \rightarrow j}$) are numerically adjusted to optimize the model fit to the experimental data.

The parameters in Table 2.4 could not directly be applied to the model since there is no one-to-one relationship between each enzyme and each flux. Some enzymes catalysed more than one flux and many fluxes may be catalysed by more than one enzyme. Because quantitative details regarding these multiple processes are lacking, enzymes

catalysing the same reaction were grouped using information in Balla [11] and Sasaki *et al.* [9].

For each group, one enzyme was chosen to define the flux parameters. The chosen enzyme was normally the one identified in the literature as the main catalyst of the respective flux. The enzymes and associated fluxes are presented in in Table 2.5 for kinases and in Table 2.6 for phosphatases.

Generally, more information is available for kinases than for phosphatases. Moreover, there is a difference concerning the assignment of kinases and phosphatases to different fluxes. As Delage *et al.* [12] observed, kinases are often specific while phosphatases are polyvalent. Of the ten fluxes catalysed by phosphatases, seven can be catalysed by synaptojanins (SYNJ) and five by suppressor of actin (SAC) [9]. This redundancy is in stark contrast with the kinases that catalyze one or two reactions at most. An exception is phosphoinositide 3-kinase (PI3K), which is polyvalent if one allows for primary and secondary reactions. It is also noteworthy that PTEN, probably the most studied phosphatase as a consequence of its role as tumour suppressor, is specific for $PI(3,4,5)P_3$ and $PI(3,4)P_2$ substrates [13].

Fine-tuning of the model was accomplished by adjusting the levels of enzymes ($E_{i\rightarrow j}$) and fluxes entering and exiting the system ($\gamma_{\rightarrow 0}$, $\gamma_{\rightarrow 3}$, $\gamma_{\rightarrow 4}$, $\gamma_{i\rightarrow}$). These parameters were manually tuned until the model reached a steady state where phosphoinositide levels agreed with values reported for the cell membrane (Table 2.1) and model simulations replicated observed phenomena (Table 2.2 and Figure 2.3). Most of the remaining parameters, that is, rate constants and kinetic orders derived from the literature were not altered. PIP5KII parameters had to be adjusted to allow a steady-state composition compatible with literature values. This enzyme catalyses the flux $v_{5\rightarrow 45}$ [11] [9]. Using the original parameters for this enzyme would make $v_{5\rightarrow 45}$ rather slow, yielding an accumulation of PI(5)P at around 700 molecules per μm^2, which is outside the intervals reported in the literature. One could slow down the sources of PI(5)P in order to obtain a smaller pool, but that would reduce the turnover of PI(5)P which is supposed to be high [11], and the model would no longer replicate the observations regarding PI(5)P, PI(3)P and $PI(3,5)P_2$ documented in the literature. Further, using the reported PIP5KII parameterization found in the literature [14], PI(5)P and $v_{5\rightarrow 45}$ would not sustain the $PI(4,5)P_2$ pool. We also had to re-estimate two rate constants, $\gamma_{3\rightarrow 35}$ and $\gamma_{35\rightarrow 5}$. Values

retrieved from BRENDA were too small to replicate observed phenomena. For example, Bulley *et al.* [15] stated that the majority of the PI(5)P pool is formed from PI(3,5)P2. With the values retrieved from the literature [16] $v_{0\rightarrow5}$ would have a greater contribution to the PI(5)P pool than $v_{35\rightarrow5}$. Increasing $\gamma_{35\rightarrow5}$ forced us to increase $\gamma_{3\rightarrow35}$, which subsequently increased the PI_Kfyve activity when PI(3)P was used as substrate rather than PI. The increase of $\gamma_{35\rightarrow5}$ could be explained by a regulation that is not implemented in the model: the activation of MTMRs by PI(5)P [17]. The amount of PIP5KII in the model is the highest as kinases are concerned. There is evidence in the literature of higher abundance of PIP5KII than PIP5KI [18].

After the manual adjustments, as described above, a genetic algorithm was used to search for a parameter set that produced the closest fit to a set of observed phenomena.

The implemented genetic algorithm has two mechanisms to create diversity: mutation and recombination. The mutated parameters are obtained multiplying the initial value by a random value from a normal distribution of mean 1 and standard deviation of 0.3 or 0.5. Each new parameter set is only accepted if a set of validity conditions is met (Table 2.7). Higher standard deviation values would make the algorithm run very slowly due to a high number of invalid sets. Recombination combines two parameter sets and thereby generates a new set where each parameter is the average of the corresponding parameters in the two parent sets.

Each generation starts with 10 distinct parameters sets. In the first generation, the initial set consists of the manual solution and 9 viable mutants are obtained from this parent set. All pairs of these 10 sets are combined producing 45 recombined sets. Additional 10 parameter sets are created by mutating all enzyme levels, inputs and outputs parameters from 10 of the existing 55 sets picked randomly. Next, 35 new sets are created recombining a random mutant with one of the previous 55 sets. The resulting 100 sets are the source for further 100 minor mutant sets that alter between 1 and 5 parameters of the 100 existing sets. The final 200 parameter sets are then scored and the 10 sets with the best score are selected to start the next generation. The criteria for scoring the sets are presented in Table 2.7.

Two versions of the genetic algorithm were employed: one where the 10 initial progenitor sets of each generation could be part of the next generation and one where

they were excluded. The former algorithm converged rapidly but the latter found best scores more quickly. In the long run, both algorithms delivered sets with similar scores that were 50% better than the manually determined set. Final parameters for the fluxes and protein amounts per μm^2 are shown in Table 2.3.

2.8.1.4. Sensitivity Analysis

Local sensitivity analysis was implemented as described in Chen *et al.* [8] and combined sensitivities, also known as global sensitivities, were computed as detailed in Kent *et al.* [19].

Parameter sensitivities were assessed numerically by increasing each parameter, one at a time, by 1% and computing the new steady state of the system. When the relative change in the steady-state value of a dependent variable is higher than 1% (or lower than -1%) the sensitivity indicates that a change in the parameter value is amplified in the steady-state of the dependent variable. Smaller sensitivities indicate attenuation of a perturbation. Although there are exceptions, most biological systems are expected to show sensitivity values between about -3 and +3. However, in signalling systems, the sensitivities may be much higher.

The model contains 64 parameters but the sensitivity analysis can be reduced to 46 parameters, because there are 21 pairs of rate constants ($\gamma_{i\rightarrow j}$) and a corresponding enzyme quantity ($E_{i\rightarrow j}$) that always appear as a product in a flux equation. Multiplying a constant to $E_{i\rightarrow j}$ or to the corresponding $\gamma_{i\rightarrow j}$ will give the same relative change in flux and, thus, in steady state. Consequently, the sensitivities for the rate constants are identical to the corresponding enzyme quantity.

The results of the sensitivity analysis are conditional on the parameter set that provides realistic steady-state values and replicate the observed phenomena. Furthermore, they reflect responses to changes in individual parameters. However, multiple small or intermediate errors in parameter values could collectively have a larger impact on the performance of the system. To address this question, combined sensitivities were studied using a Monte-Carlo approach. Specifically, we assigned a random uncertainty of ±5%, ±10%, ±20%, ±50% or ±100% for every parameter. With every combination, we created a new parameter set and recorded those combinations that led to a steady state in up to a simulation time of 1000 minutes. With this method, 5,000 new parameter

sets were retrieved for each level of uncertainty. For each parameter set sampled we calculated the local sensitivities.

2.8.1.4.1. Sensitivity Analysis Results

The complete list of local sensitivities is presented in Table 2.8. Only 20 out of 368 (~5%) computed sensitivities have an absolute value greater than 1. The highest sensitivity value indicates an decrease of 4.15% in PI(5)P when $f_{5\rightarrow45}$ is increased by 1%. The parameter $f_{0\rightarrow3}$ has the highest number of high sensitivities, and these are related to PI(3)P, PI(5)P and PI(3,5)P_2.

The high proportion of low sensitivities shows that the model system is very robust to environmental and mutational challenges that perturb a parameter value. It also implies that small errors in model parameterization will not affect model behavior in a significant manner.

We intended to investigate whether the distributions of sensitivities might suggest a different behaviour associated with a parameter change than the one suggested by the local sensitivities. Generally, if the sensitivity of a parameter exhibits large variability, it might suggest a lack of system robustness [19].

The combined sensitivity results suggest that most parameter sensitivities are concentrated closely around the local sensitivity value. 112 out of 368 sensitivities (30.4%) led to a low overall sensitivity, even if the parameters were allowed to vary up to ±100%. Of the 256 that presented higher combined sensitivities, only 42 exhibited this behaviour with uncertainties lower or equal than 50%.

Considering these results, we can conclude that small changes in parameter values do not alter the sensitivity profile of the dependent variables. These observations suggest that the model is robust with respect to uncertainties in parameters.

Studying the sets with 100% uncertainty we found that $\gamma_{i\rightarrow}$ (the rate constant of the effluxes of all pools) presented high sensitivities in all dependent variables. $f_{0\rightarrow4}$, $f_{45\rightarrow4}$, $f_{45\rightarrow345}$ and $f_{0\rightarrow45}$ presented high sensitivities in 7 dependent variables, $f_{45\rightarrow0}$ in six and $f_{4\rightarrow0}$, $f_{45\rightarrow5}$, $f_{345\rightarrow45}$, $f_{345\rightarrow34}$ and $f_{4\rightarrow34}$ in five. This result highlights the importance of the linear pathway of PI, PI(4)P, PI(4,5)P_2 and PI(3,4,5)P_3 in the model.

The result is consistent with the earlier traditional sensitivity analysis. All parameters that in the combined sensitivity study cause high sensitivities in five or more dependent variables are also presented in the individual sensitivity analysis, except for $f_{45\rightarrow 0}$, $f_{0\rightarrow 45}$ and $f_{45\rightarrow 5}$. This suggests that the model was parameterized so that $v_{0\rightarrow 45}$ and $v_{45\rightarrow 0}$ fluxes have a small influence, although their potential for high sensitivities is considerable.

2.8.1.5. Identifiability Analysis

If a model is only slightly perturbed even in response to large changes in a parameter value, does it mean that the parameter value is correct? This question becomes complicated if the sensitivities of two or more parameters are correlated and the increase in one can be compensated with an alteration in one or more others. The issue is related to the existence of infinite parameter combinations that produce essentially the same model output. This redundancy is especially important if we want to suggest an experimental design to populate the model with parameters values. These issues are related with the problem of parameter identifiability, which is defined as the ability to identify the true value of a model parameter [20].

To find the best identifiable parameters we implemented the method described by Srinath and Gunawan [20] and Yao *et al.* [21], which is based on the local sensitivity matrix. For each column of the matrix, the Euclidian norm is calculated and the column with the highest magnitude is selected. If the magnitude exceeds a certain threshold, the parameter corresponding to this column is identifiable. This column is removed from the local sensitivity matrix. The projection of the removed column on the remaining columns is computed and subtracted from them. This procedure creates a new local sensitivity matrix. The process is repeated until the highest magnitude is below the threshold. All remaining parameters are considered non-identifiable.

2.8.1.5.1. Results of the Identifiability Analysis

In the phosphoinositide pathway model, the best-identifiable parameters are $f_{4\rightarrow 0}$, $f_{3\rightarrow 35}$, $f_{5\rightarrow 45}$, $f_{45\rightarrow 345}$, $f_{35\rightarrow 5}$, $f_{4\rightarrow 34}$, $f_{45\rightarrow 4}$ and finally $\gamma_{i\rightarrow}$ (Figure 2.8d). These parameters constitute a subset of those parameters that exhibited high local sensitivities. The parameters that were considered non-identifiable either have very small sensitivities, or their effect on the dependent variables may be replicated by a linear combination of perturbations in identifiable parameters.

2.8.1.6. Monte-Carlo Exploration of the Parameter Space

The identifiability analysis suggests the existence of alternative parameter sets that replicate both, the reported steady-state levels of phosphoinositides and the observed relationships between steady-state levels. To identify possible alternative parameter sets satisfying these conditions, we explored 79,993 random parameter sets using a Monte Carlo approach. Only the most identifiable parameters (discussed in the previous section) plus the input and output fluxes were allowed to vary between 50 and 150 per cent from their reference value. These parameter sets were only accepted if they reached a steady state in up to 5000 minutes of simulation time.

Non-identifiable parameters were not varied in order to optimize the parameter space exploration, because varying non-identifiable parameters would yield small changes in system behavior. Additionally, linear combinations of perturbations in identifiable parameters can mimic most of the effects of perturbations in non-identifiable perturbations. Input fluxes were also varied although they were not identifiable. This variation was necessary to accommodate changes in effluxes ($\gamma_{i\rightarrow}$) and still allow for the system to achieve a steady state.

2.8.1.6.1. Results of the Monte-Carlo Exploration of the Parameter Space

Among the initial 79,993 combinations of parameter values, 79,985 reach a steady-state within 5000 minutes and 1452 have phosphoinositide levels within the intervals retrieved from the literature. Among these, 231 replicate the relative amounts between the phosphoinositide pools. Intriguingly, only 117 (the set used to parameterize the model and 116 alternatives), less than 0.15% of all surveyed sets, satisfy the previous conditions plus the fact that effluxes are less in magnitude than 7% and the influxes are less than 25% of the respective phosphoinositide pools. Indeed, the 116 alternative sets of parameters have outputs that are similar to the ones produced by the optimized parameter set but are less concordant with of the phenomena retrieved in the literature. For example, as can be seen in Figure 2.5, taking the score of the manually found parameter set as a base score of 20, all of the 116 admissible alternative parameter sets have a higher score, i.e., present less concordance with the conditions of the scoring function.

The results of this analysis suggest that the information available is sufficient to restrict the parameter space to a region that is compatible with all experimental observations. The alternative parameter sets are characterized by alterations that cancel each other in the system's input of PI, PI(3)P and PI(4)P and output fluxes.

The conditions imposed to find alternative parameter sets are not very restrictive. For example, we accepted data sets with the levels of PI between 200,000 and 400,000 and for PI(4)P and $PI(4,5)P_2$ between 5,000 and 20,000. As such, the small number of parameter sets that satisfy all the tests was not due to narrow test conditions but a genuine scarcity of combinations of parameters that satisfy all pertinent phenomena reported in the literature.

It is impossible to discern which set is the best representation of reality, not only because there are gaps in information, like missing measurements of the input fluxes, but also because these parameter sets can correspond to different cell types, states or membrane configurations. However, the initial parameter set used in the model has kinetic parameters in accordance with the literature and steady-state values that are closest to the center of the reported intervals for phosphoinositide levels.

2.8.1.7. Validity Test Using an siRNA Knockdown

2.8.1.7.1. Preparation of siRNA coated multi-well plates

Multi-well plates (384-well plates) (BD Falcon #353962) were coated with customized siRNAs (Silencer® Select, Ambion) for solid-phase reverse transfection adapted from a previously reported protocol (Erfle H et al., 2007). An aqueous 0.2% (w/v) gelatine solution was prepared and filtered with 0.45µM pore size filter and a 0.4M glucose solution was prepared in Opti-MEM (Gibco #51985). Then, a transfection mix was prepared by mixing 1.662mL of the sucrose/Opti-MEM solution, 969µL of Lipofectamine® 2000 (Gibco #12566014) and 969µL doubly distilled water. This transfection mix was distributed into a 96-conic well plate (35µL/well, "Plate A"). In parallel, fibronectin was diluted in the 0.2% gelatine solution to a concentration of 1%. This solution was distributed into another 96-conic well plate (96µL/well, "Plate B"). Then, 5µL of a 3µM siRNA solution and 7µL of the transfection mix ("Plate A") were incubated in each well of a low volume 384 well plate ("Plate C"). After 20-min incubation, 7µL of the fibronectin solution ("Plate B") were added. 3µL of the contents

of each well in “Plate C” were diluted fifty fold in a 384 deep well plate using doubly distilled water. Finally, 15µL of each well were transferred to a 384-well imaging plate, lyophilized and stored in an anhydrous atmosphere before cell seeding.

2.8.1.7.2. ENaC microscopy-based live-cell functional assay

2.8.1.7.2.1. Preparation of the functional assay

The live-cell assay used to identify the novel regulators of ENaC activity constricted on transfecting A549 cells with different siRNAs by solid-phase reverse transfection (previously described in the section *Preparation of siRNA coated multi-well plates*). Cells were plated in 384-well plates containing different human siRNAs (2500 cells per well) and incubated for 48h or 72h at 37ºC with 5% CO_2. Afterwards, cell nuclei were stained for 1h with Hoechst-33342 dye (Sigma-Aldrich #B2261) (1/10000) diluted in Ringer solution (145mmol/L NaCl, 0.4mmol/L KH_2PO_4, 1.6mmol/L K_2HPO_4, 5mmol/L D-glucose, 1mmol/L $MgCl_2$ and 1.3mmol/L Ca-gluconate) (30µL/well) at 37ºC. After washing with Ringer solution, cells were incubated for another 10min with diluted voltage-sensitive FLIPR® Membrane Potential Assay (FMP) (Molecular Devices, #R8042) staining solution (20µL/well) at 37ºC in the pre-warmed and humidity saturated (50-70% of humidity) microscope chamber of an automated epifluorescence Scan^R screening microscope (Olympus Biosystems), comprising a cooled 12 bit 1344x1024 pixel resolution C8484 CCD camera (Hamamatsu), Marzhauser SCAN IM IX2 scanning stage, metal halide light source (MT20), standard filter sets and an automated liquid dispenser.

2.8.1.6.2.2. Image Acquisition

The first row of the cells in the 384-well plate was imaged in the wide-field Olympus Scan^R microscope with a 10x objective (Olympus, UPSAPO) in the Cy3 channel and DAPI channel with an exposure time of 5ms and coarse auto-focus (two images per well, 5min/row). Then FMP containing 30µM amiloride hydrochloride (Sigma #A7410) was added by an automatic liquid dispenser adapted to the microscope stage. The image acquisition was initiated after 5min of incubation with amiloride.

2.8.1.6.2.3. Image Analysis

Overall transfection efficiency was assessed by observing if cells transfected with siRNAs compromising chromosome segregation exhibited mitotic phenotypes (Simpson et al., 2012). Failure to observe these phenotypes in more than 75% of images implied the rejection of the corresponding plate from analysis.

The intensity of FMP fluorescence (IF) before and after adding amiloride was quantified using the open source cell image analysis software CellProfiler. Nuclei were identified as primary objects and FMP fluorescence measured in Cy3 channel as secondary object. The amiloride-sensitive fluorescence ratio for each cell was calculated applying the following formula:

$$Ratio = \frac{IF_{\text{before amil}} - IF_{\text{after amil}}}{IF_{\text{before amil}}} \times 100 \qquad (2.2)$$

Each image was corrected for the background and several quality controls were applied: cells with too high or too low intensity; abnormal area shape, eccentricity; low number of cells per well; cells out-of-focus, localized near the edges or that changed their position in the well were not quantified. The amiloride-sensitive ratios were further analysed in R in order to automatically identify the potential "hits", which are the ones whose ratio deviate more than two standard deviations from the ratio of the negative control, as calculated from the following formula:

$$Deviation = \frac{\overline{Ratio_{\text{siRNA}}} - \overline{Ratio_{\text{Negative control}}}}{2 \times SDM_{\text{Negative control}}} \qquad (2.3)$$

Where SDM is a standard deviation of the mean and “scrambled” siRNA was used as a negative control.

We considered as significant Amil-sensitive ENaC functional effects, those whose magnitudes were larger than twice the negative control´s SDM. Therefore, we defined ENaC function enhancers as those conditions having a Deviation Score above +1 and ENaC function inhibitors as those having a Deviation Score below -1. Additionally, Student´s t-test was performed to quantify statistical significance versus the corresponding negative control.

2.9. Supplementary Figures

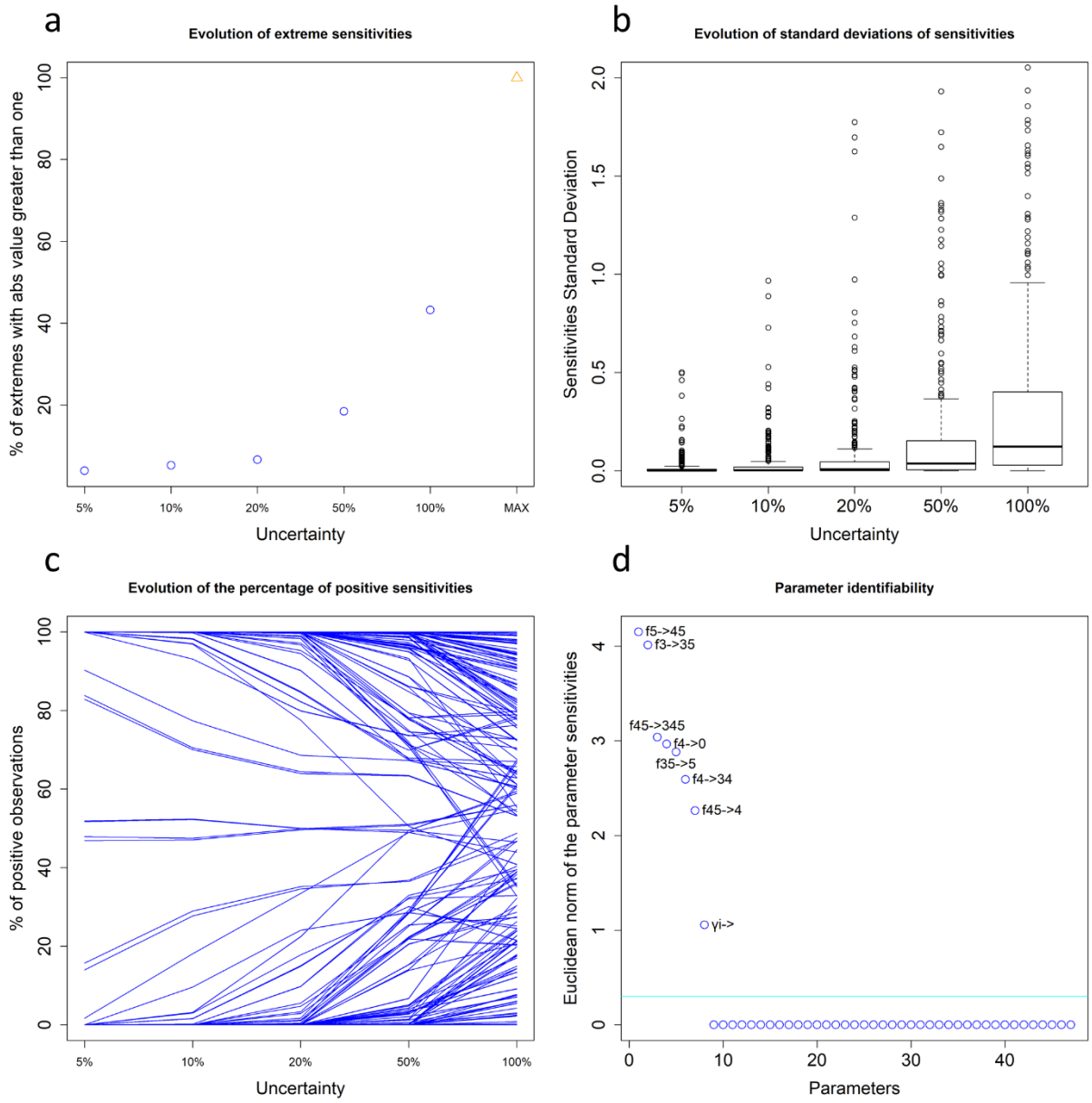

Figure 2.8. Evolution of sensitivities due to an increasing level of uncertainty and parameter identifiability.

a) Evolution of the number of extreme sensitivities with absolute values greater than 1 as a function of the level of uncertainty in parameter values. MAX corresponds to the total number of extremes in the model (736 extremes, which is twice the number of parameters). A noticeable increase begins around the 50% uncertainty level. b) Evolution of the standard deviations of sensitivities due to increasing uncertainty. The boxplot corresponding to 100% uncertainty does not show all outliers, the highest of which is 48.09. This finding suggests that the variance in sensitivity is moderate at least up to 50% uncertainty. c) Evolution of the percentage of positive sensitivities according to parameter value uncertainty. Each line corresponds to one pair of a parameter and a dependent variable. For low levels of uncertainty, the majority of the observed sensitivities are almost all positive or all negative, which

means that the sign of the sensitivities are constant for small perturbations. The reason for this consistency is that the background parameter sets lead to models with similar behaviour. The result also suggests that the model behaviour is consistent even under moderate uncertainty and only starts to vary for 50% or more uncertainty in parameter values. d) Plot showing the best-identifiable parameters. $\gamma_{i\rightarrow}$ represents for the rate constant for all exit fluxes. Graphs created in R[22].

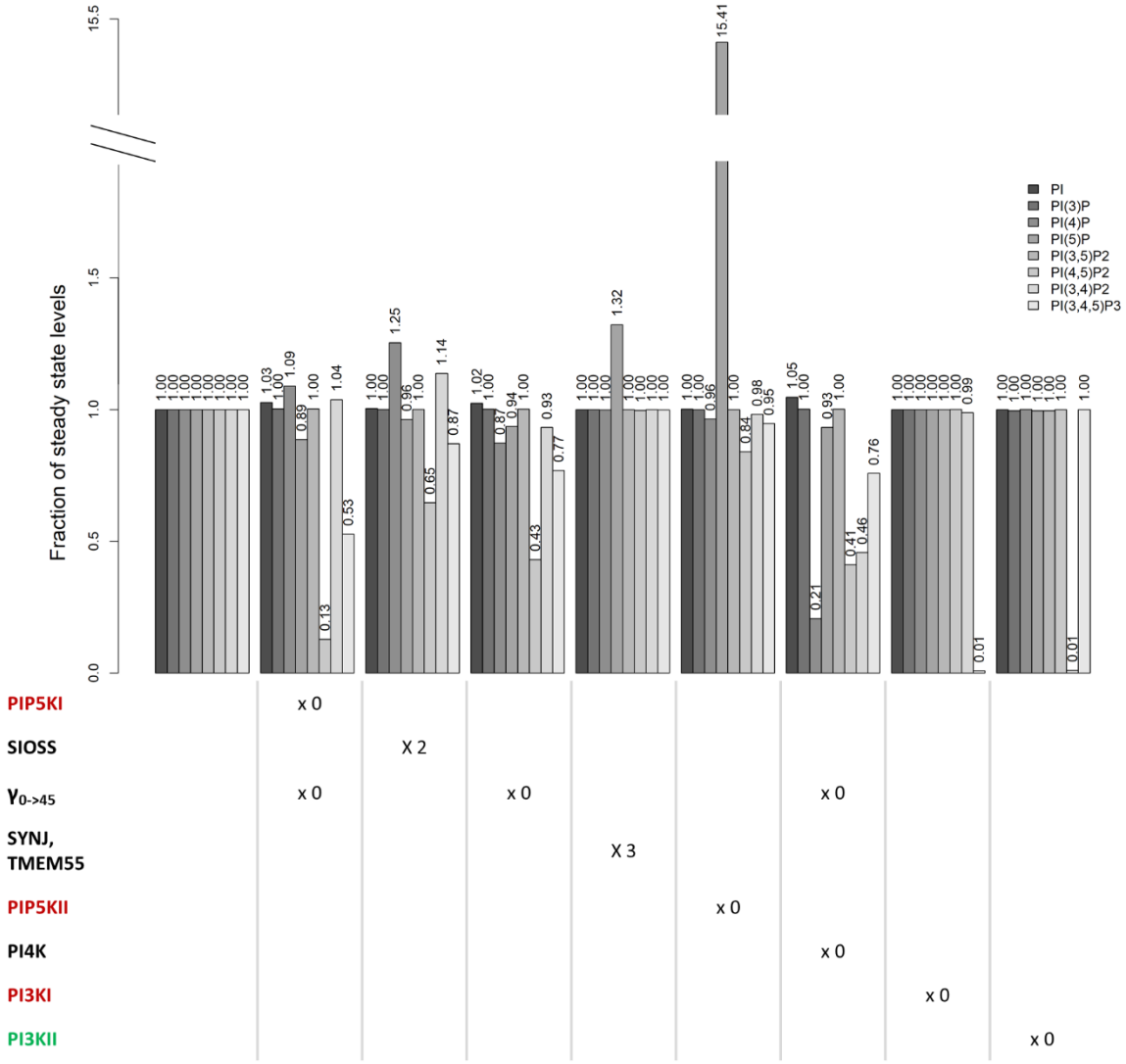

Figure 2.9. Alterations in all pools of the model as a consequence of perturbations in enzyme activities.

Changes in enzyme activity simulate the effect of an siRNA screen performed by Almaça and colleagues[23]. Graph was created in R[22] and x axis labels added in PowerPoint.

2.10. Supplementary Tables

Table 2.1. Levels of phosphatidylinositol and phosphoinositides in the membranes of mammalian cells and corresponding steady-state values in the model.

Molecule	(mol %) of total cellular inositol lipids	Molecules / μm^2	Source	Model values at steady state
PI	90%	200000 – 400000	[11] [1] [24]	304372.1
	80%	40000 - 160000	[25]	
PI(3)P	0.36%	800 – 6000	[11]	100.0
	0.05% - 1.5%	25 – 3000	[25]	
	0.2%	600	[26]	
	0.175%	525	[27]	
	0.3%	100	[13]	
PI(4)P	2,24%	5000 – 20000	[11] [28] [24] [25]	10040.1
	6%	18000	[26]	
	3%	9000	[27]	
PI(5)P	Very small	Very small	[11]	100.5
	0.5% - 2% of PI(4)P	75 – 300	[15]	
	4%	1200	[26]	
	.3%	900	[27]	
	0.1% – 0.5%	50 – 1000	[25]	
$PI(4,5)P_2$	2,24%	5000 – 20000	[11] [28] [24] [25]	10001.0
	3%	9000	[26]	
	5%	15000	[27]	
$PI(3,5)P_2$	7 to 50 fold less than PI(5)P	1 – 57	[29]	20.2
	0.1% - 1%	50 – 2000	[25]	
	0.055%	165	[26]	
	0.04%	120	[27]	
$PI(3,4)P_2$	Very small	Very small	[11]	20.6
	0.1% - 1%	50 - 2000	[25]	
$PI(3,4,5)P_3$	0.036%	80 – 1000	[11] [28]	639.5
	0.1% - 1%	50 - 2000	[25]	
Total	100%	220000 – 450000	[11]	325294.0
		50000 - 200000	[25]	

Table 2.2. Observed experimental phenomena used to calibrate the model and model performance for each phenomenon.

	Phenomenon	Model
1	$PI(4,5)P_2$ should drop (proportionally) as a consequence of depletion of PI. [5]	A 50% decrease in $\gamma_{\rightarrow 0}$ will decrease PI to 50%. This will only cause $PI(4,5)P_2$ to decrease to 88% of steady state. (Figure 2.3a)
2	$PI(4,5)P_2$ is independent of PI(4)P. [11] [30]	Even with PI(4)P at 7% of its original steady state levels, $PI(4,5)P_2$ only dropped 20%. (Figure 2.3b)
3	$PI(4,5)P_2$ is dependent on PI4K [30]. PI4K knock-down decreases PI(4)P and PI(4,5)P2 by 50%. [11]	A decrease of 95% in PI4K will decrease $PI(4,5)P_2$ to 45% and PI(4)P to 24% of original steady state values. (Figure 2.3a)
4	PI(5)P is of similar or higher abundance as compared to PI(3)P and ~20-100-fold below the levels of PI(4)P and $PI(4,5)P_2$. Steady-state PI(5)P levels are more than 5-fold higher than those of $PI(3,5)P_2$. [11], [13], [15], [26], [27], [29]	PI(5)P = 100.49 PI(3)P = 100.00 PI(4)P = 10040.13 (10040.13 / 100.49 = 99.91) $PI(4,5)P_2$ = 10000.97 (10000.97 / 100.49 = 99.52) $PI(3,5)P_2$ = 20.21 (100.49 / 20.21 = 4.97) (Table 2.1)
5	Golgi PI(4)P makes a sizeable contribution to the plasma membrane supply of PI(4)P but it is dispensable in the maintenance of $PI(4,5)P_2$. [31]	Closing $\gamma_{\rightarrow 4}$ will decrease PI(4)P to 61% of the steady-state values but only decrease $PI(4,5)P_2$ by 1% (Figure 2.3d).
6	$PI(3,4,5)P_3$ depend on PTEN concentration. [13], [32]	$PI(3,4,5)P_3$ increases 16 fold when PTEN is knocked down (Figure 2.5)
7	PTEN knockdown does not decrease the levels of $PI(4,5)P_2$ significantly. [33]	PI(4,5)P2 decreases 1% when PTEN is knocked down (Figure 2.5)
8	$PI(4,5)P_2$ levels drop around 50% if PIP5KI is knocked down 50%. [34]	A decrease in 50% on PIP5KI will decrease $PI(4,5)P_2$ to 55% of the steady-state (Figure 2.3a)
9	When PIKfyve is reduced to 10%, PI(5)P and $PI(3,5)P_2$ decrease 50%. [15]	When PIKfyve is reduced to 10%, PI(5)P and $PI(3,5)P_2$ decrease to 50.05% and 49.70% respectively (Figure 2.3c).
10	When PIKfyve is reduced to undetectable levels PI(3)P rises 5 fold, PI(5)P decreases to 15%, $PI(3,5)P_2$ is undetectable as well and $PI(4,5)P_2$ decreases to 67-80%. [15]	When PIKfyve is reduced to 0.1%, PI(3)P will increase 8.85 fold, PI(5)P decreases to 10.08%, $PI(3,5)P_2$ to 0.88% and $PI(4,5)P_2$ to 85.78% of original steady state levels (Figure 2.3c).
11	When MTMR2 is knocked out, PI(5)P is reduced to 20% and $PI(3,5)P_2$ increases to 150%. [15]	When MTMR is reduced to 65% (simulating the knockout of MTMR2), PI(5)P is only reduced to 98.97% but $PI(3,5)P_2$ is increased to 152.17% (Figure 2.3c).
12	Majority of the PI(5)P pool is created from $PI(3,5)P_2$ via myotubularins. [15]	Three fluxes supply material to the PI(5)P pool: $v_{0\rightarrow 5}$ = 5.49 molecules/s, $v_{45\rightarrow 5}$ = 17.04 molecules/s and $v_{35\rightarrow 5}$ = 102molecules/s. $v_{35\rightarrow 5}$, which is catalysed by myotubularins, is responsible for 81.91% of PI(5)P production (Figure 2.3c).
13	PI(5)P is important in the synthesis of $PI(4,5)P_2$. [15]	The flux $v_{5\rightarrow 45}$ alone is capable of maintaining $PI(4,5)P_2$ with 34% of its original steady state levels (Figure 2.3b).

Table 2.3. Values of model parameters.

Fluxes $v_{i\rightarrow j}$	$\gamma_{i\rightarrow j}$ (molecules^{1-g} μm^{2g}/min or μm^2/min/mg) where ^{g} is the kinetic order of the corresponding variable	$f_{i\rightarrow j}$ (dimensionless)	$E_{i\rightarrow j}$ (mg)
$v_{0\rightarrow 3}$	1.09e+15	0.11	2.23e-14
$v_{3\rightarrow 0}$	3.07e+12	1.00	2.56e-14
$v_{0\rightarrow 4}$	5.10e+14	0.29	2.78e-14
$v_{4\rightarrow 0}$	6.65e+12	0.91	8.93e-15
$v_{0\rightarrow 5}$	2.87e+14	0.06	8.54e-15
$v_{5\rightarrow 0}$	3.07e+12	1.00	8.93e-15
$v_{3\rightarrow 35}$	1.34e+14	1.00	8.54e-15
$v_{35\rightarrow 3}$	3.06e+12	1.00	1.71e-13
$v_{4\rightarrow 45}$	8.49e+15	0.05	1.74e-14
$v_{45\rightarrow 4}$	6.65e+12	0.91	6.35e-15
$v_{4\rightarrow 34}$	1.04e+13	0.50	1.23e-15
$V_{34\rightarrow 4}$	7.60e+12	1.00	5.30e-17
$v_{5\rightarrow 45}$	2.95e+13	0.88	6.89e-14
$v_{45\rightarrow 5}$	4.13e+12	0.65	1.05e-14
$v_{35\rightarrow 5}$	4.16e+14	1.00	1.21e-14
$v_{34\rightarrow 3}$	1.33e+12	1.00	3.81e-14
$v_{0\rightarrow 45}$	2.67e+14	0.29	4.15e-14
$V_{45\rightarrow 0}$	6.65e+12	0.91	2.79e-18
$v_{45\rightarrow 345}$	1.89e+14	0.31	1.53e-14
$v_{345\rightarrow 45}$	4.81e+14	0.98	5.30e-17
$v_{345\rightarrow 34}$	1.68e+12	1.00	7.76e-15
$v_{\rightarrow 0}$	16588.74	-	-
$v_{\rightarrow 3}$	12.37	-	-
$v_{\rightarrow 4}$	297.26	-	-
$v_{0\rightarrow}$, $v_{3\rightarrow}$, $v_{4\rightarrow}$, $v_{5\rightarrow}$, $v_{34\rightarrow}$, $v_{35\rightarrow}$, $v_{45\rightarrow}$, $v_{345\rightarrow}$, ($v_{i\rightarrow}$)	0.0519	-	-

Table 2.4. Kinetic parameters associated with enzymes in the model.

The first column contains the enzyme name and the second the corresponding gene name. The third and fourth columns exhibit Km and specific activity values, along with literature references.

Protein (EC number)	Human gene name	K_m (mM)	Specific activity (μmol/min/mg)	Localization
PI3K IA α (2.7.1.137)	PIK3CA	0.011 [35]	0.0086 [36]	C, PM
PI3K IA β (2.7.1.137)	PIK3CB		0.0017 [36]	N, C, PM
PI3K IA δ (2.7.1.137)	PIK3CD		0.0026 [36]	C, PM
PI3K IB γ (2.7.1.137)	PIK3CG		0.0016 [36]	C, PM
PI3KII α (2.7.1.154)	PIK3C2A	0.25 [37]	-	N, C, G, PM
PI3KII β (2.7.1.154)	PIK3C2B		-	N, C, ER, E, PM
PI3KII γ (2.7.1.154)	PIK3C2G		-	C, G, PM
PI3KIII (2.7.1.137)	PIK3C3	0.064 [37]	-	C, E
PI4KII α (2.7.1.67)	PI4K2A	0.2 [38]	0.044 [39]	M, E, G, PM
PI4KII β (2.7.1.67)	PI4K2B			N, C, G, E, PM
PI4KIII α (2.7.1.67)	PIK4CA	-	-	C, G, PM
PI4KIII β (2.7.1.67)	PIK4CB	-	-	C, M, ER, G
PIPK I α (2.7.1.68)	PIP5K1A	0.0012 [14]	0.023 [14]	N, C, PM
PIPK I β (2.7.1.68)	PIP5K1B	0.262 [40]		C
PIPK I γ (2.7.1.68)	PIP5K1C	-		N, C, PM
PIPK II α (2.7.1.68)	PIP4K2A	0.05 [40]	0.015 [14]	N, C, PM
PIPK II β (2.7.1.68)	PIP4K2B	-		N, C, ER, PM
PIPK II γ (2.7.1.68)	PIP4K2C	-		C, PM
PIPK III (2.7.1.68)	PIP5K3	-	-	C, G, E
PTEN (3.1.3.67)	PTEN	0.07 [41]	30.318 [41]	N, M, C, PM
TPIP (3.1.3.67)	TPTE2	-	-	C, G, ER
MTM1 (3.1.3.64)	MTM1	0.039 or 0.017 [42]	-	C, E, PM
MTMR1 (3.1.3.64)	MTMR1	0.0008 or 0.0037 [43]	-	C, PM
MTMR2 (3.1.3.64)	MTMR2		-	C, E, PM
MTMR3 (3.1.3.64)	MTMR3		-	C
MTMR4 (3.1.3.64)	MTMR4		-	C, E
MTMR6 (3.1.3.64)	MTMR6		-	N, C
MTMR7 (3.1.3.64)	MTMR7		-	C
MTMR8 (3.1.3.64)	MTMR8		-	N, C
MTMR14 (3.1.3.64)	MTMR14		-	C
INPP4A (3.1.3.66)	INPP4A	0.049 [44]	-	C, E, PM
INPP4B (3.1.3.66)	INPP4B		-	C
TMEM55A (3.1.3.78)	TMEM55A	0.046 [44]	0.01 [45]	C, E
TMEM55B (3.1.3.78)	TMEM55B			N, C, E
SYNJ1 (3.1.3.36)	SYNJ1	0.25 [46] [47]	0.765 [47]	C
SYNJ2 (3.1.3.36)	SYNJ2			C, PM
OCRL1 (3.1.3.36)	OCRL			N, C, G, E, PM
INPP5B (3.1.3.36)	INPP5B			C, G, ER, E, PM
INPP5J (3.1.3.36)	INPP5J			C, PM
SKIP (3.1.3.36)	SKIP			N, C, G, ER, PM
SHIP1 (3.1.3.36)	INPP5D			C, PM
SHIP2 (3.1.3.36)	INPPL1			C, G, PM
INPP5E (3.1.3.36)	INPP5E			C, G, PM
SAC1 (3.1.3.36)	SACM1L			G, ER
SAC2 (3.1.3.36)	INPP5F			E
SAC3 (3.1.3.36)	FIG4			G, ER, E

The last columns exhibit the localization of the enzyme. Abbreviations: PLIP: PTEN-like lipid phosphatase; TPIP: PTEN-Like Inositol Lipid Phosphatase; N: Nucleus, C: Cytosol; M: Mitochondria; G: Golgi; E: Endosome; ER: Endoplasmic Reticulum; PM: Plasma Membrane.

Table 2.5. Groups of kinases associated with each flux in the model.

Group	Enzymes	Flux	Values	Reference
pi_3KII_III	PI3KII α / β / γ, PI3K III (Vps34), (primary) PI3K IA α / β / δ, PI3K IB γ (secondary)	$v_{0\rightarrow3}$	K_m = 0.064 SA = 0.0086	[37] [36]
pi_4K	PI4KII α / β, PI4KIII α / β	$v_{0\rightarrow4}$	K_m = .2 SA = 0.044	[38] [48]
pi_Kfyve	PIPK III (secondary)	$v_{0\rightarrow5}$	K_m = 0.0034 No from humans. Bus Taurus. SA = 0.0028 (both from PI3K)	[49] [36]
pi_Kfyve	PIPK III (primary)	$v_{3\rightarrow35}$	K_m = 0.12 SA estimated	[40] [50]
pi_3KII	PI3K IA α / β / δ, PI3K IB γ, PI3KII α / β / γ (all secondary)	$v_{4\rightarrow34}$	K_m = 0.25 SA = 0.0043 (estimated)	[37] [51]
pip_5KI	PIPK I α / β / γ	$v_{4\rightarrow45}$	K_m = 0.0012 SA = 0.023	[14] [14]
pip_5KII	PIPK II α / β / γ	$v_{5\rightarrow45}$	K_m = 0.012 (No PI(5)P K_m . Using PIP_5KI K_m and SA.) SA = 0.023	[14] [14]
pi_3KI	PI3K IA α / β / δ, PI3K IB γ	$v_{45\rightarrow345}$	K_m = 0.011 SA = 0.0086	[35] [36]
pi_4K_pip_5KI	PI4K, PIP5KI and Dvl	$v_{0\rightarrow45}$	K_m = .2 (K_m of the first enzyme to contact substrate) SA = 0.023 (SA of the slowest)	[38] [14]

K_m in mM an SA in μmol/min/mg.

Table 2.6. Groups of phosphatases and associated fluxes.

Group	Enzymes	Flux	Values (problems)	Reference
SYNJ_SAC1_MTMR	SYNJ 1/2, SAC1, MTMR (9 forms)	$v_{3\rightarrow0}$		
SYNJ_SAC1	SYNJ 1/2, SAC1	$v_{4\rightarrow0}$	K_m = 0.25 (Using PI(4,5)P2 K_m of 5 phosphatase) SA = 0.765	[46]
SYNJ_SAC1	SYNJ 1/2, SAC1	$v_{5\rightarrow0}$		[47]
SYNJ_SAC1_SAC3	SYNJ 1/2, SAC1, SAC3	$v_{35\rightarrow3}$		
SYNJ	Not yet documented. Possibly synaptojanins.	$v_{45\rightarrow0}$		
S_I_O_S_S	SYNJ 1/2, INPP5 B/J/E, OCRL1, SAC2, SKIP	$v_{45\rightarrow4}$	K_m = 0.25 (Using PI(4,5)P2 K_m of 5 phosphatase) SA = 0.765	[46] [47]
S_I_O_S_S_SHIP2	SYNJ 1/2, INPP5 B/J/E, OCRL1, SAC2, SKIP, SHIP2	$v_{345\rightarrow34}$	K_m = 0.25 (Using PI(4,5)P2 K_m of 5 phosphatase) SA = 0.0765 (SA estimated)	[46]
SYNJ_TMEM55	SYNJ 1/2, TMEM55	$v_{45\rightarrow5}$	K_m = 0.046 (Using Inositol134P_3 Km) SA = 0.01	[44] [45]
PTEN	PTEN, TPTE	$v_{345\rightarrow45}$	K_m = 0.07 SA = 30.3	[41] [41]
MTMR	MTMR 7 forms, TPIP, INPP5E	$v_{35\rightarrow5}$	K_m = 0.0037 (Rattus Inositol13P2 K_m. No SA (SA estimated)	[43] [47]
INPP4	INPP4 A/B	$v_{34\rightarrow3}$	K_m = 0.046 (Using Inositol134P_3 K_m. No SA. Using PI(4,5)P2_4P SA) SA = 0.061	[44] [45]
PTEN	not yet documented	$v_{34\rightarrow4}$	K_m = 0.72 SA = 5.47	[52] [52]

K_m in mM an SA in μmol/min/mg.

Table 2.7. Performance and Score Criteria for the Genetic Algorithm.

Performance criteria:

- The solution must exist; it must not be composed of NA or NaN values
- The system must reach a stable steady state
- 200000 < PI < 400000
- 0.1< PI(3)P < 6000
- 5000 < PI(4)P < 20000
- 0.1< PI(5)P < 200
- 0.1< $PI(3,5)P_2$ < 200
- 5000 < $PI(4,5)P_2$ < 20000
- 0.1< $PI(3,4)P_2$ < 200
- 0.1< $PI(3,4,5)P_3$ < 5000
- The sum of all phosphoinositides must be between 220000 and 450000

Score criteria:

- Similar levels of PI(4)P and $PI(4,5)P_2$
- Similar levels of PI(3)P and PI(5)P
- PI(5)P levels are 5 fold of PI(3,5)P2 levels
- PI(4)P and $PI(4,5)P_2$ levels are 100 times higher than PI(5)P and PI(3)P
- Steady-state value of PI close to 300000
- Steady-state value of $PI(4,5)P_2$ close to 10000
- Steady-state value of PI(3)P close to 100
- Similar levels of $PI(3,5)P_2$ and $PI34P_2$
- $PI(4,5)P_2$ will decrease by the same percentage as PI
- PI(4)P drops to 50% after PI4K knockout
- $PI(4,5)P_2$ drops to 50% after PI4K knockout
- PI(4,5)P2 drops to 50% after PIP_5KI knockdown
- PI(5)P drops to 20% after MTMR2 knockdown (MTMR estimated to be reduced to 65%)
- $PI(3,5)P_2$ raises to 150% after MTMR2 knockdown (MTMR estimated to be reduced to 65%)
- PI(5)P should drop to 50% if pi_Kfive is reduced to 10%
- $PI35P_2$ should drop to 50% if pi_Kfive is reduced to 10%
- PI(5)P should drop to 15% if pi_Kfyve is knockout
- $PI(3,5)P_2$ should drop to 0.1% if pi_Kfyve is knockout
- $PI(4,5)P_2$ should drop to 80% if pi_Kfyve is knockout
- PI(3)P should increase 5-fold if pi_Kfyve is knockout

Table 2.8. Local sensitivity analysis. Each parameter was altered by 1% and the consequent alteration in each pool was measured. Induced changes greater than 1% are highlighted.

	PI	PI(3)P	PI(4)P	PI(5)P	PI(3,5)P2	PI(4,5)P2	PI(3,4)P2	PI(3,4,5)P3
$\gamma_{\rightarrow 0}$	**1.03456**	0.10471	0.24441	0.11920	0.10457	0.19251	0.09790	0.05926
$\gamma_{\rightarrow 4}$	0.00570	0.00165	0.38978	0.00224	0.00165	0.00698	0.12026	0.00215
$\gamma_{\rightarrow 3}$	0.00012	0.10674	0.00318	0.09998	0.10661	0.01453	0.00271	0.00448
$\gamma_{0\rightarrow 3}$	-0.00544	0.88524	0.02484	0.82935	0.88412	0.11939	0.02188	0.03676
$f_{0\rightarrow 3}$	-0.00788	**1.28161**	0.03596	**1.20096**	**1.27999**	0.17285	0.03167	0.05321
$\gamma_{3\rightarrow 0}$	0.00042	-0.06751	-0.00189	-0.06322	-0.06743	-0.00911	-0.00167	-0.00281
$f_{3\rightarrow 0}$	0.00195	-0.31694	-0.00889	-0.29675	-0.31655	-0.04275	-0.00784	-0.01317
$\gamma_{0\rightarrow 4}$	-0.02276	-0.00041	0.68316	0.00017	-0.00041	0.00622	0.20991	0.00192
$f_{0\rightarrow 4}$	-0.08381	-0.00155	**2.51637**	0.00057	-0.00155	0.02259	0.76967	0.00696
$\gamma_{4\rightarrow 0}$	0.01114	0.00020	-0.33438	-0.00009	0.00020	-0.00307	-0.10300	-0.00095
$f_{4\rightarrow 0}$	0.09480	0.00164	**-2.84494**	-0.00085	0.00164	-0.02664	-0.88199	-0.00821
$\gamma_{0\rightarrow 5}$	-0.00031	-0.00002	0.00152	0.05046	-0.00002	0.00727	0.00133	0.00224
$f_{0\rightarrow 5}$	-0.00025	-0.00002	0.00123	0.04087	-0.00002	0.00589	0.00108	0.00181
$\gamma_{5\rightarrow 0}$	0.00016	0.00001	-0.00076	-0.02521	0.00001	-0.00363	-0.00067	-0.00112
$f_{5\rightarrow 0}$	0.00073	0.00005	-0.00357	-0.11872	0.00005	-0.01711	-0.00314	-0.00527
$\gamma_{3\rightarrow 35}$	-0.00036	-0.88106	0.00320	0.10443	0.11136	0.01509	0.00279	0.00465
$f_{3\rightarrow 35}$	-0.00164	**-3.98069**	0.01448	0.47192	0.50315	0.06820	0.01259	0.02100
$\gamma_{35\rightarrow 3}$	0.00003	0.08270	-0.00030	-0.00980	-0.01045	-0.00142	-0.00026	-0.00044
$f_{35\rightarrow 3}$	0.00010	0.25230	-0.00092	-0.02990	-0.03189	-0.00432	-0.00080	-0.00133
$\gamma_{4\rightarrow 45}$	-0.00329	-0.00061	-0.22535	0.03145	-0.00061	0.31978	-0.03098	0.09840
$f_{4\rightarrow 45}$	-0.00140	-0.00026	-0.09563	0.01335	-0.00026	0.13571	-0.01313	0.04179
$\gamma_{45\rightarrow 4}$	0.00266	0.00049	0.18242	-0.02548	0.00049	-0.25884	0.02496	-0.07981
$f_{45\rightarrow 4}$	0.02277	0.00418	**1.56142**	-0.21880	0.00418	**-2.21482**	0.21030	-0.68757
$\gamma_{5\rightarrow 45}$	-0.00014	0.00001	0.00257	**-1.04473**	0.00001	0.01195	0.00222	0.00368
$f_{5\rightarrow 45}$	-0.00056	0.00002	0.01020	**-4.15151**	0.00002	0.04751	0.00880	0.01463
$\gamma_{45\rightarrow 5}$	0.00002	0.00000	-0.00038	0.15426	0.00000	-0.00177	-0.00033	-0.00054
$f_{45\rightarrow 5}$	0.00013	-0.00001	-0.00233	0.95018	-0.00001	-0.01087	-0.00202	-0.00335
$\gamma_{45\rightarrow 345}$	-0.00015	0.00340	-0.01062	-0.00175	0.00340	-0.04880	0.38096	0.99045
$f_{45\rightarrow 345}$	-0.00044	0.00973	-0.03037	-0.00501	0.00972	-0.13959	**1.08973**	**2.83323**
$\gamma_{345\rightarrow 45}$	0.00005	-0.00101	0.00316	0.00052	-0.00101	0.01451	-0.11324	-0.29441
$f_{345\rightarrow 45}$	0.00029	-0.00650	0.02027	0.00334	-0.00649	0.09317	-0.72733	**-1.89095**
$\gamma_{35\rightarrow 5}$	-0.00003	-0.08108	0.00059	0.01908	-0.97009	0.00276	0.00051	0.00085
$f_{35\rightarrow 5}$	-0.00008	-0.24026	0.00176	0.05653	**-2.87469**	0.00819	0.00152	0.00252
$\gamma_{34\rightarrow 3}$	0.00000	0.00456	0.00013	0.00427	0.00455	0.00062	-0.48909	0.00019
$f_{34\rightarrow 3}$	0.00001	0.01376	0.00039	0.01289	0.01375	0.00187	**-1.47765**	0.00058
$\gamma_{345\rightarrow 34}$	0.00000	0.00343	0.00003	0.00317	0.00342	0.00012	0.38195	-0.01704
$f_{345\rightarrow 34}$	0.00002	0.02280	0.00020	0.02112	0.02277	0.00078	**2.54154**	-0.11336
$\gamma_{i\rightarrow}$ (i=0,3,4,5,35,34,45,345)	-0.98865	-0.15655	**-1.07621**	-0.30012	-0.16558	-0.96498	**-1.21047**	-0.98028
$\gamma_{0\rightarrow 45}$	-0.02376	-0.00143	0.12280	0.05741	-0.00143	0.58758	0.10772	0.18064
$f_{0\rightarrow 45}$	-0.08750	-0.00528	0.45199	0.21086	-0.00527	**2.16408**	0.39516	0.66172
$\gamma_{4\rightarrow 34}$	-0.00002	0.00549	-0.00153	0.00514	0.00548	0.00072	0.61188	0.00022
$f_{4\rightarrow 34}$	-0.00009	0.02592	-0.00723	0.02426	0.02589	0.00339	**2.89031**	0.00104
$\gamma_{34\rightarrow 4}$	0.00000	-0.00004	0.00001	-0.00003	-0.00004	0.00000	-0.00391	0.00000
$f_{34\rightarrow 4}$	0.00000	-0.00011	0.00003	-0.00010	-0.00011	-0.00001	-0.01202	0.00000
$\gamma_{45\rightarrow 0}$	0.00000	0.00000	-0.00002	-0.00001	0.00000	-0.00011	-0.00002	-0.00004
$f_{45\rightarrow 0}$	0.00004	0.00000	-0.00021	-0.00010	0.00000	-0.00100	-0.00018	-0.00031

Table 2.9. Phenomena used to train the model, formulae used to evaluate the model for each phenomenon, and respective non-normalized scores.

Data	Formula to calculate non-normalized score	non-normalized score
Similar levels of PI4P and PI45P2	abs([PI(4)P] - [PI(4,5)P2])	617.82
Similar levels of PI3P and PI5P	abs([PI(3)P] - [PI(5)P])	17.86
PI5P levels are 5 fold of PI35P2 levels	abs([PI(5)P] - 5 * [PI(3,5)P2])	7.64
PI4P or PI45P2 is 100 times more than PI5P or PI3P	abs([PI(4)P] - 100 * [PI(5)P])	930.43
Stst value of PI close to 300000	abs([PI] - 300000)	19618.60
Stst value of PI45P2 close to 10000	abs([PI(4,5)P2] - 10000)	519.09
Stst value of PI3P close to 100	abs([PI(3)P] - 100)	7.57
similar levels of PI35P2 and PI34P2	abs([PI(3,5)P2] - [PI(3,4)P2])	17.05
PI45P2 will decrease in the same percentage as PI	abs([PI with PI input KD] / [Steady-state PI] - [PI(4,5)P2 with PI input KD] / [Steady-state PI(4,5)P2])	0.46
PI4P drops to .5 after PI4K knockout	abs(0.5 - [PI(4)P with PI4K KO] / [Steady-state PI(4)P])	0.41
PI45P2 drops to .5 after PI4K knockout	abs(0.5 - [PI(4,5)P2 with PI4K KO] / [Steady-state PI(4,5)P2])	0.31
PI45P2 drops to .5 after PIP_5KI knockdown	abs(0.5 - [PI(4,5)P2 with PIP5KI KD] / [Steady-state PI(4,5)P2])	0.04
PI5P drops to .2 after MTMR2 knockdown (MTMR estimated to be reduced to 65%)	abs(0.2 - [PI(5)P with MTMR 35% KD] / [Steady-state PI(5)P])	0.71
PI35P2 raises to 1.5 after MTMR2 knockdown (MTMR estimated to be reduced to 65%)	abs(1.5 - [PI(3,5)P2 with MTMR 35% KD] / [Steady-state PI(3,5)P2])	0.03
PI5P should drop to 50% if pi_Kfive is reduced to 10%	abs(0.5 - [PI(5)P with PIKfyve 90% KD] / [Steady-state PI(5)P])	0.07
PI35P2 should drop to 50% if pi_Kfive is reduced to 10%	abs(0.5 - [PI(3,5)P2 with PIKfyve 90% KD] / [Steady-state PI(3,5)P2])	0.03
PI5P should drop to .15 if pi_Kfyve is knockout	abs(0.15 - [PI(5)P with PIKfyve KO] / [Steady-state PI(5)P])	0.07
PI35P2 should drop to undetectable levels if pi_Kfyve is knockout	abs(0.001 - [PI(3,5)P2 with PIKfyve KO] / [Steady-state PI(3,5)P2])	0.01
PI45P2 should drop to .8 if pi_Kfyve is knockout	abs(0.8 - [PI(4,5)P2 with PIKfyve KO] / [Steady-state PI(4,5)P2])	0.04
PI3P should increase 5-fold if pi_Kfyve is knockout	abs(5 - [PI(3)P with PIKfyve KO] / [Steady-state PI(3)P])	3.07

Table 2.10. siRNAs screen used to identify candidate CF drug targets.

Effect of siRNA is measured by ENaC activity. Scores above 1 classify a gene as ENaC inhibiting and below -1 as ENaC-activating. The screen is described in detail in theses supplementary methods and in Almaça *et al.* [23].

First round of siRNA screens (*Almaça et al.* [23])		Second round of siRNA screens (siRNA KD validation tests)				
Gene name	Results	Gene name	First siRNA test	Second siRNA test	Third siRNA test	Results
INPP5A	ENaC-activating gene	INPP5A	4.628	-2.796	x	both effects
INPPL1	ENaC-activating gene	INPPL1	3.400	-1.025	x	both effects
OCRL	both effects	OCRL	1.947	0.465	-4.844	both effects
PI4KA	ENaC-activating gene	PI4KA	-0.861	-5.739	4.752	both effects
PIK3C2B	ENaC-inhibiting gene	PIK3C2B	5.777	-0.019	x	1 of 2 ENaC-inhibiting
PIK3CA	ENaC-activating gene	PIK3CA	-1.761	1.109	-1.385	both effects
PIK3CB	ENaC-activating gene	PIK3CB	-0.509	-4.154	x	1 of 2 ENaC-activating
PIK3CD	ENaC-activating gene	PIK3CD	-2.944	-1.903	0.952	2 of 3 ENaC-activating
PIK3R3	ENaC-inhibiting gene	PIK3R3	5.877	-11.030	2.551	both effects
PIP4K2A	ENaC-activating gene	PIP4K2A	-2.992	-4.393	-3.249	3 of 3 ENaC-activating
PIP5K1B	both effects	PIP5K1B	-1.986	-3.728	x	2 of 2 ENaC-activating

Table 2.11. System equations.

Fluxes

$V_{\rightarrow 0} = \gamma_{\rightarrow 0}$

$V_{\rightarrow 4} = \gamma_{\rightarrow 4}$

$V_{\rightarrow 3} = \gamma_{\rightarrow 3}$

$V_{0\rightarrow 3} = \gamma_{0\rightarrow 3} * PI^{f_{0\rightarrow 3}} * (PI3KII+PI3III)$

$V_{3\rightarrow 0} = \gamma_{3\rightarrow 0} * PI(3)P^{f_{3\rightarrow 0}} * (SYNJ+SAC1+MTMR)$

$V_{0\rightarrow 4} = \gamma_{0\rightarrow 4} * PI^{f_{0\rightarrow 4}} * PI4K$

$V_{4\rightarrow 0} = \gamma_{4\rightarrow 0} * PI(4)P^{f_{4\rightarrow 0}} * (SYNJ+SAC1)$

$V_{0\rightarrow 5} = \gamma_{0\rightarrow 5} * PI^{f_{0\rightarrow 5}} * PIKfyve$

$V_{5\rightarrow 0} = \gamma_{5\rightarrow 0} * PI(5)P^{f_{5\rightarrow 0}} * (SYNJ+SAC1)$

$V_{3\rightarrow 35} = \gamma_{3\rightarrow 35} * PI(3)P^{f_{3\rightarrow 35}} * PIKfyve$

$V_{35\rightarrow 3} = \gamma_{35\rightarrow 3} * PI(3,5)P_2^{f_{35\rightarrow 3}} * (SYNJ+SAC1+SAC3)$

$V_{4\rightarrow 45} = \gamma_{4\rightarrow 45} * PI(4)P^{f_{4\rightarrow 45}} * PIP5KI$

$V_{45\rightarrow 4} = \gamma_{45\rightarrow 4} * PI(4,5)P2^{f_{45\rightarrow 4}} * (SIOSS)$

$V_{5\rightarrow 45} = \gamma_{5\rightarrow 45} * PI(5)P^{f_{5\rightarrow 45}} * PIP5KII$

$V_{45\rightarrow 5} = \gamma_{45\rightarrow 5} * PI(4,5)P_2^{f_{45\rightarrow 5}} * (SYNJ+TMEM55)$

$V_{45\rightarrow 345} = \gamma_{45\rightarrow 345} * PI(4,5)P_2^{f_{45\rightarrow 345}} * PI3KI$

$V_{345\rightarrow 45} = \gamma_{345\rightarrow 45} * PI(3,4,5)P_3^{f_{345\rightarrow 45}} * PTEN$

$V_{35\rightarrow 5} = \gamma_{35\rightarrow 5} * PI(3,5)P_2^{f_{35\rightarrow 5}} * MTMR$

$V_{34\rightarrow 3} = \gamma_{34\rightarrow 3} * PI(3,4)P_2^{f_{34\rightarrow 3}} * INPP4$

$V_{345\rightarrow 34} = \gamma_{345\rightarrow 34} * PI(3,4,5)P_3^{f_{345\rightarrow 34}} * (SIOSS+SHIP2)$

$V_{45\rightarrow} = \gamma_{45\rightarrow} * PI(4,5)P_2$

$V_{0\rightarrow} = \gamma_{0\rightarrow} * PI$

$V_{4\rightarrow} = \gamma_{4\rightarrow} * PI(4)P$

$V_{345\rightarrow} = \gamma_{345\rightarrow} * PI(3,4,5)P_3$

$V_{3\rightarrow} = \gamma_{3\rightarrow} * PI(3)P$

$V_{35\rightarrow} = \gamma_{35\rightarrow} * PI(3,5)P_2$

$V_{5\rightarrow} = \gamma_{5\rightarrow} * PI(5)P$

$V_{34\rightarrow} = \gamma_{34\rightarrow} * PI(3,4)P_2$

$V_{0\rightarrow 45} = \gamma_{0\rightarrow 45} * PI^{f_{0\rightarrow 45}} * (PI4K+PIP5KI)$

$V_{4\rightarrow 34} = \gamma_{4\rightarrow 34} * PI(4)P^{f_{4\rightarrow 34}} * PI3KII$

$V_{34\rightarrow 4} = \gamma_{34\rightarrow 4} * PI(3,4)P_2^{f_{34\rightarrow 4}} * PTEN$

$V_{45\rightarrow 0} = \gamma_{45\rightarrow 0} * PI(4,5)P_2^{f_{45\rightarrow 0}} * SYNJ$

Differential equations

$dPI = V_{\rightarrow 0} + V_{3\rightarrow 0} + V_{4\rightarrow 0} + V_{5\rightarrow 0} + V_{45\rightarrow 0} - V_{0\rightarrow 3} - V_{0\rightarrow 4} - V_{0\rightarrow 5} - V_{0\rightarrow 45} - V_{0\rightarrow}$

$dPI3P = V_{\rightarrow 3} + V_{0\rightarrow 3} + V_{35\rightarrow 3} + V_{34\rightarrow 3} - V_{3\rightarrow 0} - V_{3\rightarrow 35} - V_{3\rightarrow}$

$dPI4P = V_{\rightarrow 4} + V_{0\rightarrow 4} + V_{45\rightarrow 4} + V32 - V_{4\rightarrow 0} - V_{4\rightarrow 45} - V24 - V_{4\rightarrow}$

$dPI5P = V_{0\rightarrow 5} + V_{35\rightarrow 5} + V_{45\rightarrow 5} - V_{5\rightarrow 0} - V_{5\rightarrow 45} - V_{5\rightarrow}$

$dPI35P2 = V_{3\rightarrow 35} - V_{35\rightarrow 5} - V_{35\rightarrow 3} - V_{35\rightarrow}$

$dPI45P2 = V_{4\rightarrow 45} + V_{5\rightarrow 45} + V_{345\rightarrow 45} + V_{0\rightarrow 45} - V_{45\rightarrow 4} - V_{45\rightarrow 5} - V_{45\rightarrow 345} - V_{45\rightarrow 0} - V_{45\rightarrow}$

$dPI34P2 = V_{345\rightarrow 34} + V_{4\rightarrow 34} - V_{34\rightarrow 4} - V_{34\rightarrow 3} - V_{34\rightarrow}$

$dPI345P3 = V_{45\rightarrow 345} - V_{345\rightarrow 45} - V_{345\rightarrow 34} - V_{345\rightarrow}$

2.11. References

[1] G. van Meer, D. R. Voelker, and G. W. Feigenson, “Membrane lipids: where they are and how they behave.,” *Nat. Rev. Mol. Cell Biol.*, vol. 9, no. 2, pp. 112–124, 2008.

[2] B. Fadeel and D. Xue, “Membrane : Roles in Health and Disease,” *Crit Rev Biochem Mol Biol*, vol. 44, no. 5, pp. 264–277, 2009.

[3] M. J. Phillips and G. K. Voeltz, “Structure and function of ER-membrane contact sites with other organelles.,” *Mol. Cell Biol.*, vol. 17, pp. 69–82, 2016.

[4] S. Lev, “Non-vesicular lipid transport by lipid-transfer proteins and beyond.,” *Nat. Rev. Mol. Cell Biol.*, 2010.

[5] Y. J. Kim, M. L. Guzman-Hernandez, and T. Balla, “A highly dynamic ER-derived phosphatidylinositol-synthesizing organelle supplies phosphoinositides to cellular membranes,” *Dev. Cell*, vol. 21, pp. 813–824, 2011.

[6] A. Johnson, B. Alberts, D. Bray, D. Lewis, K. Roberts, and M. Raff, “Molecular Biology of the Cell. (4th ed.),” *Garland Science*, 2002. .

[7] I. Schomburg *et al.*, “BRENDA: integrated reactions, kinetic data, enzyme function data, improved disease classification.,” 2015. .

[8] P. W. Chen, L. L. Fonseca, Y. A. Hannun, and E. O. Voit, “Coordination of Rapid Sphingolipid Responses to Heat Stress in Yeast,” *PLoS Comput. Biol.*, vol. 9, no. 5, 2013.

[9] T. Sasaki *et al.*, “Mammalian phosphoinositide kinases and phosphatases,” *Prog. Lipid Res.*, vol. 48, no. 6, pp. 307–343, 2009.

[10] C. J. Stefan, A. G. Manford, D. Baird, J. Yamada-Hanff, Y. Mao, and S. D. Emr, “Osh proteins regulate phosphoinositide metabolism at ER-plasma membrane contact sites,” *Cell*, vol. 144, no. 3, pp. 389–401, 2011.

[11] T. Balla, “Phosphoinositides: tiny lipids with giant impact on cell regulation,”

Physiol. Rev., vol. 93, no. 3, pp. 1019–1137, 2013.

[12] E. Delage, J. Puyaubert, A. Zachowski, and E. Ruelland, "Signal transduction pathways involving phosphatidylinositol 4-phosphate and phosphatidylinositol 4,5-bisphosphate: Convergences and divergences among eukaryotic kingdoms," *Prog. Lipid Res.*, vol. 52, no. 1, pp. 1–14, 2013.

[13] N. R. Leslie, I. H. Batty, H. Maccario, L. Davidson, and C. P. Downes, "Understanding PTEN regulation: PIP2, polarity and protein stability," *Oncogene*, vol. 27, no. 41, pp. 5464–5476, 2008.

[14] C. E. Bazenet and R. A. Anderson, "Phosphatidylinositol-4-phosphate 5-kinases from human erythrocytes.," *Methods Enzym.*, vol. 209, pp. 189–202, 1992.

[15] S. J. Bulley, J. H. Clarke, A. Droubi, M.-L. Giudici, and R. F. Irvine, "Exploring phosphatidylinositol 5-phosphate 4-kinase function.," *Adv. Biol. Regul.*, vol. 57, pp. 193–202, Jan. 2015.

[16] B. M. Emerling *et al.*, "Depletion of a putatively druggable class of phosphatidylinositol kinases inhibits growth of p53-Null tumors," *Cell*, vol. 155, no. 4, pp. 844–857, 2013.

[17] J. Schaletzky, S. K. Dove, B. Short, O. Lorenzo, M. J. Clague, and A. F. Barr, "Phosphatidylinositol-5-Phosphate Activation and Conserved Substrate Specificity of the Myotubularin Phosphatidylinositol 3-Phosphatases.," *Curr. Biol.*, vol. 13, pp. 504–509, 2003.

[18] N. Divecha, "Phosphoinositides in the nucleus and myogenic differentiation: how a nuclear turtle with a PHD builds muscle.," *Biochem. Soc. Trans.*, vol. 44, no. 1, pp. 299–306, 2016.

[19] E. Kent, S. Neumann, U. Kummer, and P. Mendes, "What can we learn from global sensitivity analysis of biochemical systems?," *PLoS One*, vol. 8, no. 11, 2013.

[20] S. Srinath and R. Gunawan, "Parameter identifiability of power-law biochemical system models," *J. Biotechnol.*, vol. 149, no. 3, pp. 132–140, 2010.

[21] K. Z. Yao, B. M. Shaw, B. Kou, K. B. McAuley, and D. W. Bacon, “Modeling Ethylene/Butene Copolymerization with Multi-site Catalysts: Parameter Estimability and Experimental Design,” *Polym. React. Eng.*, vol. 11, no. 3, pp. 563–588, 2003.

[22] R Core Team, *R: a language and environment for statistical computing*. Vienna, Austria, 2017.

[23] J. Almaça *et al.*, “High-content siRNA screen reveals global ENaC regulators and potential cystic fibrosis therapy targets,” *Cell*, vol. 154, no. 6, 2013.

[24] C. Xu, J. Watras, and L. M. Loew, “Kinetic analysis of receptor-activated phosphoinositide turnover,” *J. Cell Biol.*, vol. 161, pp. 779–791, 2003.

[25] J. Viaud *et al.*, “Phosphoinositides: Important lipids in the coordination of cell dynamics,” *Biochimie*, vol. 125, pp. 250–258, 2016.

[26] O. C. Ikonomov *et al.*, “The Phosphoinositide Kinase PIKfyve Is Vital in Early Embryonic Development: PREIMPLANTATION LETHALITY OF PIKfyve-/- EMBRYOS BUT NORMALITY OF PIKfyve+/- MICE,” *J. Biol. Chem.*, vol. 286, no. 15, pp. 13404–13413, 2011.

[27] Y. Zhang *et al.*, “Loss of Vac14, a regulator of the signaling lipid phosphatidylinositol 3,5-bisphosphate, results in neurodegeneration in mice.,” *Proc. Natl. Acad. Sci. U. S. A.*, vol. 104, no. 44, pp. 17518–17523, 2007.

[28] B. H. Falkenburger, J. B. Jensen, E. J. Dickson, B.-C. Suh, and B. Hille, “Phosphoinositides: lipid regulators of membrane proteins.,” *J. Physiol.*, 2010.

[29] A. Shisheva, “PtdIns5P: News and views of its appearance, disappearance and deeds,” *Arch. Biochem. Biophys.*, vol. 538, no. 2, pp. 171–180, 2013.

[30] G. R. V. Hammond *et al.*, “PI4P and PI(4,5)P2 are essential but independent lipid determinants of membrane identity.,” *Science (80-.).*, vol. 337, no. 6095, pp. 727–730, 2012.

[31] Z. Szentpetery, P. Várnai, and T. Balla, “Acute manipulation of Golgi phosphoinositides to assess their importance in cellular trafficking and

signaling.," *Proc. Natl. Acad. Sci. U. S. A.*, vol. 107, no. 18, pp. 8225–30, 2010.

[32] F. Martin-Belmonte *et al.*, "PTEN-Mediated Apical Segregation of Phosphoinositides Controls Epithelial Morphogenesis through Cdc42," *Cell*, 2007.

[33] A. Gericke, N. R. Leslie, M. Lösche, and A. H. Ross, "PtdIns(4,5)P2-mediated cell signaling: Emerging principles and PTEN as a paradigm for regulatory mechanism," *Adv. Exp. Med. Biol.*, vol. 991, pp. 85–104, 2013.

[34] L. A. Volpicelli-Daley *et al.*, "Phosphatidylinositol-4-phosphate 5-kinases and phosphatidylinositol 4,5-bisphosphate synthesis in the brain," *J. Biol. Chem.*, vol. 285, no. 37, pp. 28708–28714, 2010.

[35] D. R. Jones *et al.*, "Phosphorylation of glycosyl-phosphatidylinositol by phosphatidylinositol 3-kinase changes its properties as a substrate for phospholipases.," *FEBS Lett., 579(1), 59-65.*, vol. 579, no. 1, pp. 59–65, 2005.

[36] T. I. Meier *et al.*, "Cloning, expression, purification, and characterization of the human Class Ia phosphoinositide 3-kinase isoforms. Protein Expr Purif.," *Protein Expr Purif.*, vol. 35, no. 2, pp. 218–224, 2004.

[37] J. Domin, F. Pages, S. Volinia, S. E. Rittenhouse, R. C. Stein, and M. D. Waterfield, "Cloning of a human phosphoinositide 3-kinase with a C2 domain that displays reduced sensitivity to the inhibitor wortmannin.," *Biochem J.*, vol. 326, p. 139–147., 1997.

[38] R. Wetzker *et al.*, "Purification and characterization of phosphatidylinositol 4-kinase from human erythrocyte membranes.," *Eur J Biochem.*, vol. 200, no. 1, pp. 179–185, 1991.

[39] G. H. Jenkins and R. A. Subrahmanyam, G. Anderson, "Purification and reconstitution of phosphatidylinositol 4-kinase from human erythrocytes.," *Biochim Biophys Acta.*, vol. 1080, no. 1, pp. 11–28, 1991.

[40] X. Zhang *et al.*, "Phosphatidylinositol-4-phosphate 5-kinase isozymes catalyze the synthesis of 3-phosphate-containing phosphatidylinositol signaling

molecules.," *J Biol Chem.*, vol. 272, no. 28, pp. 17756–17761, 1997.

[41] S. B. Johnston and R. T. Raines, "Catalysis by the tumor-suppressor enzymes PTEN and PTEN-L," *PLoS One*, vol. 10, no. 1, pp. 1–13, 2015.

[42] T. U. Consortium, "Uniprot : a hub for Protein information.," *The UniProt Consortium.*, 2015. .

[43] K. K. Cladwell, D. L. Lips, V. S. Bansal, and P. W. Majerus, "Isolation and characterization of two 3-phosphatases that hydrolyze both phosphatidylinositol 3-phosphate and inositol 1,3-bisphosphate.," *J Biol Chem*, vol. 266, no. 27, pp. 18378–18386, 1991.

[44] F. A. Norris, R. C. Atkins, and P. W. Majerus, "The cDNA cloning and characterization of inositol polyphosphate 4-phosphatase type II. Evidence for conserved alternative splicing in the 4-phosphatase family.," *J Biol Chem.*, vol. 272, no. 38, pp. 23859–23864, 1997.

[45] K. Niebuhr *et al.*, "Conversion of PtdIns(4,5)P(2) into PtdIns(5)P by the S.flexneri effector IpgD reorganizes host cell morphology.," *EMBO J.*, vol. 21, no. 19, pp. 5069–5078, 2002.

[46] M. Matzaris, S. P. Jackson, K. M. Laxminarayan, C. J. Speed, and C. A. Mitchell, "Identification and characterization of the phosphatidylinositol-(4, 5)-bisphosphate 5-phosphatase in human platelets.," *J Biol Chem.*, vol. 269, no. 5, pp. 3397–3402, 1994.

[47] P. D. Roach and F. B. Palmer, "Human erythrocyte cytosol phosphatidyl-inositol-bisphosphate phosphatase.Human erythrocyte cytosol phosphatidyl-inositol-bisphosphate phosphatase.," *Biochim Biophys Acta.*, pp. 323–333, 1981.

[48] S. Suer, A. Sickmann, H. E. Meyer, F. W. Herberg, and L. M. Heilmeyer Jr., "Human phosphatidylinositol 4-kinase isoform PI4K92. Expression of the recombinant enzyme and determination of multiple phosphorylation sites.," *Eur J Biochem.*, vol. 268, no. 7, pp. 2099–2106, 2001.

[49] S. J. Morgan, A. D. Smith, and P. J. Parker, "Purification and characterization of

bovine brain type I phosphatidylinositol kinase.," *Eur. J. Biochem.*, vol. 191, no. 3, pp. 761–767, 1990.

[50] L. E. Ling, J. T. Schultz, L. C. Cantley, J. T. Schulz, and L. C. Cantley, "Characterization and purification of membrane-associated phosphatidylinositol-4-phosphate kinase from human red blood cells," *J. Biol. Chem.*, vol. 264, no. 9, pp. 5080–5088, 1989.

[51] C. L. Carpenter, B. C. Duckworth, B. C. Auger, B. Cohen, B. S. Schaffhausen, and L. C. Cantley, "Purification and characterization of phosphoinositide 3-kinase from rat liver.," *J Biol Chem.*, vol. 265, no. 32, pp. 19704–19711, 1990.

[52] G. McConnachie, I. Pass, S. M. Walker, and C. P. Downes, "Interfacial kinetic analysis of the tumour suppressor phosphatase, PTEN: evidence for activation by anionic phospholipids," *Biochem. J.*, vol. 371, no. 3, pp. 947–955, May 2003.

Chapter 3. Thickness of the airway surface liquid layer in the lung is affected in cystic fibrosis by compromised synergistic regulation of the ENaC ion channel

This Chapter is an integral reproduction of the paper:

Olivença, D. V., Fonseca, L. L., Voit, E. O., & Pinto, F. R. (2018). Thickness of the airway surface liquid layer in the lung is affected in cystic fibrosis by compromised synergistic regulation of the ENaC ion channel. [submitted]

3.1. Abstract

The lung epithelium is lined with a layer of airway surface liquid (ASL), which is crucial for healthy lung function. The thickness of ASL is controlled by two ion channels: The epithelium sodium channel (ENaC) and the cystic fibrosis transmembrane conductance regulator (CFTR). Here we present a minimal mathematical model of ENaC, CFTR and ASL regulation that sheds light on the control of ENaC by the short palate lung and nasal epithelial clone 1 (SPLUNC1) protein and by phosphatidylinositol 4,5-biphosphate ($PI(4,5)P_2$). The model, despite its simplicity, yields a good fit to experimental observations and is an effective tool for exploring the interplay between ENaC, CFTR and ASL. We show that the available data can constrain the model's parameters without ambiguities. The control of the ENaC opening probability, exerted by $PI(4,5)P_2$, is sufficient for fitting available experimental data. We test the hypothesis that $PI(4,5)P_2$ protects ENaC from ubiquitination and results suggest that it does not improve the model's ability to reproduce observations, but changes the sign of the steady-state sensitivity of ENaC with respect to changes in $PI(4,5)P_2$ from negative to positive. Finally, model analysis shows that ASL at the steady state is sensitive to small changes in $PI(4,5)P_2$ abundance, particularly in cystic fibrosis conditions, which suggests that manipulation of phosphoinositide metabolism may promote therapeutic benefits for cystic fibrosis patients.

3.2. Introduction

Cystic fibrosis (CF) is a genetic disease caused by mutations in a chloride channel: the cystic fibrosis transmembrane conductance regulator (CFTR). A mutated CFTR may cause loss of function or not even reach the plasma membrane, thereby not only affecting the lungs but also many other organs, such as the pancreas. In the lungs, this condition leads to the gradual destruction of tissues, due to repeated inflammation and infections [1,2]. CF cause has been known for several decades, but an effective treatment for the disease has eluded the best efforts of the biomedical community, although substantial gains in life expectancy and quality of life have been achieved by the targeted management of symptoms. Good results were recently obtained with Lumacaftor and Ivacaftor, but some mutations remain untreatable by drugs [3].

The Epithelium Sodium Channel (ENaC) may be affected in CF [2,4–6]. The upregulation of this channel function is thought to contribute of the accumulation of thick dehydrated mucus that is one of the hallmarks of CF and a frequent source of consequent lung problems [2]. Inadequately hydrated mucus and/or mucus over-production are also the cause of a number of other diseases, including primary ciliary dyskinesia, chronic obstructive pulmonary disease, bronchiectasis and asthma [1]. ENaC is furthermore important in non-mucus related conditions like blood pressure control problems, edema [7] and heart disease [8]. Given the important roles of ENaC in such a wide range of conditions it is imperative that we improve our fundamental understanding of this channel in health, disease, and with respect to novel treatments.

In this work we focus on the crosstalk between two of the crucial regulators of ENaC: the short palate lung and nasal epithelial clone 1 (SPLUNC1) extracellular protein and phosphatidylinositol 4,5-biphosphate ($PI(4,5)P_2$). Distinct parallel mechanisms of ENaC regulation have been investigated [9,10], and several models of airway surface liquid (ASL) and ENaC regulation and their impact on ion-driven water fluxes have been proposed (*e.g.*, [11–15]). However, these models do not account for the synergistic regulation of ENaC and ASL by SPLUNC1 and $PI(4,5)P_2$. Thus, our goal is to deepen our understanding of this synergism with the design of a simple, targeted mathematical model that allows us to explore the specific roles and interactions of these regulators.

3.3. Background

ENaC is a membrane-bound ion channel that transports Na^+ ions according to the electrochemical gradient. It is a constituted by three of α or δ, β or γ subunits that present common tertiary structures and similar amino acid sequence. Other stoichiometries are possible but the most common is a αβγ trimer [16].

The role of ENaC in CF is still unclear [17–19]. The majority of researchers, however, appears to be convinced that ENaC function is upregulated in CF. Indeed, several hypotheses explaining this upregulation have been proffered [2,4,7,20–22]. Among them is the postulate that the absence of functional CFTRs in the cell membrane causes the acidification of the airway surface liquid (ASL), which lines and protects the lungs [23–25]. This acidification, in turn, is suspected to inactivate SPLUNC1, a protein involved in protecting ENaC from proteolysis, among other roles. SPLUNC1 also promotes ENaC ubiquitination and disassembly, removing the α and γ subunits from the plasma membrane [6]. Taken together, the lack of CFTR activity would lead to a loss of SPLUNC1 and to an elevated ENaC activity or an increased number of channels. We analyze this hypothesis here, because it could lead to truly novel therapeutic applications [26], if it can be confirmed. The dynamics of ENaC is represented graphically in Figure 3.1.

Phosphoinositides are lipids in the cell membranes that have numerous functions [27]. One of them is the regulation of plasma membrane proteins. Several studies have shown that some phosphoinositides, specifically $PI(4,5)P_2$ and phosphatidylinositol 3,4,5-triphosphate ($PI(3,4,5)P_3$), influence ENaC [27–31]. A mechanistic explanation of this phosphoinositide control of ENaC was advanced by Kota *et al.* [32], who found that when the intracellular N-terminal of γ ENaC connects to phosphoinositides, a conformational change occurs that exposes the extracellular loops of the channel to proteases. Once these loops are cleaved, the channel channel-open probability (P_o) of ENaC is increased. While ENaC is initially cleaved by furin in the Golgi, further protease action can greatly increase the P_o [33].

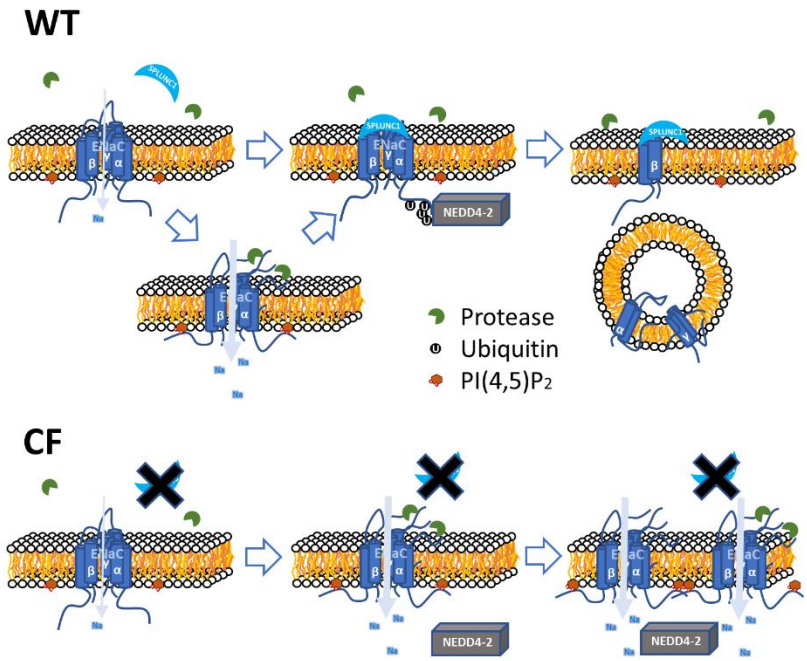

Figure 3.1. ENaC regulation by proteases, SPLUNC1, PI(4,5)P2 and NEDD4-2.

When ENaC is created and placed into the cell membrane, it presents a low activity. Full activation is contingent on the cleavage of its extracellular loops by proteases. To expose the loops, ENaC's N-termini need to interact with $PI(4,5)P_2$ in the cell membrane. The extracellular protein SPLUNC1 induces a conformation shift in ENaC that expose intracellular ubiquitination sites of α and γ subunits. These sites are ubiquitinated by the neural precursor cell expressed developmentally down-regulated protein 4 - 2 (NEDD4-2) that, in turn, cause the disassembly of the channel and the removal of the ubiquitinated subunit from the cell membrane. In CF, the ASL is more acidic due to the lack of CFTR in the membrane. The acidity inactivates SPLUNC1, which in turn reduces the ubiquitination of ENaC by NEDD4-2 and consequently decreases the removal of ENaC channels from the membrane.

Therefore, if the levels of $PI(4,5)P_2$ or $PI(3,4,5)P_3$ are decreased, proteases do not cut the extracellular loops of ENaC and the channel activity is reduced. The N-terminal can also be ubiquitinated, which marks ENaC for internalization and degradation. The fact that ENaC is sensitive to anionic phospholipids and ubiquitinated in the same region raises the question whether $PI(4,5)P_2$ or $PI(3,4,5)P_3$ could protect ENaC from ubiquitination. Kota and colleges [32] observed that the γ-N-terminal is structurally more compact in the presence of $PI(4,5)P_2$, which indicates that connecting to $PI(4,5)P_2$ or $PI(3,4,5)P_3$ might indeed protect these sites from ubiquitination. In this work we investigate the phosphoinositide and NEDD4-2 competition for the ENaC N-terminus by comparing two models: one where PI(4,5)P2 does not protect ENaC from degradation and another where it does.

While these chains of possible causes and effects appear to make *a priori* sense, it is known that intuition regarding the consequences of changes of any of the components in a complex nonlinear system are treacherous and often unreliable. We therefore incorporate all pertinent information regarding the regulation of ENaC and ASL by SPLUNC1 and $PI(4,5)P_2$ into a dynamic mathematical model, which permits explorations of every aspect of the system in a quantitative manner. In particular, this model allows us to test if the dual effect of $PI(4,5)P_2$ increasing the P_o of ENaC and decreasing ENaC degradation is compatible with experimental observations. More generally, the model enables us to investigate quantitatively if $PI(4,5)P_2$ has a significant impact on ASL thickness, which ultimately determines the severity of the CF lung phenotype.

3.4. Results

3.4.1. Model description

The proposed model of ENaC and ASL regulation by SPLUNC1 and $PI(4,5)P_2$ is diagrammed in Figure 3.2. It contains two dependent variables, ENaC and ASL, and accounts for channel production and degradation, as well as ASL influx and efflux. SPLUNC1 and $PI(4,5)P_2$ are included as independent variables with regulatory roles in the system.

The ENaC variable represents the number of channels in a μm^2 of apical plasma membrane. The rate of ENaC production is assumed to be constant (V_1). $PI(4,5)P_2$ affects ENaC´s P_o. The $PI(4,5)P_2$-dependent P_o, multiplied by ENaC, corresponds to ENaC's activity.

SPLUNC1 causes a conformational change that will expose ENaC's ubiquitination sites. This will lead to the disassembly of the channel and internalization of the α and γ subunits [6,25]. Therefore, SPLUNC1 indirectly activates one of the ENaC degradation fluxes (V_3), thereby maintaining low levels of active channels. The number of SPLUNC1 molecules is considered to be constant. To model SPLUNC1 dilution on ASL, we assume that SPLUNC1 activity is inversely proportional to ASL thickness. ENaC has a second degradation flux (V_2) that is independent of SPLUNC1. This flux is important for the system's ability to reach a steady state when SPLUNC1 activity is inhibited.

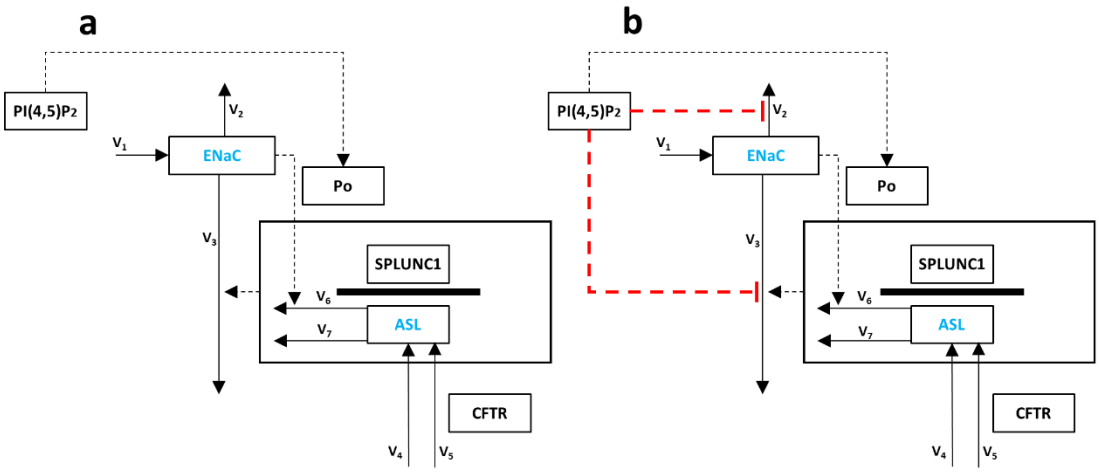

Figure 3.2. Diagrams of the two model variants.

Graphical representation of the two models tested. a) In Model A, PI(4,5)P_2 only influences ENaC's P_o but does not protect the channel from degradation. b) In Model B, PI(4,5)P_2 influences ENaC's P_o and also protects the channel from degradation. Solid arrows represent fluxes and dashed arrows regulatory processes.

The ASL variable represents the thickness or height of the liquid, expressed in μm, above the apical plasma membrane. ASL has two influxes: V_5 accounts for the influx of material, which depends on CFTR activity, whereas V_4 accounts for other channels like aquaporins and tight junctions that allow material to passes through. ENaC activity induces water absorption and reduces the thickness of ASL through the flux V_6. V_7 is an ENaC-independent efflux from ASL that ensures that a steady state is reached if ENaC activity on ASL is blocked.

To study the hypothesis that PI(4,5)P_2 additionally protects ENaC from ubiquitination, we created two model variants: in model A, PI(4,5)P_2 does not protect ENaC from ubiquitination (Figure 3.2 a), whereas in model B, PI(4,5)P_2 inhibits both degradation fluxes of ENaC (Figure 3.2 b). Differential equations for both models are presented in Table 3.1.

Table 3.1. Model equations, parameter values and initial values for model variant A and B.

Variant A, where $PI(4,5)P_2$ does not protect ENaC from degradation, and variant B, where $PI(4,5)P_2$ does protect ENaC from degradation.

	Variant A	Variant B
Differential Equations		
dENaC/dt	$V_1 - V_2 - V_3$	
dASL/dt	$V_4 + V_5 - V_6 - V_7$	
Fluxes		
V_1	γ_1	
V_2	$\gamma_2 \cdot ENaC$	$\gamma_2 \cdot ENaC \cdot (PI(4,5)P_2)^{-1}$
V_3	$\gamma_3 \cdot ENaC \cdot (SPLUNC1/ASL)$	$\gamma_3 \cdot ENaC \cdot (SPLUNC1/ASL) \cdot (PI(4,5)P_2)^{-1}$
V_4	γ_4	
V_5	γ_5	
V_6	$\gamma_6 \cdot ASL \cdot ENaC \cdot P_o(PI(4,5)P_2)$	
V_7	$\gamma_7 \cdot ASL$	
Initial conditions for the dependent variables		
ENaC	35 molecules/μm^2	
ASL	7 μm	
Parameters		
γ_1	1.73×10^{-2} molecules$\cdot min^{-1}$	
γ_2	2.17×10^{-4} molecules$^{-1} min^{-1}$	2.17 min^{-1}
γ_3	2.53×10^{-7} $\mu m \cdot$molecules$^{-1} \cdot min^{-1}$	2.53×10^{-3} $\mu m \cdot min^{-1}$
γ_4	5.92×10^{-2} $\mu m \cdot min^{-1}$	
γ_5	2.39×10^{-2} $\mu m \cdot min^{-1}$	
γ_6	2.64×10^{-4} molecules$^{-1} \cdot min^{-1}$	
γ_7	9.59×10^{-3} min^{-1}	
Independent variables		
SPLUNC1	7714 molecules/μm^2	
$PI45P_2$	10000 molecules/μm^2	

The model parameters were optimized so that the model behavior was consistent with experimental observations retrieved from the literature (Table 3.2). In particular, the model was adjusted to replicate steady states in both, wild type (WT) and CF, the known half-life of ENaC, and ASL perturbation time courses in WT epithelia. To simulate the CF phenotype, SPLUNC1 and the rate constant γ_5 were set to zero.

Table 3.2. Observed experimental phenomena used to calibrate and validate the model.

Data Description	Usage	Reference
In WT lungs, the number of ENaC channels per μm^2 of plasma membrane is between 30 and 50.	Set steady-state value of ENaC in WT to 35. Used do define γ_4, γ_5, γ_7, γ_1, $\gamma_2$and γ_3	[35]
In CF, ENaC will be degraded more slowly because of low pH inactivation of SPLUNC1 and because the channel numbers are more than double.	Set steady-state value of ENaC to 80 for CF. Used do define γ_4, γ_5, γ_7, γ_1, γ_2 and γ_3	[6]
ASL thickness has a steady state of 7 μm in WT basal conditions and a steady state of 4 μm in CF; ASL maximal thickness should not surpass 20 μm.	Used do define γ_4, γ_5, γ_7, γ_1, γ_2 and γ_3	[34,36]
Estimates for half-life of ENaC vary from 20 minutes to several hours.	Set ENaC half-life to 40 minutes. Used do define γ_1, γ_2 and γ_3	[37–39]
According to a mathematical model of epithelial ion and water transport, the relation between the ASL influx due to CFTR activity and the ASL efflux due to ENaC activity in resting WT conditions should be around 1.5.	Used do define γ_4, γ_5, γ_7,	[14]
The concentration of SPLUNC1 is about 50 ng/ml. ASL in WT has a thickness of 7 μm, and considering a 1 μm^2 patch of membrane, the number of SPLUNC1 molecules is 7714.	Set value for SPLUNC1.	[24]
ENaC activity ($N * P_o$) and mean open and closed times of ENaC for situations when $PI(4,5)P_2$ levels are low, close to basal and high (5000, 10000, 15000 molecules per μm^2, respectively).	Assuming we know N, we can determine and parameterize a function relating P_o and $PI(4,5)P_2$ levels.	[40]
ASL time courses for WT and CF.	WT data were used to adjust value of γ_6. CF data were used for validation.	[24,36,41,42]
ENaC activity, measured for WT and CF as the difference in the short circuit current with and without amiloride, which is an ENaC inhibitor. PLC was manipulated to alter $PI(4,5)P_2$ levels.	WT data were used to calibrate decrease in $PI(4,5)P_2$ due to PLC activation. CF data were used to validate model predictions.	[43]
In a normal plasma membrane there are 10,000 $PI(4,5)P_2$ molecules per μm^2	Set value for $PI(4,5)P_2$	[27,45–48]

3.4.2. Model validation

To validate the models, we compared our predictions with experimental observations that were not used to define parameter values. For this purpose, we used data from (1)time courses of ASL thickness above CF airway epithelial cultures and (2) ENaC activity changes after phospholipase C (PLC) activation (Table 3.2).

1. In the first validation, both model variants successfully replicated ASL thickness dynamics in CF airway epithelial cultures after an initial artificial increase to 25 or 30 μm (Figure 3.3, A3 and B3 plots).

2. We retrieved measurements of ENaC activity under WT and CF conditions with and without activation of phospholipase C (PLC) [43]. PLC is not a variable in our models, but PLC activity is known to decrease the level of $PI(4,5)P_2$. Thus, we estimated the degree of $PI(4,5)P_2$ reduction caused by the activation of PLC by determining the decrease in $PI(4,5)P_2$ that predicts, for a WT system, a reduction in ENaC activity similar to the experimental observation. We found that reductions of 10% and 9% in $PI(4,5)P_2$ levels, for models A and B respectively, reproduce the PLC activation effect well. This reduction is mild when compared with reports of 50% reduction after PLC activation [40]. However, this numerical discrepancy might well be attributable to differences in cell type. We are simulating human airway epithelial cells and Pochynyuk et al. used immortalized mouse renal cells from the collecting duct. Also, different experimental procedures or activation protocols could contribute to the discrepancy. Using the estimated reductions in $PI(4,5)P_2$ for both models, the levels of ENaC activity for CF without PLC activation are within the reported interval (Figure 3.3, A1 and B1 plots). Although the model predicts a large drop of ENaC activity in CF with PLC activation, results are above the experimentally observed interval. This difference suggests that the $PI(4,5)P_2$ drop may be underestimated by the models. Using a reduction by 15% of basal $PI(4,5)P_2$ levels in model A and 14.5% in model B, all predictions fall within the experimental intervals of data published by Almaça's *et al.* (Figure 3.4).

Use of an alternative CF specific ENaC open-probability function with a value of 0.6 for basal levels of $PI(4,5)P_2$, as proposed in several reports [49–51], did not improve the comparison with PLC activation data, but compromised the adjustment to ASL thickness time courses in CF.

Details on how these simulations were set in the model are in section 5.5 in Methods.

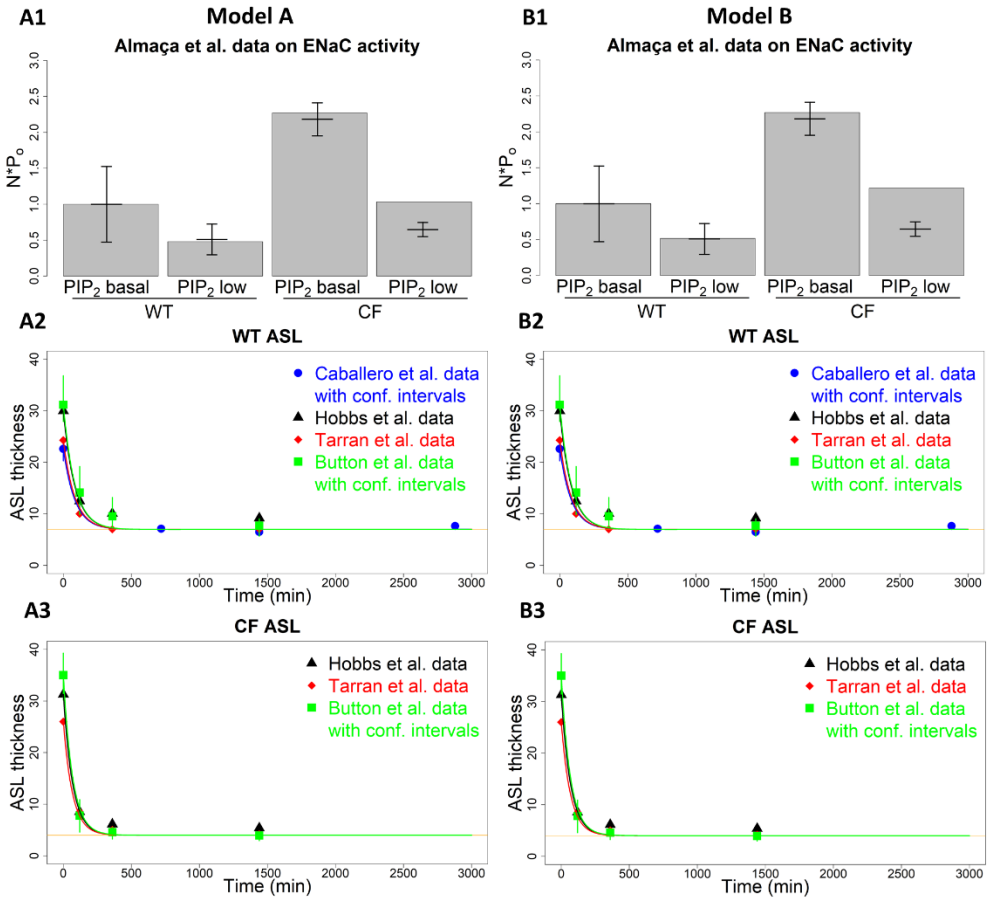

Figure 3.3. Model results corresponding to ENaC activity and ASL time courses in WT and CF.

The two columns refer to results for model A and model B. The first row exhibits a comparison between model results (bars) and Almaça's data [43] of ENaC activity for different PI(4,5)P_2 levels (means and confidence intervals). The second and third rows display model results (lines) superimposed on time course data of ASL thickness (symbols) after perturbations under WT and CF conditions, respectively [24,36,41,42].

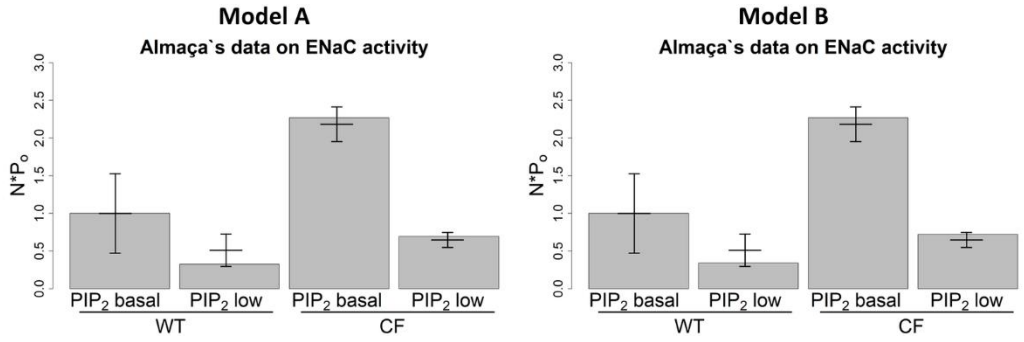

Figure 3.4. Consequences of an alternative model parameterization.

A reduction by 15% of basal PI(4,5)P2 levels in model A and 14.5% in model B causes the predictions of the two models to fall inside the confidence intervals reported by Almaça *et al.* [43].

3.4.3. ASL is sensitive to changes in $PI(4,5)P_2$

After parameterization and validation of both model variants, we assessed if changes in $PI(4,5)P_2$ have a significant impact on ASL. Toward this end, we analyzed the sensitivities of model variables relative to small changes in independent variables and parameters at the steady state (Table 3.3).

All other sensitivities to changes in parameter values are smaller than 1 (in absolute value) in the WT scenario, which means that perturbations are attenuated, which is desirable. Under CF conditions, only the sensitivity of ASL with respect to γ_4 reaches a value of 1. These low values show that the model is very robust to reasonable changes in model parameters.

Considering sensitivities to independent variables, sometimes called *gains*, only one high sensitivity stands out in both model variants, namely the gain of ASL, with respect to changes in $PI(4,5)P_2$ (Table 3.3). This sensitivity is approximately doubled in CF versus WT conditions. The fact that ASL has a high sensitivity to $PI(4,5)P_2$, especially in CF, supports the hypothesis that alterations of $PI(4,5)P_2$ could affect ASL thickness with possible therapeutic benefit for CF patients.

Table 3.3. Model sensitivity matrix for models A and B.

Sensitivities	WT				CF			
	Model A		Model B		Model A		Model B	
	ENaC	ASL	ENaC	ASL	ENaC	ASL	ENaC	ASL
$PI(4,5)P_2$	-0.67	**-1.28**	0.16	**-1.45**	0	**-2.57**	0.66	**-2.81**
SPLUNC1	-0.47	0.09	-0.47	0.09	0	0	0	0
γ_1	0.84	-0.16	0.84	-0.16	0.66	-0.23	0.66	-0.23
γ_3	-0.47	0.09	-0.47	0.09	0	0	0	0
γ_2	-0.37	0.07	-0.37	0.07	-0.66	0.23	-0.66	0.23
γ_6	-0.09	-0.17	-0.09	-0.17	0	-0.35	0	-0.35
γ_4	0.34	0.65	0.34	0.65	0	**1**	0	**1**
γ_5	0.14	0.26	0.14	0.26	0	0	0	0
γ_7	-0.38	-0.73	-0.38	-0.73	0	-0.64	0	-0.64

Note that only ASL has a high sensitivity (sensitivity greater than 1 in absolute value) with respect to $PI(4,5)P_2$, and only these $PI(4,5)P_2$ sensitivities are noticeably different between the two models.

The increase in ASL sensitivity to $PI(4,5)P_2$ from WT to CF conditions is associated with a relative change in flux distribution between the respective steady states (Table 3.4). These distributions are equal for both model variants, A and B, because the adjusted rate constants compensate for the inclusion of $PI(4,5)P_2$ in the fluxes V_2 and V_3. In WT, 56% of ENaC degradation is due to SPLUNC1 activity. CFTR is only responsible for 39% of ASL influx. ENaC activity is also a minor contributor (19%) for the ASL efflux in WT. In CF, V_3 and V_5 are set to zero to simulate the disease condition. These alterations increase the contribution of ENaC in the ASL efflux to 36%. This CF-specific increased role of ENaC in the ASL efflux may be responsible for the greater sensitivity of ASL to changes in $PI(4,5)P_2$. Reports in the literature suggest that the increase in ENaC activity in CF could be even higher, with increase ratios of 4.5 within a model of epithelial ion and water transport [14], 3 in human colon cells [52] and 2.2 in bronchial epithelial cells [43].

Table 3.4. Fluxes of the model at steady state in WT and CF. Values are identical for models A and B.

	WT	CF
V_1	0.01733	0.01733
V_2	0.00758	0.01733
V_3	0.00975	0.00000
V_4	0.05915	0.05915
V_5	0.02389	0.00000
V_6	0.01592	0.02079
V_7	0.06712	0.03836

Although it has a small absolute value, the sensitivity of ENaC with respect to $PI(4,5)P_2$ shows the main difference between model variants A and B. In variant A, where $PI(4,5)P_2$ only influences ENaC's P_o, a small increase in $PI(4,5)P_2$ leads to a *decrease* in the number of ENaC molecules present in the cell membrane. This is an indirect effect, mediated by SPUNC1/ASL feedback regulation of ENaC activity. In CF, where SPLUNC1 is absent, this sensitivity is 0. By contrast, a small increase in $PI(4,5)P_2$ within model variant B leads to a small *increase* in the value of ENaC. This qualitative change in the sign of the sensitivity is due to the $PI(4,5)P_2$-mediated protection of ENaC from degradation.

Finally, we assessed how ASL changes with larger perturbations in $PI(4,5)P_2$ and the number of ENaC molecules (Figure 3.5). These results confirm the sensitivity analysis, as ASL changes significantly when $PI(4,5)P_2$ is altered. Again, the increase in ASL is greater under CF conditions. Manipulation of the number of ENaC molecules is also able to influence ASL thickness, but with smaller efficiency.

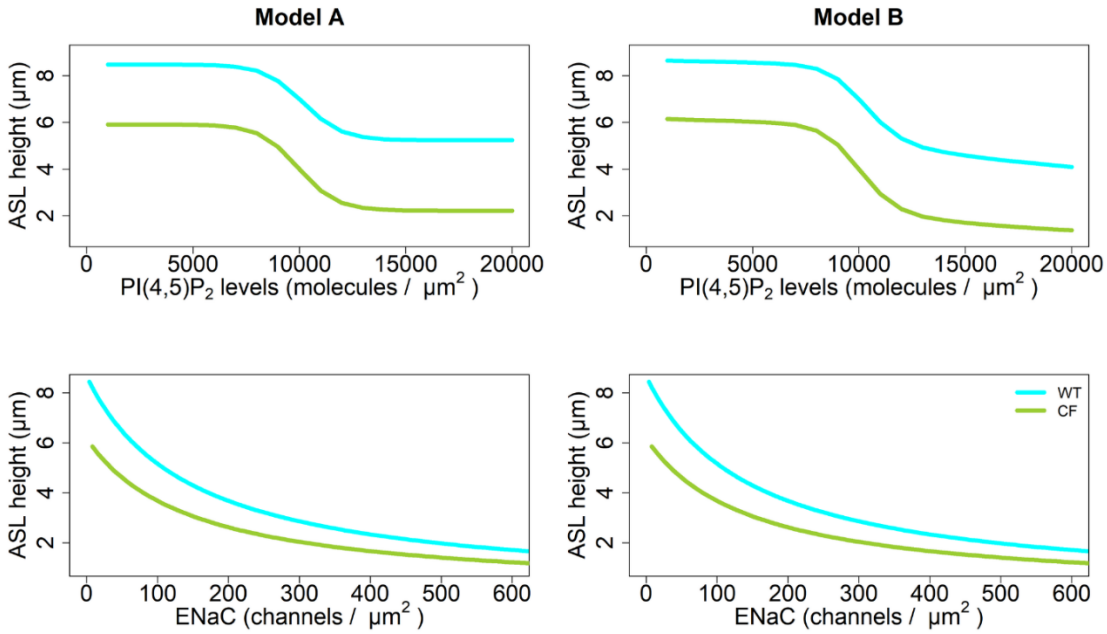

Figure 3.5. Sensitivity of ASL with respect to PI(4,5)P2 and ENaC.

Figures in the top panels show the effects of different levels of $PI(4,5)P_2$ on ASL thickness for WT and CF in the two models. Figures in the bottom panels show the effects of different numbers of ENaC channels on ASL thickness, also in WT and CF and for both models. In the bottom Figures, ENaC numbers were changed by varying the ENaC influx in the system, V_1. ENaC numbers were artificially inflated in order to reach stabilization of ASL thickness values; thus, the trends for high numbers are very unlikely to occur *in vivo*.

3.5. Discussion

In this work we propose a model of ASL regulation by ENaC, SPLUNC1 and $PI(4,5)P_2$. ENaC is subject to multiple additional regulations [53], and it could be interesting in the future to expand our model to include the effects of protein kinase C (PKC) and cyclic adenosine monophosphate (cAMP), as well as more detailed regulation by NEDD4-2. More complex models of epithelial ion and water transport are available, but do not facilitated the exploration of the role of $PI(4,5)P_2$ in the regulation of ENaC and, consequently, of ASL. By contrast, the simplicity of the model proposed here permitted the successful, direct determination of parameter values from limited experimental data, without the need for complex multi-parametric optimization. Given this direct derivation of parameter values and the good agreement between model predictions and validation data, we cautiously conclude that the model represents the ASL and ENaC regulation by SPLUNC1 and $PI(4,5)P_2$ quite well.

As our model considers $PI(4,5)P_2$ as an independent variable, it can be easily coupled with models of the phosphoinositide pathway that are now starting to emerge [54,55]. This coupling will allow a deeper exploration of potential manipulations of phosphoinositide metabolism leading to a more efficient recovery of ASL in CF patients.

Two model variants were explored to test the hypothesis whether $PI(4,5)P_2$, besides its influence on ENaC's P_o, may also protect ENaC from ubiquitination. We did not find any noticeable differences between the two variants when comparing model predictions with validation data. Both were equally successful in reproducing the systems at the WT and CF steady states, as well as the observed ASL dynamics in WT. Thus, the simpler model, where $PI(4,5)P_2$ only regulates ENaC open probability, is sufficient to explain the system behavior. However, this sufficiency does not rule out the protective role of $PI(4,5)P_2$ in ENaC ubiquitination, and if future experimental evidence supports this role of $PI(4,5)P_2$, the more complex model variant may be deemed more appropriate. This secondary role of $PI(4,5)P_2$ could be of practical interest, because the dual regulatory function would make ASL more sensitive to $PI(4,5)P_2$ changes, thereby improving the possible success of $PI(4,5)P_2$ manipulations as a therapeutic approach.

Whether or not $PI(4,5)P_2$ plays a dual role, the model analysis reveals that the synergism between SPLUNC1 and the phosphoinositide system is an important mechanism for controlling ASL in the healthy lung and that this system is compromised in CF.

3.6. Methods

3.6.1. Mathematical framework

The model of ENaC/ASL dynamics was designed within the framework of Biochemical Systems Theory (BST) [56–60], using ordinary differential equations (ODEs) in the format of a generalized mass action (GMA) system. In this approach, each ODE describes the dynamics of a dependent variable X_i, which is formulated stoichiometrically as a sum of all fluxes that are directly related to this variable; furthermore, each flux v_j is formulated as a power-law function, as indicated in Eq. 3.1.

$$\frac{dX_i}{dt} = \sum_{s=1}^{a} n_s.v_s - \sum_{p=1}^{a} m_p.v_p$$
$$v_j = \gamma_j \cdot \prod_{i=1}^{b+c} X_i^{f_{ij}} \qquad (3.1)$$

γ_j represents the rate constant for flux v_j, respectively. The effect of each substrate X_i on the flux is modeled by a kinetic order f_{ij}. If no kinetic order is depicted it's because it is equal to 1. n_s and m_p are the stoichiometric coefficients for influxes and effluxes. *a* denote the number of fluxes. b and c represent the number of dependent and independent variables, respectively.

3.6.2. Model design and equations

The core of the model consists of two dependent variables: ENaC represents the number of channels in a 1 μm^2 patch of plasma membrane and ASL represents the thickness of ASL in μm. The differential equations for each model variant (A: $PI(4,5)P_2$ only regulates ENaC's P_o; B: $PI(4,5)P_2$ regulates both ENaC's P_o and removal) are presented in Table 3.1.

3.6.3 Open-probability (P_o) of ENAC

For both models we determine the P_o of ENaC as a function of $PI(4,5)P_2$ by fitting a sigmoidal (logistic) function to data published by Pochynyuk *et al.* (Table 3.2 and Figure 3.6) [40].

The resulting function (Eq. 3.2) predicts P_o values close to 0 for very low levels of PI(4,5)P2 and 1 for very high levels of $PI(4,5)P_2$.

$$P_0\left[PI(4,5)P_2\right] = \frac{0.96}{1 + 786 \times e^{-5.6e-4 \times [PI(4,5)P_2]}} \qquad (3.2)$$

In reality, it is to be expected that the absence of $PI(4,5)P_2$ will not completely shut down P_o and that $PI(4,5)P_2$ saturation will not permanently open every ENaC channel in the membrane. To account for these reality checks, we considered different bounds and found that the minimum and maximum observed P_o's (0.02 and 0.82, respectively) are still observed when $PI(4,5)P_2$ tends to 0 or 20,000, respectively. To create a function with this behavior, we added four points with ordinates equal to 0.02 and abscissas equal to 1000, 2000, 3000 and 4000. We also added four points with ordinates equal to

.82 and abscissas of 16000, 17000, 18000 and 19000. We allowed an additional term in the function to enable a lower asymptote greater than zero for low PI(4,5)P_2 levels. The resulting function (Eq. 3.3) was used for both model variants.

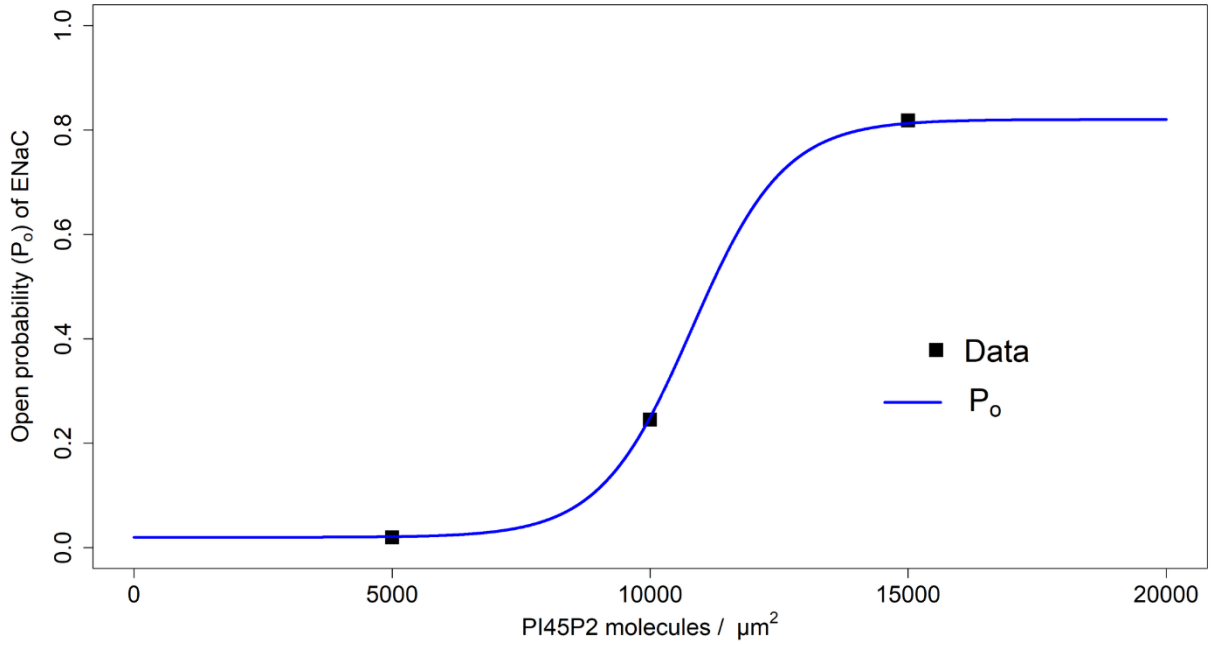

Figure 3.6. Open-probability function Po for ENaC.

A logistic function (line) represents the effect of PI(4,5)P_2 on P_o well. Squares represent data points from Pochynyuk et al. [40].

$$P_0\left[PI(4,5)P_2\right] = 0.02 + \frac{.8}{1+181429\times e^{-1.12e-3\times\left[PI(4,5)P_2\right]}} \qquad (3.3)$$

Parameter values for the functions where obtained with the general optimization function (optim) in R [61]. Initial values for the optimization where found with a TI-83 logistic regression.

It is known that channels with different subunit stoichiometries may be present [62] in the cell membrane and that they could have a different open-probability distribution. For simplification, we only considered αβγ ENaC channels and assumed that any regulation that affects one of the subunits will affect the expression of the trimeric channel with the same magnitude [62].

Additionally, ENaC cleavage by furin and extracellular proteases may be an important regulatory mechanism of ENaC's P_o [32,33,62]. SPLUNC1 may have a role in protecting ENaC from these proteases [63]. For simplicity, we did not consider this as part of the model, but this role can certainly be introduced in future versions. Making the P_o function dependent also on the concentration of extracellular proteases could render the $PI(4,5)P_2$ regulation more accurate in CF conditions. ENaC´s P_o is also dependent on another phosphoinositide, $PI(3,4,5)P_3$. We did not consider this regulation because we were interested in ENaC at the apical part of the plasma membrane of an epithelial cell, which is characterized by the absence or low levels of both $PI(3,4,5)P_3$ and the enzyme responsible for its production, PI3KI [64].

3.6.4. Parameter estimation

Values for the three parameters in the differential equation for ENaC were obtained by solving the corresponding steady-state equations using steady-state values of ENaC and ASL in WT and CF lungs from the literature (Table 3.2). The resulting two steady-state equations are not sufficient to solve for the values of the three parameters uniquely. To obtain a unique solution, we used information about the half-life of ENaC in WT (Table 3.2). Some of the ENaC half-life values in the literature appear to be very high, which could be due to the fact that they were measured in oocytes that were cultured in low temperatures, which is known to increase the half-life of ENaC [38]. A consequence of adopting high half-life values is that the transition from WT to CF will take a substantial amount of time. For example, with an ENaC half-life of 80 minutes, our model estimates that a subject would need more than a month to proceed from a WT-like to a CF-like steady state. With a shorter half-life of 20 minutes, this process will take only 14 days. This lower number is in accordance with the literature; for instance, Stoltz and colleagues [19] report that loss of CFTR does not directly increase activity of ENaC at the onset of disease. Thus, based on the range of estimates documented in the literature, we considered an ENaC half-life of $t_{1/2} = 40$ minutes in WT conditions. Assuming that ENaC degradation is well modeled by an exponential decay, we were thus able to calculate the overall rate of ENaC degradation γ (Eq. 3.4) from three equations (Eq. 3.5) that uniquely determine the values of γ_1, γ_2 and γ_3.

$$\frac{ENaC\_initial}{2} = ENaC\_initial \times e^{-\gamma \times t_{1/2}} \Leftrightarrow$$
$$\Leftrightarrow \frac{\ln(2)}{t_{1/2}} = \gamma \qquad (3.4)$$

$$\begin{cases} \left.\frac{d}{dt} ENaC\right|_{wt} = \gamma_1 - \gamma_3 \times ENaC \times \frac{SPLUNC1}{ASL} - ENaC \times \gamma_2 \\ \left.\frac{d}{dt} ENaC\right|_{CF} = \gamma_1 - ENaC \times \gamma_2 \\ \frac{\ln(2)}{t_{1/2}} = \gamma_3 \times ENaC \times \frac{SPLUNC1}{ASL} + ENaC \times \gamma_2 \end{cases} \Leftrightarrow$$

$$\Leftrightarrow \begin{cases} 0 = \gamma_1 - \gamma_3 \times 35 \times \frac{7714}{7} - 35 \times \gamma_2 \\ 0 = \gamma_1 - 80 \times \gamma_2 \\ \frac{\ln(2)}{40} = \gamma_3 \times 35 \times \frac{7714}{7} + 35 \times \gamma_2 \end{cases} \Leftrightarrow$$

$$\Leftrightarrow \begin{cases} \gamma_1 = \frac{\ln(2)}{40} \simeq 1.732868\text{e-}2 \\ \gamma_3 = \frac{9 \times \ln(2)}{24684800} \simeq 2.527193\text{e-}7 \\ \gamma_2 = \frac{\ln(2)}{3200} \simeq 2.166085\text{e-}4 \end{cases} \qquad (3.5)$$

A similar approach was followed to determine the parameters for the B model variant (Eq. 3.6). In this model variant, ENaC effluxes are divided by the PI(4,5)P_2 concentration to reflect that PI(4,5)P_2 protects ENaC from ubiquitination.

$$
\begin{cases}
\left.\dfrac{d}{dt}ENaC\right|_{WT} = \gamma_1 - \dfrac{\gamma_3 \times ENaC \times \dfrac{SPLUNC1}{ASL}}{PI(4,5)P_2} - \dfrac{ENaC \times \gamma_2}{PI(4,5)P_2} \\
\left.\dfrac{d}{dt}ENaC\right|_{CF} = \gamma_1 - \dfrac{ENaC \times \gamma_2}{PI(4,5)P_2} \\
\dfrac{\ln(2)}{t_{1/2}} = \dfrac{\gamma_3 \times ENaC \times \dfrac{SPLUNC1}{ASL}}{PI(4,5)P_2} + \dfrac{35 \times \gamma_2}{PI(4,5)P_2}
\end{cases}
\Leftrightarrow
$$

$$
\Leftrightarrow
\begin{cases}
0 = \gamma_1 - \dfrac{\gamma_3 \times 35 \times \dfrac{7714}{7}}{10000} - \dfrac{35 \times \gamma_2}{10000} \\
0 = \gamma_1 - \dfrac{80 \times \gamma_2}{10000} \\
\dfrac{\ln(2)}{40} = \dfrac{\gamma_3 \times 35 \times \dfrac{7714}{7}}{10000} + \dfrac{35 \times \gamma_2}{10000}
\end{cases}
\Leftrightarrow
$$

$$
\Leftrightarrow
\begin{cases}
\gamma_1 = \dfrac{\ln(2)}{40} \simeq 0.01732868 \\
\gamma_3 = \dfrac{225 \times \ln(2)}{61712} \simeq 0.002527193 \\
\gamma_2 = \dfrac{25 \times \ln(2)}{8} \simeq 2.166085
\end{cases}
\qquad (3.6)
$$

The differential equation for ASL has four parameters. As for the case of ENaC, we used steady-state equations for ASL under WT and CF conditions. We added a third equation imposing a ratio between the ASL fluxes induced by CFTR and ENaC in WT, according to modelling results found in the literature (Table 3.2). This system of three equations (Eq. 3.7) allowed us to express three of the parameters as functions of γ_6.

$$
\begin{cases}
\left.\frac{d}{dt}ASL\right|_{WT} = \gamma_4 + \gamma_5 - \gamma_6 \times ASL \times ENaC \times Po(PI(4,5)P_2) - ASL \times \gamma_7 \\
\left.\frac{d}{dt}ASL\right|_{CF} = \gamma_4 - \gamma_6 \times ASL \times ENaC \times Po(PI(4,5)P_2) - ASL \times \gamma_7 \quad \Leftrightarrow \\
1.5 = (\gamma_5) / (\gamma_6 \times ASL \times ENaC \times Po(PI(4,5)P_2))
\end{cases}
$$

$$
\Leftrightarrow \begin{cases}
0 = \gamma_4 + \gamma_5 - \gamma_6 \times 7 \times 35 \times 0.25 - 7 \times \gamma_7 \\
0 = \gamma_4 - \gamma_6 \times 4 \times 80 \times 0.25 - 4 \times \gamma_7 \quad \Leftrightarrow \\
1.5 = (\gamma_5) / (\gamma_6 \times 7 \times 35 \times 0.25)
\end{cases} \qquad (3.7)
$$

$$
\Leftrightarrow \begin{cases}
\gamma_4 = \frac{455}{2}\gamma_6 \\
\gamma_5 = \frac{735}{8}\gamma_6 \\
\gamma_7 = \frac{295}{8}\gamma_6
\end{cases}
$$

To define γ_6, and consequently the remaining three parameters, we adjusted its value to reproduce observed ASL dynamics data in WT (Table 3.2). Starting from an initial guess of γ_6 = 4e-4 (chosen to avoid problems with the numerical differential equation solver), the local optimizer identified the best solution as 2.6e-4.

The four parameters associated with the differential equation for ASL are equal for both model variants. The complete list of model parameter values is presented in Table 3.1.

3.6.5. Model conditions for experiments simulation presented in Figures 3.3 and 3.4

For Figure 3.3 A1 and B1, ENaC activity was measured in four situations. First, at basal conditions ($PI(4,5)P_2$ = 10000 molecules/μm^2, SPLUNC = 7714 molecules/μm^2, γ_5 = 2.39e-2 μm·min^{-1}). Second, a decrease in PI(4,5)P2 was found to match the data from Almaça (PI(4,5)P2 = 9200 molecules/μm^2, SPLUNC = 7714 molecules/μm^2, γ_5 = 2.39e-2 μm·min^{-1}). Third, the models were set to simulate CF condition with the basal level of $PI(4,5)P_2$ ($PI(4,5)P_2$ = 10000 molecules/μm^2, SPLUNC = 0 molecules/μm^2, γ_5 = 0 μm·min^{-1}). Forth, in CF condition with the same decrease in PI(4,5)P2 that was found previously ($PI(4,5)P_2$ = 9200 molecules/μm^2, SPLUNC = 0 molecules/μm^2, γ_5 = 0 μm·min^{-1}).

Figure 3.4 is similar to Figure 3.3 A1 and B1. The difference is the reduction of $PI(4,5)P_2$ in the second and fourth columns, which is more pronounced in Figure 3.4, to 8500 molecules/μm^2.in model A and 8550 molecules/μm^2 for model B.

For the simulations presented in Figures 3.3 A2 and B2, no alterations were made to the models except for the initial value of the ASL height, that was altered to match the initial ASL height of the experiments. These were 22.59, 29.96, 24.28 and 31.17 μm for the data sets that can be found in the following references. [23,35,40,41]

In Figures 3.3 A3 and B3 the models were set to simulate CF condition by setting SPLUNC1 and the rate constant γ_5 to zero. As in the previous case, the only alteration made to the model's parameters were the initial value of the ASL height. These were 31.276586, 25.993151, 35.005454 μm and these data sets can be found in the same references as in the previous case.

3.6.6. Sensitivity analysis

Local sensitivity analysis was implemented as described in Chen *et al.* [65]. Briefly, parameter sensitivities were assessed numerically by increasing each parameter, one at a time, by 1% and computing the new steady state of the system. When the relative change in the steady-state value of a dependent variable is higher than 1% (or lower than -1%) the sensitivity indicates that a change in the parameter value is amplified in the steady-state value of the dependent variable. Smaller sensitivities indicate attenuation of a perturbation.

3.6.7 Model Implementation

The model was implemented in the programming language R v3.1.0 [61] together with the package deSolve [66]. We used the ODE integration function with the LSODA method.

3.7. References

1. Livraghi A, Randell SH. Cystic fibrosis and other respiratory diseases of impaired mucus clearance. Toxicol Pathol. 2007;35(1):116–29.

2. Collawn JF, Lazrak A, Bebok Z, Matalon S. The CFTR and ENaC debate: how

important is ENaC in CF lung disease? AJP Lung Cell Mol Physiol [Internet]. 2012;302(11):L1141–6. Available from: http://ajplung.physiology.org/cgi/doi/10.1152/ajplung.00036.2012

3. Taylor-Cousar JL, Jain M, Barto TL, Haddad T, Atkinson J, Tian S, et al. Lumacaftor/ivacaftor in patients with cystic fibrosis and advanced lung disease homozygous for F508del-CFTR. J Cyst Fibros [Internet]. 2017;17(2):228–35. Available from: www.elsevier.com/locate/jcf%0Ahttps://doi.org/10.1016/j.jcf.2017.09.012

4. Hobbs CA, Da Tan C, Tarran R, Tan C Da, Tarran R. Does epithelial sodium channel hyperactivity contribute to cystic fibrosis lung disease? J Physiol. 2013;59118(591):4377–438718.

5. Althaus M. ENaC inhibitors and airway re-hydration in cystic fibrosis: state of the art. Curr Mol Pharmacol [Internet]. 2013;6:3–12. Available from: http://www.ncbi.nlm.nih.gov/pubmed/23547930

6. Kim CS, Ahmad S, Wu T, Walton WG, Redinbo MR, Tarran R. SPLUNC1 is an allosteric modulator of the epithelial sodium channel. FASEB J [Internet]. 2018 Jan 8; Available from: http://www.fasebj.org/lookup/doi/10.1096/fj.201701126R

7. Bhalla V, Hallows KR. Mechanisms of ENaC regulation and clinical implications. J Am Soc Nephrol. 2008;19(10):1845–1854.

8. Teiwes J, Toto RD. Epithelial sodium channel inhibition in cardiovascular disease. A potential role for amiloride. Am J Hypertens. 2007;20(1):109–17.

9. Kleyman TR, Kashlan OB, Hughey RP. Epithelial Na + Channel Regulation by Extracellular and Intracellular Factors. Annu Rev Physiol [Internet]. 2018 Feb 10;80(1):annurev-physiol-021317-121143. Available from: http://www.annualreviews.org/doi/abs/10.1146/annurev-physiol-021317-121143

10. Smith NJ, Solovay CF. Epithelial Na $^{+}$ channel inhibitors for the treatment of cystic fibrosis. Pharm Pat Anal [Internet]. 2017;6(4):181–90. Available from:

http://www.future-science.com/doi/10.4155/ppa-2017-0009

11. Horisberger JD. ENaC-CFTR interactions: The role of electrical coupling of ion fluxes explored in an epithelial cell model. Pflugers Arch Eur J Physiol. 2003;445(4):522–8.

12. Warren NJ, Tawhai MH, Crampin EJ. A mathematical model of calcium-induced fluid secretion in airway epithelium. J Theor Biol. 2009;259(4):837–49.

13. Garcia GJM, Boucher RC, Elston TC. Biophysical model of ion transport across human respiratory epithelia allows quantification of ion permeabilities. Biophys J [Internet]. 2013;104(3):716–26. Available from: http://dx.doi.org/10.1016/j.bpj.2012.12.040

14. Sandefur CI, Boucher RC, Elston TC. Mathematical model reveals role of nucleotide signaling in airway surface liquid homeostasis and its dysregulation in cystic fibrosis. Proc Natl Acad Sci [Internet]. 2017;114(35):E7272–81. Available from: http://www.pnas.org/lookup/doi/10.1073/pnas.1617383114

15. Sasamoto K, Marunaka R, Niisato N, Sun H, Taruno A, Pezzotti G, et al. Analysis of Aprotinin, a Protease Inhibitor, Action on the Trafficking of Epithelial Na+ Channels (ENaC) in Renal Epithelial Cells Using a Mathematical Model. Cell Physiol Biochem [Internet]. 2017;41(5):1865–80. Available from: https://www.karger.com/?doi=10.1159/000471934

16. Staruschenko A, Adams E, Booth RE, Stockand JD. Epithelial Na+ channel subunit stoichiometry. Biophys J [Internet]. 2005;88(6):3966–75. Available from: http://dx.doi.org/10.1529/biophysj.104.056804

17. Itani OA, Chen J-H, Karp PH, Ernst S, Keshavjee S, Parekh K, et al. Human cystic fibrosis airway epithelia have reduced Cl- conductance but not increased Na+ conductance. Proc Natl Acad Sci [Internet]. 2011;108(25):10260–5. Available from: http://www.pnas.org/cgi/doi/10.1073/pnas.1106695108

18. Chen J-H, Stoltz DA, Karp PH, Ernst SE, Pezzulo, Alejandro A. Moninger, Thomas O. Rector M V., Reznikov LR, et al. Loss of anion transport without increased sodium absorption characterizes newborn porcine cystic fibrosis

airway epithelia. Cell. 2010;143(6):319–35.

19. Stoltz DA, Meyerholz DK, Welsh MJ. Origins of Cystic Fibrosis Lung Disease. N Engl J Med [Internet]. 2015;372(4):351–62. Available from: http://www.nejm.org/doi/10.1056/NEJMra1300109

20. Reddy MM, Light MJ, Quinton PM. Activation of the epithelial Na+ channel (ENaC) requires CFTR Cl- channel function. Nature [Internet]. 1999;402(6759):301–4. Available from: http://dx.doi.org/10.1038/46297

21. Palma AG, Kotsias BA, Marino GI. Artículo especial funciones de los canales iónicos CFTR y ENaC. Med (Buenos Aires). 2014;74:133–9.

22. Enuka Y, Hanukoglu I, Edelheit O, Vaknine H, Hanukoglu A. Epithelial sodium channels (ENaC) are uniformly distributed on motile cilia in the oviduct and the respiratory airways. Histochem Cell Biol. 2012;137(3):339–53.

23. Walton WG, Ahmad S, Little MS, Kim CSK, Tyrrell J, Lin Q, et al. Structural features essential to the antimicrobial functions of human SPLUNC1. Biochemistry. 2016;55(21):2979–91.

24. Garcia-Caballero A, Rasmussen JE, Gaillard E, Watson MJ, Olsen JC, Donaldson SH, et al. SPLUNC1 regulates airway surface liquid volume by protecting ENaC from proteolytic cleavage. Proc Natl Acad Sci [Internet]. 2009;106(27):11412–7. Available from: http://www.pnas.org/cgi/doi/10.1073/pnas.0903609106

25. Tarran R, Redinbo MR. Mammalian short palate lung and nasal epithelial clone 1 (SPLUNC1) in pH-dependent airway hydration. Int J Biochem Cell Biol. 2014;130–5.

26. Terryah ST, Fellner RC, Ahmad S, Moore PJ, Reidel B, Sesma JI, et al. Evaluation of a SPLUNC1-derived peptide for the treatment of cystic fibrosis lung disease. Am J Physiol - Lung Cell Mol Physiol [Internet]. 2017;314(1):L192–205. Available from: http://ajplung.physiology.org/lookup/doi/10.1152/ajplung.00546.2016

27. Balla T. Phosphoinositides: tiny lipids with giant impact on cell regulation. Physiol Rev [Internet]. 2013;93(3):1019–137. Available from: http://www.ncbi.nlm.nih.gov/pubmed/23899561

28. Pochynyuk O, Bugaj V, Stockand JD. Physiologic regulation of the epithelial sodium channel by phosphatidylinositides. Curr Opin Nephrol Hypertens [Internet]. 2008;17(5):533–40. Available from: http://content.wkhealth.com/linkback/openurl?sid=WKPTLP:landingpage&an=00041552-200809000-00015

29. Pochynyuk O, Tong Q, Medina J, Vandewalle A, Staruschenko A, Bugaj V, et al. Molecular determinants of PI(4,5)P2 and PI(3,4,5)P3 regulation of the epithelial Na+ channel. J Gen Physiol [Internet]. 2007;130(4):399–413. Available from: http://www.pubmedcentral.nih.gov/articlerender.fcgi?artid=2151653&tool=pmcentrez&rendertype=abstract

30. Ma H-P, Eaton DC. Acute regulation of epithelial sodium channel by anionic phospholipids. J Am Soc Nephrol [Internet]. 2005;16(11):3182–7. Available from: http://www.jasn.org/cgi/doi/10.1681/ASN.2005040434

31. Yue G, Malik B, Yue G, Eaton DC. Phosphatidylinositol 4,5-bisphosphate (PIP2) stimulates epithelial sodium channel activity in A6 cells. J Biol Chem. 2002;277(14):11965–9.

32. Kota P, Buchner G, Chakraborty H, Dang YL, He H, Garcia GJM, et al. The N-terminal domain allosterically regulates cleavage and activation of the epthelial sodium channel. J Biol Chem. 2014;289(33):23029–42.

33. Rossier BC, Stutts MJ. Activation of the Epithelial Sodium Channel (ENaC) by Serine Proteases. Annu Rev Physiol [Internet]. 2009;71(1):361–79. Available from: http://www.annualreviews.org/doi/10.1146/annurev.physiol.010908.163108

34. Garland AL, Walton WG, Coakley RD, Tan CD, Gilmore RC, Hobbs C a, et al. Molecular basis for pH-dependent mucosal dehydration in cystic fibrosis

airways. Proc Natl Acad Sci U S A [Internet]. 2013;110(40):15973–8. Available from: http://www.pubmedcentral.nih.gov/articlerender.fcgi?artid=3791714&tool=pmcentrez&rendertype=abstract

35. Rossier BC. Hormonal Regulation of the Epithelial Sodium Channel ENaC : N or Po ? 2002;120(July):67–70.

36. Hobbs CA, Blanchard MG, Kellenberger S, Bencharit S, Cao R, Kesimer M, et al. Identification of SPLUNC1's ENaC-inhibitory domain yields novel strategies to treat sodium hyperabsorption in cystic fibrosis airways. Am J Physiol - Lung Cell Mol Physiol Mol Physiol. 2013;305(12):L990–1001.

37. Morris RG, Schafer J a. cAMP increases density of ENaC subunits in the apical membrane of MDCK cells in direct proportion to amiloride-sensitive Na(+) transport. J Gen Physiol. 2002;120(1):71–85.

38. Rotin D, Kanelis V, Schild L. Trafficking and cell surface stability of ENaC. Am J Physiol Renal Physiol [Internet]. 2001;281(3):F391–9. Available from: http://www.ncbi.nlm.nih.gov/cgi-bin/Entrez/referer?http://ajprenal.physiology.org/cgi/content/abstract/281/3/F391%5Cnhttp://ajprenal.physiology.org/content/ajprenal/281/3/F391.full.pdf

39. Butterworth MB. Regulation of the epithelial sodium channel (ENaC) by membrane trafficking. Biochim Biophys Acta - Mol Basis Dis [Internet]. 2010;1802(12):1166–77. Available from: http://dx.doi.org/10.1016/j.bbadis.2010.03.010

40. Pochynyuk O, Bugaj V, Vandewalle A, Stockand JD. Purinergic control of apical plasma membrane PI(4,5)P2 levels sets ENaC activity in principal cells. Am J Physiol Renal Physiol [Internet]. 2008;294(1):F38-46. Available from: http://www.ncbi.nlm.nih.gov/pubmed/17913833

41. Tarran R. Regulation of Airway Surface Liquid Volume and Mucus Transport by Active Ion Transport. Proc Am Thorac Soc [Internet]. 2004;1(1):42–6. Available from: http://pats.atsjournals.org/cgi/doi/10.1513/pats.2306014

42. Button B, Picher M, Boucher RC. Differential effects of cyclic and constant stress on ATP release and mucociliary transport by human airway epithelia. J Physiol [Internet]. 2007;580(2):577–92. Available from: http://doi.wiley.com/10.1113/jphysiol.2006.126086

43. Almaça J, Faria D, Sousa M, Uliyakina I, Conrad C, Sirianant L, et al. High-content siRNA screen reveals global ENaC regulators and potential cystic fibrosis therapy targets. Cell. 2013;154(6).

44. Myerburg MM, Butterworth MB, McKenna EE, Peters KW, Frizzell RA, Kleyman TR, et al. Airway surface liquid volume regulates ENaC by altering the serine protease-protease inhibitor balance: A mechanism for sodium hyperabsorption in cystic fibrosis. J Biol Chem. 2006;281(38):27942–9.

45. Falkenburger BH, Jensen JB, Hille B. Kinetics of PIP2 metabolism and KCNQ2/3 channel regulation studied with a voltage-sensitive phosphatase in living cells. J Gen Physiol [Internet]. 2010;135(2):99–114. Available from: http://www.pubmedcentral.nih.gov/articlerender.fcgi?artid=2812502&tool=pmcentrez&rendertype=abstract

46. Xu C, Watras J, Loew LM. Kinetic analysis of receptor-activated phosphoinositide turnover. J Cell Biol [Internet]. 2003;161:779–791. Available from: https://doi.org/10.1083/jcb.200301070

47. Viaud J, Mansour R, Antkowiak A, Mujalli A, Valet C, Chicanne G, et al. Phosphoinositides: Important lipids in the coordination of cell dynamics. Biochimie [Internet]. 2016;125:250–8. Available from: http://dx.doi.org/10.1016/j.biochi.2015.09.005

48. Ikonomov OC, Sbrissa D, Delvecchio K, Xie Y, Jin JPJ-PJP, Rappolee D, et al. The Phosphoinositide Kinase PIKfyve Is Vital in Early Embryonic Development: PREIMPLANTATION LETHALITY OF PIKfyve-/- EMBRYOS BUT NORMALITY OF PIKfyve+/- MICE. J Biol Chem [Internet]. 2011;286(15):13404–13. Available from: http://www.jbc.org/cgi/doi/10.1074/jbc.M111.222364

49. Stutts MJ, Rossier BC, Boucher RC. Cystic Fibrosis Transmembrane Conductance Regulator Inverts Protein Kinase A-mediated Regulation of Epithelial Sodium Channel Single Channel Kinetics. J Biol Chem [Internet]. 1997;272(22):14037–40. Available from: http://www.jbc.org/content/272/22/14037.abstract

50. Berdiev BK, Qadri YJ, Benos DJ. Assessment of the CFTR and ENaC association. Mol Biosyst. 2009;5(2):123–7.

51. Lazrak A, Jurkuvenaite A, Chen L, Keeling KM, Collawn JF, Bedwell DM, et al. Enhancement of alveolar epithelial sodium channel activity with decreased cystic fibrosis transmembrane conductance regulator expression in mouse lung. AJP Lung Cell Mol Physiol [Internet]. 2011;301(4):L557–67. Available from: http://ajplung.physiology.org/cgi/doi/10.1152/ajplung.00094.2011

52. Mall M. CFTR-mediated inhibition of epithelial sodium conductance in human colon is defective in cystic fibrosis. Neth J Med [Internet]. 1999;54:S25. Available from: http://linkinghub.elsevier.com/retrieve/pii/S0300297799900591

53. Kashlan OB, Kleyman TR. Epithelial Na+ channel regulation by cytoplasmic and extracellular factors. Exp Cell Res. 2012;318(9):1011–9.

54. Suratekar R, Panda A, Raghu P, Krishna S. Evidence of sinks and sources in the phospholipase C-activated PIP $_2$ cycle. FEBS Lett [Internet]. 2018;1–11. Available from: http://doi.wiley.com/10.1002/1873-3468.12998

55. Olivença DV, Uliyakina I, Fonseca LL, Amaral MD, Voit EO, Pinto FR. A Mathematical Model of the Phosphoinositide Pathway. Sci Rep [Internet]. 2018 Dec 2;8(1):3904. Available from: https://www.nature.com/articles/s41598-018-22226-8

56. Torres NV, Voit EO. Pathway Analysis and Optimization in Metabolic Engineering. Cambridge, U.K.: Cambridge University Press; 2002.

57. Savageau M. Biochemical Systems Analysis. 1976. 379 p.

58. Savageau MA. Biochemical systems analysis. I. Some mathematical properties of the rate law for the component enzymatic reactions. J Theor Biol [Internet]. 1969 Dec;25(3):365–9. Available from: http://www.ncbi.nlm.nih.gov/pubmed/5387046

59. Voit EO. Computational analysis of biochemical systems: a practical guide for biochemists and molecular biologists. Cambridge, U.K.: Cambridge University Press; 2000. 531 p.

60. Voit EO. Biochemical systems theory: a review. ISRN Biomath [Internet]. 2013;2013:1–53. Available from: http://www.hindawi.com/isrn/biomathematics/2013/897658/

61. R Core Team. R: a language and environment for statistical computing [Internet]. Vienna, Austria; 2017. Available from: http://www.r-project.org

62. Butterworth MB, Weisz OA, Johnson JP. Some assembly required: Putting the epithelial sodium channel together. J Biol Chem. 2008;283(51):35305–9.

63. Gaillard EA, Kota P, Gentzsch M, Dokholyan N V., Stutts MJ, Tarran R. Regulation of the epithelial Na+ volume by serine proteases channel and airway surface liquid. Pflugers Arch. 2010;460(1):1–17.

64. Kolay S, Basu U, Raghu P. Control of diverse subcellular processes by a single multi-functional lipid phosphatidylinositol 4,5-bisphosphate [PI(4,5)P2]. Biochem J [Internet]. 2016;473(12):1681–92. Available from: http://www.ncbi.nlm.nih.gov/pubmed/27288030

65. Chen PW, Fonseca LL, Hannun YA, Voit EO. Coordination of Rapid Sphingolipid Responses to Heat Stress in Yeast. PLoS Comput Biol. 2013;9(5).

66. Soetaert K, Petzoldt T, Setzer RW. Solving differential equations in R: package deSolve. J Stat Software [Internet]. 2010;2(9):1–25. Available from: http://www.jstatsoft.org/v33/i09

3.8. Acknowledgements

We would like to acknowledge the help provided by Margarida D Amaral and Maria Margarida Perestrello Ramos from the University of Lisbon, Faculty of Sciences, BIOISI: Biosystems and Integrative Sciences Institute.

3.9. Author contribution statement

D.V.O., L.L.F., E.O.V. and F.R.P. contributed to the conception of this project and the drafting of the manuscript. D.V.O. performed the literature review, retrieved data characterizing the system, created the ASL / ENaC model, created the code and performed the analysis. L.L.F. helped in the ASL / ENaC model creation. All authors reviewed the manuscript.

3.10. Additional information

Competing financial interests

The author(s) declare no competing financial interests.

Chapter 4. ENaC regulation by phospholipids and SPLUNC1 protein explained through mathematical modelling

Olivença, D. V., Voit, E. O., & Pinto, F. R. (2018). ENaC regulation by phospholipids and SPLUNC1 protein explained through mathematical modelling [submited]

4.1. Abstract

Cystic fibrosis (CF) is a condition caused by mutations in the cystic fibrosis transmembrane conductance regulator (CFTR), a chloride and bicarbonate channel. A secondary effect of CF seems to be an increase in the number of epithelial sodium channels (ENaCs), and the greater absorption of sodium and water by these channels is thought to be one of the causes of the accumulation of mucus in the lungs that characterizes the disease. This mucus is at least partially responsible for recurrent pulmonary infections and inflammation events that ultimately destroy the lungs of affected subjects.

Phosphoinositides are rare signaling lipids that constitute a complex network regulating numerous cellular processes. One of the many functions of phosphoinositides is the regulation of cell membrane proteins, and several studies specifically implicate phosphatidylinositol 4,5-biphosphate ($PI(4,5)P_2$) in ENaC regulation.

Inhibition of diacylglycerol kinase (DGK), an enzyme of the phosphoinositide pathway, is known to moderate ENaC function and therefore might become a candidate for novel therapeutics against cystic fibrosis. However, progress in this direction has been slow as the mechanism of moderation of ENaC by DGK is not sufficiently well understood. A hypothesis is that DGK modulates $PI(4,5)P_2$ production by halting phosphoinositide recycling, but this mechanism has not been proven.

Here we propose to combine two metabolic pathway models: one representing the dynamics of phosphoinositides and the other accounting for the roles of ENaC and the protein SPLUNC1 (short palate lung and nasal epithelial clone 1) in the control of Airway Surface Liquid (ASL). The merging of the models enables, for the first time, a detailed study of the intricate interactions between DGK and ENaC. The results of the computational analysis strongly suggest that, contrary to a widely accepted hypothesis,

the regulation of ENaC is primarily exerted through the control of $PI(4,5)P_2$ production by type I phosphatidylinositol-4-phosphate 5-kinase (PIP5KI), which in turn is controlled by phosphatidic acid (PA), the product of the DGK reaction.

Key words:

Cystic fibrosis, epithelium sodium channel (ENaC), airway surface liquid (ASL), phosphatidylinositol 4,5-bisphosphate ($PI(4,5)P_2$), short palate lung and nasal epithelial clone 1 (SPLUNC1), diacylglycerol kinase (DGK)

4.2. Introduction

Mutations in the cystic fibrosis transmembrane conductance regulator (CFTR), a chloride and bicarbonate membrane channel, can cause problems in several organs and, in particular, lead to cystic fibrosis (CF). In the lungs, the production of thick, dehydrated mucus associated with these mutations leads to recurrent infections and frequent inflammation events that eventually compromise organ function [1]. Life expectancy for subjects with CF has improved considerably [2], and promising new drugs containing lumacaftor or ivacaftor were recently brought to the market [3]. Despite these advancements, a complete cure for CF has not yet been achieved, in part due to mutations that are not treatable with the available drugs.

While the mutation causing CF is found in the gene for CFTR, other ion channels are affected. In particular, changes in the Epithelium Sodium Channels (ENaCs) play a role in CF. It has been hypothesized that lack of CFTR in CF lungs causes ENaC function to increase. Consequently, large amounts of sodium and water are absorbed, which implies that this channel may be one of the contributors to the accumulation of mucus in the lungs that characterizes this disease. Interestingly, ENaC was found to be dependent on CFTR in sweat glands, and inhibition or removal of the chloride channel prevents ENaC activation [4]. Perturbations in ENaC have also been linked to several other diseases, including high blood pressure control, edema [5] and heart disease [6].

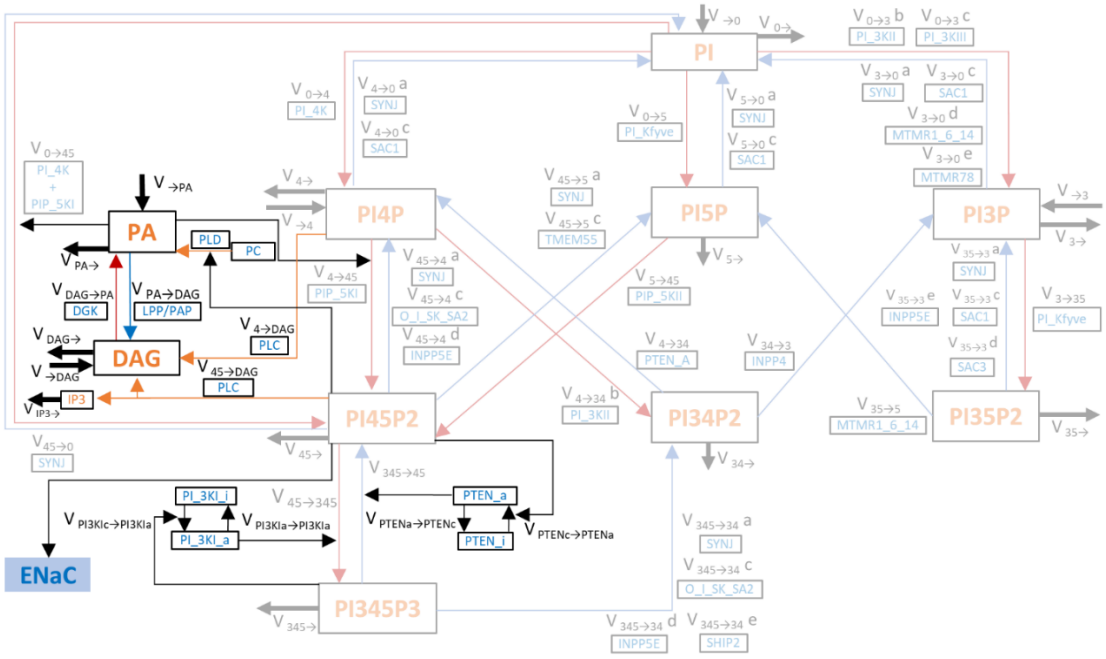

Figure 4.1. Model map.

The faint components represent our previous model [7], while the prominent components show the new modules and extensions. The arrow from $PI(4,5)P_2$ to ENaC represents the control that the lipid exerts over the channel. Thick black arrows represent input and output fluxes of material entering and leaving the system. Thin black arrows represent regulations. Red and blue arrows represent fluxes of phosphorylation and hydrolysis, respectively. For each flux, the name ($v_{i\rightarrow j}$) and the group of enzymes that catalyze the reaction are shown. Orange arrows represent phospholipase fluxes. PTEN and PI3KI have an active (a) and inactive (i) state. O_I_SK_SA2 is a group of phosphatases, consisting of OCRL1, INPP5 B/J, SAC2 and SKIP. PI4K+PIP5KI+DVL denotes a complex formed by the three proteins. Proteins separated by commas catalyze the same reaction. INPP5: Inositol polyphosphate 5-phosphatases; OCRL1: Lowe Oculocerebrorenal Syndrome Protein.

Phosphoinositides are rare membrane lipids with various signaling functions. Several studies have shown that two of these lipids, $PI(4,5)P_2$ and $PI(3,4,5)P_3$, have an effect on ENaC [8]–[12]. Their key precursor, phosphatidylinositol (PI), is created in the ER from phosphatidic acid (PA) and transported to the plasma membrane, where it is phosphorylated into the other phosphoinositide species (Figure 4.1). $PI(4,5)P_2$ is cleaved by PLC into inositol triphosphate (IP_3) and diacylglycerol (DAG) and transformed into PA, which is transported back to the ER to close the cycle.

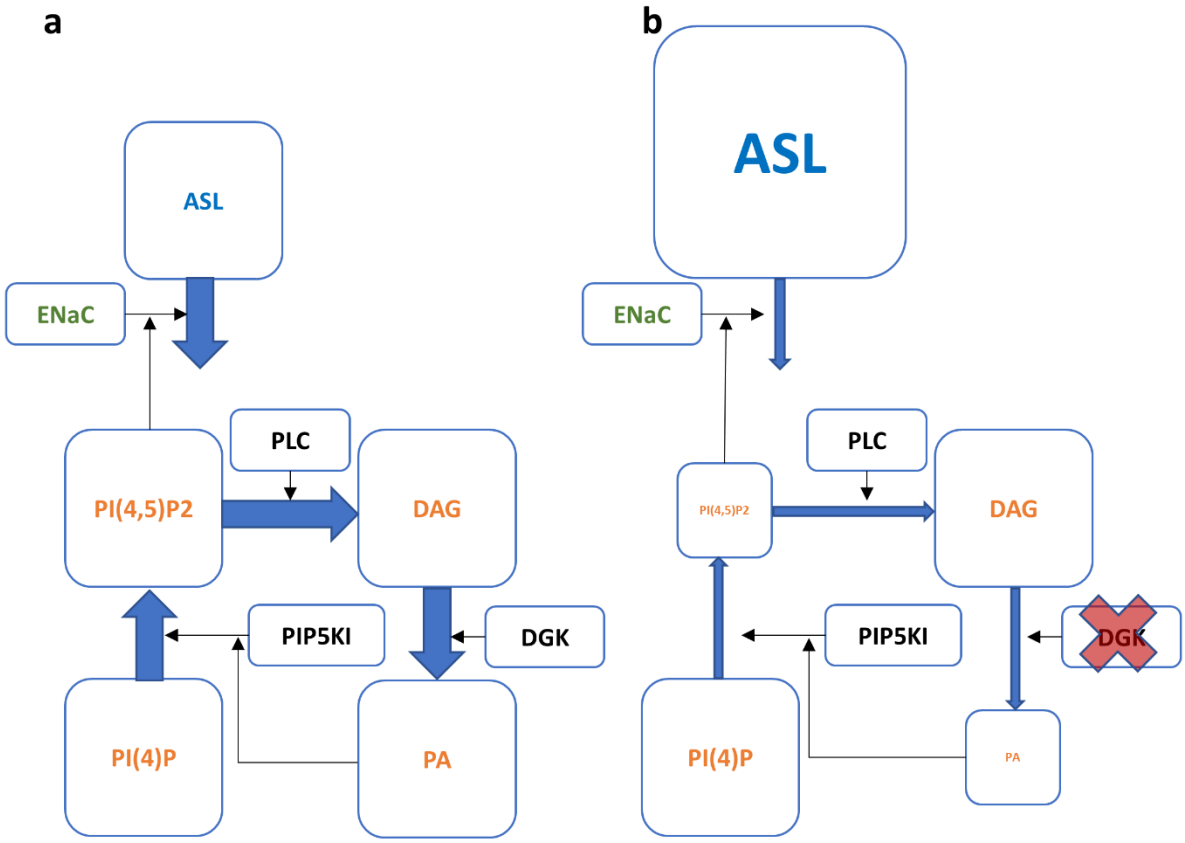

Figure 4.2. Consequences of inhibiting DGK for phosphoinositide metabolism, ENaC and ASL.

a) Normal state. **b)** DGK inhibition reduces the production of PA which, in turn, reduces the production of $PI(4,5)P_2$, which is catalyzed by PIP5KI. Low levels of $PI(4,5)P_2$ reduce ENaC activity and the absorption of ASL by this channel, which consequently leads to an increase in ASL thickness.

DGK is the kinase that transforms DAG into PA. Almaça *et al.* [13] found that inhibiting DGK causes a moderation of ENaC activity and normalizes the increased sodium channel activity in CF. These authors specifically hypothesized that inhibiting DGK might bring the recycling of the phosphoinositides to a halt, which in turn would decrease the levels of $PI(4,5)P_2$ and $PI(3,4,5)P_3$ and cause the observed ENaC moderation. However, DGK is active in the plasma membrane, while phosphoinositide synthesis occurs in the ER. Transport of lipids between membranes of different compartments is mediated by vesicles or specialized proteins, and quantitative details about the dynamics of this transport are still lacking. Thus, many open questions remain unanswered. Crucially, it is not clear what the dynamics of the control of ENaC by

DGK is, and if and how DGK could potentially be used as a therapy in situations where ENaC function is deregulated.

In the work described here, we investigate ENaC control by DGK. As an alternative to Almaça's hypothesis, we proffer that ENaC is regulated by $PI(4,5)P_2$, which is produced by PIP5KI under the control of PA, which in turn is produced from DAG under the control of DGK (Figure 4.2). We furthermore suggest that $PI(4,5)P_2$ specifically influences the probability that ENaC is open ("open-probability" P_o) but not the number of channels in the membrane (N), which is a consequence of ubiquitination by the protein NEDD4-2 (neural precursor cell expressed developmentally down-regulated protein 4 – 2) [14] and an interaction with the protein SPLUNC1 (short palate lung and nasal epithelial clone 1) [15].

Our core objective in this work is to test this hypothesis with a strategy that uses computational modelling and to achieve a deeper understanding of how DGK and phosphoinositides control ENaC activity. The proposed model consists of two modules that embedded in an appropriate context, established from the literature, and offers an explanation of the regulation of ENaC function. One of the two modules address the phosphoinositide pathway, while the other captures the regulation of ENaC and ASL. The merging of these modules allows, for the first time, a detailed study of the dynamics of ENaC regulation by phosphoinositides. The model of the phosphoinositide pathway is taken from our recent work [7], expanded with processes that are fundamental to study the pathway regulation, namely ENaC regulation and $PI(4,5)P_2$ degradation by PLC, DAG or PA, while the model of ENaC dynamics was presented in [16].

In the following, we present an extended version of the prior phosphoinositide pathway model, which takes into account the competition of enzymes for the same substrates and regulation among PTEN, PI3KI, $PI(4,5)P_2$ and $PI(3,4,5)P_3$. We further add a new module, which was constructed with similar principles and includes four new processes (Figure 4.1): first, the cleavage of $PI(4,5)P_2$ into DAG and IP_3 by phospholipase C (PLC); second, the production of PA by the phosphorylation of DAG by DGK; third, the hydrolysis of PA back to DAG by phosphatidate phosphatases (LLP's); and fourth, the replenishment of the PA pool from phosphatidylcholine (PC) by phospholipase D (PLD).

We also account for PA activation of PIP5KI, the enzyme that transforms PI(4)P into $PI(4,5)P_2$, as previously described in the literature [17]–[19]. This collective mechanism is able to sustain $PI(4,5)P_2$ levels upon PLC activation [20]–[22].

To study the influence of $PI(4,5)P_2$ and DGK on ENaC and ASL, we couple the extended model of phosphoinositide dynamics with our recent model designed to elucidate the dynamics of ENaC and ASL regulation [16].

Finally, we use Suratekar's model of the phosphoinositide pathway [23] to demonstrate that Almaça's hypothesis does not truly replicate the observed behavior. However, after adding PA regulation of PIP5KI and implementing a few other adjustments, the model replicates the observed DGK attenuation of ENaC.

Our results show that the combined and extended model of the phosphoinositide pathway fits data from different sources remarkably well. Most importantly, testing our and Suratekar's models against the observations of Almaça *et al.* yields good agreement. This agreement suggests that the models and our hypothesis, that ENaC regulation by DGK is accomplished though PA activation of PIP5KI, provide a good explanation for ENaC regulation and can be used to explore therapeutic interventions in clinical conditions where ENaC is thought to be relevant.

4.3. Background

DAG is composed of a glycerol backbone with two hydrophobic fatty acid chains attached. DAG can be transformed through the Kennedy pathway into other phospholipids [24], such as phosphatidylcholine (PC), phosphatidylserine (PS) and phosphatidylethanolamine (PE). DAG can also be phosphorylated at the last free carbons of glycerol, thereby becoming PA. An inositol ring of six carbons can be attached to this phosphate, which converts PA into phosphatidylinositol (PI). This inositol ring can be further phosphorylated at the third, fourth and fifth carbons, and these phosphorylation events give rise to the seven species of phosphoinositides. These relatively rare lipids, which comprise about 10% of the phospholipids in cell membranes [12], [25], [26], are at the center of this study.

Phosphoinositides have been implicated in nearly all aspects of cell physiology. They are identifiers of different types of cell membranes and also play a dynamic role in cell

process control as second messengers and precursors of other messengers. As a consequence, phosphoinositides are important in a myriad of cell functions like cytoskeleton formation, chemotaxis, cell polarization, T cell activation and cytokinesis [12], [27]. Here, we are particularly interested in their function as docking sites for proteins to the cell membrane and as membrane protein regulators.

Several studies have shown that phosphoinositides, especially $PI(4,5)P_2$ and $PI(3,4,5)P_3$, influence ENaC [8]–[12]. In particular, Almaça *et al.* [13] studied ENaC function with siRNA screens in the context of CF and demonstrated that the phosphatidylinositol pathway is highly influential with respect to ENaC activity. These authors found that inhibiting DGK, which can influence phosphoinositide production, moderates ENaC activity in primary human lung cells affected by CF and that ENaC function is essentially restored to normal, non-CF levels.

The reasons for ENaC's upregulation in CF are not clear, but there is no shortage of hypotheses [5], [15], [28]–[32]. Among these, Tarran and colleagues [33]–[35] advanced a hypothesis based on the protein SPLUNC1, which not only protects ENaC from cleavage by proteases but also promotes the channel disassembly and removal of ENaC α and γ subunits from the plasma membrane [15]. According to this hypothesis, the absence of CFTR in the membrane leads to a decreased secretion of bicarbonate, which in turn leads to SPLUNC1 inactivation by the now more acidic ASL. Therefore, ENaC channels with high P_o will be more common, have less probability of being removed from the plasma membrane and, ultimately, is function will be up-regulated. We adopted this view because it was at least partially validated by results obtained under practically relevant conditions [36].

Kota *et al.* [37] offered an explanation linking phosphoinositides to ENaC control. They found that when the intracellular N-termini of ENaC connect to phosphoinositides, a conformational change occurs that exposes the extracellular loops of the channel to proteases. Severing these loops leads to an increase in the "channel open probability" (P_o) of ENaC. Thus, if the levels of $PI(4,5)P_2$ or $PI(3,4,5)P_3$ are decreased, proteases will not cut ENaC's extracellular loops as often and the channel action is reduced.

It is clear that the regulation of ENaC and ASL is complex and that intuition alone may lead to faulty conclusions. To overcome this challenge, we are here employing

mathematical models that allow us to study the dynamics of ENaC and its regulation by $PI(4,5)P_2$ in an objective manner. Specifically, we expand an existing model of phosphoinositide dynamics and couple it with a model capturing the processes controlling ENaC and ASL.

To the best of our knowledge, only Sandefur and colleagues [38] made an attempt to study ENaC regulation by phosphoinositides. However, these authors did not consider SPLUNC1 and practically ignore phosphoinositides, only referring to them as mediators of $P2Y_2$ purinoreceptor signaling, which is activated by extracellular adenosine triphosphate (ATP). This simplification has the crucial disadvantage that it becomes difficult to study the regulation of PIP5KI by DGK, which could be a promising drug target.

Other models have been proposed to simulate the phosphoinositide pathway or parts of it. Falkenburger, Dickson and Hille [39], [40] studied the kinetics of PI(4)P, $PI(4,5)P_2$, PLC, DAG, IP_3 and calcium. They showed that an acceleration of $PI(4,5)P_2$ production during PLC activation is necessary for IP_3 production. Expressed differently, IP_3 production will fade or stop if $PI(4,5)P_2$ production is not accelerated. This study did not account for the activation of PIP5KI by PA, although it considered an increase in PI4K function when PLC was activated, which has a similar effect.

Narang *et al.* [41] developed a mathematical model that takes the activation of PIP5KI by PA into account. However, this model oversimplifies the phosphoinositide pathway by representing PI, PI(4)P, $PI(4,5)P_2$ and $PI(3,4,5)P_3$ with just one variable and implementing PA activation of PIP5KI with an auto-activation of the phosphoinositides.

Purvis *et al.* [22] built a model of the pathway in platelets. While generally impressive, this model does not account for all pertinent phosphoinositide species and does not include the activation of PIP5KI by PA.

PI is twice phosphorylated to become $PI(4,5)P_2$: first by PI4K and afterwards by PIP5KI. The limiting rate of this process seems to be PI4K phosphorylation, which is 20 times slower than the phosphorylation of PIP5KI. In an attempt to explain this difference, Falkenburger, Dickson and Hille [39], [40] suggested that an acceleration of the production of $PI(4,5)P_2$, which would compensate for the depletion caused by

PLC, should impact PI4K. We cannot fully agree with this rationale because of the following observations. PIP5KI is inhibited by its substrate, PI(4)P, which Falkenburger's argument ignores. Specifically, Jarquin-Pardo *et al.* [19] stated that PIP5KI has an inhibitory as well as an active site for PI(4)P and that, in the absence of PA, the K_M for the inhibitory site is 50-fold smaller than the K_M for the active site. They furthermore state that "the addition of PA increases the affinity with which the active site of mPIP5K-Ib binds PI(4)P by 67-fold." Furthermore, Moritz *et al.* [17] report that the PIP5KI activation by PA is inhibited by $PI(4,5)P_2$. These two pieces of evidence suggest that PIP5KI only functions fully in the presence of PA and with reduced levels of $PI(4,5)P_2$. Finally, PI4K has PI as its substrate, which is 300 times more abundant than PI(4)P, the substrate for PIP5KI. These observations suggest that PIP5KI is the rate limiting component of $PI(4,5)P_2$ production.

Falkenburger *et al.* [39] used in their model an amount of PI(4)P that is less than a third of the quantity of $PI(4,5)P_2$ and assumed that two thirds of $PI(4,5)P_2$ were in a bound state while all PI(4)P was free. We tried to keep the amounts of these two phosphoinositides similar, in accordance with what is commonly accepted [12], [26].

4.4. Results

All major findings in this section are inferences from analyses of our proposed model. This model is composed of two sub-models. One of these was shown in Chapter 2; it represents the phosphoinositide pathway. The other sub-model captures the dynamics of ENaC; details can be found in Chapter 3 . The main connection between the two sub-models is $PI(4,5)P_2$. This connection is critical, as it permits explorations of the interactions between phosphoinositides and the dynamics of ENaC and ASL.

The map for the expanded phosphoinositide pathway model is depicted in Figure 4.1. Fluxes and equations are presented in Table 4.1 and parameters and initial values are given in Table 4.2. References for parameters can be found in Supplementary Table 4.4 and in Chapters 2 and 3. The earlier phosphoinositide pathway model was successfully tested against a long list of phenomena reported in the literature, and the results were described in Chapter 2. Corresponding results for the extended phosphoinositide model are summarized in Figure 4.10. As is to be expected, the new modules and extensions slightly affect the model fits in comparison to the previous sub-model, but the combined

phosphoinositide-ENaC model yields fits to the data that are similar. In addition, the combined model generates genuinely new results, which are summarized in Table 4.3 and detailed in the following, along with reports from the literature.

Table 4.1. Format of the Extended Model.

Fluxes

$V_{\rightarrow 0} = \gamma_{\rightarrow 0}$

$V_{\rightarrow 4} = \gamma_{\rightarrow 4}$

$V_{\rightarrow 3} = \gamma_{\rightarrow 3}$

$V_{0\rightarrow 3b} = \gamma_{0\rightarrow 3b} * PI\hat{}f_{0\rightarrow 3b\_PI} * PI3KII$

$V_{0\rightarrow 3c} = \gamma_{0\rightarrow 3c} * PI\hat{}f_{0\rightarrow 3c\_PI} * PI(4)P\hat{}\ f_{0\rightarrow 3c\_PI(4)P} * PI3KIII$

$V_{3\rightarrow 0a} = \gamma_{3\rightarrow 0a} * PI(3)P\hat{}f_{3\rightarrow 0a\_PI(3)P} * PI(4)P\hat{}f_{3\_0a\_PI(4)P} * PI(5)P\hat{}f_{3\_0a\_PI(5)P} * PI(3,5)P_2\hat{}f_{3\_0a\_PI(3,5)P2} * PI(4,5)P_2\hat{}(f_{3\_0a\_PI(4,5)P2\_PI} + f_{3\_0a\_PI(4,5)P2\_PI(4)P} + f_{3\_0a\_PI(4,5)P2\_PI(5)P}) * PI(3,4,5)P_3\hat{}f_{3\_0a\_PI(3,4,5)P3} * SYNJ$

$V_{3\rightarrow 0c} = \gamma_{3\rightarrow 0c} * PI(3)P\hat{}f_{3\rightarrow 0c\_PI(3)P} * PI(4)P\hat{}f_{3\_0c\_PI(4)P} * PI(5)P\hat{}f_{3\_0c\_PI(5)P} * PI(3,5)P_2\hat{}f_{3\_0c\_PI(3,5)P2} * SAC1$

$V_{3\rightarrow 0d} = \gamma_{3\rightarrow 0d} * PI(3)P\hat{}f_{3\rightarrow 0d\_PI(3)P} * PI(3,5)P_2\hat{}f_{3\_0d\_PI(3,5)P2} * MTMR1\_6\_14$

$V_{3\rightarrow 0e} = \gamma_{3\rightarrow 0e} * PI(3)P\hat{}f_{3\rightarrow 0e\_PI(3)P} * MTMR78$

$V_{0\rightarrow 4} = \gamma_{0\rightarrow 4} * PI\hat{}f_{0\rightarrow 4\_PI} * PI4K$

$V_{4\rightarrow 0a} = \gamma_{4\rightarrow 0a} * PI(4)P\hat{}f_{4\rightarrow 0a\_PI(4)P} * PI(3)P\hat{}f_{4\_0a\_PI(3)P} * PI(5)P\hat{}f_{4\_0a\_PI(5)P} * PI(3,5)P_2\hat{}f_{4\_0a\_PI(3,5)P2} * PI(4,5)P_2\hat{}(f_{4\_0a\_PI(4,5)P2\_PI(4)P} + f_{4\_0a\_PI(4,5)P2\_PI(5)P} + f_{4\_0a\_PI(4,5)P2\_PI}) PI(3,4,5)P_3\hat{}f_{4\_0a\_PI(3,4,5)P3} * SYNJ$

$V_{4\rightarrow 0c} = \gamma_{4\rightarrow 0c} * PI(4)P\hat{}f_{4\rightarrow 0c\_PI(4)P} * PI(3)P\hat{}f_{4\_0c\_PI(3)P} * PI(5)P\hat{}f_{4\_0c\_PI(5)P} * PI(3,5)P_2\hat{}f_{4\_0c\_PI(3,5)P2} * SAC1$

$V_{0\rightarrow 5} = \gamma_{0\rightarrow 5} * PI\hat{}f_{0\rightarrow 5\_PI} * PI(3)P\hat{}f_{0\_5\_PI(3)P} * PIKfyve$

$V_{5\rightarrow 0a} = \gamma_{5\rightarrow 0a} * PI(5)P\hat{}f_{5\_0a\_PI(5)P} * PI(3)P\hat{}f_{5\_0a\_PI(3)P} * PI(4)P\hat{}f_{5\_0a\_PI(4)P} * PI(3,5)P_2\hat{}f_{5\_0a\_PI(3,5)P2} * PI(4,5)P_2\hat{}(f_{5\_0a\_PI(4,5)P2\_PI(4)P} + f_{5\_0a\_PI(4,5)P2\_PI(5)P} + f_{5\_0a\_PI(4,5)P2\_PI}) PI(3,4,5)P_3\hat{}f_{5\_0a\_PI(3,4,5)P3} * SYNJ$

$V_{5\rightarrow 0c} = \gamma_{5\rightarrow 0c} * PI(5)P\hat{}f_{5\_0c\_PI(5)P} * PI(3)P\hat{}f_{5\_0c\_PI(3)P} * PI(4)P\hat{}f_{5\_0c\_PI(4)P} * PI(3,5)P_2\hat{}f_{5\_0c\_PI(3,5)P2} * SAC1$

$V_{3\rightarrow 35} = \gamma_{3\rightarrow 35} * PI(3)P\hat{}f_{3\rightarrow 35\_PI(3)P} * PIKfyve$

$V_{35\rightarrow 3a} = \gamma_{35\rightarrow 3a} * PI(3,5)P_2\hat{}f_{35\_3a\_PI(3,5)P2} * PI(3)P\hat{}f_{35\_3a\_PI(3)P} * PI(4)P\hat{}f_{35\_3a\_PI(4)P} * PI(5)P\hat{}f_{35\_3a\_PI(5)P} * PI(4,5)P_2\hat{}f_{35\_3a\_PI(4,5)P2\_PI(4)P} + f_{35\_3a\_PI(4,5)P2\_PI(5)P} + f_{35\_3a\_PI(4,5)P2\_PI}) PI(3,4,5)P_3\hat{}f_{35\_3a\_PI(3,4,5)P3} * SYNJ$

$V_{35\rightarrow 3c} = \gamma_{35\rightarrow 3c} * PI(3,5)P_2\hat{}f_{35\_3c\_PI(3,5)P2} * PI(3)P\hat{}f_{35\_3c\_PI(3)P} * PI(4)P\hat{}f_{35\_3c\_PI(4)P} * PI(5)P\hat{}f_{35\_3c\_PI(5)P} * SAC1$

$V_{35\rightarrow 3d} = \gamma_{35\rightarrow 3d} * PI(3,5)P_2\hat{}f_{35\rightarrow 3d\_PI(3,5)P2} * SAC3$

$V_{35\rightarrow 3e} = \gamma_{35\rightarrow 3e} * PI(3,5)P_2\hat{}f_{35\_3e\_PI(3,5)P2} * PI(4,5)P_2\hat{}f_{35\_3e\_PI(4,5)P2} * PI(3,4,5)P_3\hat{}f_{35\_3e\_PI(3,4,5)P3} * INPP5E$

$V_{4\rightarrow 45} = \gamma_{4\rightarrow 45} * PI(4)P\hat{}f_{4\rightarrow 45\_PI(4)P} * PIP5KI * HS(PA) * PI(4,5)P_2\hat{}f_{4\_45\_PI(4,5)P2}$

$V_{45\rightarrow 4a} = \gamma_{45\rightarrow 4a} * PI(4,5)P_2\hat{}f_{45\_4a\_PI(4,5)P2\_PI(4)P} * PI(3)P\hat{}f_{45\_4a\_PI(3)P} * PI(4)P\hat{}f_{45\_4a\_PI(4)P} * PI(5)P\hat{}f_{45\_4a\_PI(5)P} * PI(3,5)P2\hat{}f_{45\_4a\_PI(3,5)P2} * PI(4,5)P_2\hat{}(f_{45\_4a\_PI(4,5)P2\_PI(5)P} + f_{45\_4a\_PI(4,5)P2\_PI}) * PI(3,4,5)P_3\hat{}f_{45\_4a\_PI(3,4,5)P3} * SYNJ$

$V_{45\rightarrow 4c} = \gamma_{45\rightarrow 4c} * PI(4,5)P_2\hat{}f_{45\_4c\_PI(4,5)P2} * PI(3,4,5)P_3\hat{}f_{45\_4c\_PI(3,4,5)P3} * (ORCL1 + INPP5BJ + SKIP + SAC2)$

$V_{45\rightarrow 4d} = \gamma_{45\rightarrow 4d} * PI(4,5)P_2\hat{}f_{45\_4d\_PI(4,5)P2} * PI(3,5)P_2\hat{}f_{45\_4d\_PI(3,5)P2} * PI(3,4,5)P_3\hat{}f_{45\_4d\_PI(3,4,5)P3} * INPP5E$

$V_{5\rightarrow 45} = \gamma_{5\rightarrow 45} * PI(5)P\hat{}f_{5\rightarrow 45\_PI(5)P} * PIP5KII$

$V_{45\rightarrow 5a} = \gamma_{45\rightarrow 5a} * PI(4,5)P_2\hat{}f_{45\_5a\_PI(4,5)P2\_PI(5)P} * PI(3)P\hat{}f_{45\_5a\_PI(3)P} * PI(4)P\hat{}f_{45\_5a\_PI(4)P} * PI(5)P\hat{}f_{45\_5a\_PI(5)P} * PI(3,5)P_2\hat{}f_{45\_5a\_PI(3,5)P2} * PI(4,5)P_2\hat{}(f_{45\_5a\_PI(4,5)P2\_PI(4)P} + f_{45\_5a\_PI(4,5)P2\_PI}) * PI(3,4,5)P_3\hat{}f_{45\_5a\_PI(3,4,5)P3} * SYNJ$

$V_{45\rightarrow 5c} = \gamma_{45\rightarrow 5c} * PI(4,5)P_2\hat{}f_{45\rightarrow 5c\_PI(4,5)P2} * TMEM55$

$V_{45\rightarrow 345} = \gamma_{45\rightarrow 345} * PI(4,5)P_2\hat{}f_{45\rightarrow 345\_PI(4,5)P2} * PI3KI\_a$

$V_{345\rightarrow 45} = \gamma_{345\rightarrow 45} * PI(3,4,5)P_3\hat{}f_{345\rightarrow 45\_PI(3,4,5)P3} * PI(3,4)P_2\hat{}f_{345\_45\_PI(3,4)P2} * PTEN\_a$

$V_{35\rightarrow 5} = \gamma_{35\rightarrow 5} * PI(3,5)P_2\hat{}f_{35\rightarrow 5\_PI(3,5)P2} * PI(3)P\hat{}f_{35\_5\_PI(3)P} * MTMR1\_6\_14$

$V_{34\rightarrow 3} = \gamma_{34\rightarrow 3} * PI(3,4)P_2\hat{}f_{34\rightarrow 3\_PI(3,4)P2} * INPP4$

$V_{345\rightarrow 34a} = \gamma_{345\rightarrow 34a} * PI(3,4,5)P_3\hat{}f_{345\_34a\_PI(3,4,5)P3} * PI(3)P\hat{}f_{345\_34a\_PI(3)P} * PI(4)P\hat{}f_{345\_34a\_PI(4)P} * PI(5)P\hat{}f_{345\_34a\_PI(5)P} * PI(3,5)P_2\hat{}f_{345\_34a\_PI(3,5)P2} * PI(4,5)P_2\hat{}(f_{345\_34a\_PI(4,5)P2\_PI(4)P} + f_{345\_34a\_PI(4,5)P2\_PI(5)P} + f_{345\_34a\_PI(4,5)P2\_PI}) * SYNJ$

$V_{345\rightarrow 34c} = \gamma_{345\rightarrow 34c} * PI(3,4,5)P_3\hat{}f_{345\rightarrow 34c\_PI(3,4,5)P3} * PI(4,5)P_2\hat{}f_{345\_34c\_PI(4,5)P2} * (ORCL1 + INPP5BJ + SKIP + SAC2)$

$V_{345\rightarrow 34d} = \gamma_{345\rightarrow 34d} * PI(3,4,5)P_3\hat{}f_{345\rightarrow 34d\_PI(3,4,5)P2} * PI(3,5)P_2\hat{}f_{345\_34d\_PI(3,5)P2} * PI(4,5)P_2\hat{}f_{345\_34d\_PI(4,5)P2} * INPP5E$

$V_{345\rightarrow 34e} = \gamma_{345\rightarrow 34e} * PI(3,4,5)P_3\hat{}f_{345\rightarrow 34e\_PI(3,4,5)P3} * SHIP2$

$V_{45\rightarrow} = \gamma_{i\rightarrow} * PI(4,5)P_2$

$V_{0\rightarrow} = \gamma_{i\rightarrow} * PI$

$V_{4\rightarrow} = \gamma_{i\rightarrow} * PI(4)P$

$V_{345\rightarrow} = \gamma_{i\rightarrow} * PI(3,4,5)P_3$

$V_{3\rightarrow} = \gamma_{i\rightarrow} * PI(3)P$

$V_{35\rightarrow} = \gamma_{i\rightarrow} * PI(3,5)P_2$

$V_{5\rightarrow} = \gamma_{i\rightarrow} * PI(5)P$

$V_{34\rightarrow} = \gamma_{i\rightarrow} * PI(3,4)P_2$

$V_{0\rightarrow 45} = \gamma_{0\rightarrow 45} * PI\hat{}f_{0\rightarrow 45\_PI} * (PI4K\_PIP5KI) * HS(PA) * PI(4,5)P_2\hat{}f_{0\_45\_PI(4,5)P2}$

$V_{45\rightarrow 0} = \gamma_{45\rightarrow 0} * PI(4,5)P_2\hat{}f_{45\_0\_PI(4,5)P2\_PI} * PI(3)P\hat{}f_{45\_0\_PI(3)P} * PI(4)P\hat{}f_{45\_0\_PI(4)P} * PI(5)P\hat{}f_{45\_0\_PI(5)P} * PI(3,5)P_2\hat{}f_{45\_0\_PI(3,5)P2} * PI(4,5)P_2\hat{}f_{45\_0\_PI(4,5)P2\_PI(4)P} * PI(4,5)P_2\hat{}f_{45\_0\_PI(4,5)P2\_PI(5)P} * PI(3,4,5)P_3\hat{}f_{45\_0\_PI(3,4,5)P3} * SYNJ$

$V_{4\rightarrow 34a} = \gamma_{4\rightarrow 34a} * PI(4)P\hat{}f_{4\rightarrow 34a\_PI(4)P} * PI3KI\_a$

$V_{4\rightarrow 34b} = \gamma_{4\rightarrow 34b} * PI(4)P\hat{}f_{4\rightarrow 34b\_PI(4)P} * PI\hat{}f_{4\_34b\_PI} * PI3KII$

$V_{34\rightarrow 4} = \gamma_{34\rightarrow 4} * PI(3,4)P_2\hat{}f_{34\rightarrow 4\_PI(3,4)P2} * PI(3,4,5)P_3\hat{}f_{34\_4\_PI(3,4,5)P3} * PTEN\_a$

$PI3KI\_c = PI3KI - PI3KI\_a$

$V_{PI3KIc\rightarrow PI3KIa} = \gamma_{PI3KIc\rightarrow PI3KIa} * (PI3KI - PI3KI\_a) \hat{} f_{PI3KIc\rightarrow PI3KIa\_PI3KI\_c} * PI(3,4,5)P_3 \hat{} f_{PI3KIc\rightarrow PI3KIa\_PI(3,4,5)P3}$

$V_{PI3KIa \rightarrow PI3KIc} = \gamma_{PI3KIa \rightarrow PI3KIc} * PI3KI\_a$

$PTEN\_c = PTEN - PTEN\_a$

$V_{PTENc \rightarrow PTENa} = \gamma_{PTENc \rightarrow PTENa} * (PTEN - PTEN\_a) \wedge f_{PTENc \rightarrow PTENa\_PTEN\_c} * PI(4,5)P_2 \wedge f_{PTENc \rightarrow PTENa\_PI(4,5)P2}$

$V_{PTENa \rightarrow PTENc} = \gamma_{PTENa \rightarrow PTENc} * PTEN\_a \wedge f_{PTENa \rightarrow PTENc\_PTEN\_a}$

$V_{45 \rightarrow DAG} = \gamma_{45 \rightarrow DAG} * PI(4,5)P_2 \wedge f_{45 \rightarrow DAG\_PI(4,5)P2} * PI(4)P \wedge f_{45 \rightarrow DAG\_PI(4)P} * PS \wedge f_{45 \rightarrow DAG\_PS} * PLC$

$V_{PA \rightarrow DAG} = \gamma_{PA \rightarrow DAG} * PA \wedge f_{PA \rightarrow DAG\_PA} * LPP$

$V_{DAG \rightarrow PA} = \gamma_{DAG \rightarrow PA} * DAG \wedge f_{DAG \rightarrow PA\_DAG} * DGK$

$V_{\rightarrow DAG} = \gamma_{\rightarrow DAG}$

$V_{DAG \rightarrow} = \gamma_{DAG \rightarrow} * DAG \wedge f_{DAG \rightarrow\_DAG}$

$V_{\rightarrow PA} = \gamma_{\rightarrow PA}$

$V_{PA \rightarrow} = \gamma_{PA \rightarrow} * PA \wedge f_{PA \rightarrow\_PA}$

$V_{PC \rightarrow PA} = \gamma_{PC \rightarrow PA} * PI(4,5)P_2 \wedge f_{PC\_PA\_PI(4,5)P2}$

$V_{IP3 \rightarrow} = \gamma_{IP3 \rightarrow} * IP3 \wedge f_{IP3 \rightarrow\_IP3}$

$V_{PI4P \rightarrow DAG} = \gamma_{4 \rightarrow DAG} * PI(4)P \wedge f_{4 \rightarrow DAG\_PI4P} * PI(4,5)P_2 \wedge f_{4\_DAG\_PI(4,5)P2} * PS \wedge f_{4 \rightarrow DAG\_PS} * PLC$

Table 4.2. Initial Values and Model Parameters.

PI3KI	1000	$f_{5\rightarrow 0a\_PI4P}$	-0.04385	$f_{35\rightarrow 5\_PI3P}$	-0.00066
PTEN	50	$f_{5\rightarrow 0a\_PI5P}$	0.999562	$\gamma_{34\rightarrow 3}$	1.33E+12
PI3KII	75	$f_{5\rightarrow 0a\_PI35P2}$	-0.00022	$f_{34\rightarrow 3\_PI34P2}$	0.998198
PI3KIII	5	$f_{5\rightarrow 0a\_PI45P2\_PI4P}$	-0.04385	$\gamma_{345\rightarrow 34a}$	2.48E+12
PI4K	400	$f_{5\rightarrow 0a\_PI45P2\_PI5P}$	-0.23834	$f_{345\rightarrow 34a\_PI3P}$	-0.00044
PIKfyve	48	$f_{5\rightarrow 0a\_PI345P3}$	-0.00167	$f_{345\rightarrow 34a\_PI4P}$	-0.04385
PIP5KI	330	$f_{5\rightarrow 0a\_PI45P2\_PI}$	-0.01096	$f_{345\rightarrow 34a\_PI5P}$	-0.00044
PIP5KII	845	$\gamma_{5\rightarrow 0c}$	5.1E+12	$f_{345\rightarrow 34a\_PI35P2}$	-0.00022
PI4K_PIP5KI	230	$f_{5\rightarrow 0c\_PI5P}$	0.999378	$f_{345\rightarrow 34a\_PI45P2\_PI4P}$	-0.04385
SYNJ	30	$f_{5\rightarrow 0c\_PI3P}$	-0.00062	$f_{345\rightarrow 34a\_PI45P2\_PI5P}$	-0.23834
SAC1	100	$f_{5\rightarrow 0c\_PI4P}$	-0.06219	$f_{345\rightarrow 34a\_PI345P3}$	0.998332
SAC2	1	$f_{5\rightarrow 0c\_PI35P2}$	-0.00031	$f_{345\rightarrow 34a\_PI45P2\_PI}$	-0.01096
SAC3	5	$\gamma_{3\rightarrow 35}$	1.62E+16	$\gamma_{345\rightarrow 34c}$	2.79E+11
INPP4	50	$f_{3\rightarrow 35\_PI3P}$	0.999622	$f_{345\rightarrow 34c\_PI345P3}$	0.997636
TMEM55	20	$f_{3\rightarrow 35\_PI}$	-0.45347	$f_{345\rightarrow 34c\_PI45P2}$	-0.06214
MTMR1_6_14	63	$\gamma_{35\rightarrow 3a}$	4.56E+13	$\gamma_{345\rightarrow 34d}$	2.79E+11
MTMR78	18	$f_{35\rightarrow 3a\_PI3P}$	-0.00044	$f_{345\rightarrow 34d\_PI345P3}$	0.997637
ORCL1	3	$f_{35\rightarrow 3a\_PI4P}$	-0.04385	$f_{345\rightarrow 34d\_PI35P2}$	-0.00031
INPP5BJ	1	$f_{35\rightarrow 3a\_PI5P}$	-0.00044	$f_{345\rightarrow 34d\_PI45P2}$	-0.06212
INPP5E	1	$f_{35\rightarrow 3a\_PI35P2}$	0.999781	$\gamma_{345\rightarrow 34e}$	1.68E+11
SKIP	5	$f_{35\rightarrow 3a\_PI45P2\_PI4P}$	-0.04385	$f_{345\rightarrow 34e\_PI345P3}$	0.998198
SHIP2	1	$f_{35\rightarrow 3a\_PI45P2\_PI5P}$	-0.23834	$\gamma_{I\rightarrow}$	0.045
PS	150000	$f_{35\rightarrow 3a\_PI345P3}$	-0.00167	$\gamma_{0\rightarrow 45}$	2.67E+14
PLC	5	$f_{35\rightarrow 3a\_PI45P2\_PI}$	-0.01096	$f_{0\rightarrow 45\_PI}$	0.286462
DGK	50	$\gamma_{35\rightarrow 3c}$	5.1E+12	$f_{0\rightarrow 45\_PA}$	0.2
LPP	100	$f_{35\rightarrow 3c\_PI35P2}$	0.999689	$f_{0\rightarrow 45\_PI45P2}$	-0.05
$\gamma_{\rightarrow 0}$	15000	$f_{35\rightarrow 3c\_PI3P}$	-0.00062	$\gamma_{4\rightarrow 34b}$	5.64E+14
$\gamma_{\rightarrow 4}$	150	$f_{35\rightarrow 3c\_PI4P}$	-0.06219	$f_{4\rightarrow 34b\_PI4P}$	0.929698
$\gamma_{\rightarrow 3}$	10	$f_{35\rightarrow 3c\_PI5P}$	-0.00062	$f_{4\rightarrow 34b\_PI}$	-0.82386
$\gamma_{0\rightarrow 3b}$	8.80959e+14	$\gamma_{35\rightarrow 3d}$	3.06E+12	$\gamma_{34\rightarrow 4}$	5.04E+11
$f_{0\rightarrow 3b\_PI}$	0.1761429	$f_{35\rightarrow 3d\_PI35P2}$	0.999934	$f_{34\rightarrow 4\_PI34P2}$	0.99989
$f_{0\rightarrow 3b\_PI4P}$	-0.07030248	$\gamma_{35\rightarrow 3e}$	5.14E+12	$f_{34\rightarrow 4\_PI345P3}$	-0.04443
$\gamma_{0\rightarrow 3c}$	5.45988E+14	$f_{35\rightarrow 3e\_PI35P2}$	0.999689	$\gamma_{45\rightarrow 0}$	1.14E+12
$f_{0\rightarrow 3c\_PI}$	0.1138439	$f_{35\rightarrow 3e\_PI45P2}$	-0.06212	$f_{45\rightarrow 0\_PI3P}$	0.999562
$\gamma_{3\rightarrow 0b}$	4.55762E+13	$f_{35\rightarrow 3e\_PI345P3}$	-0.00236	$f_{45\rightarrow 0\_PI4P}$	-0.04385
$f_{3\rightarrow 0a\_PI3P}$	0.9995615	$\gamma_{4\rightarrow 45}$	8.49E+15	$f_{45\rightarrow 0\_PI5P}$	-0.00044
$f_{3\rightarrow 0a\_PI4P}$	-0.04385422	$f_{4\rightarrow 45\_PI4P}$	0.045962	$f_{45\rightarrow 0\_PI35P2}$	-0.00022
$f_{3\rightarrow 0a\_PI5P}$	-0.00043854	$f_{4\rightarrow 45\_PA}$	0.2	$f_{45\rightarrow 0\_PI45P2\_PI4P}$	-0.04385
$f_{3\rightarrow 0a\_PI3SP2}$	-0.00021927	$f_{4\rightarrow 45\_PI45P2}$	-0.05	$f_{45\rightarrow 0\_PI45P2\_PI5P}$	-0.23834
$f_{3\rightarrow 0a\_PI45P2\_PI4P}$	-0.04385422	$\gamma_{45\rightarrow 4a}$	4.56E+13	$f_{45\rightarrow 0\_PI345P3}$	-0.00167
$f_{3\rightarrow 0a\_PI45P2\_PI5P}$	-0.2383381	$f_{45\rightarrow 4a\_PI3P}$	-0.00044	$f_{45\rightarrow 0\_PI45P2\_PI}$	-0.01096
$f_{3\rightarrow 0a\_PI345P3}$	-0.00166827	$f_{45\rightarrow 4a\_PI4P}$	-0.04385	$\gamma_{PI3KIc\rightarrow PI3KIa}$	3.35E-06
$f_{3\rightarrow 0a\_PI45P2\_PI}$	-0.01096355	$f_{45\rightarrow 4a\_PI5P}$	-0.00044	$f_{PI3KIc\rightarrow PI3KIa\_pi\_3KI\_c}$	1
$\gamma_{3\rightarrow 0c}$	5.09681E+12	$f_{45\rightarrow 4a\_PI3SP2}$	-0.00022	$f_{PI3KIc\rightarrow PI3KIa\_PI345P3}$	0.7
$f_{3\rightarrow 0c\_PI3P}$	0.9993781	$f_{45\rightarrow 4a\_PI45P2\_PI4P}$	0.956146	$\gamma_{PI3KIa\rightarrow PI3KIc}$	0.000622

$f_{3\rightarrow 0c\_PI4P}$	-0.06218905
$f_{3\rightarrow 0c\_PI5P}$	-0.00062189
$f_{3\rightarrow 0c\_PI35P2}$	-0.00031095
$\gamma_{3\rightarrow 0d}$	3.05908E+12
$f_{3\rightarrow 0d\_PI3P}$	0.9993364
$f_{3\rightarrow 0d\_PI35P2}$	-0.00033179
$\gamma_{3\rightarrow 0e}$	3.06733E+12
$f_{3\rightarrow 0e\_PI3P}$	0.9993362
$\gamma_{0\rightarrow 4}$	5.10064E+14
$f_{0\rightarrow 4\_PI}$	0.2864618
$\gamma_{4\rightarrow 0a}$	4.55762E+13
$f_{4\rightarrow 0a\_PI3P}$	-0.00043854
$f_{4\rightarrow 0a\_PI4P}$	0.9561458
$f_{4\rightarrow 0a\_PI5P}$	-0.00043854
$f_{4\rightarrow 0a\_PI35P2}$	-0.00021927
$f_{4\rightarrow 0a\_PI45P2\_PI4P}$	-0.04385422
$f_{4\rightarrow 0a\_PI45P2\_PI5P}$	-0.2383381
$f_{4\rightarrow 0a\_PI345P3}$	-0.00166827
$f_{4\rightarrow 0a\_PI45P2\_PI}$	-0.01096355
$\gamma_{4\rightarrow 0c}$	5.09681E+12
$f_{4\rightarrow 0c\_PI4P}$	0.937811
$f_{4\rightarrow 0c\_PI3P}$	-0.00062189
$f_{4\rightarrow 0c\_PI5P}$	-0.00062189
$f_{4\rightarrow 0c\_PI35P2}$	-0.00031095
$\gamma_{0\rightarrow 5}$	4.70283E+11
$f_{0\rightarrow 5\_PI}$	0.5465332
$f_{0\rightarrow 5\_PI3P}$	-0.00037789
$\gamma_{5\rightarrow 0a}$	4.55762E+13
$f_{5\rightarrow 0a\_PI3P}$	-0.00043854
$f_{45\rightarrow 4a\_PI45P2\_PI5P}$	-0.23834
$f_{45\rightarrow 4a\_PI345P3}$	-0.00167
$f_{45\rightarrow 4a\_PI45P2\_PI}$	-0.01096
$\gamma_{45\rightarrow 4c}$	5.13E+12
$f_{45\rightarrow 4c\_PI45P2}$	0.937861
$f_{45\rightarrow 4c\_PI345P3}$	-0.00236
$\gamma_{45\rightarrow 4d}$	5.14E+12
$f_{45\rightarrow 4d\_PI45P2}$	0.937881
$f_{45\rightarrow 4d\_PI35P2}$	-0.00031
$f_{45\rightarrow 4d\_PI345P3}$	-0.00236
$\gamma_{5\rightarrow 45}$	2.95E+13
$f_{5\rightarrow 45\_PI5P}$	0.87844
$\gamma_{45\rightarrow 5a}$	3.24E+12
$f_{45\rightarrow 5a\_PI3P}$	-0.00044
$f_{45\rightarrow 5a\_PI4P}$	-0.04385
$f_{45\rightarrow 5a\_PI5P}$	-0.00044
$f_{45\rightarrow 5a\_PI35P2}$	-0.00022
$f_{45\rightarrow 5a\_PI45P2\_PI4P}$	-0.04385
$f_{45\rightarrow 5a\_PI45P2\_PI5P}$	0.761662
$f_{45\rightarrow 5a\_PI345P3}$	-0.00167
$f_{45\rightarrow 5a\_PI45P2\_PI}$	-0.01096
$\gamma_{45\rightarrow 5c}$	4.13E+12
$f_{45\rightarrow 5c\_PI45P2}$	0.648722
$\gamma_{45\rightarrow 345}$	1.89E+14
$f_{45\rightarrow 345\_PI45P2}$	0.306333
$\gamma_{345\rightarrow 45}$	2.9E+15
$f_{345\rightarrow 45\_PI345P3}$	0.955575
$f_{345\rightarrow 45\_PI34P2}$	-0.00011
$\gamma_{35\rightarrow 5}$	6.06E+14
$f_{35\rightarrow 5\_PI35P2}$	0.999668
$f_{PI3KIa\rightarrow PI3KIc\_pi\_3KI\_a}$	1
$\gamma_{PTENc\rightarrow PTENa}$	1.25E-07
$f_{PTENc\rightarrow PTENa\_PTEN\_c}$	1
$f_{PTENc\rightarrow PTENa\_PI45P2}$	1
$\gamma_{PTENa\rightarrow PTENc}$	0.003
$f_{PTENa\rightarrow PTENc\_PTEN\_a}$	1
$f_{PTENa\rightarrow PTENc\_PI345P3}$	1
$\gamma_{45\rightarrow DAG}$	1.88E+19
$f_{45\rightarrow DAG\_PI45P2}$	0.977042
$f_{45\rightarrow DAG\_PI4P}$	-0.0126
$f_{45\rightarrow DAG\_PS}$	-0.96424
$\gamma_{PA\rightarrow DAG}$	5.54E+11
$f_{PA\rightarrow DAG\_PA}$	0.96528
$\gamma_{DAG\rightarrow PA}$	1.65E+13
$f_{DAG\rightarrow PA\_DAG}$	0.947551
$\gamma_{\rightarrow DAG}$	0.00001
$\gamma_{DAG\rightarrow}$	0.1
$f_{DAG\rightarrow\_DAG}$	1
$\gamma_{\rightarrow PA}$	4
$\gamma_{PA\rightarrow}$	0.1
$f_{PA\rightarrow\_PA}$	1
$\gamma_{PC\rightarrow PA}$	14.35507
$f_{PC\rightarrow PA\_PI45P2}$	0.3
$\gamma_{IP3\rightarrow}$	2
$f_{IP3\rightarrow\_IP3}$	1
$\gamma_{4\rightarrow DAG}$	2.55E+18
$f_{4\rightarrow DAG\_PI4P}$	0.987396
$f_{4\rightarrow DAG\_PI45P2}$	-0.02296
$f_{4\rightarrow DAG\_PS}$	-0.96424

Table 4.3. Observed experimental phenomena used to calibrate the model and model performance for each phenomenon.

	Phenomenon	Model
1	In the apical part of the cell membrane, inhibiting PLC should cause an increase of 50 % in $PI(4,5)P_2$ in the first 15 min. [42]	Figure 4.3 a, blue line and points.
2	In the apical part of the cell membrane, PLC activation will decrease $PI(4,5)P_2$ by 50% in the first 15 min. [42]	Figure 4.3 a, red line and points.
3	Intense activation of PLC can lead to 75% [21] or 90% [43] of $PI(4,5)P_2$ depletion.	Increasing 7 times the basal activity of PLC will deplete $PI(4,5)P_2$ by 73%, but PLC must be increased 20 times to deplete $PI(4,5)P_2$ by 90%.
4	Inhibition of class I DGK in BSC-1 cells results in a 50% reduction in total PA levels, indicating the majority of cellular PA is synthesized by type I DGKs. [44]	Inhibiting DGK by 75% will reduce PA in 52%. Knockout of DGK will reduce PA by 75%.
5	Time series data for activation and inhibition of PI3KI and PI(3,4,5)P3 dynamics. [45]	Figure 4.4 a, b.
6	Time series data on PI3KI inhibition with LY294002 and readings of PI(3,4,5)P3 levels in a cell-attached patch made on a principal cell from a collecting duct freshly isolated from a salt restricted rat. [46]	Figure 4.4 c.

4.4.1. $PI(4,5)P_2$ behavior in PLC perturbations

Xu *et al.* [20], Gericke *et al.* [21] and Purvis *et al.* [22] state that $PI(4,5)P_2$ recovers rapidly form an initially steep decrease in response to activation of PLC. For this

recovery, the activation of PIP5KI by PA is essential [17]–[19]. These reports do not quantify the magnitude of the recovery or the magnitude of PLC activation that allows a recovery, but it is known that a strong activation of PLC causes $PI(4,5)P_2$ depletion [40].

The model confirms $PI(4,5)P_2$ recovery for a range of levels of PLC activation, which is presented in Supplement Figure 4.11. The original parameter set allows only a modest recovery, but a combination of stronger PA / PIP5KI activation and an adequate activation of PLC produces very clear $PI(4,5)P_2$ recovery.

If the activation of PIP5KI by PA is sufficiently strong, the model system becomes bistable, and the levels of the dependent variables do not return to the initial steady state, even if PLC activation is returned to its initial level. Instead, the system becomes locked into a state of high PA levels that increase $PI(4,5)P_2$ production so much that the basal activity of PLC produces enough PA to keep the high PA levels and maintain the new steady state. This model result could be an artifact because PLC saturation would prevent high DAG and PA production only as a consequence of a great increase in $PI(4,5)P_2$. However, if this bistability were real, it would be an effective way to maintain the signal after the initial stimulus has ceased. Interestingly, Purvis *et al.* [22] encountered the same phenomenon with their model.

Pochynyuk *et al.* [42] measured the levels of $PI(4,5)P_2$ for the first 15 minutes after altering PLC activity. The data and model results can be seen in Figure 4.3a. The model presents a good fit to these data. Furthermore, although no data exist for later time points, the simulation can be extended and shows that, after about 500 minutes, $PI(4,5)P_2$ reaches a steady state that is increased to 1.6-fold for PLC inhibition and decreased to 0.4-fold for a 4-fold activation of PLC activity in comparison to the basal level.

4.4.2. Degradation of PI(4)P and $PI(4,5)P_2$

Várnai *et al.* [47] presented data using reporters for PI(4)P and $PI(4,5)P_2$ that derived from two experiments: one where SAC1 4-phosphatase was used to degrade PI(4)P and another where the INPP5E 5-phosphatase was used to degrade $PI(4,5)P_2$. For the SAC1 experiment, our model produced a good fit (Figure 4.3b) with an initial 8-fold increase

in the model's SAC1 activity followed by an attenuation to a 2-fold activation after 4 minutes.

Our model was initially unable to reproduce the INPP5E results when we used perturbations of a reasonable magnitude. This failure was probably due to the fact that we had underestimated the amount of enzyme in the cell membrane or the enzyme activity. Raising the activity of the enzyme 30-fold, we obtain noticeable alterations to the PI(4)P and PI(4,5)P2 levels. Furthermore, the shape of the data seems to suggest that the chimera INPP5E used by Várnai *et al.* was, in addition to its 5-phosphatase ability, able to hydrolyze the 4-phosphate of $PI(4,5)P_2$. To test this speculation, we increased the activity of the SYNJ phosphatase, which is able to hydrolyze the 4^{th} and 5^{th} position of the inositol ring in $PI(4,5)P_2$. With this activation, the model presented a reasonable fit to the time course (Figure 4.3c).

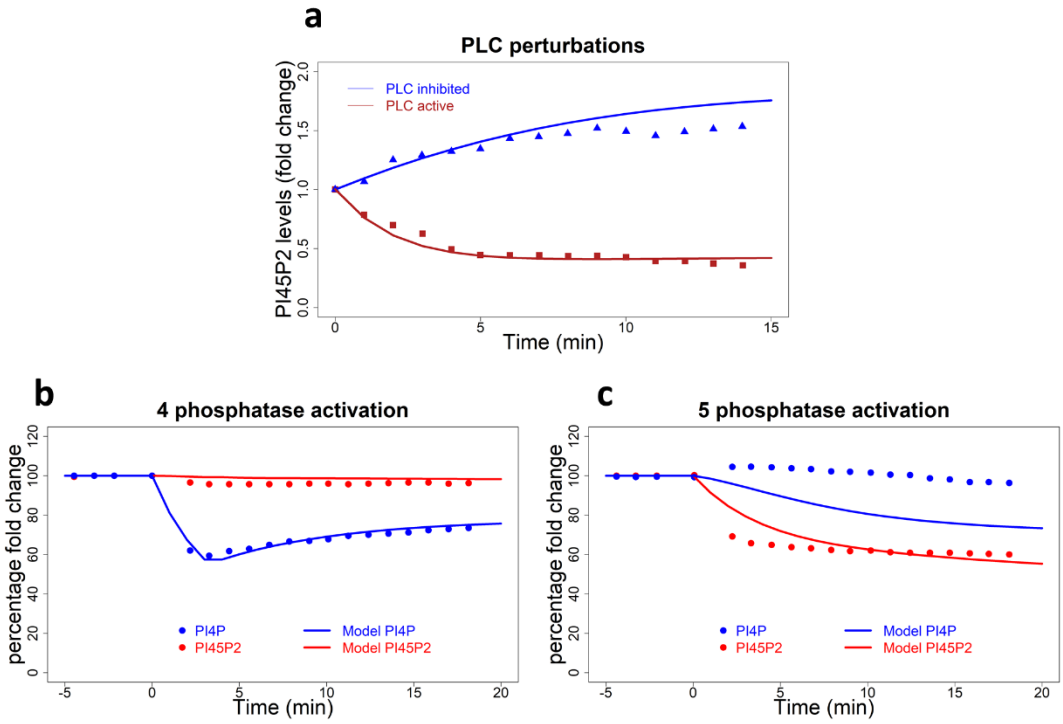

Figure 4.3. Perturbation that affect PI(4)P and PI(4,5)P2.

a) PLC was inhibited (blue) or activated (red) and levels of $PI(4,5)P_2$ were measured. Triangles and squares represent data points [42] and lines the model time courses where PLC was inhibited to 1% or activated to 4-fold of the enzyme's basal activity. **b)** PI(4)P and $PI(4,5)P_2$ time course in a 4-phosphatase activation. Points represent data [47] and lines show model results. **c)** PI(4)P and $PI(4,5)P_2$ time courses following 5-phosphatase activation. Points represent data [47] and lines show model results.

4.4.3. Perturbations in PTEN, PI3KI, $PI(4,5)P_2$ and $PI(3,4,5)P_3$

Fitting the earlier phosphoinositide model to data reported by Feng *et al.* [45] and Pochynyuk *et al.* [8] indicates that the specific activity of PTEN must be greater than the value retrieved from the enzyme database BRENDA [48]. This discrepancy is in line not only with Feng's conclusions, but also with reports by McConnachie *et al.* [49] and Johnston and Raines [50]. We proceed by using the values presented by Johnston and Raines [50]. We also adjust the amounts of total and active PI3KI to obtain an adequate quantity of $PI(3,4,5)P_3$.

Feng *et al.* [45] presented two time courses that resulted from first activating PI3KI with rCD1 at time point t=5 min and then inhibiting the enzyme with FK506 at time point t=40 min. We simulate these perturbations with a 28-fold increase in the activation flux of PI3KI at t=5 min and a return of PI3KI to its steady state values at t=40 min (Figure 4.4a). Figure 4.4b shows results of blocking PTEN activity with H_2O_2 at t=2 min and inhibiting PI3KI with FK506 at t=8 min. We simulate these perturbations with a decrease of 50% in PTEN at t=2 min and a decrease of PI3KI of 30% values at t=8 min. The simulation results reflect the observations quite well.

Pochynyuk *et al.* [46] present a $PI(3,4,5)P_3$ time course where PI3KI is inhibited with LY294002. We simulate this perturbation with a 90% decrease in PI3KI (Figure 4.4c). Again, our model was able to reproduce this experimental observation.

4.4.4. Connection of two sub-modules through $PI(4,5)P_2$

We previously created a model of ENaC and ASL regulation by SPLUNC1 and $PI(4,5)P_2$ that was elsewhere described in detail [16]. In fact, we tested two versions of this ENaC model, with similar results. Here, we opt for the simpler version, which is briefly summarized below. The model simulates the numbers of ENaCs, which are regulated by SPLUNC1 and ASL thickness. ASL thickness, in turn, is regulated by CFTR influx, ENaC numbers and ENaC's open probability (P_o), which is determined by $PI(4,5)P_2$ levels. The ENaC and ASL model can be set to simulate healthy and CF lungs. Specifically, CF is simulated by setting to zero the SPLUNC1 parameter and the influx of material to the ASL, V_5, which is dependent of CFTR.

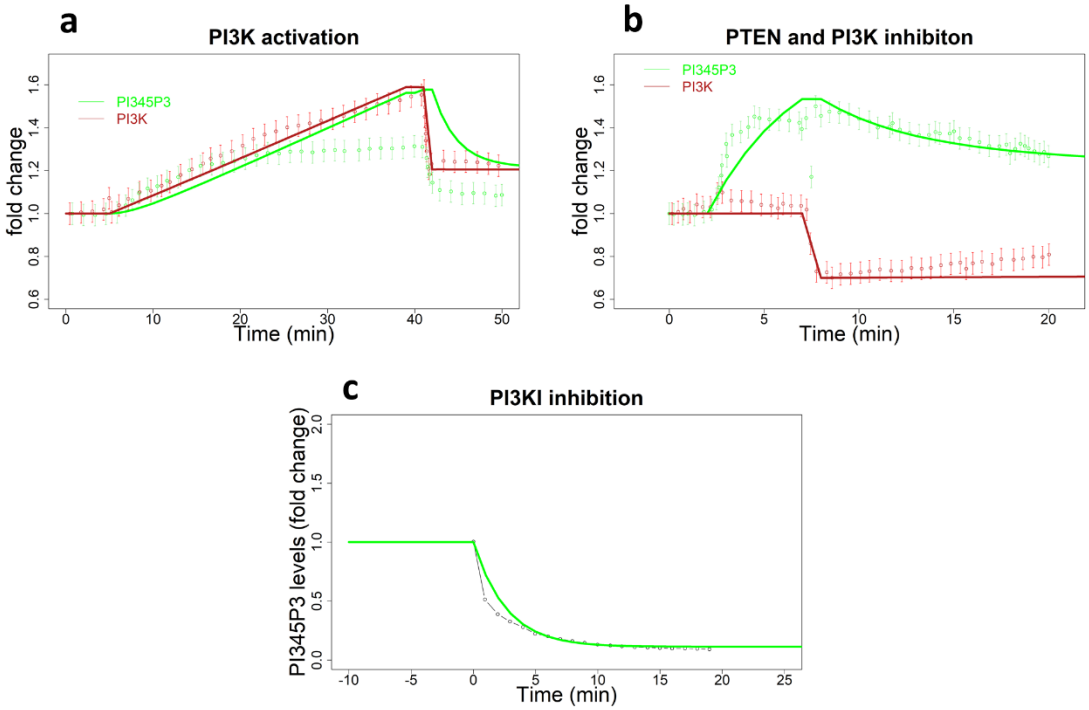

Figure 4.4. Perturbations that affect PI(3,4,5)P3.

a) PI3KI and PI(3,4,5)P_3 time courses in response to enzyme activation at t = 5 and inhibition at t = 40. Circles and intervals represent data [45], lines are model results. **b)** PI3KI and PI(3,4,5)P_3 time courses in response to PTEN inhibition at t = 3 and PI3KI inhibition at t = 8. Circles and intervals represent data [45], lines are model results. **c)** PI(3,4,5)P_3 time courses in a PI3KI inhibition. Black circles represent data [46] and green line shows model results.

The combined model proposed here accepts information regarding the PI(4,5)P_2 level from the phosphoinositide model and translates it into P_o. P_o contributes to the determination of the ENaC activity level that regulates ASL thickness and, through SPLUNC1 dilution, the number of ENaC channels.

4.4.5. ENaC control by DGK

Our hypothesis for the combined model is that ENaC is regulated by PI(4,5)P_2 though PA control of PIP5KI. To test this hypothesis, we performed a series of simulations with the combined model where we perturbed the phosphoinositide pathway and evaluated the consequences for ENaC. The extended phosphoinositide sub-model was used to supply the appropriate level of PI(4,5)P_2. With this input, the model for the

dynamics of ENaC generates the number of active ENaC channels in the plasma membrane (N), while results on $PI(4,5)P_2$ and the effect on ENaC reveal ENaC's open probability (P_o). Multiplying N and P_o results in the activity of ENaC.

The work of Antonescu *et al.* [44] demonstrated that the inhibition of DGK causes a decrease of about 50% in the level of PA. If our hypothesis regarding the role of DGK is valid, the reduction in PA should decrease $PI(4,5)P_2$ production by PIP5KI. Indeed, the model exhibits a decrease of 52% in PA when DGK is inhibited 75%. The same perturbation reduces $PI(4,5)P_2$ by 28%.

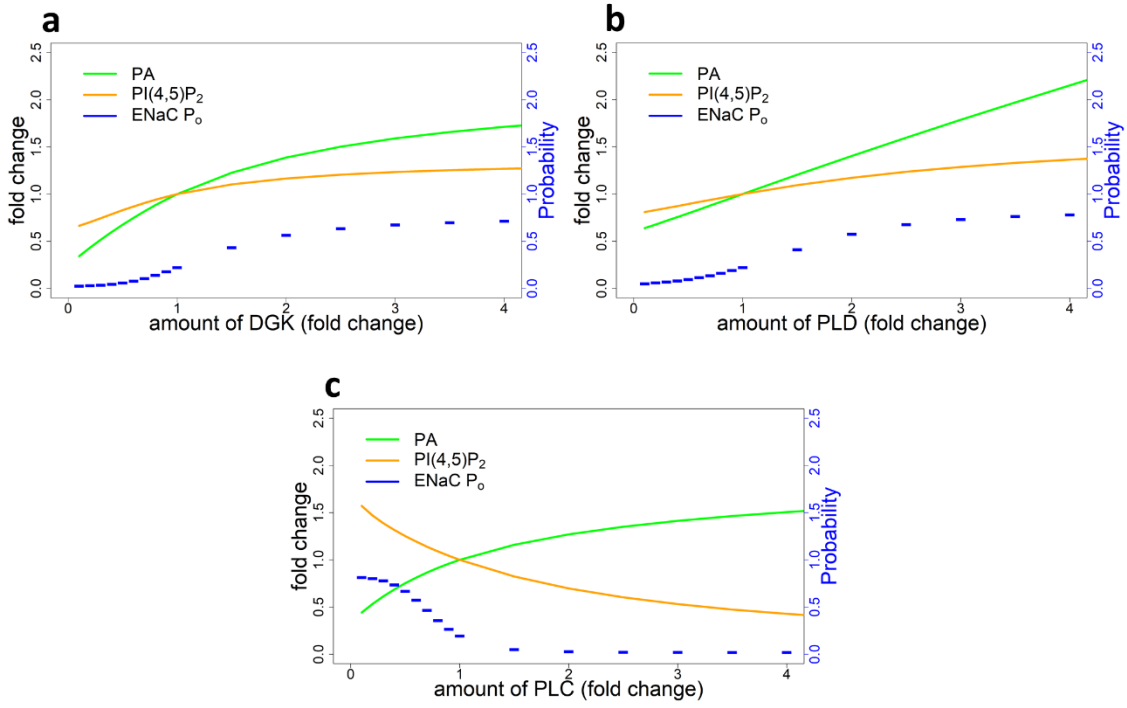

Figure 4.5. PA, PI(4,5)P2 and ENaC open probability.

PA has two sources in the model. One is through PLC that produces DAG, which is transformed by DGK into PA. The other is through PLD that produces PA from PC. **a)** DGK, **b)** PLD and **c)** PLC levels where varied from 0.1 to 10-fold and the levels of PA, $PI(4,5)P_2$ and the open probability (P_o) of ENaC here recorded.

The PA pool is fed by two sources: $PI(4,5)P_2$/PLC/DAG and PLD/PC (recall Figure 4.2). According to our hypothesis, alterations in these elements of the system should yield changes in PA, $PI(4,5)P_2$ and ENaC. We tested different values for PLC, PLD and

DGK to characterize the dynamic effects of these perturbations on PA, $PI(4,5)P_2$ levels and P_o. The results are shown in Figure 4.5. For the basal levels of the involved compounds, the model predicts $P_o = 0.22$, which is similar to the value presented in Pochynyuk *et al.* [42].

Almaça *et al.* [13] preformed siRNA screens to find modulators of ENaC activity and noticed the following phenomena: DGK inhibition reduces ENaC activity to WT basal levels in CF F508del cells, but does not have a significant effect in WT cells. Also, DGK has no effect on ENaC when PLC is activated or inhibited. This information is summarized in Figure 4F of their paper.

To explore these findings with our model, we start by studying the effects of SPLUNC1 and DGK perturbations. In WT, inhibition of DGK decreases the activity of ENaC roughly in 40%. This effect is caused by a decrease in P_o and a slightly increase in N; the estimated drop in ENaC's activity is mainly due to the reduction in P_o (Figure 4.6a). Almaça *et al.* report a non-significant change in ENaC activity, and it appears that the remaining ENaC activity could be similar to basal conditions. The reason is that this reduction is similar to what should be expected in an individual with just one functional copy of scnn1, which codes for ENaC proteins, and there are no reports of problems in heterozygotes, only in homozygotes [1].

When we simulate CF conditions, by setting SPLUNC1 and the $V_{\square}$ flux equal to zero (CF), N increases to 2.26 times the number of channels in WT, which is close to the value reported by Tarran's group [34]. Concerning ENaC activity, ENaC is projected to be 2.26 more active in CF than in WT (Figure 4.6a). It should be noted that, in the model, the increase of ENaC activity is due to an increase in the number of channels. In CF, N is affected by DGK inhibition but, due to the drop in P_o, the activity of ENaC decreases to about half. Almaça *et al.* report a reduction of ENaC in this condition, and the model predictions agree, yielding a difference of ENaC activity between WT / DGK+ and CF / DGK- of only 1.91, which corresponds to only 25% of the basal activity of ENaC in WT. This result is significant if one takes into account that ENaC activity in CF is increased to 126% of the basal activity of ENaC in WT. Overall, the model predicts a DGK induced reduction of ENaC activity under CF conditions similar to the basal activity of ENaC in WT, which can be classified, with a high degree of certainty, as a considerable decrease.

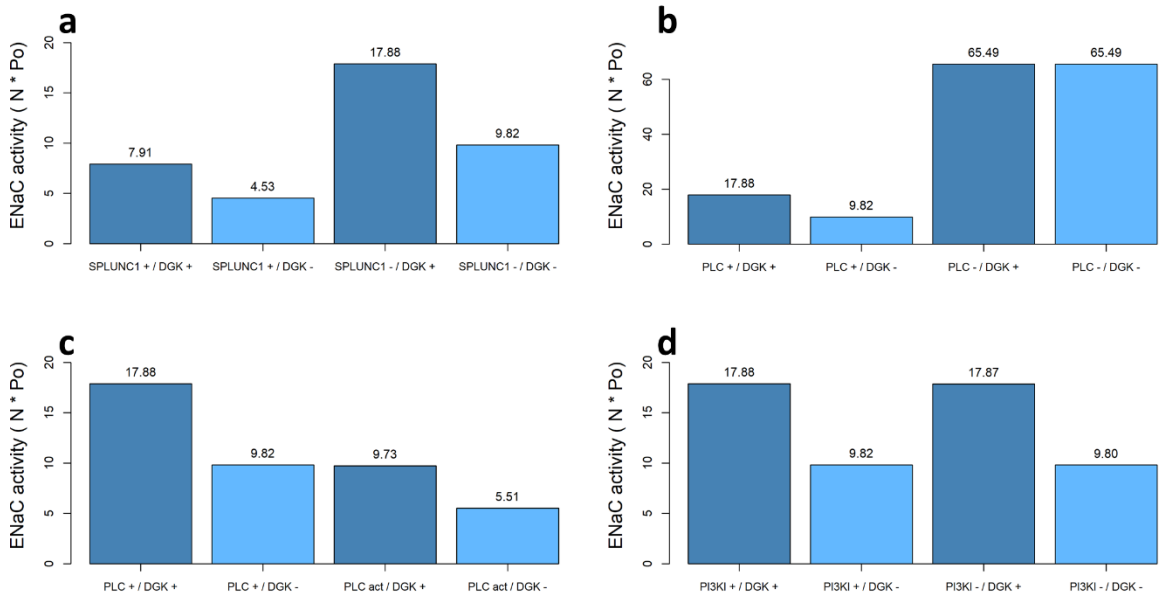

Figure 4.6. Consequences of DGK inhibition on ENaC activity in a) WT and CF, b) CF with PLC inhibition, c) CF with PLC activation and d) CF with PI3KI inhibition.

In all four plots, the first and third bar in dark blue correspond to basal levels of DGK activity level (DGK +), the second and forth bar in light blue to DGK 25% inhibition (DGK -). **a)** DGK inhibition in CF (CF / DGK -) induces ENAC's activity to a similar level as the channel activity in WT (WT / DGK +), as reported by Almaça *et al.* [13]. **b)** With PLC inhibition, a decrease in $PI(4,5)P_2$ caused by DGK inhibition does not affect ENaC's action. **c)** When PLC is activated, DGK inhibition still reduces ENaC activity. d) The model suggests that PI3KI inhibition in the apical part of the plasma membrane has no effect on ENaC activity, which is expected.

Next, we study PLC inhibition and DGK perturbations in CF (Figure 4.6b). With basal activity levels of PLC (PLC +), inhibition of DGK produces the same result as in Figure 4.6a under CF conditions, as expected. By contrast, if PLC is inhibited by 99%, the effect of DGK vanishes. The estimated levels of $PI(4,5)P_2$ are around 16,000 molecules/μm^2 when PLC is inhibited, which corresponds to an increase of approximately 50% over the basal level. The levels of PA, and even more so DAG, are greatly reduced to 2600 and 42 molecules/μm^2, which corresponds to 33% and 1% of their basal levels, respectively. The severe reduction of DAG explains the lack of DGK's influence over PA and $PI(4,5)P_2$ production, as well as the activity of ENaC.

We can also explore PLC activation and DGK perturbations in CF (Figure 4.6c). Again, if the activity of PLC is normal (PLC +), inhibition of DGK will reduce ENaC activity to levels similar to WT. By contrast, if PLC is activated to 20% over its basal activity, ENaC activity is reduced to levels similar to those in WT, which is due to the decrease in $PI(4,5)P_2$ consumed by PLC. With DGK inhibition, the levels of ENaC activity drop further, but not much.

Finally, inhibition of PI3KI, even by 99%, has no effect on ENaC activity (Figure 4.6d). This result is actually to be expected because the extended phosphoinositide model used here was calibrated to simulate the apical part of the plasma membrane, which is characterized, among other features, by the lack of PI3KI and its product $PI(3,4,5)P_3$ within this region.

Given the good agreement between all available data and the results from our model analyses, we can cautiously conclude that our hypothesis regarding the mechanisms of ENaC regulation, combined with the models of ENaC regulation by DGK and SPLUNC1, provides a good explanation for the activity of ENaC in WT and CF.

4.4.6. Almaça's *et al.* hypothesis tested with our phosphoinositide model

The model allows us to test the hypothesis of Almaça and colleagues that the damping of ENaC activity by DGK is caused by a general decrease in phosphoinositides due to their reduced recycling. To assess this hypothesis, we alter the extended phosphoinositide model in two ways. First, we allow the efflux from the PA pool, $V_{PA\rightarrow}$, to supply the PI pool with material, which simulates the transformation of PA into PI in the ER. This additional, simplified step in a crude way closes the circle of phosphoinositide recycling. Because the efflux of PA is only 5% of the influx of PI, we maintain the already present influx into the PI pool, which is now reduced by an amount equal to the PA efflux. The new flux $V_{\rightarrow 0}$ in this model extension can be interpreted biologically as the amount of PI produced in the ER from PA that did not originate in the plasma membrane; expressed differently, it represents PA created *de novo*. Second, we remove the regulation of PIP5KI by PA.

With these presumably reasonable settings, the model does not replicate the observation by Almaça and colleagues that, if DGK is inhibited, it no longer affects ENaC activity, whether in WT or CF (Figure 4.7a). To remedy the situation, it would be necessary to

balance the input into PI and the efflux out of PA. Specifically, the input into PI would have to be an exact multiple of the efflux $V_{PA\rightarrow}$ out of PA such that this multiple would be equal to the original PI influx. Such a coupling would make the PI pool dependent on the PA efflux. In a simulation with these settings, the ENaC activity is more sensitive to DGK inhibition, but the decrease in cation channel activity is very small (Figure 4.7b). If the inhibition of DGK in the model is made stronger, this configuration of the model can actually replicate the data reported by Almaça and colleagues (Figure 4.7c). However, to achieve this configuration, PI would have to be hypersensitive to the PA efflux, or the levels of PA and PI in the plasma membrane would somehow have to be closely coordinated. There is no evidence of PI hypersensitivity to PA efflux, and while there are no exact measurements for these lipids in the plasma membrane, all existing cell measurements suggest that PI is 10 times more abundant than PA [25], [51]. Moreover, it is known that PA is produced *de novo* in the ER, and this production affects the sensitivity of PI to plasma membrane PA. Thus, the model does not support the hypothesis of Almaça *et al.* [13] that inhibiting DGK brings the recycling of the phosphoinositides to a halt, which in turn decreases $PI(4,5)P_2$ and $PI(3,4,5)P_3$ and causes reduced ENaC activity.

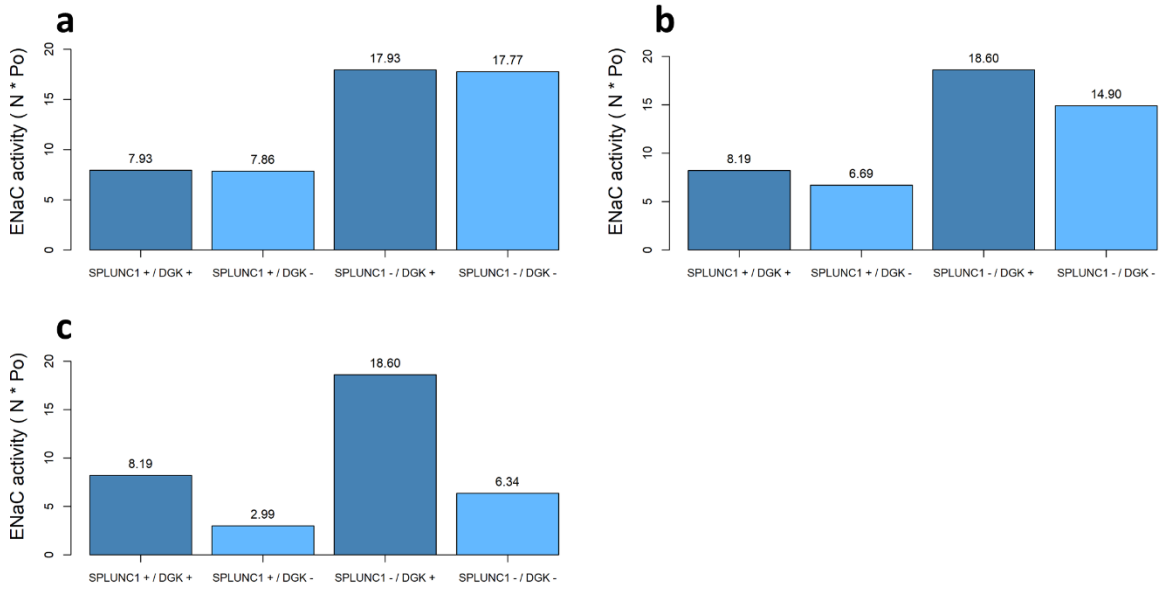

Figure 4.7. Extended phosphoinositide model, altered to simulate PI recycling without PIP5KI regulation by PA.

To test Almaça's hypothesis, we altered the extended phosphoinositide model to simulate phosphoinositide recycling and removed the regulation of PIP5KI by PA. **a)** Under these conditions the model does not replicate the observation of ENaC moderation when DGK is inhibited, as reported by Almaça and colleagues. **b)** Making the influx of PI a multiple of the PA efflux, the model does not replicate the observation from Almaça and colleagues either. **c)** With the same conditions as in b), we furthermore inhibited DGK by 75% instead of the usual 25%. With these alterations, the model does replicate the observation of Almaça and colleagues. However, this degree of sensitivity of PI to plasma membrane PA efflux is not an accurate representation of reality.

4.4.7. A puzzling result regarding P_o

ENaC is usually composed of three subunits: α, β and γ [52]. Channels with alternate stoichiometries have been reported to have very low activity [53], so that it is imaginable that some ENaC channels could be constitutively closed. Also, not all ENaC channels are necessarily equal, due to variability introduced by alternative splicing, alternative folding, glycosylation and ubiquitination. Thus, one might expect a range of ENaCs where, at one end, some channels are open even if ENaC controllers are signaling a closed configuration, and where the opposite is true at the other end. If there are indeed constitutively open and closed ENaC channels, the open probability function would have a much higher minimum than the reported value, which is about 0.02 [54]. By the same token, as a result of constitutively closed channels, the maximum should be lower than reported. To explore this situation, we tested an alternative ENaC P_o function with a minimum of 0.12, a basal ENaC P_o of 0.22, and maximum of 0.72. With this P_o function, the model exhibit results that are similarly good as previous result but yields much improved results with respect to perturbations in PLC activation. This alteration would likely make the activity of ENaC less sensitive to DGK inhibition and yield model results that are more similar to observations by Almaça and colleagues. Unfortunately, there are no data supporting this strategy.

4.4.8. Suratekar's phosphoinositide cycle model

Phosphoinositides are created from PA in the ER and transported to the plasma membrane where they are phosphorylated, cleaved by PLC into IP_3 and DAG and transformed back to PA, which is transported back to the ER, thereby closing the cycle. Almaça *et al.* [13] hypothesized that inhibiting DGK would bring the recycling of

phosphoinositides to a halt, which in turn would decrease $PI(4,5)P_2$, and consequently reduce ENaC action.

Suratekar and colleagues [23] recently simulated the phosphoinositide cycle in the PM and in the ER. Using their information on $PI(4,5)P_2$ levels and coupling Suratekar's model with our ENaC and ASL model allowed us to test Almaça's hypothesis in a different, almost independent manner. Suratekar and colleagues [23] tested many versions of the model, including open and closed cycles and even a model where they considered PA as a regulator of PIP5KI. We used this model, implemented with Michaelis–Menten kinetics, which was shown to be consistent with all data available to the authors, an open cycle with influx of PA into the ER and efflux out of DAG in the plasma membrane, and without PA regulation of PIP5KI. Alas, this representation of the phosphoinositide pathway turned out to be unable to replicate Almaça's observations of ENaC moderation under DGK inhibition (Figure 4.8a). The reason seems to be the following: Suratekar's model contains an influx of PA into the ER that is independent of plasma membrane PA. This influx suffices to maintain phosphoinositide levels, when we inhibit DGK, and severely reduces PA in the plasma membrane.

It is interesting to note that PA in the plasma membrane decreases by 90% when DGK is inhibited. This strong effect raises the question if including regulation of PIP5KI by PA in the plasma membrane would enable Suratekar's model to replicate Almaça's observations. We implemented this regulation of PIP5KI in two ways: first, by making the V_{max} of PIP5KI dependent of PA in the plasma membrane according to a Hill function and, second, by making the K_M of PIP5KI inversely proportional to plasma membrane PA. In both cases, the inhibition of DGK decreases PA in the membrane, and this information is passed on to PIP5KI, resulting in a decreased rate of $PI(4,5)P_2$ production. But as PIP5KI loses efficiency, PI(4)P accumulates rapidly because there is no other exit from the pool. This chain of events continues until the amount of PI(4)P compensates the reduced efficiency of PIP5KI, thereby establishing a new, very elevated steady state of PI(4)P and restoring the levels of $PI(4,5)P_2$.

Assigning an efflux from the pool of PI(4)P with a small rate constant (0.08) creates an escape valve that prevents PI(4)P from unduly accumulating when DGK is inhibited. This setting alters the steady state, but only very slightly, and can be balanced by

increasing the endoplasmic reticulum PA source by 1.1%, which compensates for the new loss of material from the system. These settings lead to a model that is consistent with Suratekar's data and replicates Alamaça's observations (Figure 4.8b).

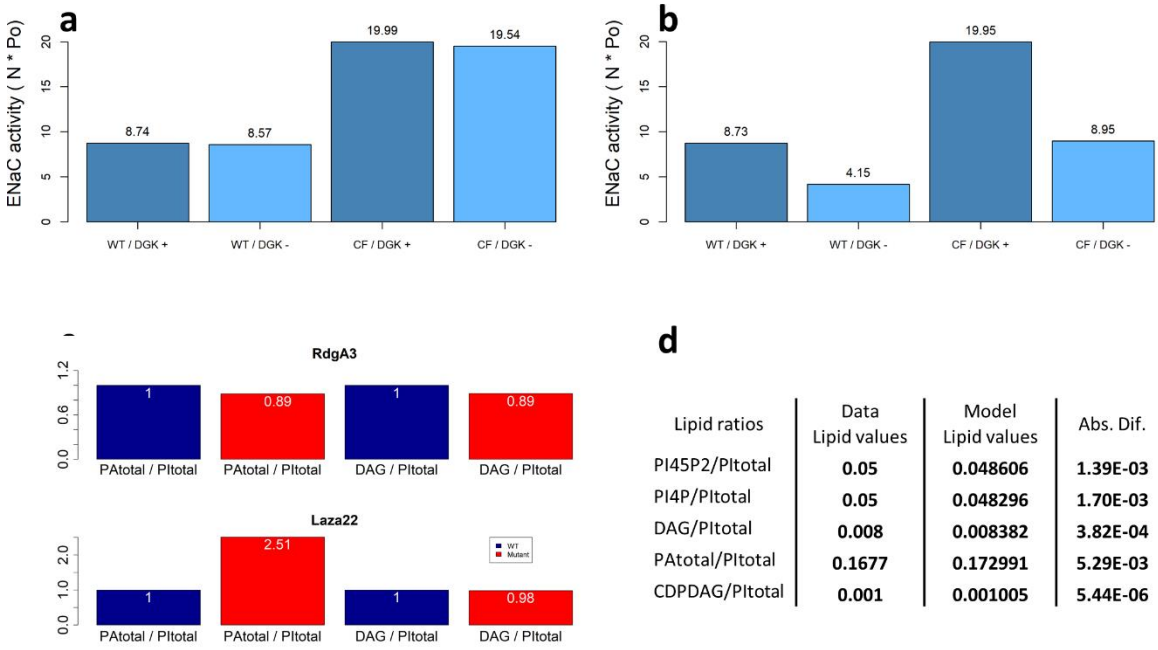

Lipid ratios	Data Lipid values	Model Lipid values	Abs. Dif.
PI45P2/PItotal	**0.05**	**0.048606**	**1.39E-03**
PI4P/PItotal	**0.05**	**0.048296**	**1.70E-03**
DAG/PItotal	**0.008**	**0.008382**	**3.82E-04**
PAtotal/PItotal	**0.1677**	**0.172991**	**5.29E-03**
CDPDAG/PItotal	**0.001**	**0.001005**	**5.44E-06**

Figure 4.8. Suratekar's model of phosphoinositide recycling does not replicate Almaça's observations of ENaC moderation when DGK is inhibited.

a) This discrepancy happens because the external influx of PA into the ER sustains the phosphoinositide recycling and consequently the $PI(4,5)P_2$ levels, when DGK is inhibited. **b)** Suratekar's model of phosphoinositide recycling is modified to include PA regulation of PIP5KI and an efflux out of the PI(4)P pool. This refined model does replicate Suratekar's data and Almaça's observations of DGK control of ENaC. DGK inhibition causes a moderation of ENaC action. In CF, this moderation brings the ENaC activity close to the WT ENaC activity. **c)** Modified Suratekar's model replicates data from mutants in *Drosophila melanogaster* photoreceptor cells. **d)** Lipid ratios from the literature, from the model simulation and absolute difference between the two.

Taking all results together gives us confidence that our hypothesis of DGK moderating ENaC through PA control of PIP5KI convincingly explains the available data.

4.5. Discussion and Conclusions

The objective of the work described here and previously was to shed light on the effect of phosphoinositides and the protein SPLUNC1 on the functionality of the ion channel

ENaC, which plays an important role in several diseases and, especially, in CF. We started by creating two models, one representing the phosphoinositide pathway and the second capturing the dynamics of the ENaC ion channel and its effects on ASL, which is dependent on the transport protein CFTR that is typically mutated in CF. After expanding the phosphoinositide model, by accounting for all elements necessary to our study, we merged the two models. The combined model allowed us to test our hypothesis, that moderation of ENaC, observed after DGK inhibition, is accomplished through a decrease in PA, which in turn ceases to activate the $PI(4,5)P_2$ producing enzyme, PIP5KI. We compared the model results from several pathway perturbations with observed data from reports by Almaça *et al.* of the same perturbations and obtained good agreement.

In a second step we modified the model of the phosphoinositide pathway to enable an assessment of opposing hypotheses suggested by Almaça and colleagues, namely, that moderation of ENaC in response to DGK inhibition is caused by stopping phosphoinositide recycling. We found that, for the model to replicate the data, one possibility is that plasma membrane and endoplasmic reticulum PA would have to have similar concentrations, which is contrary to the best data available on the subject [25], [51]. Another possibility could be that the production of PA in the endoplasmic reticulum and its transport to the plasma membrane would exhibit high sensitivity to $PI(4,5)P_2$ degradation by PLC, to plasma membrane PA levels, or to plasma membrane PA transport to the endoplasmic reticulum. There is no evidence in the literature supporting any of these possibilities.

Finally, we used a model of the phosphoinositide cycle created by Suratekar *et al.* [23] to test both hypotheses independently of our earlier conclusions. This model failed to replicate Almaça's data when activation of PIP5KI by plasma membrane PA was not taken into account, but succeeded when this regulation was included.

The past years have witnessed numerous new discoveries regarding lipid transfer proteins (LPTs) (*e.g.*, [55]). Thus, it is conceivable that a so-far unknown cellular mechanism could create the high sensitivity of PA production in the endoplasmic reticulum to the levels of PA in the plasma membrane, which would validate the hypothesis of Almaça *et al.* At the same time, extensive research over several decades has not identified such a mechanism. Thus, all things considered, it appears that our

hypothesis regarding ENaC regulation by DGK has a higher likelihood of being correct than the earlier hypothesis of Almaça and colleagues. According to this new hypothesis, which is supported by our computational analyses here, the regulation of ENaC is primarily exerted through the control of $PI(4,5)P_2$ production by type I phosphatidylinositol-4-phosphate 5-kinase (PIP5KI), which in turn is controlled by phosphatidic acid (PA), the product of the DGK reaction.

4.5.1. Future directions

Tarran and colleagues [15] proffer that SPLUNC1 causes channel disaggregation and internalization of ENaC α and γ subunits. If so, the β subunit persists in the plasma membrane with SPLUNC1 attached. SPLUNC1 is known to exert bacteriostatic and antibiofilm effects, bind to lipopolysaccharide, and act as a fluid-spreading surfactant [33]. In CF patients, with SPLUNC1 inactivated by the acidic ASL, these normal tasks cannot be accomplished. Thus, it will be interesting to study the importance of attaching an antimicrobial molecule to the pulmonary epithelial cell membrane in an attempt to control lung infections.

It would also be beneficial to study more deeply the positive feedback loop between $PI(4,5)P_2$, PLC, PA and PLD. Not only would it be interesting to see the regulatory capabilities of this functional arrangement, but there are intriguing observations like the one made by Antonescu *et al.* [44], where the knock-down of an PLD isoform led to increased PA levels. There are ten DGK isoforms [56], [57], thirteen PLC isoforms [58], two PLD isoforms [59] and nine PKC isoforms. In the present work, we did not account for these details but the diversity could be important for explaining some of the surprising observations in the field.

Our computational results point to the conclusion that DGK inhibition and the consequent decrease in $PI(4,5)P_2$ levels moderate ENaC gain of function in CF by compensating for SPLUNC1 inactivation, which is caused by an increase in acidity of the airway surface liquid. Also, there is strong indication that this regulatory mechanism is mediated through the regulation of PIP5KI by PA. While altering the levels of $PI(4,5)P_2$ could seem to be an interesting therapeutic target, caution is necessary as such alterations will probably have unpredictable and possibly undesirable consequences. A case in point is Balla's work [12], which shows that $PI(4,5)P_2$ not only influences ENaC but many other proteins in the cell. In addition, alterations in the levels of $PI(4,5)P_2$

obviously lead to changes in other phosphoinositide levels, such as $PI(3,4,5)P_3$, which can have further ramifications, such as alterations in the AKT signaling pathway, to name just one.

A promising aspect of this research is that there is evidence that phosphoinositides act locally [12], [60] and that this fact can possibly be exploited to create safe and effective therapies for CF and other diseases. However, before we pursue such avenues, we need to understand far better how these local activities interact and how they are controlled.

4.6. Materials and Methods

4.6.1 Available Datasets and their limitations

For the calibration of the model proposed here, we used numerous datasets and other types of information from the literature. As far as this information pertains to the original phosphoinositide pathway model, it was presented in Chapter 2 [7]. It mainly consists of concentrations of phosphoinositides and changes in their amounts in response to numerous perturbations of the pathway. These perturbations usually affected enzymes and their activators and inhibitors or consisted of alterations to influxes or effluxes of the system. The results of these experiments are summarized in the supplementary information of Chapter 2 [7].

The new additions to the model resulted in data fits of a similar quality as for the simpler version of the model, but allowed us to assess a host of new features. In particular, they permitted assessments of the effects of alterations in phosphoinositides on the dynamics of ENaC, as shown in the *Results* section and also in the *Supplements*, which provide further details on the interactions between PI, PI(4)P, PI(5)P, $PI(4,5)P_2$, PI4K and PIP5KI.

In the new model proposed here, which consists of a combination of the phosphoinositide model and a model describing the dynamics of ENaC, we used several additional datasets that were not used in the previous sub-models. They are summarized below.

4.6.2. Almaça's data

Almaça and colleagues [13] investigated A549 cell, which are adenocarcinomic human alveolar basal epithelial cells. Because these are cancer cells, they probably are not

completely polarized. This feature is not ideal for studying ENaC because the majority of ENaC channels is found in the apical part of the membrane [54].

Almaça also studied the effects of PKC activation and DGK perturbations on ENaC activity in CF. PKC has an enormous variety of effects [61], [62] but, in our model, we assume that this kinase will solely activate PLD and regulate the DGK independent PA production. Consequently, an activation of PKC immediately increases PA production and, through an increase in $PI(4,5)P_2$, raises ENaC activity; which is contrary to Almaça's observations. Instead, it might be that the inhibiting effect of PKC activation on ENaC is mediated by cAMP or the MAPK pathway [63], [64], which are not parts of the model.

Finally, Almaça *et al.* tested the possibility that ENaC could be inhibited by a PI3KI knockdown [13]. The authors state that ENaC is activated by $PI(3,4,5)P_3$, an observation confirmed by others [9], [65]. Unfortunately, these studies do not take into account the polarity of human pulmonary epithelial cells. In these cells, ENaC and its influence on ASL tickness are found in the apical part of the plasma membrane, which contains very small quantities of $PI(3,4,5)P_3$ and PI3KI; indeed these low quantities are among the hallmarks of the apical part of human pulmonary epithelial cells. Further studies are necessary to confirm that polarity is truly important in this context, but given the known facts it seems improbable that PI3KI inhibition would have any practical effect on apical located ENaC activity *in vivo*.

It is imaginable that the effect on ENaC could come from $PI(4,5)P_2$ rather than from $PI(3,4,5)P_3$ but it is not clear if PI3KI activity influences $PI(4,5)P_2$ levels in the plasma membrane. So far, the data of the highest quality are pointing to a uniform distribution of PI(4,5)P2 throughout the plasma membrane in polarized cells [66].

4.6.3. Moritz' data

Moritz *et al.* [17] studied PIP5KI activation as a function of PA concentration (Figure 4.12) using Triton X-100 which, as Jones *et al.* [67] report, greatly inhibits the basal PIP5KI activity. This inhibition causes the reported basal activity to be lower and the apparent fold change activation to be increased. The authors report a basal activity of 1 pmol/min and a maximum activation of the enzyme of 20-fold. We adjusted for the effects of the detergent, as described in the *Methods*.

4.6.4. Jarquin-Pardo's data

Jarquin-Pardo and colleagues [19] reported on an impressive amount of work addressing PIP5KI kinetics and its activation by PA. Unfortunately, they also used Triton X-100. Their data on PIP5KI activation as a function of PA concentration can be seen in Figure 4.12. The authors report a basal activity of 0.2 molecule/min/unit of PIP5KI and a maximum activation of the enzyme of 30-fold.

To find the range of PA concentrations in Jarquin-Pardo's experiments we had to estimate the total concentration of Triton X-100 they used. Our calculations suggested that a pure Triton X-100 solution at 0.1% volume will have a concentration of 1,600 μM. Because the Triton X-100 was in a mixture, we searched for a number that would produce a better agreement between Jarquin-Pardo's and Moritz' data. We found that a Triton X-100 concentration of 35,000 μM would produce good agreement between the two datasets and was close enough to the calculated value. Furthermore, although we do not know the exact figure for PA levels, different sources report them close to the levels of PI(4)P and $PI(4,5)P_2$ [17], [22], [25], which is in good agreement with Moritz' data.

4.6.5. Jenkins' data

Jenkins *et al.* [68] studied PIP5KI activation by PA with and without triton X-100. Unfortunately, they only showed the data for the experiment with the detergent. The authors report a maximum activation of the enzyme of 8, 15 and in some cases even 50-fold with Triton X-100. For the experiment without the detergent they reported that the maximum activation was around 3-fold, which agrees with reports by Jones and colleagues.

4.6.6. Other pertinent data

Pochynyuk *et al.* [42] provided information about the concentrations of $PI(4,5)P_2$ under different levels of PLC activity and measured 15 minutes after the perturbations occurred. We used this information from Pochynyuk's article, as well as the levels of DAG, PA and IP_3, for the parameterization of PLC activity in the model.

The paper by Sampaio *et al.* [25] contains values for PA and DAG levels that correspond to 0.5% – 1% of total cell lipids in polarizing MDCK cells. This level makes

them similarly rare as PI(4)P and PI(4,5)P_2, which are found at around 10,000 molecules/μm^2. PA and DAG values were set in the model to 5,600 and 7,800 molecules/μm^2, respectively.

Studies on platelets [22], [69] suggest that the levels of IP_3 are between 300 to 700 molecules/μm^3; the model uses a value of 500 molecules/μm^3. This value was achieved by enabling fast removal of IP_3 from the system, which is in agreement with the fact that IP_3 is a soluble molecule.

Some components of the system are faced with a large dispersion of parameter values, especially in specific enzyme activity. For instance, according to James *et al.* [70], PLC is inhibited by many detergents commonly used in laboratory experiments, specially Triton X-100. James *et al.* used dodecylmaltoside, which was shown not to affect the activity of PLC. They report values between 0.11 and 0.18 μM for the K_M and between 31.3 and 38.9 μmol/min/mg for the specific activity. We decided to use these parameter values but deemed the activity of PLC too strong. As a correction, we considered that PI(4)P competes for PLC, as shown by Ginger, Seifert and others [71], [72] and that PLC is inhibited by PS [72]. Values for PS were taken from Sampaio *et al.* [25].

4.6.7. Parameter values from BRENDA

Several papers cited in the BRENDA database [48] suggest very different values for the kinetic parameters of PLC. In particular, values for the K_M of human PLC are listed between 0.0123 and 0.0391 mM, and values for specific activity range between 0.5784 and 200 μmol/min/mg. For *Rattus norvegicus* the ranges are also quite large, namely, between 0.006 and 0.182 mM for K_M and between 3.1 and 204.1 μmol/min/mg for specific activity.

Similarly, it is not clear which parameters for PI3KI that are listed in BRENDA are most appropriate here, and we are therefore not fully confident about the representation of the function of this enzyme. The large amount of enzyme necessary to balance the powerful action of PTEN could be an indication that the values retrieved from BRENDA are not entirely suited for our purposes.

For our model calibration, we ensured that all pertinent values fell into the ranges provided by BRENDA and obtained specific values through various fitting procedures.

4.6.8. Mathematical framework

A dynamical model of phosphoinositide metabolism was recently designed within the framework of Biochemical Systems Theory (BST) [73]–[79], using ordinary differential equations (ODEs) in the format of a generalized mass action (GMA) system. In this approach, each ODE describes the dynamics of a dependent variable X_i, which is formulated as a sum of all fluxes that are directly related to this variable; furthermore, each flux $v_{i\rightarrow j}$ is formulated as a power-law function, as shown in Eq. (4.1).

$$\frac{dX_i}{dt} = \sum_s n_{s\rightarrow i}.v_{s\rightarrow i} - \sum_p m_{i\rightarrow p}.v_{i\rightarrow p} \qquad (4.1)$$
$$v_{i\rightarrow j} = \gamma_{i\rightarrow j} \cdot E_{i\rightarrow j} \cdot X_i^{f_{i\rightarrow j}}$$

Each quantity $\gamma_{i\rightarrow j}$ or $E_{i\rightarrow j}$ represents the rate constant or enzyme activity for a given flux, respectively, $f_{i\rightarrow j}$ is the kinetic order, and $n_{s\rightarrow i}$ and $m_{i\rightarrow p}$ are the stoichiometric coefficients for the influxes and outfluxes.

4.6.9. Model design, equations and parameters estimation

The model proposed here is a functional merger of two sub-models. The first in an extension of a phosphoinositide pathway model that was recently published, along with all pertinent information regarding equations and parameter values [7]. The second sub-model captures the dynamics of ENaC and ASL and is described elsewhere [16]. The main coupling point between the two sub-models is PI(4,5)P_2. This coupling, for the first time, permits an investigation of the complex regulation of ENaC and ASL by phosphoinositides.

Functionally connecting the phosphoinositide pathway to the dynamics of ENaC suggests slight modifications to the phosphoinositide model, which are depicted Figure 4.1; the fluxes and equations are presented in Table 4.1 and parameters and initial values are given in Table 4.2. References for parameters can be found in Supplementary Table 4.4 and in Chapters 2 and 3.

The rather complex phosphoinositide sub-model accounts for all phosphoinositide species and their interconversions, as well as PI, the precursor of all phosphoinositides. It reproduces several phenomena described in the literature that characterize the

pathway, even for phosphoinositides present in small quantities. Notably, however, this model does not account for ENaC or other elements that are needed to study the regulation of this channel.

Thus, we connect this model to a module containing all biochemical components that are necessary for studying ENaC regulation by $PI(4,5)P_2$. Specifically, we add phospholipase C (PLC), which cleaves $PI(4,5)P_2$ into DAG and IP_3, and allow for competitive inhibition of this phospholipase by PI(4)P and PS. In addition to DAG and IP_3, we explicitly define the enzyme DGK, which facilitates the transformation of DAG into PA. We also add LPPs that hydrolyze PA back to DAG.

A new input flux of material to the PA pool now accounts for the transformation of PC into PA by phospholipase D (PLD). We opted for this implementation because PC exists in abundance in the cell membrane, with approximately 3,000,000 molecules/μm^2, which corresponds to approximately 25% of the cell membrane [25], and will therefore never be significantly depleted by the action of PLD. It also has a structural role in the cell membrane, and severe depletion of PC causes the cell to lyse. The flux rate constant is adjusted to include the contribution of PC.

We also include the observed activation of PLD by $PI(4,5)P_2$ [80], [81] by letting the levels of phosphoinositide influence the influx of material. This activation creates a positive feedback between $PI(4,5)P_2$ and the production of PA by PLD, which enables the system very elegantly to increase the sensitivity of $PI(4,5)P_2$ production to alterations in PA when PLC is active (Figure 4.9). This mechanism appears to do the following: PA has two main sources. It may be created from PC by PLD, or it may be derived from the cleavage of $PI(4,5)P_2$ by PLC. When PLC displays low activity, a good amount of PA is being produced by PLD. However, when PLC is activated, more PA is produced via degradation of $PI(4,5)P_2$. Less $PI(4,5)P_2$ reduces the activation of PLD and leads to less PA production from PC. Not only does this dual mechanism contribute to the stability of PA levels, but it also alters the ratio between PA coming from PLC and PA coming from PLD.

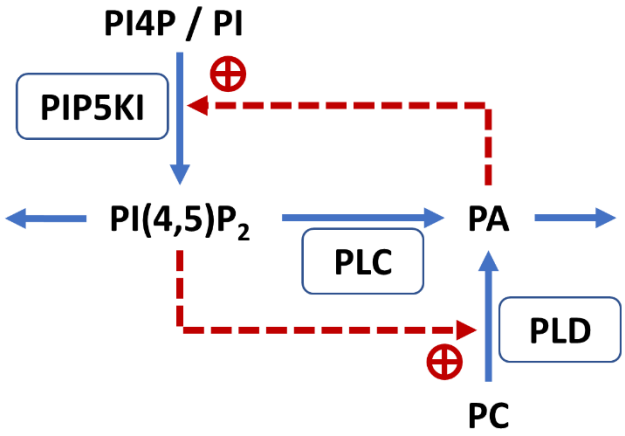

Figure 4.9. Positive feedback regulation of PI(4,5)P2 and PA.

In the plasma membrane, PA may be created from PC by PLD and by cleavage of $PI(4,5)P_2$ by PLC. When PLC displays low activity, PA is mainly produced by PLD. When PLC activity increases, more PA is produced via degradation of $PI(4,5)P_2$, which lowers the pool of $PI(4,5)P_2$, secondarily reduces the activation of PLD, and ultimately leads to less PA production from PC. This dual activation mechanism could alter the ratio between PA coming from PLC and from PLD and contribute to the stability of PA and $PI(4,5)P_2$ levels; however, confirmation of this mechanism will require further laboratory investigation.

The combined model moreover accounts for the activation of PIP5KI by PA, a regulation frequently described in the literature [17]–[19]. This regulation renders $PI(4,5)P_2$ production dependent on DGK and allows us to study the activity of ENaC under different DGK levels of activation.

In addition to including these mechanisms, we introduce three minor refinements. First, we separate some enzymes catalyzing the same reaction into different fluxes when there is sufficient information to do so. For instance, we define two groups of the myotubularin phosphatase family: MTMR_1_6_14, which corresponds to myotubularins 1 to 6 plus 14, and MTMR78, which contains myotubularins. We cannot really separate these groups into individual enzymes because no information is available for specific differences among MTMR's. For the same reason, ORCL1, INPP5 B/J, SKIP and SAC2 are grouped into O_I_SK_SA2. Outside these exceptions, the enzyme separation allows a better understanding of the mechanics in the model and a more accurate replication of experimental perturbations to the pathway, especially with respect to explorations that involve the inhibition or activation of enzymes.

Finally, we account for substrate competition in accordance to observations of wet lab experiments that reported the existence of multiple substrates, especially in the case of phosphatases [82]. The regulation among PTEN, PI3KI, $PI(4,5)P_2$ and $PI(3,4,5)P_3$ is implemented by creating pools of active (PTENa and PI3KIa) and inactive (PTENc and PI3KIc) PI3KI and PTEN and allowing the products of these enzymes to activate the enzymes. Parameters for this part of the model were found by fitting the model behavior to data reported by Feng *et al.* [45], which were not used in the earlier phosphoinositide model.

As for the earlier models, rate constants and kinetic orders are derived from enzyme kinetic information provided by the BRENDA database [48] or from the literature, after the necessary unit transformations. In this model, K_M values are in molecules/μm^3, specific activities in molecules/min/mg of enzyme and enzymes in mg. Details can be found in the Supplementary information, or in Table 2.3 of Chapter 2 [7]. The kinetic parameters of enzymes used only in the combined model are presented in Table 4.4 of the Supplements. Enzyme activities and transport fluxes where manually set to approximate reported phosphoinositide steady-state values. In some cases, the rate constants were estimated based on data fits.

The parameters were derived from different data sources. Initially, we manually adjusted the parameters to fit the data adequately. Next, for each dataset, a local, general-purpose optimization function implemented in the R language was used to search for the best fit. The Nelder–Mead method was used. In the final step, a hybrid genetic algorithm was implemented in the GA package to search for the global minimum.

With regard to the ENaC model, Chapter 3 explored two models: one where $PI(4,5)P_2$ protected ENaC from ubiquitination and another where this was not the case. As we did not detect significant differences in results, we chose here the simpler model, where $PI(4,5)P_2$ does not protect ENaC from ubiquitination. The equations, parameters and initial values for this model are presented in Chapter 3.

While most of the information regarding the two sub-models was presented somewhere, the connection of the two models requires additional effort. Most of this effort concerns the dynamics of $PI(4,5)P_2$.

4.6.10. Activation of PIP5KI by PA

PIP5KI is the enzyme responsible for phosphorylating the fifth carbon on the PI(4)P inositol ring and transforming it into $PI(4,5)P_2$. It has two identified binding sites for PA in the C-terminal domain [19]. PIP5KI also has two binding sites for is substrate, PI(4)P, and these have different functions. One allows inhibition of the enzyme, whereas the other is a catalytic site that phosphorylates PI(4)P into $PI(4,5)P_2$. According to Jarquin-Pardo *et al.*, [19], the catalytic site has a K_M of 134 μM in the absence of PA, which is much higher than the inhibitory site with 2.4 μM. Consequently, the enzyme is inactive or in a reduced activity state if the concentration of PA is low. In the presence of PA, the situation is reversed: the K_M for the catalytic site is 2 μM and the K_M for the inhibitory site is 4.2 μM. The values of the k_{cat} for both these cases are 16.4 and 17 min^{-1}. They suggest that PA will mainly alter the affinity of the catalytic site for PI(4)P.

To identify a function that describes the PIP5KI activation by PA, we consulted three papers containing data on $PI(4,5)P_2$ production under different levels of PA [17], [19], [68]. These articles were described before, and we focus here specifically on PIP5KI activation. Unfortunately, all three studies used Triton X-100, which Jones *et al.* [67] describe as greatly inhibiting the basal lipid kinase activity. We explored different means of compensating for this inhibition. In Moritz' case, we altered the basal activity of PIP5KI from 1 to 1.5 molecules/min/unit of PIP5KI and scaled the data in such a manner that the maximum activation was 3, as reported by Jenkins and colleagues. We achieved this scaling by multiplying the values of $PI(4,5)P_2$ production with 3/20. For Jarquin-Pardo's data, we performed two transformations of the data. First, we altered the basal activity of PIP5KI from 0.2 to 1.5 molecules/min/unit of PIP5KI. Second, we scaled the data so that the maximum activation was again 3. In this case, we achieved this scaling by multiplying the values of $PI(4,5)P_2$ production with 3/30. Finally, for Jenkins' data, we altered the basal activity of PIP5KI to 1.5 molecules/min/unit of PIP5KI and scaled the data so that the maximum activation was again 3. In this case, we multiplied the values of $PI(4,5)P_2$ production with 2.2/13.

4.6.11. Creating a PIP5KI PA activation function

Because data presented by Moritz and Jarquin-Pardo both suggest a sigmoid function, we chose a shifted Hill function to describe the activation of PIP5KI by PA. This

function (Eq. 4.2) has a K_M of 10,000, a Hill coefficient of 2 and a maximal fold-activation of PIP5KI of 2; it is furthermore shifted by 1.

$$\text{PIP5KI\_activation}\left(PA\right) = 1 + \frac{2 \times PA^2}{10000^2 + PA^2} \qquad (4.2)$$

These settings ensure that the maximum activation of the PIP5KI enzyme is 3-fold (4.5 molecules/min/unit of PIP5KI), which is in line with the range of 2.2 and 3-fold activation reported by Jones *et al.* [67] and Jenkins *et al.* [18]. When PA has a concentration of 10,000 molecules/μm^3, the enzyme is activated at half the maximum rate, and this value is within the physiological range for PA [17], [22], [25]. The Hill coefficient of 2 agrees well with the two reported binding sites for PA [19].

4.6.12. Modified Suretekar's phosphoinositide pathway model

To explore the likelihood that Almaça's hypothesis regarding the regulation of ENaC by DGK, we used a model that in some sense represents a coarse alternative to our combined model. This model was proposed by Suratekar and colleagues [23] and uses data from photoreceptor cells of *Drosophila melanogaster*. One must note that this model, although addressing the same phosphoinositide pathway, may have features that are not entirely representative of human cells.

Suratekar and colleagues tested many versions of their phosphoinositide pathway model and ultimately decided on one that was in accordance with all data available to them. It contains an open cycle with influx of PA in the ER and efflux of DAG into the plasma membrane, but does not include PA regulation of PIP5KI. We used this version implemented with Michaelis–Menten kinetics, as proposed by the authors.

The steady-state levels of our model and Suratekar's do not completely agree. In order to successfully link Suratekar's and our ENaC-ASL model, we therefore divided the $PI(4,5)P_2$ level by its steady-state value and multiplied it by 10,000. In this way, the steady state of $PI(4,5)P_2$ becomes similar to the one considered by our model.

For the model to be able to replicate Almaça's observations of DGK regulation of ENaC, we must make three alterations. The first is an implementation of a PA dependent V_{max} for PIP5KI, according to the Hill function in (4.3), which makes the production of $PI(4,5)P_2$ dependent on the levels of PA.

$$H_{pip5KI} = 0.3 + \frac{V_{\max, pip5KI^*} \times PMPA^2}{K_{M, pip5KI^*}{}^2 + PMPA^2} = \\ = 0.3 + \frac{1.51 \times PMPA^2}{0.01672982^2 + PMPA^2} \qquad (4.3)$$

The shift constant 0.3 guarantees that PIP5KI is still active without PA, $K_{M,pip5KI}{}^*$ corresponds to the steady-state level of PMPA and $V_{max,pip5KI}{}^*$ was calculated for $V_{max,pip5KI}$ to have the same value as in the original model at the steady state of PMPA. We substituted $V_{max,pip5KI}$ in the flux equation for PIP5KI by this new expression.

Because this alteration would cause an explosive increase of PI(4)P when DGK is inhibited, we added an efflux from the PI(4)P pool. The efflux is shown in Eq. (4.4) and included in the differential equation for PI(4)P as a negative term.

$$V_{PI4P\_exit} = .08 * \mathrm{PI}(4)\mathrm{P} \qquad (4.4)$$

The value for the rate constant in this flux was obtained by trial and error until the model exhibited the behavior coherent with experimental observations. We are not aware of any direct biological evidence of a significant efflux of this type but it seems reasonable to assume that every phosphoinositide pool should have an efflux representing the phospholipids that exit the plasma membrane by vesicle or non-vesicle transport. It is not clear how relevant this postulated efflux is for the phosphoinositide pools, but we have implemented effluxes in our phosphoinositide pathway model.

Finally, although the steady-state levels of the model are not drastically perturbed by these alterations, we compensated for the new exit of material from the system by increasing the ER PA source flux by 1.1%. Again, trial and error were used to determine this parameter.

One should note that we are not trying to find an optimized set of parameter values for the model. Our objective is solely to test whether Suratekar's model can replicate Almaça's observations when regulation of PIP5KI by PA accounted for.

4.6.13. Model Implementation

The model was implemented in the programming language R v3.1.0 [83] together with the package deSolve [84]. We used the ODE integration function with the LSODA method.

4.6. References

[1] M. Adachi *et al.*, "Compound heterozygous mutations in the γ subunit gene of ENaC (1627delG and 1570-1G→A) in one sporadic japanese patient with a systemic form of pseudohypoaldosteronism type 1.," *J. Clin. Endocrinol. Metab.*, vol. 86, no. 1, pp. 9–12, Jan. 2001.

[2] M. Lopes-Pacheco, "CFTR modulators: Shedding light on precision medicine for cystic fibrosis," *Front. Pharmacol.*, vol. 7, no. 275, pp. 1–20, 2016.

[3] J. L. Taylor-Cousar *et al.*, "Lumacaftor/ivacaftor in patients with cystic fibrosis and advanced lung disease homozygous for F508del-CFTR.," *J. Cyst. Fibros.*, vol. 17, no. 2, pp. 228–235, 2017.

[4] M. M. R. P. M. Quinton, "Functional interaction of CFTR and ENaC in sweat glands," pp. 499–503, 2003.

[5] V. Bhalla and K. R. Hallows, "Mechanisms of ENaC regulation and clinical implications.," *J. Am. Soc. Nephrol.*, vol. 19, no. 10, pp. 1845–1854, 2008.

[6] J. Teiwes and R. D. Toto, "Epithelial sodium channel inhibition in cardiovascular disease. A potential role for amiloride," *Am. J. Hypertens.*, vol. 20, no. 1, pp. 109–117, 2007.

[7] D. V. Olivença, I. Uliyakina, L. L. Fonseca, M. D. Amaral, E. O. Voit, and F. R. Pinto, "A Mathematical Model of the Phosphoinositide Pathway," *Sci. Rep.*, vol. 8, no. 1, p. 3904, Dec. 2018.

[8] O. Pochynyuk, V. Bugaj, and J. D. Stockand, "Physiologic regulation of the epithelial sodium channel by phosphatidylinositides," *Curr. Opin. Nephrol. Hypertens.*, vol. 17, no. 5, pp. 533–540, 2008.

[9] O. Pochynyuk *et al.*, “Molecular determinants of PI(4,5)P2 and PI(3,4,5)P3 regulation of the epithelial Na+ channel.,” *J Gen Physiol*, vol. 130, no. 4, pp. 399–413, 2007.

[10] H.-P. Ma and D. C. Eaton, “Acute regulation of epithelial sodium channel by anionic phospholipids.,” *J. Am. Soc. Nephrol.*, vol. 16, no. 11, pp. 3182–3187, 2005.

[11] G. Yue, B. Malik, G. Yue, and D. C. Eaton, “Phosphatidylinositol 4,5-bisphosphate (PIP2) stimulates epithelial sodium channel activity in A6 cells,” *J. Biol. Chem.*, vol. 277, no. 14, pp. 11965–11969, 2002.

[12] T. Balla, “Phosphoinositides: tiny lipids with giant impact on cell regulation,” *Physiol. Rev.*, vol. 93, no. 3, pp. 1019–1137, 2013.

[13] J. Almaça *et al.*, “High-content siRNA screen reveals global ENaC regulators and potential cystic fibrosis therapy targets,” *Cell*, vol. 154, no. 6, 2013.

[14] J. Almaça *et al.*, “AMPK controls epithelial Na+ channels through Nedd4-2 and causes an epithelial phenotype when mutated,” *Pflugers Arch. Eur. J. Physiol.*, vol. 458, no. 4, pp. 713–721, 2009.

[15] C. S. Kim, S. Ahmad, T. Wu, W. G. Walton, M. R. Redinbo, and R. Tarran, “SPLUNC1 is an allosteric modulator of the epithelial sodium channel,” *FASEB J.*, Jan. 2018.

[16] D. V. Olivença, L. L. Fonseca, E. O. Voit, and F. R. Pinto, “Thickness of the airway surface liquid layer in the lung is affected in cystic fibrosis by compromised synergistic regulation of the ENaC ion channel,” *Unpubl. results*.

[17] A. Moritz, P. N. De Graan, W. H. Gispen, and K. W. Wirtz, “Phosphatidic acid is a specific activator of phosphatidylinositol-4-phosphate kinase.,” *J. Biol. Chem.*, vol. 267, no. 11, pp. 7207–7210, 1992.

[18] G. H. Jenkins, P. L. Fisette, and R. A. Anderson, “Type I phosphatidylinositol 4-phosphate 5-kinase isoforms are specifically stimulated by phosphatidic acid.,” *J. Biol. Chem.*, vol. 269, no. 15, pp. 11547–54, Apr. 1994.

[19] M. Jarquin-Pardo, A. Fitzpatrick, F. J. Galiano, E. A. First, and J. N. Davis, "Phosphatidic acid regulates the affinity of the murine phosphatidylinositol 4-phosphate 5-kinase-1β for phosphatidylinositol-4-phosphate," *J. Cell. Biochem.*, vol. 100, no. 1, pp. 112–128, 2007.

[20] C. Xu, J. Watras, and L. M. Loew, "Kinetic analysis of receptor-activated phosphoinositide turnover," *J. Cell Biol.*, vol. 161, pp. 779–791, 2003.

[21] A. Gericke, N. R. Leslie, M. Lösche, and A. H. Ross, "PtdIns(4,5)P2-mediated cell signaling: Emerging principles and PTEN as a paradigm for regulatory mechanism," *Adv. Exp. Med. Biol.*, vol. 991, pp. 85–104, 2013.

[22] J. E. Purvis, M. S. Chatterjee, L. F. Brass, and S. L. Diamond, "A molecular signaling model of platelet phosphoinositide and calcium regulation during homeostasis and P2Y1 activation.," *Blood*, vol. 112, pp. 4069–4079, 2008.

[23] R. Suratekar, A. Panda, P. Raghu, and S. Krishna, "Evidence of sinks and sources in the phospholipase C-activated PIP $_2$ cycle," *FEBS Lett.*, pp. 1–11, 2018.

[24] F. Gibellini and T. K. Smith, "The Kennedy pathway-de novo synthesis of phosphatidylethanolamine and phosphatidylcholine," *IUBMB Life*, vol. 62, no. 6, pp. 414–428, 2010.

[25] J. L. Sampaio *et al.*, "Membrane lipidome of an epithelial cell line.," *Proc. Natl. Acad. Sci. U. S. A.*, vol. 108, no. 5, pp. 1903–1907, 2011.

[26] J. Viaud *et al.*, "Phosphoinositides: Important lipids in the coordination of cell dynamics," *Biochimie*, vol. 125, pp. 250–258, 2016.

[27] G. Di Paolo and P. De Camilli, "Phosphoinositides in cell regulation and membrane dynamics.," *Nature*, vol. 443, no. 7112, pp. 651–657, 2006.

[28] M. M. Reddy, M. J. Light, and P. M. Quinton, "Activation of the epithelial Na+ channel (ENaC) requires CFTR Cl- channel function.," *Nature*, vol. 402, no. 6759, pp. 301–4, 1999.

[29] A. G. Palma, B. A. Kotsias, and G. I. Marino, "Artículo especial funciones de

los canales iónicos CFTR y ENaC.," *Med. (Buenos Aires)*, vol. 74, pp. 133–139, 2014.

[30] J. F. Collawn, A. Lazrak, Z. Bebok, and S. Matalon, "The CFTR and ENaC debate: how important is ENaC in CF lung disease?," *AJP Lung Cell. Mol. Physiol.*, vol. 302, no. 11, pp. L1141–L1146, 2012.

[31] C. A. Hobbs, C. Da Tan, and R. Tarran, "Does epithelial sodium channel hyperactivity contribute to cystic fibrosis lung disease?," vol. 18, pp. 4377–4387, 2013.

[32] Y. Enuka, I. Hanukoglu, O. Edelheit, H. Vaknine, and A. Hanukoglu, "Epithelial sodium channels (ENaC) are uniformly distributed on motile cilia in the oviduct and the respiratory airways," *Histochem. Cell Biol.*, vol. 137, no. 3, pp. 339–353, 2012.

[33] W. G. Walton *et al.*, "Structural features essential to the antimicrobial functions of human SPLUNC1," *Biochemistry*, vol. 55, no. 21, pp. 2979–2991, 2016.

[34] A. Garcia-Caballero *et al.*, "SPLUNC1 regulates airway surface liquid volume by protecting ENaC from proteolytic cleavage," *Proc. Natl. Acad. Sci.*, vol. 106, no. 27, pp. 11412–11417, 2009.

[35] R. Tarran and M. R. Redinbo, "Mammalian short palate lung and nasal epithelial clone 1 (SPLUNC1) in pH-dependent airway hydration," *Int J Biochem Cell Biol.*, pp. 130–135, 2014.

[36] S. T. Terryah *et al.*, "Evaluation of a SPLUNC1-derived peptide for the treatment of cystic fibrosis lung disease," *Am. J. Physiol. - Lung Cell. Mol. Physiol.*, vol. 314, no. 1, pp. L192–L205, 2017.

[37] P. Kota *et al.*, "The N-terminal domain allosterically regulates cleavage and activation of the epthelial sodium channel," *J. Biol. Chem.*, vol. 289, no. 33, pp. 23029–23042, 2014.

[38] C. I. Sandefur, R. C. Boucher, and T. C. Elston, "Mathematical model reveals role of nucleotide signaling in airway surface liquid homeostasis and its

dysregulation in cystic fibrosis," *Proc. Natl. Acad. Sci.*, vol. 114, no. 35, pp. E7272–E7281, 2017.

[39] B. H. Falkenburger, E. J. Dickson, and B. Hille, "Quantitative properties and receptor reserve of the DAG and PKC branch of Gq-coupled receptor signaling," *J Gen Physiol*, vol. 141, no. 5, pp. 537–555, 2013.

[40] E. J. Dickson, B. H. Falkenburger, B. Hille, H. Bertil, and B. Hille, "Quantitative properties and receptor reserve of the IP3 and calcium branch of Gq-coupled receptor signaling," *J Gen Physiol*, vol. 141, no. 5, pp. 521–535, 2013.

[41] A. Narang, K. K. Subramanian, and L. D. A., "A mathematical model for chemoattractant gradient sensing based on receptor-regulated membrane phospholipid signaling dynamics.," *Ann. Biomed. Eng.*, vol. 29, no. 8, pp. 677–691, 2001.

[42] O. Pochynyuk, V. Bugaj, A. Vandewalle, and J. D. Stockand, "Purinergic control of apical plasma membrane PI(4,5)P2 levels sets ENaC activity in principal cells.," *Am. J. Physiol. Renal Physiol.*, vol. 294, no. 1, pp. F38-46, 2008.

[43] G. R. V. Hammond *et al.*, "PI4P and PI(4,5)P2 are essential but independent lipid determinants of membrane identity.," *Science (80-.).*, vol. 337, no. 6095, pp. 727–730, 2012.

[44] C. N. Antonescu, G. Danuser, and S. L. Schmid, "Phosphatidic acid plays a regulatory role in clathrin-mediated endocytosis.," *Mol. Biol. Cell*, vol. 21, no. 16, pp. 2944–2952, Aug. 2010.

[45] S. Feng *et al.*, "A rapidly reversible chemical dimerizer system to study lipid signaling in living cells," *Angew. Chemie - Int. Ed.*, vol. 53, no. 26, pp. 6720–6723, 2014.

[46] O. Pochynyuk, Q. Tong, A. Staruschenko, and J. D. Stockand, "Binding and direct activation of the epithelial Na+ channel (ENaC) by phosphatidylinositides," *J Physiol*, vol. 580, no. Pt. 2, pp. 365–372, 2007.

[47] P. Várnai, G. Gulyás, D. J. Tóth, M. Sohn, N. Sengupta, and T. Balla,

"Quantifying lipid changes in various membrane compartments using lipid binding protein domains," *Cell Calcium*, vol. 64, pp. 72–82, 2017.

[48] I. Schomburg *et al.*, "BRENDA: integrated reactions, kinetic data, enzyme function data, improved disease classification.," 2015. .

[49] G. McConnachie, I. Pass, S. M. Walker, and C. P. Downes, "Interfacial kinetic analysis of the tumour suppressor phosphatase, PTEN: evidence for activation by anionic phospholipids," *Biochem. J.*, vol. 371, no. 3, pp. 947–955, May 2003.

[50] S. B. Johnston and R. T. Raines, "Catalysis by the tumor-suppressor enzymes PTEN and PTEN-L," *PLoS One*, vol. 10, no. 1, pp. 1–13, 2015.

[51] F. C. Charalampous, "Levels and distributions of phospholipids and cholesterol in the plasma membrane of neuroblastoma cells," *BBA - Biomembr.*, vol. 556, no. 1, pp. 38–51, 1979.

[52] A. Staruschenko, E. Adams, R. E. Booth, and J. D. Stockand, "Epithelial Na+ channel subunit stoichiometry.," *Biophys. J.*, vol. 88, no. 6, pp. 3966–3975, 2005.

[53] C. M. Canessa *et al.*, "Amiloride-sensitive epithelial Na+ channel is made of three homologous subunits," *Nature*, vol. 367, no. 6462, pp. 463–467, 1994.

[54] R. G. Morris and J. a Schafer, "cAMP increases density of ENaC subunits in the apical membrane of MDCK cells in direct proportion to amiloride-sensitive Na(+) transport.," *J. Gen. Physiol.*, vol. 120, no. 1, pp. 71–85, 2002.

[55] L. H. Wong, A. Čopič, and T. P. Levine, "Advances on the Transfer of Lipids by Lipid Transfer Proteins," *Trends Biochem. Sci.*, vol. 42, no. 7, pp. 516–530, 2017.

[56] G. Baldanzi, "Inhibition of diacylglycerol kinases as a physiological way to promote diacylglycerol signaling," *Adv. Biol. Regul.*, vol. 55, pp. 39–49, 2014.

[57] M. K. Topham and R. M. Epand, "Mammalian diacylglycerol kinases: Molecular interactions and biological functions of selected isoforms," *Biochim. Biophys. Acta - Gen. Subj.*, vol. 1790, no. 6, pp. 416–424, 2009.

[58] D. M. Béziau *et al.*, “Expression of phosphoinositide-specific phospholipase C isoforms in native endothelial cells.,” *PLoS One*, vol. 10, no. 4, pp. 1–14, 2015.

[59] X. Peng and M. A. Frohman, “Mammalian phospholipase D physiological and pathological roles,” *Acta Physiol. Oxford*, vol. 204, no. 2, pp. 219–226, 2012.

[60] A. H. Lystad and A. Simonsen, “Phosphoinositide-binding proteins in autophagy,” *FEBS Lett.*, vol. 590, no. 15, pp. 2454–2468, Aug. 2016.

[61] A. C. Newton, “Protein kinase C : structure , function , and regulation.,” *Am. Soc. Biochem. Mol. Biol.*, vol. 270, no. 48, pp. 28495–28498, 1995.

[62] T. I. Igumenova, “Dynamics and membrane interactions of protein kinase C.,” *Biochemistry*, vol. 54, no. 32, pp. 4953–4968, 2015.

[63] R. E. Booth and J. D. Stockand, “Targeted degradation of ENaC in response to PKC activation of the ERK1/2 cascade.,” *Am. J. Physiol. Renal Physiol.*, vol. 284, no. 5, pp. F938–F947, 2003.

[64] J. D. Stockand *et al.*, “Stimulation of the epithelial sodium channel (ENaC) by cAMP involves putative ERK phosphorylation sites in the C termini of the channel’s β- and γ-subunit,” *J. Biol. Chem.*, vol. 281, no. 15, pp. 9859–9868, 2006.

[65] M. He-Ping, S. Saxena, and D. G. Warnock, “Anionic phospholipids regulate native and expressed epithelial sodium channel (ENaC),” *J. Biol. Chem.*, vol. 277, no. 10, pp. 7641–7644, 2002.

[66] S. Kolay, U. Basu, and P. Raghu, “Control of diverse subcellular processes by a single multi-functional lipid phosphatidylinositol 4,5-bisphosphate [PI(4,5)P2].,” *Biochem. J.*, vol. 473, no. 12, pp. 1681–92, 2016.

[67] D. R. Jones, M. A. Sanjuan, and I. Mérida, “Type I alpha phosphatidylinositol 4-phosphate 5-kinase is a putative target for increased intracellular phosphatidic acid,” *FEBS Lett.*, vol. 476, no. 3, pp. 160–165, 2000.

[68] G. H. Jenkins and R. A. Subrahmanyam, G. Anderson, “Purification and reconstitution of phosphatidylinositol 4-kinase from human erythrocytes.,”

Biochim Biophys Acta., vol. 1080, no. 1, pp. 11–28, 1991.

[69] L. F. Brass and S. K. Joseph, "A role for inositol triphosphate in intracellular Ca2+ mobilization and granule secretion in platelets," *J. Biol. Chem.*, vol. 260, no. 28, pp. 15172–15179, 1985.

[70] S. R. James, A. Paterson, T. H. Harden, and C. P. Downes, "Kinetic analysis of phospholipase C beta isoforms using phospholipid-detergent mixed micelles.," *J. Biol. Chem.*, vol. 270, no. 20, pp. 11872–11881, 1995.

[71] J. P. Seifert, M. R. Wing, J. T. Snyder, S. Gershburg, J. Sondek, and T. K. Harden, "RhoA activates purified phospholipase C-ε by a guanine nucleotide-dependent mechanism," *J. Biol. Chem.*, vol. 279, no. 46, pp. 47992–47997, 2004.

[72] R. S. Ginger and P. J. Parker, "Expression, purification and characterisation of a functional phosphatidylinositol-specific phospholipase C-delta 1 protein in Escherichia coli.," *Eur. J. Biochem.*, vol. 210, no. 1, pp. 155–60, Nov. 1992.

[73] E. O. Voit, *Computational analysis of biochemical systems: a practical guide for biochemists and molecular biologists*. Cambridge, U.K.: Cambridge University Press, 2000.

[74] E. O. Voit, "Mesoscopic modeling as a starting point for computational analyses of cystic fibrosis as a systemic disease," *Biochim. Biophys. Acta - Proteins Proteomics*, vol. 1844, no. 1, pp. 258–270, Jan. 2014.

[75] M. A. Savageau, "Biochemical systems analysis. I. Some mathematical properties of the rate law for the component enzymatic reactions.," *J. Theor. Biol.*, vol. 25, no. 3, pp. 365–9, Dec. 1969.

[76] E. O. Voit, "Biochemical systems theory: a review," *ISRN Biomath.*, vol. 2013, pp. 1–53, 2013.

[77] M. A. Savageau, *Biochemical systems analysis : a study of function and design in molecular biology*. Addison-Wesley, 1976.

[78] E. O. Voit, "The best models of metabolism," *Wiley Interdiscip. Rev. Syst. Biol. Med.*, vol. 9, no. 6, p. e1391, Nov. 2017.

[79] N. V. Torres and E. O. Voit, *Pathway Analysis and Optimization in Metabolic Engineering.* Cambridge, U.K.: Cambridge University Press, 2002.

[80] V. A. Sciorra, S. A. Rudge, J. Wang, S. McLaughlin, J. Engebrecht, and A. J. Morris, "Dual role for phosphoinositides in regulation of yeast and mammalian phospholipase D enzymes," *J. Cell Biol.*, vol. 159, no. 6, pp. 1039–1049, 2002.

[81] M. N. Hodgkin, M. R. Masson, D. Powner, K. M. Saqib, C. P. Ponting, and M. J. O. Wakelam, "Phospholipase D regulation and localisation is dependent upon a phosphatidylinositol 4, 5-bisphosphate-specific PH domain," *Curr. Biol.*, vol. 10, no. 1, pp. 43–46, 2000.

[82] T. Sasaki *et al.*, "Mammalian phosphoinositide kinases and phosphatases," *Prog. Lipid Res.*, vol. 48, no. 6, pp. 307–343, 2009.

[83] R Core Team, *R: a language and environment for statistical computing*. Vienna, Austria, 2017.

[84] K. Soetaert, T. Petzoldt, and R. W. Setzer, "Solving differential equations in R: package deSolve," *J. Stat. Software.*, vol. 2, no. 9, pp. 1–25, 2010.

4.7 ACKNOWLEDGEMENTS

Work supported by UID/MULTI/04046/2013 centre grant (to BioISI) and DIFFTARGET PTDC/BIM-MEC/2131/2014 grant (to MDA), both from FCT, Portugal. DO is a recipient of a PhD fellowship from BioSys PhD programme (Ref: SFRH/BD/52486/2014), from FCT, Portugal. This work was supported in part by the grants MCB-1517588 (PI: EOV) of the U.S. National Science Foundation. The funding agencies are not responsible for the content of this article.

4.8. Supplements

4.8.1. Model Extensions

The new additions have some effect on the model's fit, but overall, the fits to the data are similar to the earlier, simpler version of the model. Figures 4.10 a and c show model

results as bar plots, while the blue lines represent data. When PI is depleted, the decreases in PI(4)P and PI(4,5)P_2 are now slightly closer to 50%, whereas the results of perturbations in PI4K and PI4P5KI are somewhat inferior (Figure 4.10 a). Perturbations that affect the lipids in small amounts produce similar results (Figure 4.10 c).

Figure 4.10 b indicates that we can still create conditions where PI(4,5)P_2 levels are maintained with low levels of PI(4)P, but the PI(4,5)P_2 pool is much more dependent on the $V_{0\rightarrow 45}$ flux. In the new model, the contribution of PI(5)P to the PI(4,5)P_2 pool is small. Figures 4.10 c and d show that PI(4)P is also more dependent on the $V_{0\rightarrow 4}$ flux.

4.8.2. Supplementary figures

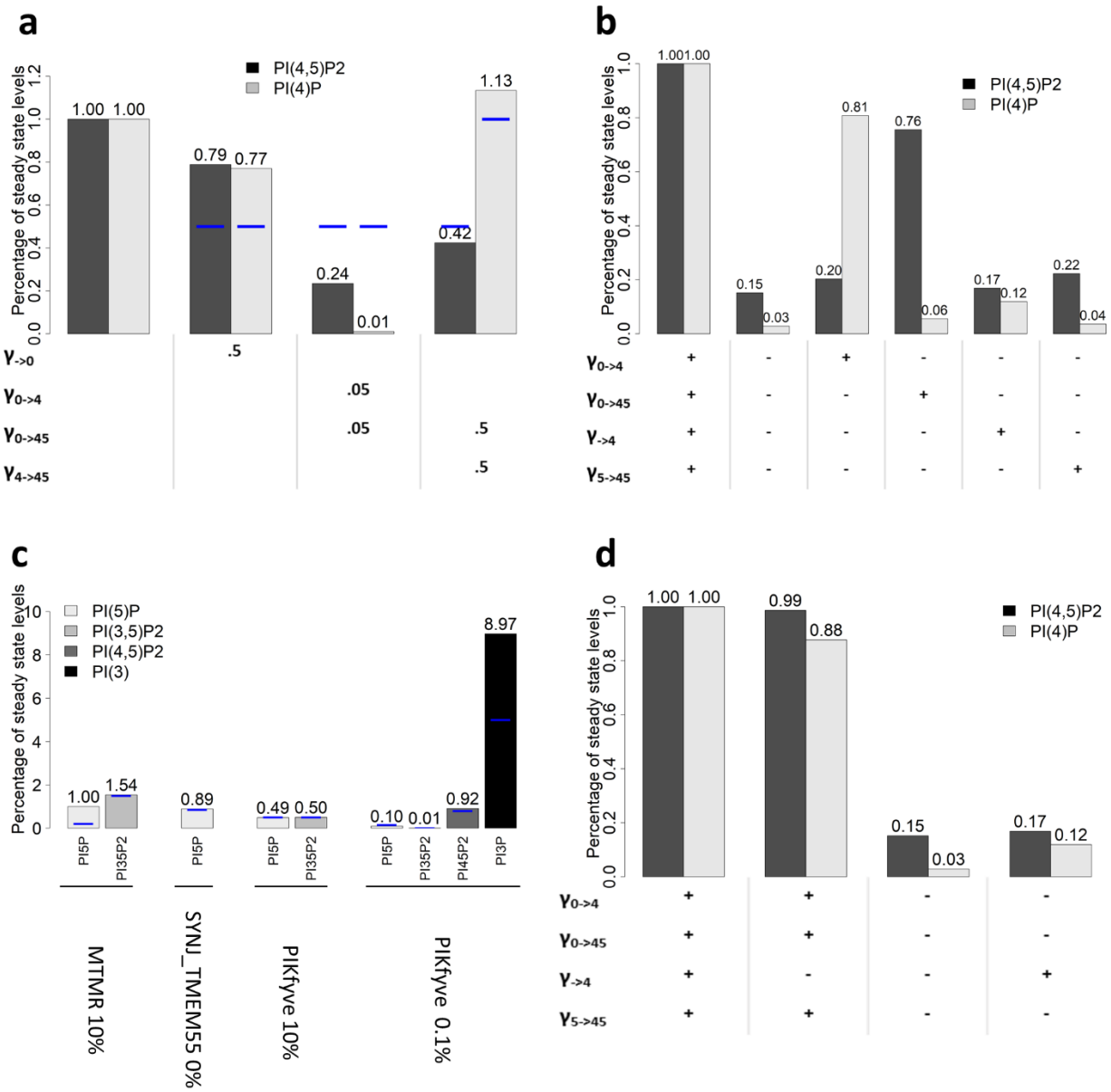

Figure 4.10. Perturbations to the phosphoinositide pathway.

Blue lines represent experimental observations and bars represent model predictions. **a)** Perturbation of PI levels and PI4K and PI5KI activities and resulting effects on PI(4,5)P_2 and PI(4)P. $\gamma_{\rightarrow 0}$ is decreased to 50% to trigger a decrease of 50% in PI. **b)** Perturbation of input fluxes into the poos of PI(4)P and PI(4,5)P_2. After stopping all inputs into PI(4)P and PI(4,5)P_2, the inputs are re-activated, one at a time, to test if they are sufficient to restore PI(4,5)P_2 levels. Enzyme knockouts were simulated by setting the rate constant of the corresponding fluxes to zero, except for $\gamma_{0\rightarrow 4}$, which was decreased to 20% of its original value, in order to avoid numerical errors in the simulation due to very small levels of PI(4)P. **c)** Perturbations to MTMR, SYNJ_TMEM55 and PIKfyve that were used to fit the model to the behavior of phosphoinositides with small pools: PI5P, PI(3,5)P_2 and PI(3)P. **d)** Consequences of Golgi PI(4)P input ($\gamma_{\rightarrow 4}$) for the levels of PI(4)P and PI(4,5)P_2 pools. Golgi PI(4)P has a significant impact on the PI(4)P pool but barely affects the PI(4,5)P_2 pool.

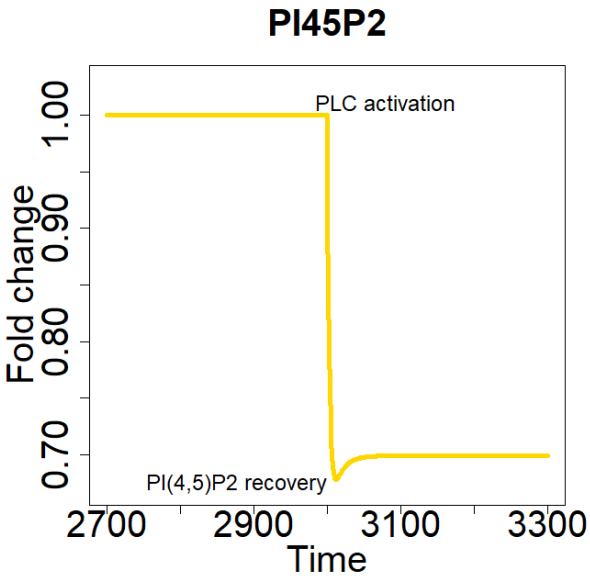

Figure 4.11. PI(4,5)P_2 recovery after 0.5-fold activation of PLC.

PLC cleaves PI(4,5)P_2 into DAG and IP_3. Several authors report a recovery of PI(4,5)P2 for some magnitudes of PLC activation [1–3]. The model shows modest recovery of PI(4,5)P_2 after an 50% increase in PLC action.

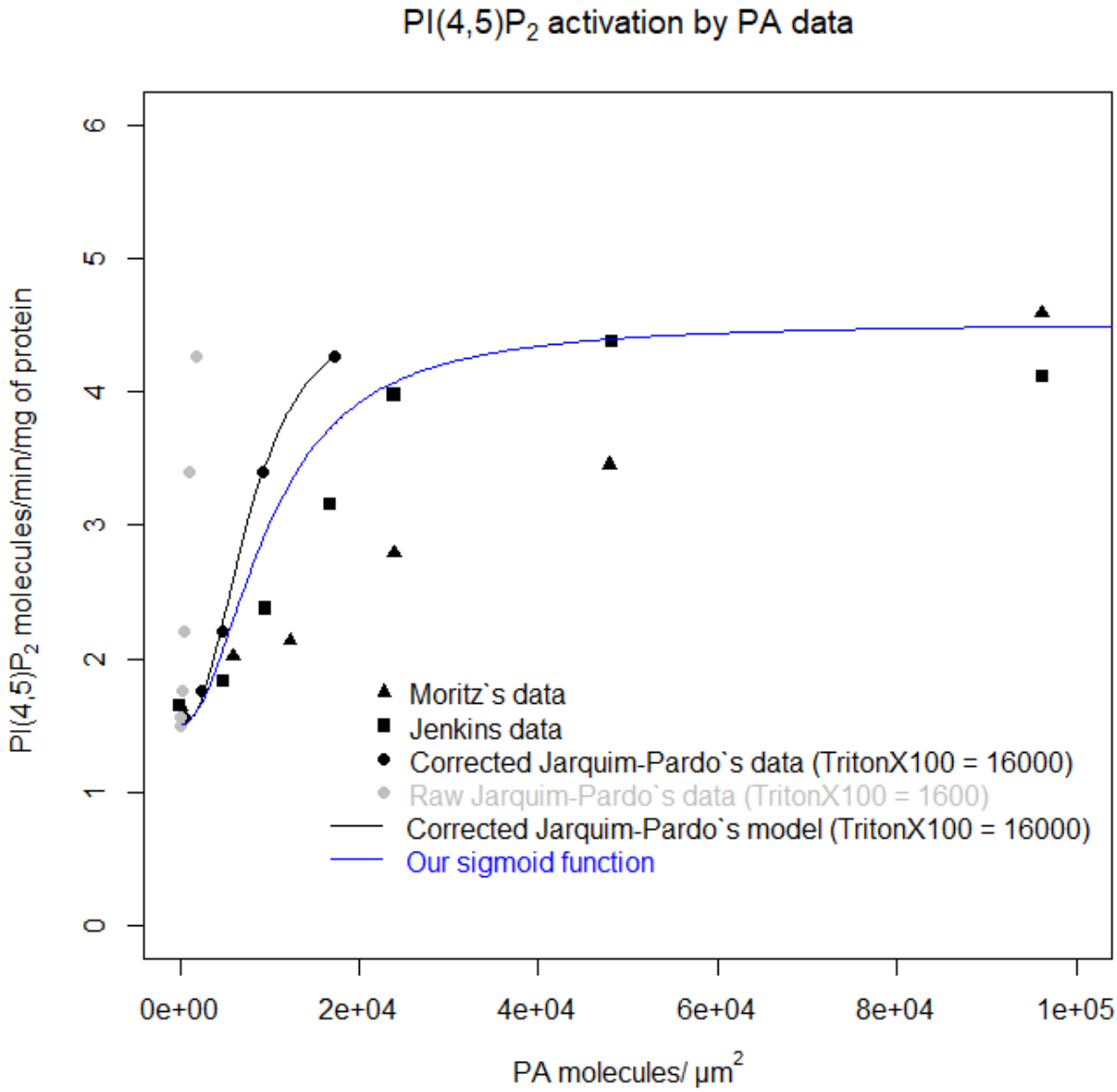

Figure 4.12. Data and model results regarding PIP5KI activation by PA.

Model results are shown as lines and points represent data. Black symbols represent data used to estimate the sigmoid function in the model, which is shown in blue. Grey points represent Jarquim-Pardo's data with the estimated correction for the use of Triton X-100.

4.8.3. Supplementary table

Table 4.4. Enzymes added to the phosphoinositide model and their characteristics.

Model enzyme	Enzymes	Flux	Values	Reference
DGK	DGK	$V_{DAG \rightarrow PA}$	K_m = 0.25 SA = 2.207	[4,5]
LPP	phosphatidate phosphatase	$V_{PA \rightarrow DAG}$	K_m = 0.277 SA = 0.1175	[6,7]
PLC	PLC β/γ/δ/ε/η	$V_{45 \rightarrow DAG}$	K_m = 0.00014 SA = 35	[8,9]
		$V_{4 \rightarrow DAG}$	K_m = 0.000255 SA = 12.7	[8,9]
PLD	PLD I/II	$V_{PC \rightarrow PA}$	*estimated*	

4.8.4. References

[1] C. Xu, J. Watras, L.M. Loew, Kinetic analysis of receptor-activated phosphoinositide turnover, J. Cell Biol. 161 (2003) 779–791. doi:10.1083/jcb.200301070.

[2] A. Gericke, N.R. Leslie, M. Lösche, A.H. Ross, PtdIns(4,5)P2-mediated cell signaling: Emerging principles and PTEN as a paradigm for regulatory mechanism, Adv. Exp. Med. Biol. 991 (2013) 85–104. doi:10.1007/978-94-007-6331-9-6.

[3] J.E. Purvis, M.S. Chatterjee, L.F. Brass, S.L. Diamond, A molecular signaling model of platelet phosphoinositide and calcium regulation during homeostasis and P2Y1 activation., Blood. 112 (2008) 4069–4079. doi:10.1182/blood-2008-05-157883.

[4] Y. Yada, T. Ozekis, H. Kanohlf, Y. Nozawasii, Purification and Characterization of Human Platelets of Cytosolic Diacylglycerol Kinases, Biochemistry. 265 (1990) 19237–19243.

[5] J.B. Wissing, K.G. Wagner, Diacylglycerol kinase from suspension cultured plant cells : characterization and subcellular localization, Plant Physiol. 98 (1992) 1148–1153. http://www.ncbi.nlm.nih.gov/pubmed/16668739.

[6] M. Takeuchi, M. Harigai, S. Momohara, E. Ball, J. Abe, K. Furuichi, N. Kamatani, Cloning and characterization of DPPL1 and DPPL2, representatives of a novel type of mammalian phosphatidate phosphatase, Gene. (2007). doi:10.1016/j.gene.2007.05.009.

[7] D. English, M. Martin, K.A. Harvey, L.P. Akard, R. Allen, T.S. Widlanski, J.G. Garcia, R.A. Siddiqui, Characterization and purification of neutrophil ecto-phosphatidic acid phosphohydrolase, Biochem J. 324 (Pt 3 (1997) 941–950. http://www.ncbi.nlm.nih.gov/entrez/query.fcgi?cmd=Retrieve&db=PubMed&dopt=Citation&list_uids=9210420.

[8] D.R. Jones, M.A. Sanjuan, I. Mérida, Type I alpha phosphatidylinositol 4-phosphate 5-kinase is a putative target for increased intracellular phosphatidic acid, FEBS Lett. 476 (2000) 160–165. doi:10.1016/S0014-5793(00)01702-6.

[9] M. Jarquin-Pardo, A. Fitzpatrick, F.J. Galiano, E.A. First, J.N. Davis, Phosphatidic acid regulates the affinity of the murine phosphatidylinositol 4-phosphate 5-kinase-1β for phosphatidylinositol-4-phosphate, J. Cell. Biochem. 100 (2007) 112–128. doi:10.1002/jcb.21027.

Chapter 5. **Conclusion and future directions**

The objectives for this PhD project were to build a dynamic model of the phosphoinositide pathway, expand the model to include ion channels, plan laboratory experiments and search for therapeutic approaches in the context of cystic fibrosis.

Our strategy to find therapeutic approaches is deeply rooted in the fact that ENaC is influenced by phosphoinositides and proteins related to the phosphoinositide pathway. As previously referred, the ASL in CF is dehydrated and the ability to moderate ENaC action could contribute to improve ASL hydration. Also, $PI(4,5)P_2$ and $PI(3,4,5)P_3$ are known to stimulate ENaC function [1]–[3] and DGK inhibition was found to moderate ENaC action [4].

The first objective was completed with the paper presented in Chapter 2 of this work. There we present a model that simulates the pathway in a 1 μm^2 patch of plasma membrane and looked for ways to manipulate $PI(4,5)P_2$, in order to influence ENaC action.

The model suggests that $PI(4,5)P_2$ can be supplied by a variety of sources apart from the one that is traditionally seen as the main source, PIP5KI phosphorylation of PI(4)P. Another source of $PI(4,5)P_2$ is the direct transformation of PI into $PI(4,5)P_2$ catalyzed by a complex of proteins that includes PI4K and PIP5KI. Also, the $PI(4,5)P_2$ pool can be supplied by PIP5KII transformation of PI(5)P. These multiple sources make manipulation of $PI(4,5)P_2$ not trivial.

Sensitivity analysis reveals that the system is robust to perturbations in most of the parameters and the high sensitivities reveal the pressure points for controlling the phosphoinositide pathway.

The model also suggests that inhibiting PIP5KI, PI4K or promoting the disassembly of the protein complex that catalyzes the direct transformation of PI, are the best strategies to decrease $PI(4,5)P_2$ levels. Alternatively, one could increase the action of phosphatases like SYNJ 1/2, INPP5 B/J/E, OCRL1, SAC2, SKIP, but increasing the action of a protein is usually more difficult than inhibiting it and phosphatases, at least

in this pathway, seem more promiscuous comparing to the kinases. This conclusion fulfilled the search for therapeutic targets objective.

In the second paper, presented in Chapter 3, we create a model of ENaC and ASL that are influenced by SPLUNC1 and $PI(4,5)P_2$. This enables us to connect the phosphoinositide model and fulfill the second objective of the project, expand the model to include ion channels. Also, it enables us to study ENaC and ASL by perturbations in the phosphoinositide pathway. In this paper, the model suggests that $PI(4,5)P_2$ can influence, not only ENaC but also ASL thickness. Also, the model suggests that alterations ENaC activity in CF are not caused by an increase in open probability but are caused by the increase in the numbers of this ion channel.

Finally, in the third paper, presented in Chapter 4, we expand the phosphoinositide model with PLC, DAG, DGK, LPPs, PA and PIP5KI regulation by PA. These additions and the merge of the phosphoinositide model with the ENaC-ASL model allow us to compare two hypotheses on how DGK influences the activity ENaC.

The first hypothesis was advanced by Almaça *et al.* [4]. DGK inhibition stops the recycling of phosphoinositides by the phosphoinositide cycle, reducing the levels of $PI(4,5)P_2$ that is being consumed by PLC. Consequently, the depletion of $PI(4,5)P_2$ will cause the moderation of ENaC action.

We explore a second hypothesis, that DGK inhibition reduces PA levels and PIP5KI activation by PA. This will decrease $PI(4,5)P_2$ production by PIP5KI and the reduction of $PI(4,5)P_2$ levels will cause ENaC moderation.

The model analysis strongly favors the second hypothesis. This is also observed when we use a phosphoinositide cycle model by Suratekar and colleagues [5]. This conclusion enabled us to challenge the established view on the mechanisms of the DGK regulation of ENaC.

Despite the encouraging results, we should point that $PI(4,5)P_2$ influences many membrane proteins [6] and tinkering with its levels will probably cause unforeseen and undesirable consequences.

Plan laboratory experiments was, as referred above, one of the objectives of this project. We can suggest several experiments but two stand out since we think the results would clarify certain obscure aspects of the phosphoinositide pathway, both in CF and WT conditions. Moreover, the experiment implementation would be simple and straightforward.

First, we would like to know if the levels of $PI(4,5)P_2$ and $PI(3,4,5)P_3$ are different in the plasma membrane of WT and CF human bronchial epithelial cells. CF human bronchial epithelial cells present a lower level of differentiation relative to their WT counterparts and this could impact the levels of $PI(4,5)P_2$ and $PI(3,4,5)P_3$ [7]. The experiment would be done as follows: 1) culture cells from the cystic fibrosis bronchial epithelial (CFBE) cell line with normal and mutated CFTR that also express a chimera with a green fluorescence protein fused to a $PI(4,5)P_2$ binding PH domain; 2) Measure the florescence in the apical and basolateral part of the plasma membrane; 3) Compare the florescence measurements between WT and CF cells. If $PI(4,5)P_2$ or $PI(3,4,5)P_3$ levels are altered in CF, this would lead research to normalize it. If not, we should keep our focus on normalizing ENaC action.

Second, we would like to validate the significance of the role of the protein complex formed by PI4K, PIP5Ki and DVL that transform PI into $PI(4,5)P_2$. The experiment would be done as follows: 1) culture cells from the cystic fibrosis bronchial epithelial (CFBE) cell line with normal and mutated CFTR that also express a chimera with a green fluorescence protein fused to a $PI(4,5)P_2$ binding PH domain; 2) create five cell lines: control, *PI4K* knockdown, *PIP5KI* knockdown, *DVL* knockdown and *WNT3A* knockdown; 3) Measure the florescence in the plasma membrane; 4) Compare the florescence measurements in the different cell lines. We would like to highlight that even if this protein complex prove not to be relevant to the levels of $PI(4,5)P_2$, other protein complexes could fulfill this role and the conclusions of Chapter 2 will not be disproved. Even so, it would be important to identify a protein complex that directly transforms PI into $PI(4,5)P_2$.

As for future perspectives, concerning the phosphoinositides, much remains to be studied. Better understanding of the distribution of phosphoinositides in the different cell organelles and the distribution of the different acyl chains in the phosphoinositide

subspecies will certainly shed light into some of the less understood aspects of the pathway.

At the start of this PhD project, the study of the phosphoinositide cycle was hindered by the lack of information on LTPs. Now, due to advances in LTPs research, a clearer picture of the cycle is emerging [8], [9]. When the information is available, I would like to build and study the model corresponding to the map depicted in Figure 5.1.

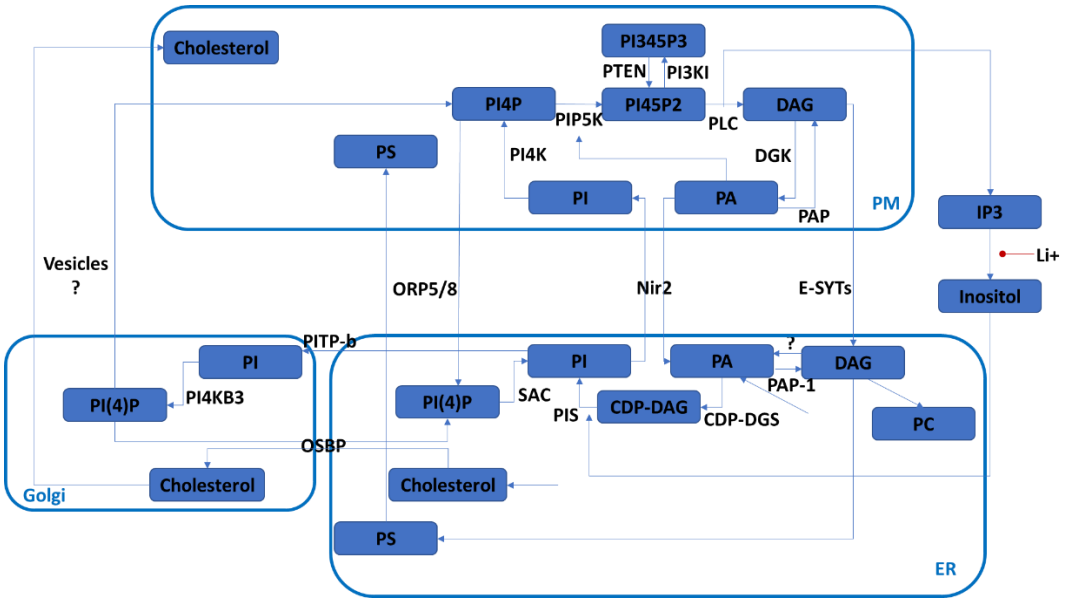

Figure 5.1. Phosphoinositide pathway map in different compartments.

This model will enable the study of the transport of phosphoinositides between organelles and of phosphoinosidide powered cholesterol transport. OSBP, PITP-b, ORB5/8 Nir2 and E-SYTs are LTP's.

Nir2's exchanges PA from the PM for PI from the ER and are very important for the recycling of phosphoinositides when PLC is activated [9], as are extended-synaptotagmins (E-SYTs) that transport DAG from the PM to the ER [10]. OSBP's exchange PI(4)P and cholesterol between the Trans-Golgi network and the ER [11]. ORP5/8 exchanges PI(4)P from the PM for PS from the ER [11]. Wong and colleagues studied the rates at which PA is transported in yeast. One lipid per second for transport between two liposomes and twelve lipids per second for import of PA in mitochondria [8]. Unfortunately, information about the kinetics of the LTPs and levels of the phosphoinositides in the different organelles is missing.

Another part of the phosphoinositide pathway that I am very keen to study is the control of $PI(4,5)P_2$ and PA levels by PLC, PLD and PIP5KI.

There are two positive feedback loops between PA and $PI(4,5)P_2$. The first is created by PLC and PIP5KI. PLC will transform $PI(4,5)P_2$ into DAG that is transformed in to PA by DGK. In turn, PA will activate the synthesis of $PI(4,5)P_2$ by PIP5KI. Because $PI(4,5)P_2$ is consumed, this is more of a replenishing mechanism than a positive feedback. However, in a system with higher PA levels, more $PI(4,5)P_2$ and PA are produced. The second is mediated by PLD. PLD transforms PC into PA that will activate the production of $PI(4,5)P_2$ by PIP5KI and we know PLD is activated by $PI(4,5)P_2$ [12], [13]. For a graphical representation of these systems see Figure 5.2.

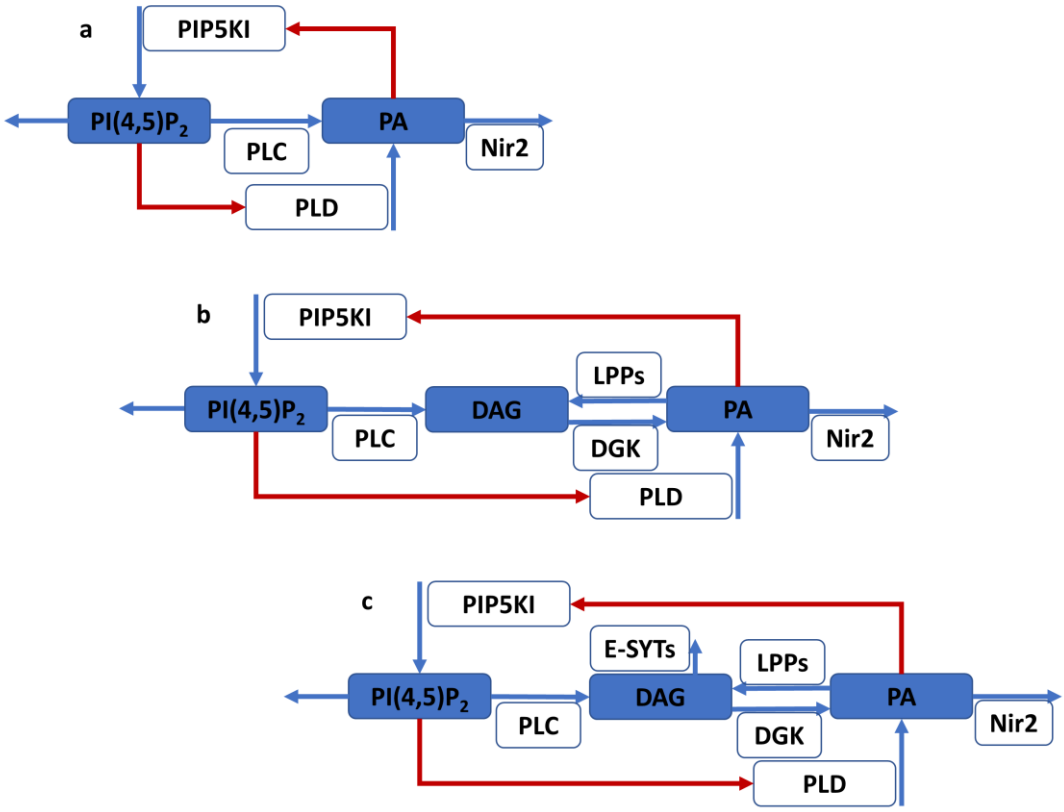

Figure 5.2. Maps of the PA, PI(4,5)P2, PLC, PLD and PIP5KI subsystem with different levels of granularity.

a) the simplest representation of the subsystem. **b)** The subsystem with the intermediate intervenients that mediate the transformation of $PI(4,5)P_2$ into PA. **c)** The same case as in b) but with an exit to the DAG pool catalyzed by E-SYTs [10].

The interesting aspect of these loops is that they seem to self-regulate the amounts of PA and $PI(4,5)P_2$, especially when PLC is activated. When $PI(4,5)P_2$ is high, the PA is predominantly synthesized by PLD. When PLC is activated, $PI(4,5)P_2$ decreases and PA is momentarily increased. Less $PI(4,5)P_2$ will reduce PA production by PLD but the increase in PA will activate $PI(4,5)P_2$ production by PIP5KI that will replenish the phosphoinositide. By these mechanisms, the levels of PA and $PI(4,5)P_2$ could be maintained.

Also, it would be interesting to study this system with the newly found regulation of PI(4)P and $PI(4,5)P_2$ by ORP5/8 found by Sohn and colleagues [14].

I would like to study more deeply these positive feedback loops, not only to evaluate their regulatory capabilities, but also to understand its purpose, if there is one, of the many isoforms of the enzymes present in this subsystem. There are ten isoforms for DGK [15], [16], thirteen PLC isoforms [17], two PLD isoforms [18] and nine PKC isoforms. PKC is a kinase that increase the levels and is activated by many of the components in the subsystem depicted in figure 5.2.

Recent developments highlight the subversion of phosphoinositide signaling by pathogens [19]. Several picornaviruses and hepatitis C virus employ a similar mechanism depending on PI4Ks, PI(4)P and OSBP [20], [21]. In order to get cholesterol for their viral replication compartments, they recruit PI4KIIIb to enrich them with PI(4)P. PI(4)P will function as an anchor for OSBP, an LPT that exchanges PI(4)P for ER cholesterol. There are several questions that could be answered with a study of these mechanisms. Can we prevent the virus from high-jacking these proteins? Will this hinder the virus development? Also, some virus are sensitive to pharmacological inhibitors of PI4Ks and OSBP, other are not [20]. What are the differences in the mechanisms between sensitive and insensitive virus?

Finally, it would be important to bring together the signaling of phosphoinositides, sphingolipids and the remaining phospholipids like PC, PS and PE.

There is much to be done.

5.1. References

[1] O. Pochynyuk, V. Bugaj, A. Vandewalle, and J. D. Stockand, "Purinergic control of apical plasma membrane PI(4,5)P2 levels sets ENaC activity in principal cells.," *Am. J. Physiol. Renal Physiol.*, vol. 294, no. 1, pp. F38-46, 2008.

[2] G. Yue, B. Malik, G. Yue, and D. C. Eaton, "Phosphatidylinositol 4,5-bisphosphate (PIP2) stimulates epithelial sodium channel activity in A6 cells," *J. Biol. Chem.*, vol. 277, no. 14, pp. 11965–11969, 2002.

[3] H.-P. Ma and D. C. Eaton, "Acute regulation of epithelial sodium channel by anionic phospholipids.," *J. Am. Soc. Nephrol.*, vol. 16, no. 11, pp. 3182–3187, 2005.

[4] J. Almaça *et al.*, "High-content siRNA screen reveals global ENaC regulators and potential cystic fibrosis therapy targets," *Cell*, vol. 154, no. 6, 2013.

[5] R. Suratekar, A. Panda, P. Raghu, and S. Krishna, "Evidence of sinks and sources in the phospholipase C-activated PIP $_2$ cycle," *FEBS Lett.*, pp. 1–11, 2018.

[6] T. Balla, "Phosphoinositides: tiny lipids with giant impact on cell regulation," *Physiol. Rev.*, vol. 93, no. 3, pp. 1019–1137, 2013.

[7] E. Hollande *et al.*, "Targeting of CFTR protein is linked to the polarization of human pancreatic duct cells in culture," *Eur. J. Cell Biol.*, vol. 76, no. 3, pp. 220–227, 1998.

[8] L. H. Wong, A. Čopič, and T. P. Levine, "Advances on the Transfer of Lipids by Lipid Transfer Proteins," *Trends Biochem. Sci.*, vol. 42, no. 7, pp. 516–530, 2017.

[9] Y. J. Kim, M. L. Guzman-Hernandez, E. Wisniewski, and T. Balla, "Phosphatidylinositol-Phosphatidic Acid Exchange by Nir2 at ER-PM Contact Sites Maintains Phosphoinositide Signaling Competence," *Dev. Cell*, vol. 33, no. 5, pp. 549–561, 2015.

[10] Y. Saheki *et al.*, "Control of plasma membrane lipid homeostasis by the extended

synaptotagmins," *Nat. Cell Biol.*, vol. 18, no. 5, pp. 504–515, 2016.

[11] G. Drin, J. M. von Filseck, and A. Čopič, "New molecular mechanisms of inter-organelle lipid transport," *Biochem. Soc. Trans.*, vol. 44, no. 2, pp. 486–492, 2016.

[12] V. A. Sciorra, S. A. Rudge, J. Wang, S. McLaughlin, J. Engebrecht, and A. J. Morris, "Dual role for phosphoinositides in regulation of yeast and mammalian phospholipase D enzymes," *J. Cell Biol.*, vol. 159, no. 6, pp. 1039–1049, 2002.

[13] M. N. Hodgkin, M. R. Masson, D. Powner, K. M. Saqib, C. P. Ponting, and M. J. O. Wakelam, "Phospholipase D regulation and localisation is dependent upon a phosphatidylinositol 4, 5-bisphosphate-specific PH domain," *Curr. Biol.*, vol. 10, no. 1, pp. 43–46, 2000.

[14] M. Sohn *et al.*, "PI(4,5)P 2 controls plasma membrane PI4P and PS levels via ORP5/8 recruitment to ER–PM contact sites," *J. Cell Biol.*, vol. 217, no. 5, pp. 1797–1813, May 2018.

[15] G. Baldanzi, "Inhibition of diacylglycerol kinases as a physiological way to promote diacylglycerol signaling," *Adv. Biol. Regul.*, vol. 55, pp. 39–49, 2014.

[16] M. K. Topham and R. M. Epand, "Mammalian diacylglycerol kinases: Molecular interactions and biological functions of selected isoforms," *Biochim. Biophys. Acta - Gen. Subj.*, vol. 1790, no. 6, pp. 416–424, 2009.

[17] D. M. Béziau *et al.*, "Expression of phosphoinositide-specific phospholipase C isoforms in native endothelial cells.," *PLoS One*, vol. 10, no. 4, pp. 1–14, 2015.

[18] X. Peng and M. A. Frohman, "Mammalian phospholipase D physiological and pathological roles," *Acta Physiol. Oxford*, vol. 204, no. 2, pp. 219–226, 2012.

[19] S. Qiu and M. Côté, "From hitchhiker to hijacker: pathogen exploitation of endosomal phosphoinositides," *Biochem. Cell Biol.*, no. C, p. bcb-2017-0317, May 2018.

[20] J. R. Strating and F. J. van Kuppeveld, "Viral rewiring of cellular lipid metabolism to create membranous replication compartments," *Curr. Opin. Cell*

Biol., vol. 47, pp. 24–33, 2017.

[21] N. Altan-Bonnet and T. Balla, “Phosphatidylinositol 4-kinases: Hostages harnessed to build panviral replication platforms,” *Trends in Biochemical Sciences*. 2012.